universität wien

DISSERTATION

Titel der Dissertation

„The role of WNT2 in human colon carcinoma development“

verfasst von

Mag. rer. nat. Nina Kramer

angestrebter akademischer Grad

Doctor of Philosophy (PhD)

Wien, 2014

Studienkennzahl lt. Studienblatt:	A 094 437
Dissertationsgebiet lt. Studienblatt:	Biologie
Betreut von:	Ao. Univ.-Prof. Mag. Dr. Ernst Müllner Mag. Dr. Helmut Dolznig

Acknowledgements

I would like to thank Assoc. Prof. Mag. Dr. Helmut Dolznig and ao. Univ.-Prof. Mag. Dr. Ernst Müllner for providing me with the opportunity to work on this PhD thesis, for all their help, encouragment and chocolate.

A special thank goes to Christine Unger, Matthias Scheinast and Martin Scherzer for their support, interesting discussions and comments regarding this thesis during our beer and chocolate breaks.

Further thanks go to my lab members Johannes Schmöllerl, Daniela Unterleuthner and Angelika Walzl for their support.

Finally, I would like to thank my husband, my family and my friends for their never-ending patience!

Summary

Colorectal cancer is the third most common cancer accounting for about 10% of cancer deaths. As in all solid cancers colon cancer cells are interwoven with the tumor stroma, which has an impact on tumor progression, metastasis and prognosis. However, the molecular mechanism of tumor-stroma crosstalk was extensively studied, but remains widely elusive. Full-genome covering expression profiling of laser-capture microdissected colon cancer stroma and normal stroma identified Wnt2 as one of the most significantly upregulated genes in the tumor stroma. Aberrant Wnt-signaling is an early event in colon cancer development; however, the impact of stromal Wnt2 expression on carcinoma progression was not addressed so far. We found that Wnt2 is expressed specifically in colon cancer-associated fibroblasts (CAFs) but not in normal colon-derived fibroblasts (NCFs). Furthermore, we demonstrated that Wnt2 expressing fibroblasts, like CAFs, induced Wnt/β-catenin signaling in colon fibroblasts but not in skin fibroblasts as shown by a 7TGP reporter construct. Furthermore, siRNA-mediated Wnt2 knock-down significantly decreased migration and invasion of CAFs. RT-qPCR analysis revealed enhanced smooth-muscle cell-myofibroblast marker expression in Wnt2 treated fibroblasts. Furthremore, transgelin expression was enhanced upon simultaneous treatment with Wnt2 and TGF-β. Co-culture of DLD1 tumor cells with Wnt2 knock-down CAFs resulted in reduced tumor cell invasion than co-culture with control CAFs. A xenograft cancer model with Wnt2 expressing HT29 and HCT116 tumor cells led to increased tumor growth compared to controls. In summary we identify Wnt2 as a novel stromal marker, inducing colon fibroblast invasion via canonical Wnt-signaling thereby affecting tumor progression.

Zusammenfassung

Kolorektale Karzinome sind die dritthäufigste Tumorerkrankung weltweit und eine häufige Todesursache. Tumorzellen solider Tumore sind eingebettet im Tumorstroma, welches einen großen Einfluss auf den Verlauf der Tumorerkrankung, Metastasierung und die Prognose hat. Trotz umfangreicher Untersuchungen wurden die Mechanismen dieser Tumor-Tumorstroma Interaktion noch nicht vollständig geklärt. Eine Genexpressionsanalyse von Kolon-Karzinom-Gewebe und gesundem Gewebe, welches mithilfe von lasergestützter Mikrodissektion in normales Stroma und Tumorstroma getrennt wurde, identifizierte Wnt2 als eines der am meist induzierten Gene im Tumorstroma. Aberrante Wnt-Signaltransduktion in Epithelzellen ist ein frühes Ereignis der Kolon-Karzinom-Entwicklung, jedoch wurde die Auswirkung von stromalem Wnt2 auf den Tumor Verlauf noch nicht untersucht. Wir konnten zeigen, dass Wnt2 spezifisch in Kolon-Karzinom-assoziierten Fibroblasten (CAFs) exprimiert wird und nicht in Fibroblasten eines gesunden Kolons (NCFs). Weiters fanden wir, dass Wnt2 exprimierende Fibroblasten, wie Wnt2 über-exprimierende Fibroblasten und CAFs, einen Wnt/β-catenin Signaltransduktions-Reporter in Kolon-Fibroblasten aktivieren, aber nicht in Haut Fibroblasten-Reporter-Zellen. Ein siRNA mediierter Knock-down von Wnt2 reduzierte die Migration und Invasion von CAFs signifikant. RT-qPCR Analyse Wnt2 behandelter Fibroblasten zeigte, dass diese mehr „smooth-muscle cell-myofibroblast marker“ exprimieren als Kontroll-Fibroblasten. Die Expression des Myofibroblasten Markers Transgelin wurde durch zeitgleiche Behandlung mit Wnt2 und TGF-β drastisch induziert. Ko-Kultivierung von Wnt2 knock-down CAFs mit DLD1 Kolon-Tumorzellen, in einem organotypischem Assay, zeigte reduzierte Invasions-Fähigkeit der Tumorzellen im Vergleich zu Ko-Kulturen mit Kontroll-Fibroblasten. Ein Xenograft Tumormodell mit Wnt2 exprimierenden HT29 und HCT116 Tumorzellen führte zu einer Zunahme des Tumorwachstums im Vegleich zu Kontroll-Tumorzellen. Zusammenfassend konnten wir Wnt2 als neuen Tumorstroma Marker identifizieren, der Kolon-Fibroblasten-Invasion über kanonische Wnt-Signaltransduktion induziert und dadurch tumorprogressiv wirkt.

Table of contents

Introduction

The Wnt signaling pathway

Wnt ligands

The first member of the Wnt pathway was discovered in 1973. A screen of an ethyl methanesulphonate mutagenized *Drosophila* population revealed a phenotype with loss of wings and halteres and impaired segmentation of the epidermis. This condition was regulated by a single recessive gene that was then called *wingless* [1, 2]. In 1982 Nusse et al identified a preferential integration site of the Mouse Mammary Tumor Virus in virally induced breast cancer, which they originally named *int-1* [3, 4]. Further investigations could show that the *Drosophila* homolog of *int-1* (D*int-1*) was identical to *wingless* [5]. For a new nomenclature *wingless* and *int-1* were combined to *wnt1* (wingless-type MMTV integration site family, member 1).

In 1991 Wnt5a was discovered in *Xenopus laevis* [6]. Injection of Wnt5a in *Xenopus* embryos resulted in loss of ectopic axis and perturbation of cellular movements in contrast to injection of Wnt1, which induced a secondary embryonic axis [7]. This finding indicated that Wnt5a signaling is different from Wnt1 [8]. In the next years Wnt5a was recognized as one of the major ligands responsible for non-canonical Wnt signaling and more Wnt ligands were discovered.

To date 19 Wnt ligands were identified in mammalian cells. They comprise a large family of secreted hydrophobic ligands with a highly conserved distribution of cysteins [9, 10]. Wnts can be clustered to subgroups that share higher sequence similarity (58-83 %) compared to Wnt ligands overall sequence identity (~35 %) [11]. Although several Wnts are localized in close proximity on the same chromosome [11, 12] members of the same subgroup are spread across the genome, indicating that they were developed through genome-duplication events or gene-translocation [11]. Wnts comprise an evolutionary conserved family of proteins that is demonstrated by 98 % sequence identity between human and mouse Wnt1 and 42 % between human and Drosophila Wnt1/Wg [11].

Post-translational modifications are the reason for the insolubility of Wnt proteins in aqueous solutions [10, 13]. Fully functional, purified Wnt3a and Wnt5a from conditioned medium were reported [14-18], though Wnt1, Wnt2b, Wnt7a and Wnt11 have been reported to be functional at least in conditioned medium [19-23]. Experiments with different Wnt proteins revealed that they enter the endoplasmic reticulum (ER) and are

glycosylated at residues that differ from Wnt to Wnt protein [24]. It could be shown that Wnt3a and Wnt5a are further palmitoylated at conserved cysteine residues (Cys77 and Cys104 for the latter) by ER-membrane bound O-acyl transferases (Porcupines) (**Figure 1**) [15, 18, 25, 26]. This palmitoylation has no effect on secretion but it is necessary for the interaction between Wnt3a and its receptors frizzled 8 (Fzd8) and low-density lipoprotein receptor-related protein 6 (LRP6) [18]. Mutation of the palmitic residue at Ser209 resulted in Wnt3a accumulation in the ER with impaired Wnt secretion [27]. Though, Wnt3a with mutated palmitic residue Ser77 was normally secreted, but could not bind its receptor. Furthermore glycosylation of Wnt3a was necessary for subsequent palmitoylation, but palmitoylation was not required for glycosylation [28]. This indicates that glycosylation could be necessary for proper protein folding that is needed for subsequent palmitoylation or secretion [10].

A highly conserved multiple-pass transmembrane protein called Wntless (Wls or Evenness interrupted, Evi; Sprinter; Mig-14; or Gpr177) was shown to be involved in Wnt secretion, since Wls mutants show a lack of secreted Wnt proteins [29-31]. Wls is localized to the cell membrane, endocytic compartments and Golgi apparatus, where it mediates membrane protein trafficking between endosomes and the Golgi [32, 33]. It was postulated that Wnts are modified in the ER, trafficked by Wls from the Golgi to the cell membrane and that Wls is internalized via endocytosis and brought back to the Golgi by a retromer complex (**Figure 1**) [32, 34, 35]. It could be shown that glycosylation of Wnt proteins is not needed for Wls mediated secretion [29]. After secretion Wnt proteins bind tightly to the cell membrane via interaction with heparan sulfate proteoglycans (HSPGs) [36, 37]. HSPGs modulate Wnt protein localization on the cell membrane and promote signal transduction [37, 38]. Due to Wnt posttranslational modifications they are hydrophic and stick to the cell membrane [39]. However, they can activate target gene transcription over 20 cell diameters from the secreting cells possibly via forming multimeric complexes to hide their hydrophobic residues inside a “Wnt micelle” [40] or via binding to lipoprotein particles thereby forming “argosomes” (**Figure 1**) [41, 42].

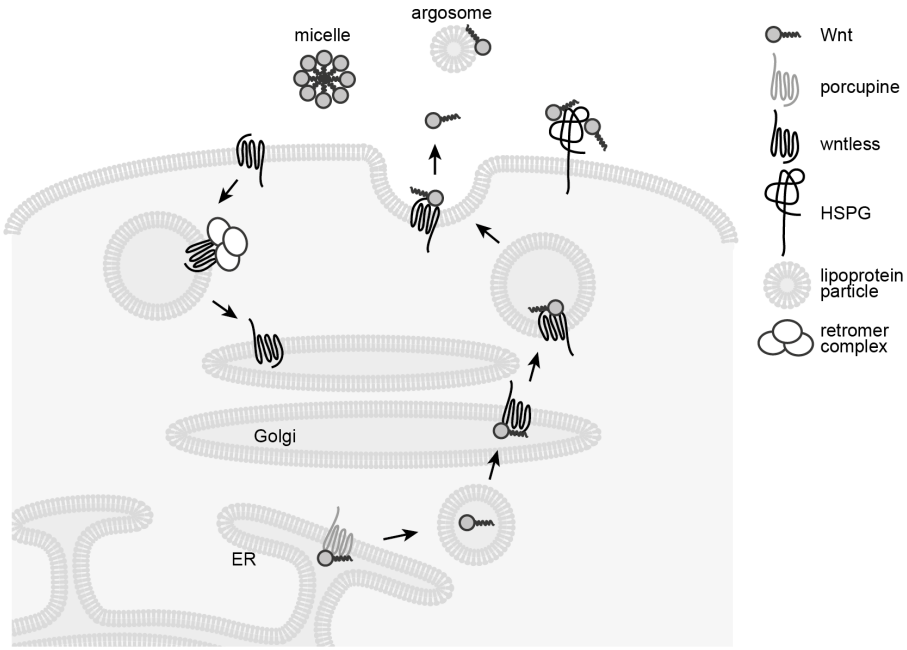

Figure 1 Wnt ligand secretion
Wnt ligands are post-translationally modified (glycosylation, palmitoylation) by porcupine in the ER. Then they are shuttled to the Golgi Apparatus, where Wntless mediates Wnt trafficking to the cell membrane. After release Wnt ligands can stick to HSPGs and remain bound to the cell membrane or they contribute to long distance signaling via aggregation to micelles or via binding to lipoprotein particles. Illustration inspired by [43].

Wnt signal transduction is mediated through transmembrane receptors. It could be shown that the primary receptors for Wnt signaling are the seven-pass transmembrane proteins Fzd [44]. In mammals 10 Fzd members are reported that are highly conserved [45]. These receptors harbor a N-terminal cysteine-rich domain (CRD) and Wnt proteins bind directly to it [44, 46, 47]. Furthermore the presence of the single-pass transmembrane proteins called LRP5/6 is necessary for canonical Wnt signaling (**Figure 2**) [48, 49], whereas non-canonical Wnt5a can also interact with the receptor tyrosine kinase Ror1/2 [50]. A comprehensive explanation of Wnt binding and downstream signaling events will be discussed in detail below.

Several Wnt antagonists could be identified like secreted Frizzled-related proteins (sFRPs). They share 30-50 % sequence similarity in their cysteine-rich domain (CRD) with other Fzd receptors [51]. sFRPs define boundaries in the developing organism in order to limit the range of Wnt proteins [52]. Furthermore expression of sFRPs is reduced in carcinomas indicating their important function in controlling Wnt signaling activity [53, 54]. sFRPs bind directly to Wnts thereby inhibiting their function to activate Wnt signaling (**Figure 2**) [55-57]. Different studies demonstrated the importance of either the

CRD alone [56] or the netrin-related (NTR) motif alone [58] or the CRD and NTR motif in combination [59] in activate canonical signaling via inhibition of the non-canonical pathway [60]. These controversial results could indicate that sFRPs harbor multiple Wnt binding sites or that sFRP/Wnt pairs interact via different domains [61]. It could be shown that only sFRP1 and 2 could abolish Wnt3a mediated signaling in L cells and that not all sFRPs could bind the same Wnt proteins [62], thereby favoring the latter possibility of distinct sFRP/Wnt pairs. Another potential mechanism of Wnt pathway inhibition could be that sFRPs and Fzd CRDs form complexes thereby rendering Fzd receptors inoperable [46, 63, 64].

Another antagonizing ligand is Dickkopf (Dkk). Like Wnts and sFRP also Dkk proteins harbor CRD [65]. In contrast to sFRPs that directly bind to Wnts, Dkk-1 interacts with LRP5/6 thereby inhibiting its activation by a Wnt ligand [66, 67]. Dkk-1 links LRP6 to another single-pass transmembrane protein called Kremen1 that induces clathrin mediated endocytosis of LRP6 (**Figure 2**) [68-70]. This internalization leads to decreased receptor distribution on the cell membrane followed by abolished canonical Wnt signaling [71].

Wnt-inhibitory factor 1 (WIF1) was shown to bind directly to Wnt ligands, thereby inhibiting its interaction with Fzd receptors (**Figure 2**) [72]. Similar to sFRPs WIF1 binds Wnt proteins that activate both pathways [73].

A type 1 transmembrane protein called TIKI was discovered in the Spemann-Mangold organizer of gastrulating Xenopus embryos [74]. Its over-expression resulted in reduced Wnt signaling activity. TIKI cleaved 8 amino acids from the N-terminus of mature human Wnt3a protein, resulting in the formation of large, soluble oligomeric complexes due to disulfide bonds with other Wnts (**Figure 2**) [74].

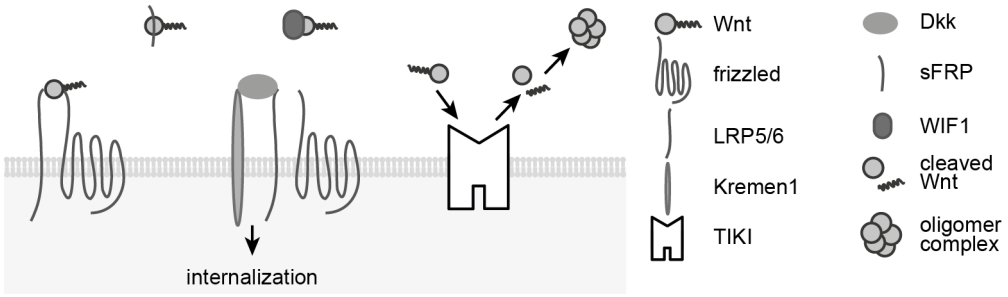

Figure 2 Wnt binding factors
Wnt ligands can bind to the CRD of frizzled family members and LRP5/6. The antagonizing Dkk ligand binds to LRP6 thereby linking it to Kremen1. The transmembrane protein TIKI cleaves 8 amino acids of the N-terminus of Wnt ligands, which leads to the formation of large oligomere complexes rendering Wnt ligands inactive. Wnts can also be bound by sFRP and WIF1 resulting in abrogated Wnt signaling.

Canonical Wnt signaling pathway

Researchers mainly focused on dissecting the canonical Wnt signaling pathway. This strong bias can partly be explained by a methodological imbalance between tools for analyzing canonical and non-canonical pathway components [75]. For analyzing the canonical pathway there are for instance β-catenin responsive TOPFlash reporters [76] and methods for β-catenin stability and nuclear translocation available and direct target genes are known [77]. Methods for dissecting non-canonical pathways often lack robust and simplistic assays. The assays used are mostly technically difficult, confusing, confounding and/or show modest fold changes of activation [77]. Development of methods and assays will improve with a better understanding of biological processes that are involved in non-canonical Wnt signaling. This in turn explains the development of excellent tools for analyzing canonical Wnt signaling components, since Wnt/β-catenin signaling was recognized as a main pathway involved in stem cell maintenance [78, 79], cancer development, progression and metastasis [13, 80] and extensive studies are therefore still going on.

In the absence of a Wnt ligand a multiprotein destruction complex tightly regulates the stability of β-catenin (**Figure 3A**). This complex consists of the two tumor suppressor proteins axis inhibiting protein 1 (Axin1) and adenomatous polyposis coli (APC) [81], the Ser/Thr kinases casein kinase1 (CK1) [82] and GSK-3 [81, 83], protein phosphatase 2A (PP2A) [84, 85] and the E3-ubiquitin ligase β-TrCP [86]. The destruction complex binds to β-catenin, which is initially phosphorylated at Ser45 by CK1 [87, 88]. Subsequently, GSK-3β phosphorylates Thr41 that primes GSK-3β mediated phosphorylation of Ser37

and Ser33 [88-91]. These successive phosphorylations of highly conserved Ser/Thr residues generate a β-TrCP binding site [92, 93]. β-TrCP interacts with Skp1/Cullin machinery to attach ubiquitin to β-catenin [94-98]. It is then presented to the proteasome and degraded (**Figure 3A**) [92, 99].

The key component of the canonical Wnt signaling pathway is the protein β-catenin. It was first identified as part of adherens junctions, where it binds E-cadherin and α-catenin [100]. 20 years ago, β-catenin was found to interact with APC [101] and further studies revealed its role as the major effector of canonical Wnt signaling [102-105].

The scaffold of the destruction complex is Axin. It interacts with all other components directly via its CK1, GSK-3, PP2A, APC and β-catenin binding sites [84, 88, 106-112]. Binding of a kinase and β-catenin to Axin brings both proteins in close proximity, thereby enhancing the effectiveness of the kinase to phosphorylate its substrate [83, 113, 114]. In vertebrates two Axin genes were reported, Axin1 [115] and Axin2/Conductin [110, 116]. Both isoforms are interchangeable for β-catenin destruction, however they differ in their transcriptional regulation. Axin1 is widely expressed in contrast to Axin2/Conduction that is a target gene of canonical Wnt signaling and therefore functions in a negative feedback loop [117-119].

Although APC has an essential role in destructing β-catenin, since mutated APC is involved in the accumulation of β-catenin in familial and sporadic colon cancers [102, 120-123], its function remains widely elusive. Two isoforms are known, APC and APC2 [124]. They have central β-catenin and Axin binding regions, furthermore they contain a N-terminal situated dimerization [125] and armadillo repeat domain [126]. Human APC contains four 15-mer and seven 20-mer repeats for β-catenin binding [127]. In between the 20-mer repeats Axin-binding sequences are present [110, 112]. It was shown that Axin and APC could bind at the same region of β-catenin indicating that APC could stabilize the Axin-β-catenin complex [114]. However, if this binding of APC, Axin and β-catenin has an impact on β-catenin phosphorylation is not clarified so far [128, 129]. There is evidence that phosphorylation of a 20-mer repeat of APC enhances its binding to a part of β-catenin that overlaps the Axin binding site [86, 102, 114, 130, 131] leading to higher binding affinity compared to Axin [114, 132, 133]. This could enable the displacement of β-catenin after phosphorylation from Axin and freeing Axin to interact with another β-catenin molecule [86, 132]. PP2A was shown to dephosphorylate APC leading to disengaged phosphorylated β-catenin in order to start a new cycle [106].

However, phosphorylation of APC must occur after β-catenin phosphorylation otherwise it would prevent Axin from binding to β-catenin. It seems difficult to orchestrate these phosphorylation events, since Axin and APC bear unstructured and flexible domains and random collisions could not produce a strict order of interaction [86]. Furthermore, the role of PP2A in this model could not be verified, since PP1, sharing the same catalytic domain as PP2A, did not dephosphorylate APC that was bound to β-catenin [114]. Also, there is no evidence that β-catenin has to dissociate from the destruction complex for degradation [94, 97, 134-136].

The protein GSK-3 is expressed as two isoforms, GSK-3α and GSK-3β. In principal the only difference between these distinct proteins is the absence of a glycine-rich amino terminus in GSK-3β [137]. Both proteins are thought to function redundantly in the destruction of β-catenin [138], although isoform specific functions were reported in other pathways [139-141].

A number of CK1 family members are known (α, β, γ1, γ2, γ3, δ, ε) [82] from which CK1α, δ and ε were found to phosphorylate β-catenin [87]. However, there is evidence that only CK1α is the β-catenin kinase *in vivo* [82, 88]. CK1γ harbors a C-terminal palmitoylation site that anchors CK1γ to the membrane. Furthermore this palmitoylation site is required for interaction with LRP6 during pathway activation [142].

Wnt signal transduction is mediated through binding of a Wnt ligand to Fzd/LRP co-receptor complex (**Figure 3B**) [44, 46-49]. It had been proposed that Wnts bind to Fzd/LRP5/6 and form a trimeric receptor complex [49]. However, this finding could not be observed in *Drosophila* [143]. Upon Wnt binding to Fzd/LRP5/6 Dishevelled (Dsh, Dvl in vertebrates) binds to Fzd's C-terminal cytoplasmic Lys-Thr-X-X-X-Trp motif [144] and becomes phosphorylated [145]. It could be demonstrated that binding of Dsh/Dvl to Fzd triggers co-clustering of Fzd and LRP6 to form signalosomes [146, 147]. How the Wnt signal is forwarded from the receptor to Dsh/Dvl is not clarified so far. There is evidence that G-protein signaling is involved, since Fzd shares the same serpentine topology as all G-protein-coupled receptors [148, 149]. Though it could be shown that Wnt signaling induces G-protein activation [150, 151] the mechanism underlying the coupling of Fzd and G-proteins remain unclear.

The cytoplasmic tail of LRP, containing Pro-Pro-Pro-(Ser/Trp)-Pro (PPP(S/T)P) motifs becomes phosphorylated by GSK-3 and the membrane bound CK1γ (**Figure 3B**) [49, 142, 152]. This phosphorylation results in the heterodimerization of Axin and LRP6 via a DIX (Dishevelled-Axin) domain in both proteins [153-155], leading to disintegration of the destruction complex and promoting β-catenin stabilization (**Figure 3B**) [156, 157]. However, Beagle et al demonstrated that PPP(S/T)P phosphorylation of LRP6 is not required to activate canonical Wnt signaling [158]. The complex formation of Fzd/Dsh/Dvl/LRP5/6, the recruitment and phosphorylation of Dsh/Dvl and the inhibition of the destruction complex are not elucidated on a molecular level so far [13, 75]. It was proposed that not the inhibition of the destruction complex, rather the limiting number of Axin proteins within the cell [159] that are relocated to the membrane upon Wnt ligand binding rapidly interrupts the degradation of β-catenin [160, 161]. Another protein that is required for the elevation of β-catenin in the cytoplasm is PP2A [162] that binds to Axin [84] and might dephosphorylate GSK-3 substrates [13]. How PP2A is regulated is not known so far [13].

Binding of a Wnt ligand to its receptor ultimately leads to the inhibition of β-catenin phosphorylation and subsequent degradation, thereby promoting the accumulation of β-catenin in the cytoplasm and nucleus [163-165]. The mechanisms leading to β-catenin translocation are not clarified so far. It could be shown that β-catenin neither possesses a nuclear localization or export signal required for exportin/importin transportation pathway, nor does it require Ran-GTPase [166-168]. Recent studies revealed the armadillo domain of β-catenin interacts with nucleoporins (Nup62, Nup98, Nup153 and Nup385) [169] and that FoxM1 binding to β-catenin enhanced its nuclear localization [170]. Deletion of nucleoporins and FoxM1 resulted in abrogated β-catenin translocation [169, 170].

In the nucleus, β-catenin forms a complex with members of the T cell factor/lymphoid enhancer factor (TCF/LEF) transcription factor family (**Figure 3B**) [103, 104, 171]. The vertebrate genome harbors genes for four different TCF/LEF DNA-binding proteins (TCF1, LEF, TCF3 and TCF4) [172]. They are highly similar on a biochemical basis, however they differ dramatically in their embryonic and adult expression, explaining the extensive redundancy that was found in double knockout experiments [123, 173]. TCF3 and TCF4 often function to reduce expression of transcriptional targets, whereas TCF1 and LEF1 are more likely transcriptional enhancers [174-176]. In the absence of Wnt

signaling TCF factors bind their recognition motif (AGATCAAAGG) in the minor groove of the DNA helix, thereby inducing a bend of 90 ° [171]. TCFs act as transcriptional repressors when they form a complex with Groucho proteins (**Figure 3A**) [177, 178] that interact with histone deacetylases to compact DNA and hinder transcriptional activation [179]. Upon canonical Wnt signaling activation and following translocation of β-catenin to the nucleus β-catenin displaces groucho from TCF/LEF [180]. Binding of β-catenin to TCF affects the local chromatin by recruiting histone acetyltransferases (CBP/p300 [181, 182], Brg-1 [183]) and Cdc37 (**Figure 3B**) that is a component of the PAF complex, which interacts with RNA polymerase II to induce transcription initiation and elongation in yeast [184]. Furthermore Legless (Lgs)/Bcl9 and pygopus interact with the TCF/β-catenin complex (**Figure 3B**) [185-187], where Bcl9 bridges Pygopus to β-catenin's N-terminus [185]. This complex is thought to be involved in nuclear import and retention of β-catenin in the nucleus [188] and in the ability of β-catenin to activate target gene transcription [189]. Mutations in either of theses genes resulted in a *wingless*-like phenotype indicating that Wnt signaling events are dependent on Bcl9 and Pygopus in *Drosophila* [187]. Furthermore in cell culture experiments it could be shown that both genes promote canonical Wnt signaling in mammalian cells [187].

More than 100 target genes of canonical Wnt signaling have been identified and many of them are associated with malignant transformation and cancer. However the signaling output seems to be cell-type specific, since loss of a single Wnt gene can trigger phenotypes varying from embryonic lethality to kidney and limb defects [13]. Loss of cells or tissue in Wnt mutants is often interpreted as a dysfunction in cell fate specification, though failing expansion of progenitor cells could also be an issue in some cases. Regulation of cell proliferation may be a function of canonical Wnt signaling during development, since genes like c-Myc [190] and cyclin D1 [191, 192] are direct targets of Wnt signaling in colon cancer cells. Interestingly, activated canonical Wnt signaling was implicated in telomerase regulation in stem cells and cancer cells [193]. β-catenin binds to the Tert promoter (a telomerase subunit) in a mouse intestinal tumor model and in human carcinomas and regulates Tert expression via interaction with Klf4 that is a core component of the pluripotency transcriptional network [193]. It is unclear if there are universal target genes, but there are few candidates, which are Wnt pathway components like Axin2/conduction [117, 194] and Fzds [195-198]. Upon Wnt target gene

transcription Axin2 is expressed resulting in reestablishment of the destruction complex and subsequent β-catenin degradation [110]. This was observed in normal cells, however in colorectal carcinomas with mutations in APC or CTNNB1 (β-catenin gene) Axin2 was found to act as a tumor promoter via inducing Snail1 dependent epithelial-to-mesenchymal transition (EMT) at the invasive front [199]. In colon cancer cells with loss of APC LEF1 is up-regulated, leading to increased mis-regulation of target gene transcription [200]. However, this mutation also increased the expression of a dominant negative splice variant of TCF1 that lacks an N-terminal β-catenin binding site, thereby attenuating the dysfunction that occurs from loss of APC [201].

Negative regulators of β-catenin mediated target gene transcription are for example Chibby (nuclear antagonist binds to C-terminal end of β-catenin [202]) and ICAT (blocks binding of β-catenin and TCF leading to the dissociation of the β-catenin/TCF/LEF/CBP/p300 complex [203-205]). An important role in the regulation of Wnt target gene expression plays LEF/TCF's ability to bind to DNA. The mitogen-activated protein kinase-related protein kinase NLK/Nemo phosphorylates TCF in order to diminish the affinity of the β-catenin/TCF/LEF complex to bind DNA [206, 207].

Interestingly nuclear import/export sequences could be found in cytoplasmic Wnt regulators like APC and Axin [208, 209]. It was found that APC promotes the export of β-catenin [210], thereby directly counteracting β-catenin activation at Wnt target genes that is mediated by GSK-3 and CK1δ phosphorylation of APC to interrupt β-catenin interaction with LEF1 [114, 211]. This periodic turnover of co-repressors and co-activators is thought to allow active genes to rapidly switch to a repressed state [212], like in other pathways with rapidly induced genes that are regulated by nuclear receptors and NF-κB [212]. A scenario was hypothesized in which a subset of destruction complex proteins enter the nucleus as part of a larger complex in order to mediate β-catenin nuclear export. This complex could comprise Axin, APC, Lgs/Bcl-9 and pygopus [188]. Alternatively proteins of the destruction complex independently shuttle to the nucleus, where they then reassemble at Wnt target genes [213]. This could be in part confirmed, since other Wnt regulators are also shuttling in and out of the nucleus (Dsh [214], ICAT [203], CK1, CK2 and GSK-3β [215]) [213].

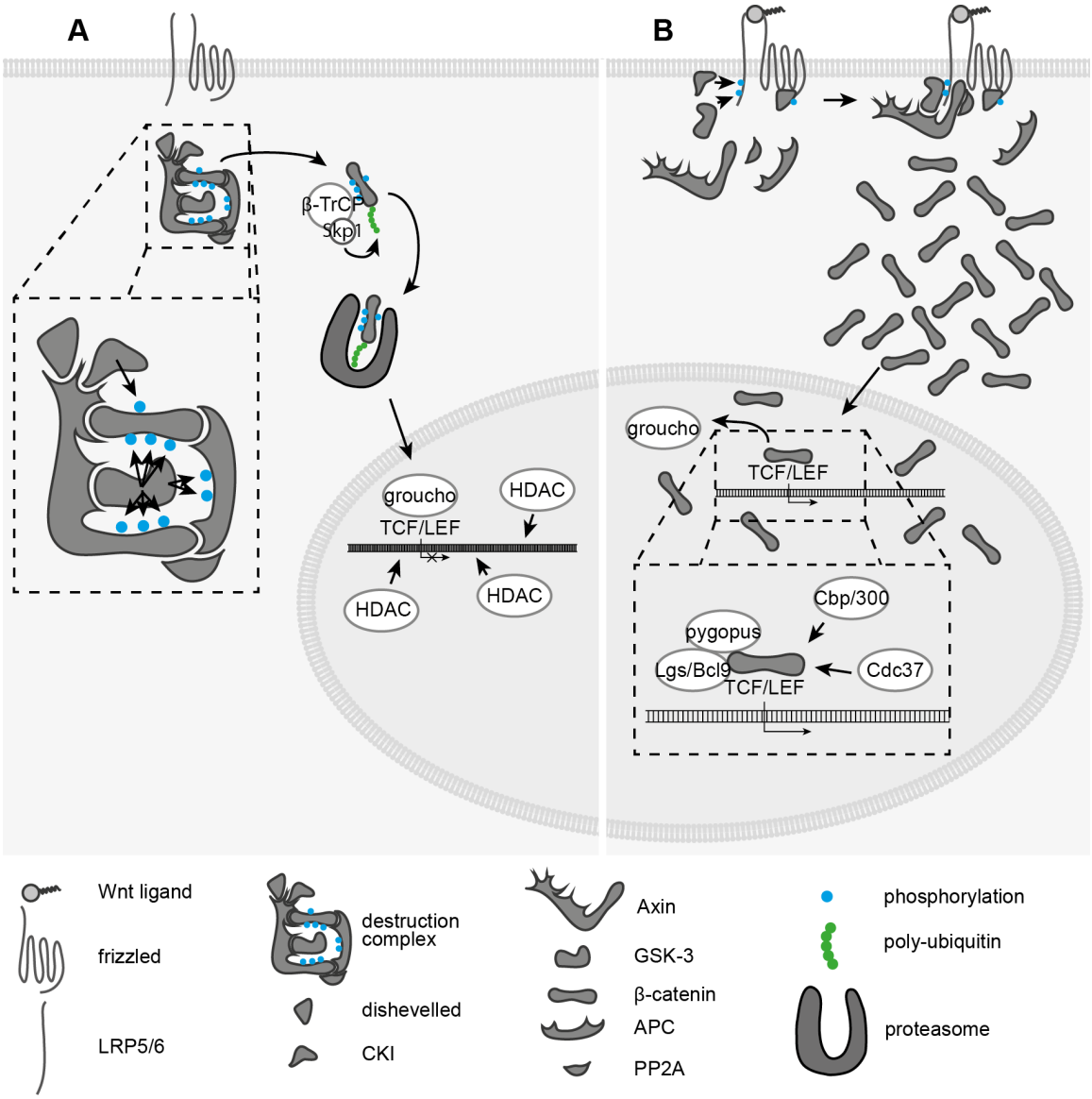

Figure 3 Scheme of canonical Wnt signaling

A In the absence of a Wnt ligand the destruction complex is assembled, CK1 initially phosphorylates β-catenin at Ser45, followed by GSK-3 mediated phosphorylation of Thr41 that primes phosphorylation of Ser37 and Ser33. These consecutive phosphorylation events generate a β-TrCP binding site, which interacts with Skp1/Cullin machinery in order to attach ubiquitin to β-catenin. Poly-ubiquitinylated β-catenin is then degraded by the proteasome. Target gene transcription is repressed by binding of groucho to TCF/LEF transcription factors and by HDAC that compact the DNA in order to hinder transcriptional activation. B Upon binding of a Wnt ligand to Fzd/LRP5/6 co-receptor complex Dsh/Dvl is recruited to Fzd and becomes phosphorylated. The cytoplasmic tail of LRP becomes phosphorylated by GSK-3 and CK1γ leading to the recruitment of Axin and PP2A to LRP and the disintegration of the destruction complex. Consequently, β-catenin stabilizes and accumulates in the cytoplasm and translocates to the nucleus, where it forms a complex with TCF/LEF transcription factors, thereby replacing groucho. Cdc37, histone acetyltransferases (Cbp/300) are recruited resulting in an open chromatin structure and transcription initiation. Lgs/Bcl9 and pygopus are thought to be involved in the nuclear import and retention of β-catenin and are necessary to activate target gene transcription. Scheme of destruction complex was inspired by [216].

In response to Wnt3a mediated canonical Wnt signaling activation LRP6 is phosphorylated and was shown to form intracellular aggregates that co-localize with the endocytic marker caveolin (**Figure 4**) [146]. Caveolin and LRP6 were found in lipid rafts of the cell membrane, where cholesterol and sphingolipids are enriched [217-219]. In HEK293 and HeLa S3 cells LRP6 bound to caveolin after Wnt3a mediated phosphorylation and was then internalized [70, 219, 220]. Inhibition of endocytosis resulted in suppressed internalization of LRP6 and abolished β-catenin stabilization [221, 222]. It was proposed that upon binding of Wnt3a to Fzd/LRP6 LRP6 is phosphorylated and Axin is recruited. A vesicle that contains a complex of LRP6, Axin, caveolin and other proteins is formed and delivered to the early endosome by Rab5 thereby altering the complex resulting in inactivated GSK-3 [223] and β-catenin dissociation from Axin (**Figure 4**) [10, 219]. Furthermore inhibition of clathrin-mediated endocytosis also resulted in impaired canonical Wnt signaling activation in mouse fibroblasts [224], indicating that receptor internalization is either mediated by caveolin or clathrin. The clathrin adaptor β-arrestin was found to interact with Dvl and thereby synergistically activating Wnt target gene transcription [225, 226]. This data indicate that receptor internalization plays critical roles in activation and enhancement of canonical Wnt signaling.

Taelman et al demonstrated that activation of canonical Wnt signaling resulted in the sequestration of GSK-3 from the cytosol in multivesicular bodies (MVBs) (**Figure 4**) [227]. They could show that GSK-3 co-localized with acidic vesicles that were positive for endosomal markers and that its activity in the cytosol decreased. Depletion of two proteins, which are necessary for MVB formation, resulted in blocked β-catenin accumulation. They conclude that Wnt stimulation leads to binding of GSK-3 to phosphorylated LRP6 (and possibly other substrates like Axin, APC, β-catenin and Dvl) with subsequent sequestration from the cytosol in MVBs in order to effectively inhibit GSK-3 activity (**Figure 4**) [227].

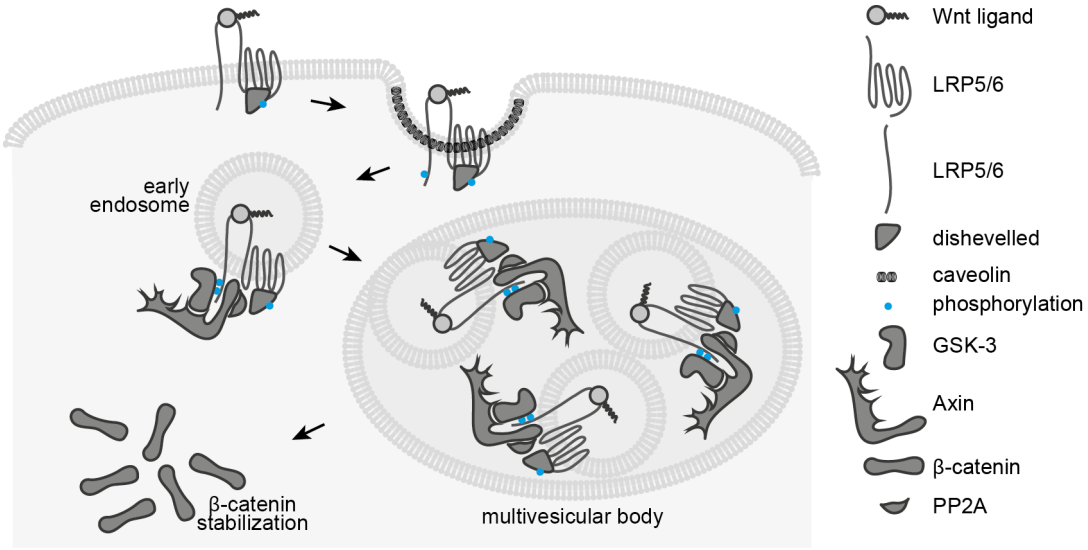

Figure 4 Receptor internalization upon Wnt ligand binding
When a Wnt ligand binds to the Fzd/LRP co-receptor complex Dsh/Dvl is recruited and phosphorylated. Consequently LRP6 is phosphorylated and is internalized via clathrin or caveolin mediated endocytosis. The Axin/GSK3/PP2A complex binds to LRP6, which is then sequestrated to MVB in order to stabilize β-catenin in the cytosol. Illustration was inspired by [227].

Not only Wnt ligands can stimulate the canonical Wnt signaling pathway, but also growth factors, like insulin [228], insulin-like growth factor-1 [228] and PDGF [229, 230], can activate β-catenin/TCF/LEF target gene transcription. Furthermore, Inoki et al demonstrated that besides stabilization of β-catenin and target gene transcription canonical Wnt signaling also activates the mTOR pathway in a GSK-3 dependent manner [231]. For detailed reading please refer to [228-231].

Besides Wnt proteins, other ligands show the ability to interact with Fzd and LRP receptors. Norrin is a secreted protein that specifically interacts with Fzd4/LRP5/6, thereby activating canonical Wnt signaling [232]. It is not related with Wnt ligands and plays a central role in eye and ear vascular development. Another group of ligands that interact with Fzd receptors are R-spondins (Rspo), which were discovered in a screening for canonical Wnt signaling activators in *Xenopus* [233]. Rspo harbor cysteine-rich furin-like (CR) domains, thrombospondin type I repeats (TSR) and basic amino acid-rich (BR) domains that are responsible for canonical Wnt signaling activation, since loss of the CR domain results in abolished activation [234] and loss of TSR and BR domains leads to decreased activation [235]. Rspo are also capable of potentiating Wnt ligand mediated pathway activation, although the molecular mechanism for this synergistic effect remains controversial due to conflicting results [233, 235-238]. Various studies suggested that

Rspo1 either binds to LRP6 [236, 238], that it blocks Kremen proteins [237] or that it blocks DKK1 interaction with LRP6 [235]. Leucine-rich repeat containing G protein-coupled receptors 4 to 6 (LGR4-6) were found to be receptors of Rspo [239] [240]. Interestingly, in Wnt signaling dependent stem cell compartments like small intestine and hair follicles Rspo1 demonstrated mitogenic activity on LGR5 positive cells [241, 242]. LGR5 is a validated marker for stem cells in these compartments and is a target gene of canonical Wnt signaling that is required for the maintenance of stem cells [241-243]. It could be shown that LGR5 physically interacts with Fzd and LRP5/6 [239] and that loss-of LGR5 or Rspo1 results in demise of crypt organoids [239], which are dependent on active proliferating stem cells [242]. Furthermore it could be shown that LGR5 forms a complex with Fzd/LRP5/6 and that this complex is rapidly internalized [244]. These data indicate an important function of Rspo1/LGR5 induced canonical Wnt signaling in the colonic stem cell compartment [239] and that Rspo/LGR5/Wnt/Fzd/LRP5/6 complexes allow the enhancement of short-range Wnt signaling that is mediated from Paneth cells [245].

Non-canonical Wnt signaling pathways

During the last two decades different non-canonical Wnt pathways were discovered that are β-catenin/TCF/LEF transcription independent. They were categorized in several groups for clarity and simplicity, however, these pathways overlap or intersect one another and still new insights are gained [246]. The following chapter will mainly focus on Wnt/Rho and on Wnt/Ca^{2+} pathway as outlined in [246].

Wnt/Rho pathway

During xenopus gastrulation, convergent extension (CE) elongates the body axis via medio-lateral convergence and anterior-posterior extension of mesodermal tissue [247]. The main element is cytoskeletal reorganization that results in changes of cell shape (polarized cell protrusions) and migration in the dorsal marginal zone of the embryo [248]. It could be shown that Wnt11 and Fzd7 play major roles in these processes [249]. Upon Wnt ligand binding to Fzd, Dsh/Dvl is recruited to the plasma membrane (**Figure 5**) [250]. A yeast two-hybrid screen identified Daam1 (Dishevelled-associated activator of morphogenesis 1) as a novel binding partner of Dsh/Dvl that acts as a bridging factor

between Dsh/Dvl and Rho, where the C-terminus binds PDZ and DEP domains of Dsh/Dvl and its N-terminus interacts with Rho [251]. The small GTPases of the Rho family, like Rho, Rac and Cdc42, rotate between GTP-bound (active) and GDP-bound (inactive) conformations. Guanine nucleotide exchange factors (GEFs) and GTPase-activating proteins (GAPs) control Rho family members [248]. Daam1 mediates complex formation with Dsh/Dvl and is thought to interact with Rho GDP and Rho GEF to enhance Rho GTP formation [251]. At the cell periphery Cdc42 and Rac facilitate actin polymerization to form lamellipodia and filopodia, while Rho regulates contractile forces via the assembly of actin and myosin [252]. In areas undergoing CE, pull-down assays revealed activated Rho and Rac proteins that could be blocked by dominant negative Wnt11 or an extracellular fragment of Fzd7 or by inhibition of Dsh [251].

The Rho-associated protein kinase (Rock) binds the activated form of Rho resulting in abolished autoinhibitory interaction within Rock [253]. Rock then phosphorylates myosin regulatory light chain (MRLC) of myosin II at Ser19 in mammalian cells leading to a conformational change in myosin II from a folded to an extended state. This change results in F-actin bundling and stress fiber formation (**Figure 5**) [254].

Daam1 was also shown to directly interact with Profilin1, a conserved actin binding protein. This Dsh/Dvl/Daam1/Profilin1 complex localizes in stress fibers and can mediate cytoskeletal changes independently from Dsh/Dvl/Daam1/Rho/Rock signaling in xenopus blastopore closure (**Figure 5**) [255].

Dsh/Dvl can also form a complex with Rac via its DEP domain to activate c-Jun N-terminal kinase (JNK) in a Dsh/Dvl/Daam1/Rho-independent manner [256]. JNK family members (JNK1, JNK2 and JNK3) are mitogen-activated protein kinases (MAPK) that are activated via phosphorylation of their threonine and tyrosine residues in Thr-X-Tyr motifs [257] by Misshapen (Msn, a STE20 kinase) [258] and subsequently phosphorylate AP1 transcription factors (**Figure 5**). The dimeric AP1 transcription factor complex consists either of hetero- or homodimers of the Jun and Fos transcription factor family [259]. Another MAPK, namely p38, was also activated by Msn and acted redundantly with JNK in the Wnt/Rho pathway [260]. These data suggest that Dsh/Dvl can regulate Wnt/Rho pathway via Rho or Rac mediated signaling [248].

Furthermore, it could be shown that Rock and JNK synergistically regulate *Xenopus* CE and that Rock was not necessary for JNK activation [261]. However, this could be explained by the finding that the receptor tyrosine kinase Ror2 acts as a receptor for

Wnt5a and induces AP1 dependent transcription via JNK activation in a Wnt/Rac independent manner [262, 263].

Hakeda and Suzuki reported that loss of all three Rac isoforms (Rac1, Rac2, Mtl) had no effect on Wnt/Rho signaling [264]. However, a more recent study revealed that triple loss-of-function mutants displayed a mild phenotype that could be enhanced with a hypomorphic mutation of Cdc42 [265], indicating that Rac1, Rac2, Mtl and Cdc42 share functional redundancy [248]. Though dominant negative Cdc42 and Rac mutants do not result in the same phenotype and show therefore at least some specificity [266].

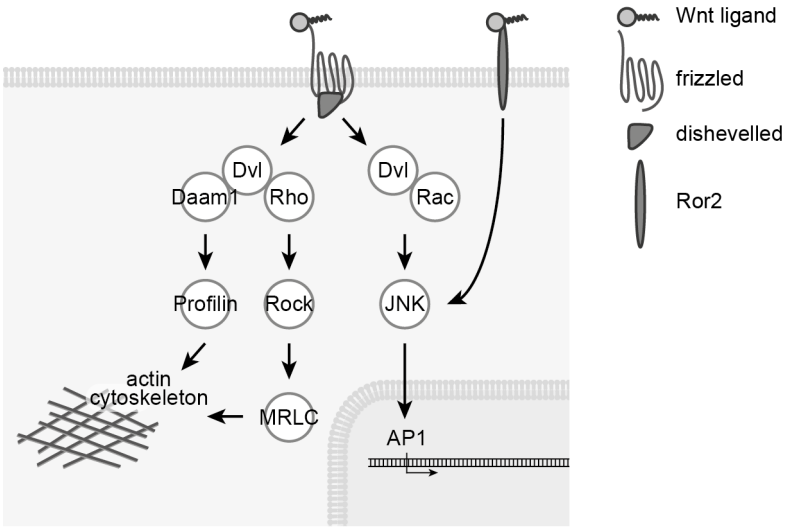

Figure 5 Wnt/Rho signaling pathway
Upon binding of a Wnt ligand to Fzd Dsh/Dvl is recruited to the plasma membrane. It is then bound by Daam1, which acts as a bridging factor between Dsh/Dvl and Rho. Rho is activated and bound by Rock that subsequently phosphorylates MRLC leading to actin cytoskeletal rearrangements. This is also achieved via Daam1, which directly interacts with Profilin1. Dsh/Dvl can also bind directly to Rac resulting in JNK activation and subsequent activation of AP1-depenendent target gene transcription.

Wnt/Ca^{2+} pathway

The primary Wnt ligand that was found to elevate intracellular Ca^{2+} ion concentrations in zebrafish embryos was Wnt5a [267]. It could be shown that Wnt5a interacts with Fzd2 in order to release intracellular Ca^{2+} ions [148]. Binding of Wnt5a to Fzd2 mediates G-protein dependent activation [268, 269] of phospholipase C (PLC) that generates inositol 1,4,5-triphosphate (IP_3) and 1,2-diacylglycerol (DAG) from membrane-bound phospholipid phophatidyl inositol 4,5-bisphosphate (**Figure 6**) [148]. IP_3 interacts with calcium channels that are present on the membrane of the ER in order to release Ca^{2+} ions

[270]. These Ca^{2+} ions in combination with cytoplasmic calmodulin enhanced the activity of calcium calmodulin-dependent protein kinase II (CAMKII) (**Figure 6**) as proven with an *in vitro* kinase assay and increased autophosphorylation of CAMKII [271]. Simultaneously, DAG and Ca^{2+} ions activate protein kinase C (PKC) that translocates to the cell membrane [270, 272]. CAMKII and PKC activate transcription factors like NF-κB and CREB (**Figure 6**) [270]. Furthermore Ca^{2+} ions can activate calcineurin, which dephosphorylates and thereby mediates the nuclear translocation of cytoplasmic NF-AT (nuclear factor associated with T cells) transcription factors (**Figure 6**) [269, 273, 274]. NF-AT dependent transcription can enhance the expression of genes in neurons, cardiac and skeletal muscle cells and pro-inflammatory genes in lymphocytes [275, 276].

Wnt5a/Fzd signaling can also activate heterotrimeric GTP-binding proteins that stimulate phosphodiesterase 6 (PDE6) activation leading to depletion of cyclic guanosine monophosphate (cGMP) [148, 277], which in turn inactivates the sensor protein kinase G (PKG) [246, 269]. This decline of PKG results in an increase of Ca^{2+} ions and enhanced NF-AT mediated target gene transcription (**Figure 6**) [269]. Ma et al could show that changes in Ca^{2+} ion levels can be measured before activity of PKG changes. The concomitant process of phosphatidyl-mediated signaling could explain this observation [268].

The role of Dsh/Dvl in regulating the Wnt/Ca^{2+} pathway is not known so far. It could be shown that in *Xenopus* a Dsh deletion construct that cannot induce canonical Wnt signaling (DshΔDIX) was shown to activate intracellular Ca^{2+} flux, PKC and CAMKII [278]. However, in mammalian cells Dvl3ΔDIX and Dvl3ΔC (lack of C-terminal His repeats) constructs resulted in abolished NF-AT target gene transcription and expression of Dvl1 and Dvl2 could not rescue non-canonical signaling in Dvl3 deficient cells [279].

Ishitani and coworkers could show that activation of TAK1, a member of mitogen-activated protein-kinase-kinase kinase (MAP3K), stimulates the MAP kinase-related protein NEMO-like kinase (NLK). This activation of NLK mediates down-regulation of β-catenin dependent target gene transcription [206]. In the presence of Ca^{2+} ions CAMKII binds TAK1 leading to its phosphorylation and activation [207], which in turn activates NLK, resulting in phosphorylation of TCF4 and LEF-1 [206]. Consequently, the β-catenin/TCF/LEF complex cannot bind to DNA anymore resulting in the inhibition of target gene transcription (**Figure 6**) [206]. These results indicate that Wnt/Ca^{2+} pathway antagonizes canonical Wnt signaling through Ca^{2+} ions and CAMKII activity via the

TAK1-NLK-MAPK cascade [207]. Furthermore canonical Wnt signaling in *Xenopus* is blocked by PKC via phosphorylation of Dsh [280, 281]. The Wnt/Ca^{2+} pathway inhibits canonical Wnt signaling via PKC-Dsh signaling upstream and Ca^{2+}/CAMKII TAK1-NLK-MAPK cascade downstream of β-catenin [207, 280].

Injection of human PKC-alpha in *Xenopus* embryos resulted in inhibition of CE movements that could be rescued by co-injection of a double negative XCdc42 mRNA indicating that Cdc42 acts downstream of PKC [282]. XWnt5a over-expression in xenopus embryonic cells resulted in decreased cell adhesion that could be reverted by co-injection with the double negative XCdc42 mRNA suggesting that Cdc42 acts downstream of Wnt5a induced Wnt/Ca^{2+} signaling thereby regulating cell adhesion and tissue separation during vertebrate gastrulation (**Figure 6**) [278, 282]. However, in mammalian cells Wnt5a stimulation induced a Yes/Cdc42/CK1alpha signaling cascade resulting in the formation of a cytoplasmic CK1alpha/NF-AT complex that antagonizes Wnt5a/Ca^{2+} dependent NF-AT target gene transcription [283].

Wnt5a can also interact with other receptors like the receptor tyrosine kinase Ror1/2 [50]. A Wnt5a/Ror complex activates Ca^{2+}/CAMKII signaling, thereby cleaving the cytoskeleton protein spectrin by the calcium-dependent non-lysosomal cysteine protease calpain (**Figure 6**) [284]. This cleavage promotes formation of an axonal cone that plays an important role in axonal path finding in the mammalian brain [13, 285]. In melanoma cells motility was induced via cleavage of the cytoskeleton protein filamin by calpain [286, 287], indicating that the Wnt/Ca^{2+} pathway plays a role in cancer.

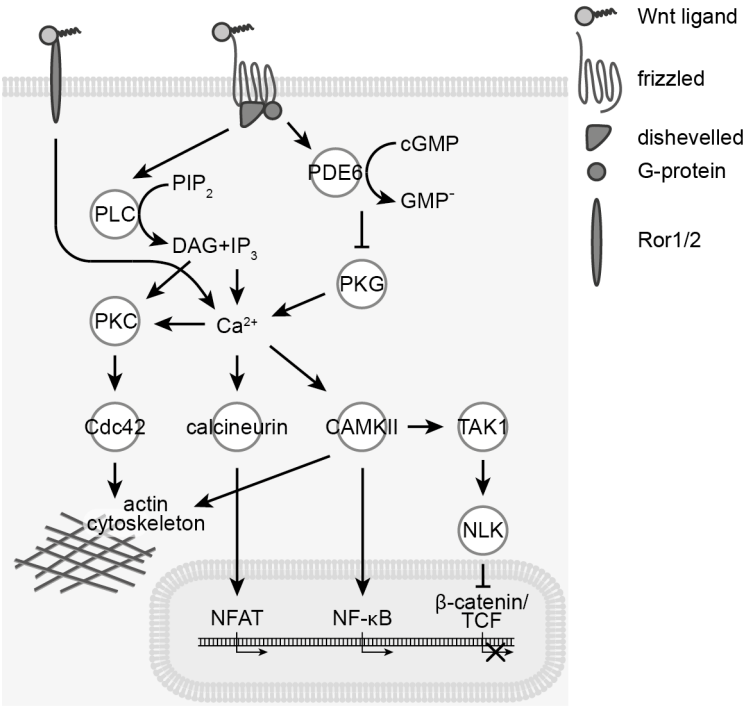

Figure 6 Wnt/Ca2+ signaling pathway
When Fzd is bound by a Wnt ligand Dsh/Dvl and G-proteins are recruited and PLC generates DAG+IP_3 from PIP_3. IP_3 then interacts with calcium channels of the ER to release Ca^{2+} ions. This elevation of ions activates calcineurin, which dephosphorylates NF-AT, thereby mediating its nuclear translocation and target gene transcription. Ca^{2+} ions and calmodulin increases the activity of CAMKII leading to NF-κB-dependent target gene transcription. Furthermore, DAG and Ca^{2+} ions activate PKC, leading to Cdc42 mediated changes of the cytoskeleton. Heterotrimeric G-proteins are also activated by binding of a Wnt ligand to Fzd, leading to PDE6 activation, which in turn depletes cGMP in the cytoplasm. This depletion results in inactivation of PKG, that stimulates the release of Ca^{2+} ions and NF-AT mediated target gene transcription. Interestingly, CAMKII can bind TAK1 leading to its activation that stimulates NLK, which in turn inhibits β-catenin/TCF mediated target gene transcription. It was also shown that Wnt could interact with Ror1/2 receptors, thereby activating Ca^{2+}/CaMKII signaling that results in the cleavage of cytoskeletal proteins.

In addition, it could be shown that Wnt5a binding to Fzd promotes the internalization of the receptor. As already mentioned upon ligand binding Dsh/Dvl is recruited to the cell membrane, where β-arrestin binds phosphorylated Dsh/Dvl and internalization is mediated via a clathrin mediated route [288]. It could further be proved that Dvl2 interacts with another clathrin binding protein (μ2-adaptin of adaptor protein 2) and that this interaction is necessary for Fzd internalization and activation of non-canonical Wnt signaling (**Figure 7**) [289]. In metastatic melanoma cells Wnt5a, Ror2 and syndecan 1 were thought to be internalized in a clathrin-dependent manner [290].

As previously mentioned, Rspo was shown to enhance canonical Wnt signaling. This might also be true for non-canonical Wnt signaling as one study reported on the interaction of Rspo with syndecan 4 (a HSPG) in order to cooperate with Wnt5a via syndecan 4 dependent Wnt5a/Fzd internalization (**Figure 7**) [291].

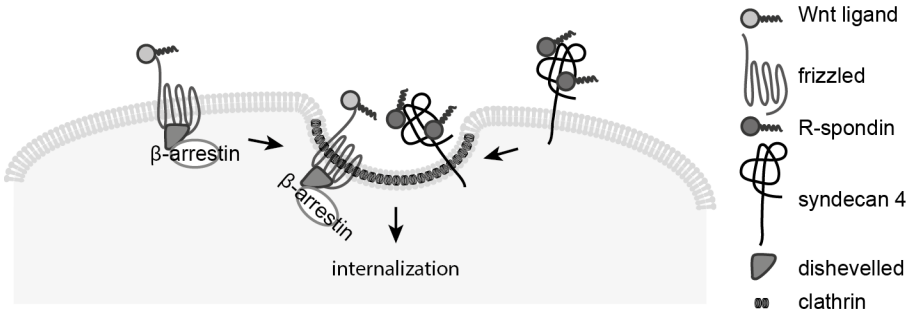

Figure 7 Receptor internalization upon activation of non-canonical Wnt signaling
Activated Fzd receptors are internalized, when β-arrestin binds Dsh/Dvl via a clathrin mediated route. Furthermore, Rspo bound syndecan 4 can also be internalized in order to cooperate with Wnt5a mediated signaling.

Distinguishing between canonical and non-canonical Wnt signaling

Studies revealed that canonical and non-canonical Wnt pathways could intersect one another. For example, Wu and co-workers found that the canonical Wnt3a ligand activated the non-canonical GTPase Rac1 via the G-protein/PI3K pathway. Rac1 then activates JNK, which in turn phosphorylates β-catenin at Ser191 and Ser605 thereby mediating its translocation to the nucleus [292].

But how do cells decide to proceed with canonical or non-canonical pathway upon Wnt ligand binding? A first assumption was that Dsh/Dvl is differentially phosphorylated depending on the Wnt/receptor complex that is activated [293]. However, Grumolato and co-workers found that GSK-3 phosphorylates Dsh/Dvl to similar extent after activation of canonical Wnt pathway by Wnt3a/Fzd/LRP5/6 or non-canonical pathway by Wnt5a/Fzd/Ror2 activation [294]. They could show that *in vitro* expression of a fusion receptor containing an extracellular Ror2 domain and an intracellular LRP6 domain resulted in activation of canonical Wnt signaling by Wnt5a. For the reverse experiment a fusion ligand of Wnt5a with a Dickkopf2's (DKK2) LRP6 binding domain was established, since Wnt5a cannot bind to LRP6 directly. It was demonstrated that Wnt5a/DKK2 could activate canonical Wnt signaling via interaction with the Fzd/LRP6 receptor complex [294]. Ser864 of Ror2 was further specified as a critical phosphorylation residue for non-canonical signaling activation that is phosphorylated by

GSK-3, analogous to GSK-3 mediated LRP6 priming phosphorylation after Wnt3a binding. The authors of this study propose that "canonical" and "non-canonical" Wnt ligands compete for Fzd binding at the cell surface in order to achieve reciprocal pathway inhibition [294]. Further studies could show that the canonical Wnt1 ligand could activate non-canonical signaling via PKC signaling [295] and that non-canonical Ryk receptor could be activated by Wnt3a [296]. Vice versa the non-canonical Wnt5a could induce axis duplication in *Xenopus laevis* in the presence of Fzd5 [297]. These findings allow the conclusion that the signaling output does not only depend on the Wnt itself, but more likely on a combination of Wnt ligand and receptor that is presented on the responder cell [270]. Furthermore binding of Wnt ligands to HSPGs and collagen triple-helix-repeat containing proteins are involved in the decision whether canonical or non-canonical Wnt signaling is activated [298, 299].

Characterization of Wnt2

In 1988 a methylation-free CpG island at chromosome 7q31 was cloned from a human lung cDNA library. The protein sequence possessed cysteine-rich domains, two potential glycosylation sites and showed high similarity with human and mouse int-1 [300]. The protein was then called int-1 related protein (IRP). It was only detected in culture medium after treatment with suramin, which is a chemical compound routinely used to prevent the binding of growth factors to cell surface receptors [301, 302], indicating that it is tightly bound to the cell membrane [303]. In the same year IRP expression was found to be elevated during cystic fibrosis [304]. Levay-Young and Navre found in 1992 that Wnt2 (wingless-type MMTV integration site family member 2), as IRP is now called, is expressed in the mesenchyme of fetal rat lungs and in human fetal lung fibroblast cell lines. They proposed that Wnt2 producing cells stimulate lung epithelial cells indicating its importance in lung development [305]. This assumption could be verified by Wnt2 knock-out ($Wnt2^{-/-}$) mice bearing poorly developed lung mesenchyme and a dilated and dysfunctional vascular endothelial plexus [306]. In addition, further analysis discovered that Wnt2 promotes early stages of airway smooth muscle cell development via FGF10, mycardin, Mrtf-B and Wnt7b [307]. These data indicate that Wnt2 is a necessary factor during lung development via specifying lung endoderm progenitors in the foregut and via the development of airway smooth muscle cells [306, 307]. Furthermore, a double knock-

out of Wnt2 and a close relative (Wnt2b) resulted in complete lung agenesis [306, 307] underlining the importance of Wnt2 during lung development.

Wnt2 was also shown to be relevant during cardiac development, where a knock-down (KD) of Wnt2 resulted in impaired cardiomyocyte differentiation from embryonic stem cells [308]. Furthermore Onizuka et al provided evidence that Wnt2 mediated cardiomyocyte differentiation in a β-catenin independent and JNK/AP1 dependent manner [308]. Activation of non-canonical Wnt pathway was also observed in dendrites [309], however activation of Wnt/β-catenin signaling is also described. In the ventral midbrain expression of Wnt2 was relatively high [310] and Wnt2 increased proliferation of ventral midbrain progenitor cells thereby activating canonical Wnt signaling [311].

Wnt2 was also found to be an important factor for liver regeneration. Klein and co-workers found that Wnt2 mRNA was highly expressed in rat hepatic sinusoidal endothelial cells (HSECs) [312]. Addition of Wnt2 to HSECs resulted in highly induced proliferation that was diminished via Wnt2 KD. Furthermore they found that vascular endothelial growth factor receptor-2 (VEGFR-2) is a target gene of Wnt2 [312]. Inducible VEGFR-2 deficiency (Rosa-creER^{T2} VEGFR-2$^{fl/fl}$; VE-cadherine-creER^{T2} VEGFR-2$^{fl/fl}$) resulted in decreased hepatocyte proliferation and impaired reconstitution of the hepatocellular mass in a mouse model for partial hepatectomy [313]. Interestingly the transcription factor Id1 was up-regulated in endothelial cells after partial hepatectomy. Conditional Id1 knockout in endothelial cells resulted in reduced liver mass due to impaired hepatocyte proliferation and furthermore expression of Wnt2 and hepatocyte growth factor (HGF) was abolished. Liver regeneration could be restored by intrasplenic transplantation of Id1$^{-/-}$ cells ectopically expressing Wnt2 and HGF [313], indicating that Wnt2 plays an important role in hepatocyte proliferation after liver injury. In non-sinusoidal endothelial cells of rat and human liver tissue Wnt2 expression was not present, however, treatment with Wnt2 resulted in enhanced endothelial proliferation and induced sprouting ability in an angiogenesis assay [314]. Klein et al provided evidence that in wound healing and in vascularized tumors Wnt2 and VEGFR-2 are over-expressed in cells of close proximity to endothelial cells [314].

Wnt2 was thought to play an important role in development of malignant structures. Expression of Wnt2 was elevated in mammary carcinomas [315] and ectopic expression of Wnt2 in normal mammary epithelial cells induced a transformed phenotype [303]. MCF-7 breast cancer cells transiently up-regulated Wnt2 mRNA expression upon β-

estradiol treatment, consistent with the finding of two estrogen-receptor binding motifs that are located within the 5'-flanking region of the mouse WNT2 gene [316]. Further putative binding sites were detected for GATA-1, AP-2, TCF1, basic helix-loop-helix transcription factors, p53 and HNF-5 [316]. In malignant glioma cells [317], colorectal cancer cells [318] and in non-small-cell lung cancer cells [319] a Wnt2 KD was reported to lead to growth suppression and induction of apoptosis. Furthermore in non-small-cell lung cancer cells [319] and in malignant melanoma cells a Wnt2 neutralizing antibody induced apoptosis and inhibited melanoma tumor growth [320]. Fzd8 was identified as the receptor for Wnt2 mediated signaling in non-small cell lung cancer cells [321]. Interestingly, co-culture with Wnt2 expressing cells abolished Fzd4 expression in normal mucosa cells, but not in tumor cell lines indicating that Wnt2 prevents normal mucosa from Fzd4 mediated Wnt signaling activation [322].

Wnt2 expression was elevated in tumor tissue from esophageal, gastric and colorectal carcinomas (stage A-C) compared to normal mucosa, where it is almost not detectable [316, 323-327]. However, in gastric cancer cell lines (OKAJIMA, TMK1, MKN7, MKN28, MKN45, MKN75 and KATO-III) Wnt2 mRNA is not detectable, indicating that Wnt2 is up-regulated via cancer-stromal interaction in primary gastric carcinomas [316]. Fibroblasts isolated isolated from matched pairs of esophageal squamous cell carcinoma (OSCC) and normal tissue revealed that WNT2 RNA is induced in the cancer-associated fibroblasts (CAFs) compared to the normal tissue-derived fibroblasts as judged by qPCR. In OSCC cell lines WNT2 RNA was almost not detectable. Furthermore high Wnt2 expression in the OSCC samples correlated with significantly shorter disease-free survival (median survival time 16 months) than compared to $Wnt2^-$ OSCC patients (median survival time 51 months, $p<0.0001$) [327]. Furthermore elevated expression was found in premalignant polyps and in liver metastasis of colorectal cancer [316, 323]. However, the cellular source of Wnt2 was not identified in these studies. These independent results demonstrate that Wnt2 up-regulation is a common feature in the development of carcinomas in the gastrointestinal tract [316].

The mechanism behind Wnt2 up-regulation in gastrointestinal cancers is not known so far, though it could be shown that in colon tumor cell lines (HCT116, Caco2 BBE) and colon mucosa cells bacterial infection with *Salmonella* induced Wnt2 expression, thereby inhibiting *Salmonella*-induced apoptosis and inflammation [328]. This data indicates that Wnt2 might contribute to host protection [328].

Wnt signaling and stem cell control

Embryonic stem cells (ESCs)

Stem cells have the ability to proliferate and remain in an undifferentiated state. Upon stimulation they can differentiate in all cell lineages in case of ESCs or in a limited repertoire of cells in the case of adult stem cells [78]. As long as core pluripotency factors like Oct4, Sox2 and Nanog are expressed ESCs remain in their undifferentiated state [329].

During embryonic development progenitor cells use Wnt signaling for lineage choice, however, if canonical Wnt signaling is required for ESC maintenance remains controversial [78]. There are reports indicating that canonical Wnt signaling is necessary for the establishment and self-renewal of ESCs [330, 331], but others demonstrated that activation of canonical Wnt signaling resulted in differentiation into cells of the mesoderm and endoderm lineages [332, 333]. However, these contradictory results could be due to the use of different ES cell sources (mouse or human) and differences in the levels of Wnt signaling [334].

On the one hand, it could be shown that TCF3 acts as a repressor for pluripotency gene transcription [335]. $TCF3^{-/-}$ murine ESCs (mESCs) self-renewed even in the absence of LIF (leukemia inhibitory factor, a cytokine supplemented to ESC growth medium that retains self-renewal [336]) and Wnt ligands indefinitely. Stabilized β-catenin mediated by GSK-3 inhibitors interfered with TCF3 binding to core pluripotency target genes thereby enhancing their transcription. This effect was promoted by β-catenin's binding ability to TCF3, since β-cateninΔC that can interact with TCF/LEF factors but cannot activate target gene transcription had the same effect as wild type β-catenin [337]. In the reverse approach mESCs were not capable of GSK-3 inhibitor mediated self-renewal in the presence of TCF3 lacking the β-catenin binding domain [338]. However, additional expression of TCF1 was necessary for target gene transcription and self-renewal upon stimulation with Wnt3a [175].

On the other hand, it was demonstrated that canonical Wnt signaling is not necessary for the maintenance of mESCs pluripotent ground state, though β-catenin mediates an additional resistance to differentiation and its absence abolished GSK-3 inhibitor mediated self-renewal [337]. These data indicate that TCF3 acts as a cell-intrinsic

inhibitor of self-renewal in mESCs via competing with Oct3/4, Sox2 and Nanog activity [339]. Another indication of the importance of canonical Wnt signaling for undifferentiated ES cells is that blocking the production of active Wnt ligands with a porcupine inhibitor (IWP2) in ESCs results in a morphology and gene expression that is more similar to primed epiblast stem cells, a developmentally more advanced stage of ESCs [331, 337]. However, it was also reported that β-catenin$^{-/-}$ mESCs continued with self-renewal and remained naïve pluripotent stem cells [340].

Adult stem cell niches

Wnt signaling also plays an important role in adult stem cell niches like hematopoietic stem cells (HSCs), mesenchymal stem cells (MSCs), adult hippocampal stem/progenitor cells (AHPs) and intestinal stem cells (ISCs). For detailed reading please refer to [341] (HSCs), [342] (MSCs) and [343] (AHPs). Before going into detail in the intestinal stem cell regulation a short overview of the structure of the intestinal epithelium is given below.

The intestinal epithelium

The epithelium of the small intestine consists of villi emerging toward the gut lumen and of crypts of Lieberkuhn that are invaginations in the mucosa (**Figure 8**) [344]. Each villus is surrounded by at least six crypts [345]. The villi harbor terminal differentiated enterocytes for absorption, goblet cells for mucus secretion and enteroendocrine cells for hormone secretion [344]. Paneth cells that secrete lysozymes and defensins reside in the crypt base interspersed with crypt base columnar cells (CBC cells) that were thought to be the origin of all differentiated intestinal cells (**Figure 8**) [344, 346]. Potten et al found that CBC cells at position +4 relative to the crypt base were slowly dividing or quiescent and were therefore supposed to be ISCs [347]. Using LGR5-EGFP-IRES-creER^{T2} knock-in mice for lineage tracing Barker et al demonstrated that CBC cells express the stem cell marker LGR5 and that these LGR5^{+} CBC cells yield all types of intestinal epithelial cells indicating that CBC cells are true ISCs [348]. ISCs at position +4 were shown to express the stem cell marker Bmi1 [349]. Yan et al demonstrated that these cells were resistant to irradiation and could give rise to Lgr5^{+} cells upon irradiation induced Lgr5^{+} ISC ablation thereby acting as a stem cell reservoir [350]. These data indicate that there are at least two distinct stem cell populations, the actively proliferating Lgr5^{+} ISCs in the crypt base that are responsible for tissue homeostasis and the quiescent BMI^{+} ISC pool at position +4 relative to the crypt base, that replenish the active ISCs in case of crypt damage [350]. Interestingly, upon intestinal damage Notch ligand delta-like 1 (Dll1) expressing secretory progenitor cells were able to dedifferentiate to LGR5^{+} ISCs [351]. These results indicate that reserve pools of progenitor cells can regain typical ISC signature to restore the intestinal epithelium upon damage [344].

Within the intestinal crypt a Wnt gradient with high activity in the crypt base contributes to the cellular fate of the residing cells [352]. However, the source of secreted Wnt ligands is not elucidated so far. Paneth cells that are interspersed with the ISCs were shown to secrete Wnt3a and knock-out of the transcriptional repressor Gfil (Gfil$^{-/-}$) resulted in decreased number of Paneth cells and concomitantly ISCs [245]. Conflicting results were obtained by Paneth cell ablation via inducible knock-out of the transcription factor Math1 (also called Atoh1; Vil-creER^{T2}; Math1$^{fl/fl}$) [353, 354] and loss of Wnt3a in epithelial cells (Vil-creER^{T2}; Wnt3a$^{fl/fl}$) [355], which could not inhibit the renewal of the epithelial layer, indicating that there are non-epithelial sources of Wnt ligands. Inhibition of canonical Wnt signaling either via β-catenin deficiency, DKK1 treatment or via loss of

TCF4 resulted in abolished ISCs and intestinal crypts indicating that β-catenin/TCF4 target gene transcription is necessary for proliferation and maintenance of ISCs [356-358]. Further importance of Wnt/β-catenin signaling in the maintenance of murine intestine was demonstrated by single ISCs that were isolated from Lgr5-EGFP reporter mice, which generated self-renewing organoids. These organoids recapitulated a functional intestinal epithelium as long as R-spondin was administrated in order to activate canonical Wnt signaling and BMP signaling was inhibited by Noggin [242]. Interestingly the more quiescent ISCs (crypt +4 cells) reside in a more Wnt-restricted environment, than compared to active stem cells in the crypt base (crypt 0 - +3 cell) [349, 359-362]. However, tissue homeostasis in the intestinal epithelium not only depends on Wnt gradients but also on bone morphogenic protein (BMP) and ephrin signaling gradients [352].

Transient amplifying cells (TA cells) are the progenies of ISCs and reside above the crypt base [344]. These TA cells rapidly proliferate, thereby generating 16-32 undifferentiated cells every day. While these cells are moving toward the tip of the villi they differentiate into all intestinal epithelial cells by committing to the secretory or adsorptive cell lineage (enterocytes, goblet cells and endocrine cells) (**Figure 8**) and finally are sloughed off every 4-5 days [344, 363]. This process is called anoikis or "detachment-induced apoptosis" [364].

TA cells do not produce Paneth cells; instead secretory progenitor cells located beneath the TA compartment differentiate into Paneth cells every 3-6 weeks, whilst migrating downward to the crypt base. These secretory progenitor cells are $Lgr5^{+}$ label-retaining cells [365] [366] [345].

The small intestine is divided in the duodenum, jejunum and ileum. Interestingly, the duodenum harbors the longest villi and predominantly absorptive enterocytes, which secrete hydrolytic enzymes in order to break-down partly digested food efficiently [345]. The short villi of the ileum contain more goblet cells, which lubricate the compacted stool that is moved to the colon [345].

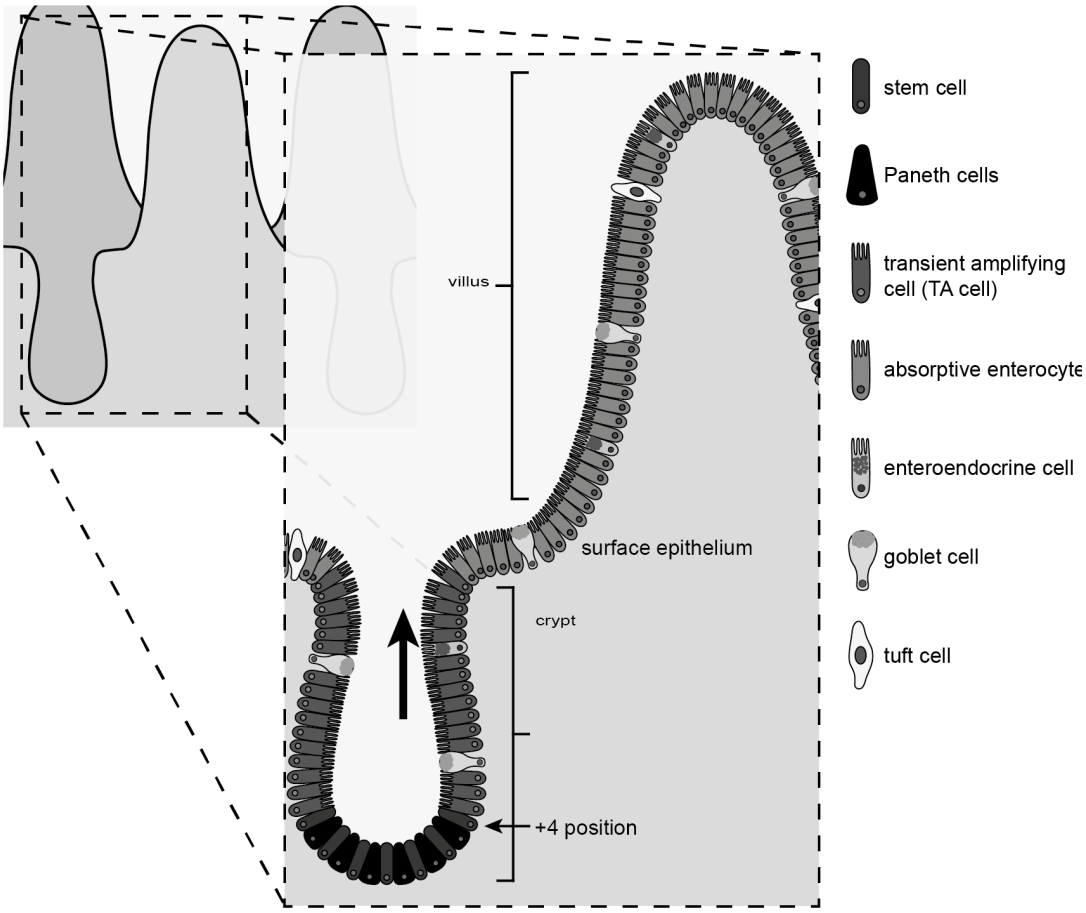

Figure 8 Structure of the small intestine
The epithelium of the small intestine harbors crypts and villi. Paneth cells that are interspersed with stem cells secrete lysozymes and defensins. Stem cells at position +4 relative to the crypt base act as a reserve stem cell pool, which give rise to $Lgr5^+$, actively proliferating stem cells. These $Lgr5^+$ stem cells give rise to transient amplifying cells, which migrate upwards the crypt, thereby proliferating and differentiating into absorptive enterocytes, enteroendocrine cells, goblet cells and tuft cells. After 4-5 days these cells are sloughed off and undergo anoikis. Illustration was inspired by [345].

In contrast, the colorectal epithelium consists of crypts that transist to a flat surface lacking the characteristic villi of the small intestine. Furthermore, within the crypts Paneth cells are absent and goblet cells are enriched though the overall crypt structure is similar to that of the small intestine (**Figure 9**) [344].

Interestingly, ephrin type B receptor 2 (EPHB2) expressing cells in the crypt base were isolated and functioned as stem cells in organoid *ex vivo* cultures, thereby expressing high levels of Lgr5. This indicates that stem cell identity in murine and human intestinal epithelium is conserved [367].

Though colonic crypts do not harbor a label retaining cell population, they can survive acute injuries, indicating that to date unknown, active proliferating cells can function as a stem cell reserve in the colon as previously described for small intestinal crypts [345].

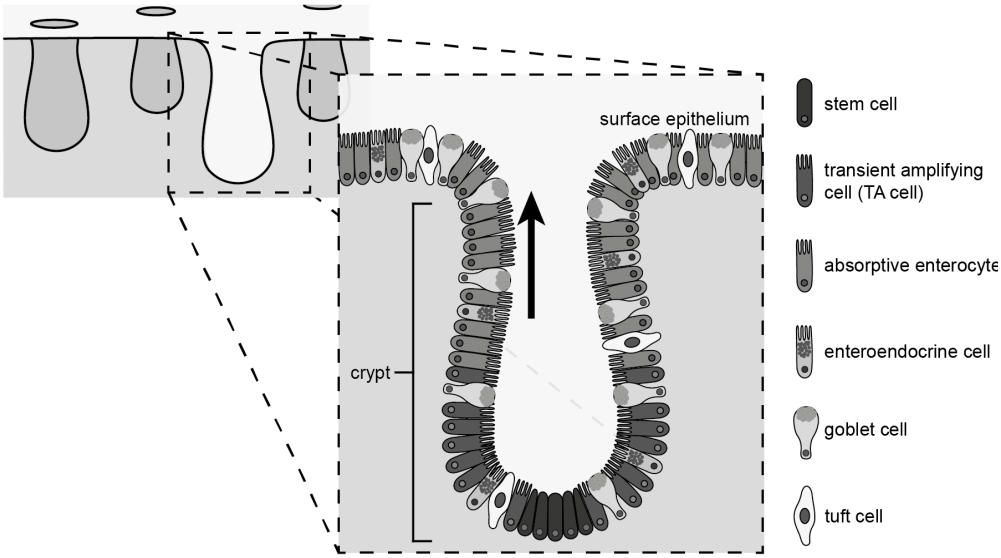

Figure 9 Structure of the colonic epithelium
The colonic epithelium is characterized by crypts that transist to a flat surface epithelium. Within the crypt base Paneth cells are absent and goblet cells are enriched. Illustration inspired by [345].

Colon carcinogenesis

General aspects of colorectal carcinomas

Every year colorectal cancer accounts for about 1.2 million newly diagnosed cases and 600,000 deaths globally making it the third most common cancer disease and the fourth most common cancer cause of death worldwide [368]. More developed countries show a higher burden for colorectal cancer with almost 60 % of all cases. The highest incidence rates were estimated in Australia, New Zealand (age standardized rate, ASR 45.7 per 100,000 for man and 33 per 100,000 for woman) and Western Europe (ASR 41.2 and 26.3), whereas Africa (except for South Africa) (ASR 4.3-7 and 3.3-5.8) and South-Central Asia (ASR 4.9 and 4.1) have the lowest rates [368]. Furthermore, worldwide incidence rates are higher in man (ASR 20.4) compared to woman (ASR 14.6). The highest mortality rates were found in Central an Eastern Europe (ASR 20.3 and 12.1), compared to Middle Africa with the lowest mortality rate (ASR 3.5 and 2.7) [368]. These estimates indicate that colorectal cancer is mainly a disease of the Western culture, however, a high degree of underreporting could also be the case for the low incidence rates in developing countries [369]. Countries that transisted from relatively low- to relatively high-income economies are confronted with rapidly increasing incidence rates (like Japan, Singapore and Eastern Europe) [369], possibly due to changes in diet and/or better health care.

Risk factors for colorectal carcinomas are age (90 % of colorectal tumors occur in people aged >50), familial history of adenomatous polyps, inflammatory bowel disease, colorectal cancer and adenomatous polyps [369]. Another factor that strongly affects the risk for colorectal cancer is diet [369]. It was estimated that a change in eating habits would reduce almost 70 % of colorectal cancer burden [370]. The major risk factor in typical “Western diet” is high fat intake, especially of animal fat [371] [372]. This diet promotes the growth of a bacterial flora that is able to degrade bile salts to *N*-nitroso compounds, which are potentially carcinogenic [373]. Meat consumption was implicated in the development of colon cancers and to a lesser extent of rectal cancer [373]. It was suggested that heme iron in red meat [374] [375] and cooking at high temperatures, which leads to the formation of heterocyclic amines and polycyclic aromatic hydrocarbons [374] [376], are the reason for the higher incidence rates. Furthermore diet with low fruit, vegetable and fiber intake are associated with higher risk for colorectal carcinoma

development [369]. Dietary differences might explain the gap in incidence rates between developing countries and westernized countries, since intake of meat and animal fat is lower and intake of vegetables and fibers [369] is higher in developing countries [377]. Other risk factors are physical inactivity, obesity, cigarette smoking, heavy alcohol consumption [369] and chronic intestinal inflammation [378].

A subgroup of intestinal inflammation is also referred to as inflammatory bowel disease (IBD). The two major disorders that are combined under the name IBD are ulcerative colitis and Crohn disease [379]. It was reported that about 20 % of IBD patients develop colorectal cancer [380] and furthermore, IBD patients with reported familial history of colorectal cancer are reckoned to the high-risk group [381]. This data indicates that mechanisms, which lead to colitis-associated cancer and colorectal cancer, are at least partially overlapping [378]. This notation is substantiated by patient studies, which revealed that non-steroidal anti-inflammatory drugs (NSAIDs) can reduce colorectal cancer by 40-50 % [382] [383]. Animal studies confirmed this result since 90 % of 110 preclinical mouse studies reported the same anti-neoplastic effect of NSAIDs [384]. It is thought that IBD is linked to environmental and to commensal microbial factors, though molecular functions are not elucidated so far [379].

Colorectal cancers are histologically diagnosed from biopsy samples that were collected during endoscopy or after surgery [385]. The basis for therapeutic decisions is provided by the TNM classification into different stages (0 to IV) according to UICC (Union Internationale Contre le Cancer), which depends on local invasion depth (T stage), lymph node involvement (N stage) and the presence of distant metastasis (M stage) [386]. Colorectal carcinomas primarily spread to the liver (10-25 % of patients with primary colorectal cancer resection [387]) or to the lung (11 % [388]) but can also be found in other organs like bone (1.3 % [389]) and brain (2.3 % [390]). The standard therapy is surgical resection and adjuvant chemotherapy for carcinomas of stages III/IV and stage II with high risk of relapse. Liver and lung metastases are surgically resected and in case of irresectable distant metastases palliative chemotherapy is administered [385]. In the past decades prognosis of patients with colorectal carcinoma slowly improved to 64 % (5-year relative survival) in high-income countries.

Colon carcinoma development

Colon carcinomas originate through a multistage process [391]. During this time epithelial cells accumulate different mutations leading to the formation of premalignant polyps that develop to adenomas and then to carcinomas (adenoma-carcinoma sequence) [385]. In 90 % of colorectal carcinomas initial mutations mostly affect the Wnt signaling pathway thereby leading to stabilization and accumulation of β-catenin in the cell nucleus [392]. This aberrant canonical Wnt signaling activation is mediated either by impairing the formation of the destruction complex due to loss-of-function mutations in the *APC* or *AXIN* gene [393, 394] or via gain-of-function mutations within the proto-oncogene β-catenin (*CTNNB1*) itself [394].

The *APC* gene is impaired in 85 % of sporadic colorectal cancers with over 300 different reported mutations [395]. Interestingly, *APC* is proned to two interdependent mutations. When the first hit lies in a region known as mutation cluster region (MCR, between codon 1194-1392) the second hit leads to loss-of heterozygosity, whereas when the first hit occurs outside the MCR the second one falls within it (**Figure 10**) [396]. This mutation leads to frameshift and premature stop codons in the mRNA of APC resulting in a truncated form of APC protein [396, 397]. Another possibility is that truncated APC still harbors its N-terminal coiled-coiled domain, which is responsible for dimerization, and interferes with wild type APC [398] thereby acting in a dominant negative way. This theory was substantiated by experiments in which interference of APC with β-catenin/TCF-mediated transcription was inhibited by a truncated form of APC [399]. However, truncated APC associated with attenuated polyposis (mutations in codons 386-1465) could only weakly inhibit wild-type APC activity [399].

Mutations in the *CTNNB1* gene are involved in 10 % of colorectal carcinomas [392]. Mutations in the *APC* and *CTNNB1* gene within the same cells are rare, since both mutations have the same effect on β-catenin/TCF target gene transcription. However, APC and β-catenin mutations are thought to function in different ways, since small adenomas with aberrant *CTNNB1* do not seem to develop to larger adenomas or invasive carcinomas as likely as *APC* mutated adenomas [400]. Mutations in *CTNNB1* gene occur around or in exon 3, which lead to missense mutation or deletion of phosphorylation sites for GSK-3β and the consequent stabilization of β-catenin [122, 401]. In some colorectal cancer cell lines inactivating mutations within the *AXIN* gene were reported [402] leading to interfered binding of Axin to GSK-3 and Dsh/Dvl. In summary, mutations in different

genes that result in β-catenin stabilization and translocation to the nucleus are prerequisites for neoplastic transformation in the colon mucosa [392].

The adenoma-carcinoma sequence is triggered by mutations in the *APC* gene followed by frequent alterations of the *KRAS* oncogene, *SMAD4* [344], *TP53* [393] and chromosome instability (**Figure 10**) [403]. K-ras is a member of the mitogen-activated protein kinases and is part of the RAS/RAF/MAPK pathway that regulates cell proliferation, differentiation, senescence and apoptosis [404]. Mutations within the *KRAS* oncogene leads to constitutive pathway activation with enhanced cell proliferation and cell survival independently from upstream signals (EGF receptor, EGFR) [404]. Consequently, treatment with EGFR antibodies is inefficient and the National Comprehensive Cancer Network recommends testing for *KRAS* mutation before starting a treatment with cetuximab or panitumumab (EGFR monoclonal antibodies) [404]. Mutations of the *SMAD4* gene were found in an increased frequency with the progression of colorectal cancers [405]. *SMAD4* displays frameshift, nonsense and missense mutations leading to altered homo- and hetero-oligomer formation with Smad2 and Smad3 proteins [406]. This abrogation results in loss-of cell-cycle control, since heterotrimeric complexes of Smad4/Smad2/Smad3 facilitate target gene transcription of cell-cycle inhibiting proteins like p15(ink4B) [407]. Wild type p53 induces apoptosis, when DNA repair was unsuccessful, thereby acting as a tumor suppressor [404]. Mutations within the *TP53* gene were thought to increase cell survival, cell proliferation and genetic instability [408]. Therefore mutations of *TP53* were associated with the transition from adenomas to carcinomas [409] [410]. However, mutations in different genes are reported for 30 % of colorectal cancer [411]. For example, carcinomas that developed from serrated benign precursor lesions often display activating mutations of the BRAF oncogene [411].

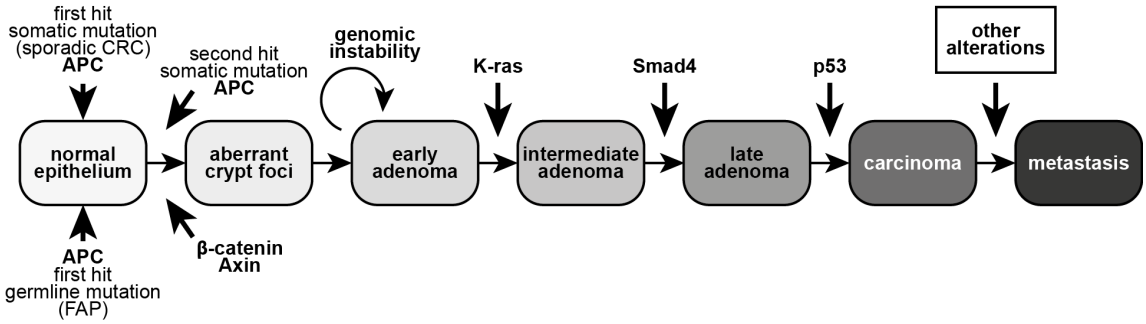

Figure 10 Adenoma-carcinoma sequence
Colorectal carcinomas develop through a multistage process called the adenoma-carcinoma sequence. Initial mutations within normal epithelial cells affect the Wnt pathway leading to hyper-proliferation. However, these mutations are insufficient to initiate carcinoma development and hence additional, mutations of K-ras, Smad4 and p53 are necessary. In order to obtain a metastatic phenotype other genetic alterations are required. Scheme was adapted from [412].

As in the most cancers the cell of origin remains elusive, however, in the literature two models for adenoma formation are discussed. The "top-down model" is characterized by mutated epithelial cells in the intracryptal zones that expand, mutated cells migrate laterally and downwards, where they displace normal epithelium of adjacent crypts [413]. Histological sections stained with β-catenin, which is often highly expressed in lesions in the upper part of the crypts and localized in the nucleus, support this model. Since in most colorectal carcinomas both alleles of the APC gene are inactivated, loss of heterozygosity in the APC gene was determined via SNP analysis (single-nucleotide polymorphism), which revealed that in 50 % APC was inactivated in the adenomatous top portion of the crypts [413]. The alternative hypothesis, the "bottom-up model", describes stem cells that acquire a second hit and expand, thereby resulting in progeny colonizing the entire crypt. The adenomatous crypt then divides via crypt fission or budding and the adenoma progresses [414]. Clevers and coworkers provided evidence for this model. They established a mouse model, in which $Lgr5^{+}$ stem cell express a tamoxifen-inducible Cre recombinase and floxed APC. They could show that deletion of APC in the stem cell compartment resulted in transformation within days and adenoma formation within 3-5 weeks, whereas APC deletion in TA cells using a different mouse model rarely showed large adenomas even after 30 weeks [415]. However, the group of Florian Greten recently found that enterocytes could re-express stem cell markers and could give rise to adenomas. These results indicate that the above-mentioned models do not exclude each other and that tumor initiation could occur in $Lgr5^{+}$ stem cells in the crypts or in

differentiated cells upon dedifferentiation and re-expression of Lgr5 in the upper part of the crypt [416].

Hereditary forms of colorectal carcinomas

Colorectal carcinomas can also develop in hereditary forms, where cells in the germ line harbor monoallelic mutations in tumor suppressors or DNA repair genes and a second hit in somatic cells leads to tumor formation of premalignant polyps [385]. Hereditary non-polyposis colon cancer (Lynch Syndrome) and familial adenomatous polyposis (FAP) are the two most common forms. FAP develops through the adenoma-carcinoma sequence with an incidence rate of 1:10,000 [385], whereas the Lynch Syndrome is characterized by deficient mismatch repair and high microsatellite instability with an estimated allele frequency of 1:350 to 1:1,700 [417]. FAP is caused by germline mutations of the *APC* gene [418]. Patients develop hundreds of colonic adenomas and further display cancerous extra-colonic manifestations in the duodenum, thyroid, pancreas, liver, as well as osteomas, epidermoid cysts and desmoid tumors [418]. In FAP patients mutations between codon 450 and 1578 of the *APC* gene result in a truncated protein, which are the most severe and common mutations. Especially mutations between codons 1359 and 1578 result in very high colorectal polyp counts, whereas mutations in the far 5' region of *APC* trigger an attenuated form of FAP with onset at a later age and fewer polyps, which is believed to be caused by alternative splicing. Mutations in the 3' result in undetectable levels of truncated APC protein with an attenuated form of FAP [419].

In 1895 Aldred Scott Warthin of the Department of Pathology at the University of Michigan in Ann Arbor reported of a familial predisposition to cancer in the so-called "Family-G". At this point Family-G comprised 70 members with 33 cases of various cancers (uterine, gastric and "abdominal cancer") [420]. Over the next 70 years, Warthin, Hauser and Weller and Henry T. Lynch revisited Family-G. Warthin recognized in 1925 that cancers of the gastrointestinal tract and uterus developed most frequently and that the median age of onset is 37.9 years in the now 146 members of Family-G [421]. In 1971 Henry T. Lynch conducted medical genetic investigations of the now over 650 family members. He recognized that progenies of affected family members had a high risk for early-onset of cancer and the autosomal dominant inheritance [422]. In 1985 Lynch used the term "hereditary non-polyposis colorectal cancer" for the first time [423] [424]. In

2005, 110 years after the first report of Family-G, Douglas et al investigated 929 descendants and reported a specific mutation in the *MSH2* gene [425]. In a Lynch Syndrome family in Sweden *MLH1* gene mutations were found [426]. Furthermore, *PMS2* and *MSH6* gene mutations were linked to Lynch Syndrome and HNPCC was linked to microsatellite instability due to mutations in DNA mismatch repair genes [427]. An international collaborative group on HNPCC that was founded in 1989 characterized families with colorectal cancers and developed the "Amsterdam Criteria" in order to identify families with Lynch Syndrome (1. At least three family members with CRC, two of whom are first-degree relatives; 2. At least two generations represented; 3. At least one individual less than 50 years old at diagnosis [428]) [429] [430]. The "Bethesda Guidelines" were developed to provide standardized diagnosis with a panel of microsatellite markers and abnormal immunohistochemistry [431]. However, not all HNPCC affected families meet the Amsterdam Criteria or the Bethesda Guidelines and conversely, many patients that meet these criteria do not have germline mutations in DNA mismatch repair genes (Familial Colorectal Cancer Type X) [432]. Therefore, it was proposed that any colorectal cancer patient under the age of 70 years should be tested for microsatellite instability for possible Lynch Syndrome [433]. Carriers of mutations within the mismatch repair genes have a 25-75 % risk of developing colorectal cancer throughout their lifetime [434].

The tumor microenvironment

Tumor cells are interwoven with extracellular matrix (ECM) components, fibroblasts, endothelial cells and immune cells, which comprise together the tumor stroma (**Figure 11**) [435]. The tumor stroma evolves of normal stroma that is "activated" in response to neoplasm, similar to the adaption of a reactive phenotype during wound healing [436]. This response drives the stroma from maintaining tissue homeostasis [437] to supporting tumor cell survival, nutrient supply, invasion and metastasis [438]. One of the main components in the tumor stroma are cancer-associated fibroblasts (CAF). CAFs display an activated phenotype that is also present in fibroblasts during wound healing or inflammation [439], however, CAFs retain in a permanent state of activation as observed during fibrosis [440] whereas activated fibroblasts that were recruited during wound healing are removed via a process called nemosis [441]. Nemosis is a form of fibroblast activation induced by fibronectin-integrin interaction, which leads to a proteolytic,

proinflammatory and growth factor response via secretion of MMP1, MMP10, IL1, IL6 and IL8 among other factors [441].

CAFs comprise a heterogeneous cell population, since local fibroblasts and fibroblast precursor cells (mesenchymal stem cells) could become incorporated and activated by the growing tumor [442]. Another possible origin of CAFs are tumor cells that develop through EMT to activated fibroblasts [443] or from endothelial cells via EndMT [444]

Compared to their normal counterparts CAFs secrete components of the ECM [445] and express proteins like fibroblast-specific protein (FSP-1), fibroblast-activating protein (FAP) and are frequently positive for α-smooth muscle actin (α-SMA), which is a marker for myofibroblasts [446]. They secrete growth factors (e.g. vascular endothelial-derived growth factor, VEGF; transforming growth factor-β, TGF-β; hepatocyte growth factor, HGF; epidermal growth factor, EGF; fibroblast growth factors, FGFs), cytokines and chemokines, thereby besides the paracrine functions described below, maintaining their CAF phenotype via an autocrine loop [435]. CAFs display a tumor-promoting effect on pre-malignant tumor stages [447] and furthermore they can support metastasis [448]. These effects are mediated by paracrine signaling on different cell types within the tumor. CAFs stimulate tumor cell proliferation [449], migration and invasion [450]; they secrete pro-inflammatory factors, thereby attracting tumor-promoting immune cells [451] and stimulate blood vessel formation via VEGF secretion [452]. Interestingly, in squamous cell carcinomas (SCC) it could be shown that CAFs provide tracks for tumor cells via remodeling the ECM [453]. This remodeling is achieved by producing different types of collagen (type I, III, IV, V), fibronectin and laminin [454] and by secreting matrix metalloproteinases (MMPs), which degrade the ECM [455], thereby affecting the stiffness of tumors and enhancing its aggressiveness and metastatic potential [456, 457]. Furthermore, CAFs can induce EMT in tumor cells [458] and provide an appropriate niche for cancer stem cells [459]. However, it could also be shown that tumor resident fibroblasts could inhibit tumorigenesis indicating that CAFs act in a context-dependent fashion. Their tumor promoting or inhibiting ability is determined by intrinsic properties but depend also on the processing of the tumor microenvironment [435].

Like fibroblasts also immune cells are attracted and activated by the tumor and have an impact on tumor growth and progression. Tumor-associated macrophages (TAM) display an M2 polarized phenotype lacking the cytotoxic activity of normal macrophages [460, 461]. These TAMs are members of myeloid-derived suppressor cells, which are rapidly

expanding in cancers [462]. TAMs accumulate in necrotic regions, where they secrete interleukin 10 (IL-10) to protect the tumor cells from normal immune cells [463], they secrete VEGF in order to aid angiogenesis [464] and EGF to promote tumor growth [452]. Macrophages are a main source of TGFβ, which promotes transdifferentiation of fibroblasts to myofibroblasts [465]. Furthermore, macrophages are the main producer of several MMPs (MMP1, MMP7, MMP8, MMP9 and MMP12) and tissue inhibitors of MMPs (TIMP) [466] thereby modifying the ECM composition, disrupting the basal membrane and promoting angiogenesis [467]. Therefore TAMs are associated with bad prognosis [468].

Tumor vascularization takes place, when a proangiogenic microenvironment was build by tumor cells, CAFs and inflammatory cells [469]. They secrete growth factors like VEGF in order to attract endothelial cells away from their vasculature to the tumor. Furthermore MMPs, secreted by CAFs and macrophages, enable migration and vascular morphogenesis [469, 470]. Tumor vessels display a leaky phenotype, rendering them inefficient in providing the tumor with nutrients and oxygen and in removing metabolic by-products. Macromolecules like fibrinogen leak into the tumor stroma, where it is cleaved and polymerizes to fibrin gel clots, which trap growth factors and protect them from degradation [471] promoting a constant wound healing response, which is never turned off [436].

As the tumor mass increases some parts become hypoxic. This is a consequence of low oxygen availability due to the poor and leaky blood perfusion [472]. Tumor cells shift their metabolism from oxidative phosphorylation to glycolysis, because of mutations in the tumor suppressor p53, which regulates glycolysis [473]. Altered PI3K/AKT signaling increases the expression of the transcription factor hypoxia-inducible factor 1 that in turn induces the transcription of glycolytic enzymes in order to elevate ATP production [474]. Enhanced metabolism then leads to an increase of metabolic acid production (lactic acid) and release to the ECM, which therefore acidifies [475]. This acidosis promotes tumor invasion due to ECM degradation [476] and inhibits the activity of natural killer cells [477]. Lactic acid was recently shown to be the major metabolite, which polarizes macrophages to an M2 phenotype [478].

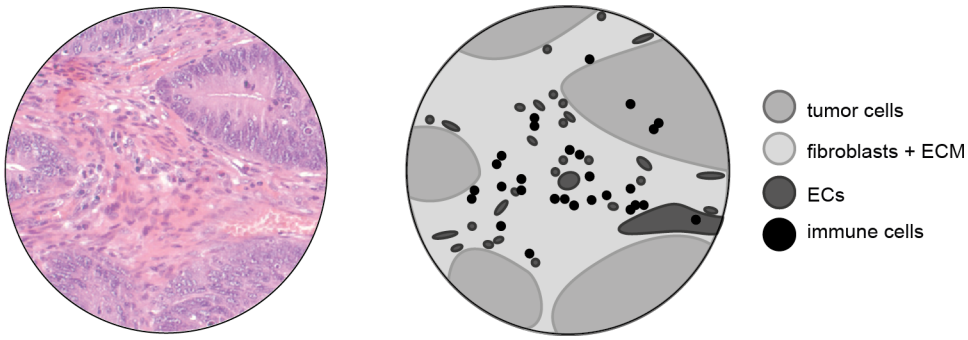

Figure 11 Tumor heterogeneity
Cancer cells of solid tumors are embedded in the tumor stroma, which comprises the ECM, fibroblasts (CAFs), endothelial cells and immune cells. The tumor stroma has a major impact on tumor initiation, progression, invasion and metastasis. Illustration adapted from {ADDR Unger}.

As depicted in the previous sections, the tumor microenvironment has a major impact on tumor progression, metastasis and prognosis [438], however many of the molecular mechanisms and functions between tumor and stroma still remain widely elusive.

Aim of this thesis

The molecular crosstalk between fibroblasts and cancer cells in colon cancer is the main focus of this work. A whole genome covering expression analysis of laser-capture microdissected colon cancer samples and normal colon samples revealed that 1,299 genes were significantly upregulated in the activated tumor stroma compared to the stroma of the corresponding normal tissue counterparts [479, 480]. One of the most significantly induced genes in the tumor stroma versus normal stroma was identified as Wnt2. We hypothesized that this selective induction in the stroma of colon cancers is functionally involved in colon cancer progression. This thesis focused on the autocrine effect of Wnt2 on fibroblasts and its paracrine effect on tumor cells in order to gain more insights into the regulation of the tumor cells by the stromal fibroblasts.

Material and Methods

Cell Culture

Reagents and solutions

Trypsin-EDTA solution (TE):

- *2200 U trypsin*
- *2 % Na EDTA pH 7.4*
- *1x PBS*

DMEM with 10% FCS:

- *DMEM high glucose (4.8 g/L glucose)*
- *10 % FCS*
- *1 % (v/v) Antibiotics stock solution*
- *2 mM l-glutamine*

Antibiotics stock solution:

- *10 g/l streptomycin sulfate*
- *6 g/l penicillin*
- *10 % 10x PBS*

General issues

All cell lines were incubated in a Heraeus BBD 6220 incubator at 5 % CO_2, 80 % relative humidity and 37 °C. All cell culture procedures were performed under sterile conditions using laminar flow hoods (Thermo Scientific, MSC Advantage) and equipment that was wiped with 70 % ethanol (EtOH) (gloves, tweezers, pipettes). Microcentrifuge tubes, pipette tips and silicon forms were sterilized in an autoclave at 121 °C for 20 min.

Cells

Primary human colon fibroblasts (CCD18Co) were obtained from ATCC (Cat. No. CRL-1459) and cultivated in fibroblast growth medium (FGM) consisting of fibroblast basal medium and FGM SingleQuot Kit. The medium was supplemented with 2.5 % fetal bovine serum (FBS). Cells used in the entire study were from passages 10-16, in order to avoid artifacts due to the onset of senescence. The mouse fibroblast lines L par, L Wnt3a, L Wnt5a and L Wnt2 were cultivated in Dulbecco's Modified Eagle Medium (DMEM) supplemented with 10 % FBS. L pWnt3a and L Wnt5a were selected with 0.4 mg/mL G418 and L Wnt2 cells were cultivated with 10 µg/mL Pyromycin. The cancer-associated fibroblasts 3 (CAF3) were cultivated in endothelial growth medium (EGM) consisting of endothelial basal medium and EGM SingleQuot Kit. Human immortalized skin fibroblasts (BJ1) and colon cancer lines HCT116, HT-29, LS174T and DLD-1 were cultivated in DMEM with 10 % FBS.

Passaging of cells

For cell passaging 1x PBS, TE and medium was pre-warmed. Culture dishes were carefully rinsed with 7 mL of PBS that was subsequently discarded and 0.5 ml of TE was added to a 10 cm tissue culture dish. For smaller dishes amount of TE was proportionately reduced. Cell detachment was monitored under the microscope and detached cells were resuspended in culture medium, centrifuged at 300 g for 3 min and supernatants were discarded. Cells were resuspended in fresh medium and splitted in new tissue culture dishes, which were incubated at 37 °C in the incubator.

Freezing of cell

Cells were harvested as described before. Cryo tubes were prepared by adding 100 µl of DMSO. After centrifugation cells were resuspended in 900 µl of FBS and pipetted into these cryo tubes, which were then incubated on ice for 20 min. Thereafter vials were transferred to -80 °C and then to liquid nitrogen tanks the next day.

Thawing of cells

Cryo tubes were taken out of the liquid nitrogen tank and thawed in 37 °C water bath. Meanwhile, centrifuge tubes were filled with 5 mL of pre-warmed medium, thawed cell suspension was transferred to the tubes and centrifuged at 300 g for 3 min. Supernatant was discarded, cells were resuspended in fresh medium and transferred to tissue culture plates. Plates were incubated at 37 °C in the incubator.

mRNA isolation and RT-qPCR

For RNA isolation CCD18Co were co-cultured with L cells and L Wnt2 cells, respectively using co-culture inserts. Therefore 100,000 CCD18Co were seeded on top of the inserts and were harvested after 72 hours. To determine siRNA mediated Wnt2 KD efficiency CAF3 were harvested 3 days after conducting Wnt2 KD and 100,000 cells were transferred to microcentrifuge tubes. Remaining cells were used to determine phenotypical parameters. For comparison of CAF3 and NCF3 mRNA expression 100,000 cells of both cell types were seeded in 6 cm tissue culture plates, which were harvested by trypsinization after 48 hours.

mRNA isolation

The ReliaPrep™ RNA Cell Miniprep System was used for mRNA isolation. In brief, collected cells were washed twice with cold 1x PBS and centrifuged for 5 min. at 300 g. Then 250 µl of BL+TG lysis buffer was added and cells were mixed thoroughly by vortexing. Thereafter 85 µl of Isopropanol was added and tubes were mixed for 5 seconds. Cell lysates were transferred to minicolumns and centrifuged for 30 seconds at 12,000 g at room temperature. The columns were then washed with 500 µl of RNA Wash Solution and centrifuged for 30 seconds at 12,000 g. Next columns were incubated with 30 µl of DNase I mix containing 24 µl of Yellow Core Buffer, 3 µl of 0.09 M $MnCl_2$ and 3 µl of DNase I enzyme per sample. The mixture was pipetted on the membrane and incubated for 15 min. at room temperature. Then 200 µl of Column Wash Solution was added to each column and centrifuged for 15 seconds at 12,000 g. After a further washing step with 500 µl of RNA Wash Solution and following centrifugation for 30 min. at 12,000 g the columns were placed in fresh collection tubes. Then 300 µl of RNA Wash Solution was added to every column and were centrifuged at 18,000g for 2 min. to remove residual ethanol. Columns were transferred to elution tubes and 30 µl of nuclease-Free water was added on the membrane. After centrifugation at 12,000 g for 1 min. the columns were discarded and purified amount of mRNA was determined using a Nanodrop. Samples were stored at -80 °C.

Reverse transcription of mRNA

First-strand cDNA synthesis was carried out using the GoScript™ Reverse Transcription System. In brief, the calculated amounts for 400 ng of mRNA were pipetted in PCR tubes, 0.5 µg of $Oligo(dT)_{15}$ primer were added and reactions were filled to 5 µl with nuclease-free water. Tubes were placed in a thermocycler, which was preheated to

70 °C. After 5 minutes tubes were chilled in ice-water for additional 5 minutes. In a separate tube a bulk reverse transcription mixture was prepared. Therefore 7.3 µl of nuclease-free water, 4 µl of GoScript™ 5x Reaction Buffer, 1.2 µl of $MgCl_2$, 1µl of PCR Nucleotide Mix, 0.5 µl of Recombinant RNasin® and 1 µl of GoScript™ Reverse Transcriptase were mixed for each sample. Before adding the reverse transcriptase 14 µl of the mixture were transferred to a non-reverse transcriptase control sample, after addition of reverse transcriptase 15 µl of the mix were added to all samples. Tubes were then placed in a thermocycler equilibrated to 25 °C for 5 min., thereafter temperature was raised to 42 °C. After 1 hour of incubation reverse transcriptase was inactivated at 70 °C for 15 min. Samples were then stored at -20 °C.

qPCR

The GoTaq® qPCR Master Mix was used to evaluate mRNA transcription. Primer pairs for target mRNAs were reconstituted to 100 µM stocks, working dilutions of 10 µM were prepared and everything was stored at -20 °C (Table 1). cDNA was diluted in a 1:1 ratio with nuclease-free water and 1 µl of cDNA was pipetted in each well of a 48-well PCR plate. For each well 10 µl of qPCR Master Mix was pipetted into a microcentrifuge tube and 5 µl of nuclease-free water was added. The needed amount of master mix for each primer pair was then pipetted into new microcentrifuge tubes and 0.2 µl of each primer was added for every single well to obtain a final primer concentration of 1 µM. Thereafter 19 µl of master mix was added to the preplated cDNA in each well, the plate was sealed with Microseal® 'B' seals and spinned for 30 seconds at 1,000 rpm. On every plate GAPDH and OAZ1 primer were measured for normalization. Amplification protocol was used as indicated in Table 2.

Evaluation of qPCR results

RT-qPCR was carried out in duplicates from three independent experiments. Rel. expression levels of our mRNAs were calculated using following formulas:

$$dCq = Cq_{\text{gene of interest}} - Cq_{\text{reference gene}}$$

$$ddCq = dCq - dCq_{\text{calibrator}}$$

$$\text{rel. mRNA expression} = 2^{(-ddCq)}$$

Values were presented as bar graphs, where the bar represents the mean values and whiskers indicate standard deviation.

Table 1 List of qPCR primers
All primer pairs were ordered from Sigma-Aldrich. Tm is indicated as calculated by Sigma-Aldrich.

mRNA	sense	Sequence 5' to 3'	Tm
CD34	fw	CCCAGCCAACGTTTCAACTC	66.7 °C
	rev	GCAAGGCTAGTGCTAGTGGT	61.1 °C
CD44	fw	GGACAAGTTTTGGTGGCACG	67.6 °C
	rev	TCCGTCCGAGAGATGCTGTA	66.0 °C
CD90	fw	GAGGCAAGCCATGGAGTGAG	67.2 °C
	rev	GCTGTGGTGGCACTATACACA	63.6 °C
CD105	fw	TCACCACAGCGGAAAAAGGT	66.7 °C
	rev	AGGAAGTGTGGGCTGAGGTA	63.7 °C
FAP	fw	GCAGTGTATCGAAAGCTGGG	64.6 °C
	rev	ATCCTCCATAGGACCAGCCC	66.3 °C
FGF10	fw	TTCTTGGTGTCTTCCGTCCC	66.3 °C
	rev	AAGGTGATTGTAGCTCCGCA	64.6 °C
GAPDH	fw	AACAGCGACACCCACTCCTC	66.7 °C
	rev	CATACCAGGAAATGAGCTTGACAA	65.9 °C
MKL2	fw	CCCCAGATCATTCCAGGCAG	69.0 °C
	rev	AGGCCAAGTCCATTTGAGGA	65.8 °C
OAZ1	fw	TTGAGATTGTGAGACCGGGG	67.3 °C
	rev	CTCGAACGTGTAGGCCATGA	66.2 °C
PDGFRα	fw	GTTGGTGTGGGTTCATTGGC	67.5 °C
	rev	GCCGATAGCACAGTGATTGC	65.7 °C
PDGFRβ	fw	TATCCACCCAGGAGCTAGGG	65.1 °C
	rev	GCAGGGACTGGCATCATAGG	66.8 °C
SMA	fw	ACTGCCTTGGTGTGTGACAA	64.4 °C
	rev	CACCATCACCCCCTGATGTC	67.8 °C
TAGLN	fw	CAGTGCAGAGGACCCTGATG	66.0 °C
	rev	CCTCTTATGCTCCTGCGCTT	65.6 °C
Wnt2	fw	CCAGCCTTTTGGCAGGGTC	69.1 °C
	rev	GCATGTCCTGAGAGTCCATG	63.5 °C

Table 2 Program for qPCR amplification

Temp.	Time	Cycles	Comments
95 °C	2 min.		Denaturation
95 °C	15 sec.	40	Denaturation
60 °C	60 sec.		Annealing/Extension
			Read Step
95 °C	10 sec.		Dissociation
65°C – 95 °C	5 sec./ 0.5 °C increment		Melting curve

siRNA mediated Wnt2 knock-down

Preparation of siRNA stock solutions

The siRNA containing tube was briefly centrifuged. Then 1x siRNA buffer was prepared by adding 200 µl of 5x siRNA buffer to 800 µl of nuclease-free water. Thereafter 250 µl of 1x siRNA buffer was added to a vial with 5 nmol siRNA to get a 20 µM stock solution. The vial was mixed thoroughly and placed on an orbital shaker for 30 min. Afterwards it was centrifuged briefly, the stock solution was aliquoted into volumes of 10 µl in 500 µl microcentrifuge tubes, which were then stored at -20 °C.

Transfection

CAF3 were seeded 16 hours before conducting Wnt2 knock-down (KD) at a ratio of 1:3 in 6 cm tissue culture plates in antibiotic-free medium. Cells were incubated over night at 37 °C in the incubator. Next day, an aliquot of OptiMEM I was prewarmed in a 37 °C water bath. For each KD experiment two 6 cm tissue culture plates were transfected either with Wnt2 siRNA or non-targeting control (NTC) siRNA. Therefore 490 µl of OptiMEM I was transferred into a microcentrifuge tube and 10 µl of Lipofectamine RNAiMAX were added. The tube was inverted 3 times, spinned shortly and incubated for 5 min. at room temperature. Meanwhile 245 µl of OptiMEM I was pipetted in two microcentrifuge tubes and 5 µl of Wnt2 siRNA and NTC siRNA, respectively were added. The vials were mixed by inverting and spinned shortly. After the 5 min. of incubation 250 µl of the OptiMEM I-Lipofectamine solution was transferred to each siRNA containing microcentrifuge tube, which was then inverted 3 times and spinned shortly. After 20 min. of incubation at room temperature 500 µl were added to 2.5 mL of antibiotic-free medium in both 6 cm tissue culture plates. Plates were mixed gently by swaying and cells were incubated for 72 hours at 37°C in the incubator.

Co-culture methods and conditioned medium treatment

Buffers and Solutions

Methylcellulose (MC):

- 1.5 % (w/v) Methylcellulose

- 2 mM of l-glutamine

- DMEM

Collagen gel:

- 40 % (v/v) MC

- 2 mg/mL Collagen I

- 10 % (v/v) 10x PBS

- 1 % (v/v) 1M NaOH

Conditioned medium treatment

Conditioned medium was prepared by splitting L par, L Wnt3a, L Wnt5a and L Wnt2 cells, respectively in a ratio of 1:10 in 10 cm tissue culture plates. Cells were grown in 10 mL of DMEM supplemented with 10 % FBS for 4 days. Medium was then harvested, sterile filtered using and stored at 4 °C. Another 10 mL of fresh DMEM, 10 % FBS was added to the plates. After 3 days the second batch of medium was harvested, sterile filtered and mixed with the first batch. The fully overgrown cells were discarded. Conditioned medium was aliquoted and stored at -80 °C.

For conditioned medium treatment 15,000 CCD18Co and BJ1, respectively were seeded in 24-well plates. After 24 hours conditioned medium was added in a ratio of 1:1 to growth medium (**Figure 12A**). Cells were incubated for 72 hours at 37 °C in the incubator.

Simple co-culture

Under simple co-culture conditions CCD18Co, BJ1 and CAF3, respectively were cultivated for a defined period (as indicated) in the same culture vessel with different Wnt ligand expressing L cells (**Figure 12B**). Cell numbers and co-cultivation times are indicated in the corresponding figure legends. For determination of phenotypical parameters CCD18Co have to be distinguishable from the mouse L cells, therefore a α-vimentin antibody that binds only to vimentin of human cells was used.

Co-culture using cell culture inserts

In this approach two different cell types were cultivated using cell culture inserts with a pore size of 0.4 µm (**Figure 12C**). Each L cell line is seeded on the bottom of separate cell culture inserts. Therefore 600,000 cells were resuspended in 750 µl of DMEM supplemented with 10 % FBS and evenly distributed on membranes, which were placed

upside down in 10 cm tissue culture dishes. After 6 hours at 37 °C, when cells were attached, collagen gel was prepared. Therefore methylcellulose, collagen I, 10x PBS and 1 M NaOH were mixed and spinned in a centrifuged at 1,000 rpm at 4 °C. The Medium was removed from the cells, which were immediately submerged with 200 µl of collagen gel per insert. Culture dishes were then placed on 37 °C until the collagen gel had completely polymerized. In 6-well plates 3 mL of culture medium were preplated, the inserts were placed the right way up. A defined amount of CCD18Co (as indicated in corresponding methods sections) was resupended in 1 mL of culture medium and added to the top well of the inserts. 6-well plates were placed in a humidified incubator at 37 °C. Incubation times were indicated in corresponding method sections.

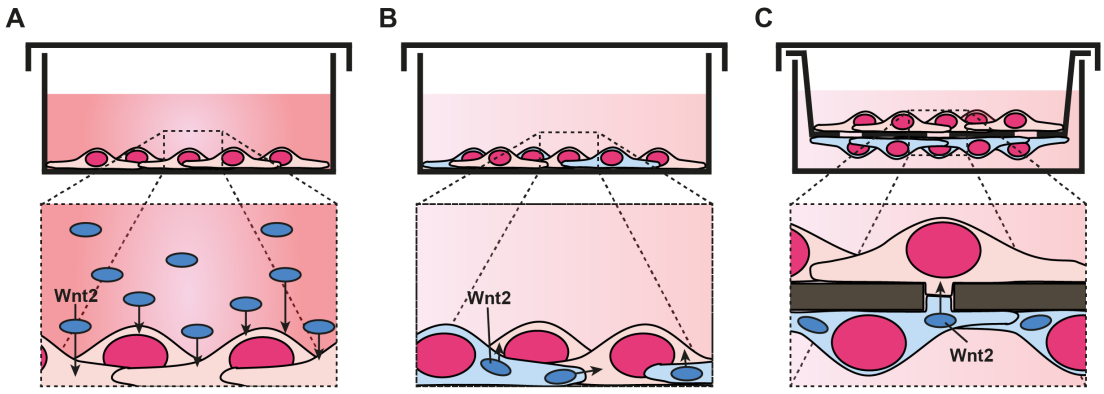

Figure 12 Schemes of culture models
Top panels illustrate different culture conditions; lower panels describe cell-cell interactions; Wnt2 expressing mouse L cells are shown in green, receiver cells in pink and Wnt2 is illustrated as blue spheres. Permeable membrane is indicated in brown. **A** Conditioned medium treatment; fibroblasts were cultivated with medium that was previously conditioned by a different type of fibroblasts. **B** Simple co-culture assay; different types of fibroblasts were cultivated together in the same culture vessel for direct cell-cell contact. **C** Co-culture using cell-culture inserts; different fibroblasts were seeded at the bottom and the top, respectively of a permeable membrane with 0.4 µm pore size, so that fibroblasts can not migrate through, but still have direct cell-cell contact.

Activation of canonical Wnt signaling

Culture conditions

A reporter construct was used to study paracrine and autocrine effects of Wnt2 on canonical Wnt signaling. This reporter harbors seven repeats of the TCF responsive element and GFP as reporter gene. Furthermore it exhibits a puromycin resistance for selection of transfected cells. Cells were constantly grown in growth medium supplemented with puromycin to keep high shields of positively transfected cells. The colon cancer cell lines were cultivated with 5 µg/ml puromycin, BJ1 and CCD18Co with 1 µg/mL puromycin. To determine canonical Wnt signaling activation 15,000 7TGP reporter cells were seeded in 24-well plates and were incubated over night at 37 °C in the incubator. For co-cultivation different L cells (L par, L Wnt3a, L Wnt5a, L Wnt2) were harvested and 15,000 cells were added to the reporter cells. In different wells conditioned medium was added in a ratio of 1:1 to the reporter cells. After 72 hours at 37 °C in the incubator cells were harvested by trypsinization, were resuspended in growth medium and reporter activation was measured via flow cytometric analyses.

Flow cytometric evaluation

For flow cytometric evaluation a BD FACSCalibur with CellQuest Pro software was used. Instrument settings were modulated with untreated and therefore non-fluorescent cells. At first voltage of FSC and SSC were adjusted so that live cells form a cluster in FSC-SSC dot plots (**Figure 13A**). Next voltages of FL1 (green) and FL2 (red) channels were set so that non-fluorescent cells form a cluster of auto-fluorescence at an angle of 45 ° in a FL1-FL2 dot plot (**Figure 13B**). Pathway activation was measured by determining the number of cells that shift towards FL1 (**Figure 13C**). Cell numbers were exported to GraphPad Prism5 and bar charts were created.

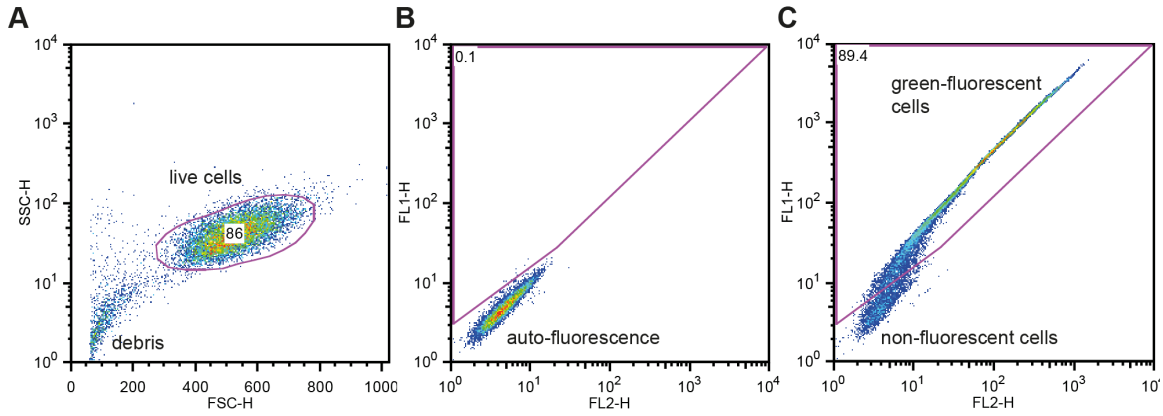

Figure 13 Description of flow cytometric evaluation

A FSC and SSC were adjusted so that live cells form a compact cluster. **B** With non-fluorescent cells voltages of FL1 and FL2 were modulated to set the autofluorescence cluster at an angle of 45 ° in the lower left corner of a dot plot. **C** Green-fluorescent cells shift towards FL1.

Immunofluorescence staining and evaluation

Buffers and Solutions

4 % Paraformaldehyde (PFA) pH 7.4:

- *4 % (w/v) PFA*
- *1 % 1M NaOH*
- *10 % 10x PBS*
- *Aqua dest.*

TBS-Tween:

- *150 mM NaCl*
- *50 mM Tris pH 7.4*
- *0.5 % Tween-20*
- *Aqua dest.*

PBS-Tween:

- *0.5 % Tween-20*
- *1x PBS*

Blocking buffer:

- *1 % BSA*
- *0.3 % Triton X-100*
- *1x PBS*

Antibody dilution buffer:

- *0.5 % Tween-20*
- *1 % BSA*
- *1x PBS*

Immunofluorescence staining for β-catenin translocation

In 4-well chamber slides 7,500 CCD18Co and 7,500 cells of different Wnt expressing L cells were seeded and incubated for 72 hours at 37 °C in the incubator. Cells were fixed with 4 % PFA for 10 min. at room temperature, washed twice with TBS-Tween for 5 min. each, then washed twice with PBS-Tween for 5 min. each. Thereafter cells were permeabilized with pre-chilled (-20 °C) 100 % methanol at -20 °C for 10 min. Methanol was discarded and cells were washed with PBS-Tween for 5 min. Chamber slides were incubated with 500 µl of blocking buffer for one hour at room temperature. Cells were then washed with PBS-Tween. The chambers were removed and wells were encircled with a paraffin pen. Thereafter, α-human vimentin and α-β-catenin antibodies were mixed in antibody dilution buffer and 30 µl of this mixture were added to each well and were incubated for 1.5 hours at room temperature in a humidified chamber. Cells were washed with PBS-Tween for 5 min. and 30 µl of an antibody solution with goat-α-mouse Alexa Fluor 594 and goat-α-rabbit Alexa Fluor 488 in antibody dilution buffer was added. After 1.5 hours of incubation at room temperature in a humidified chamber slides were washed with PBS-Tween and 30 µl of 1 µg/mL DAPI solution was added for 15 min. at room temperature in a humidified chamber. Cells were washed with PBS-Tween and mounted with Vectashield mounting medium and stored at 4 °C. Confocal images were acquired

using a Zeiss LSM 700 microscope. For dilutions of primary and secondary antibodies and other dyes see Table 3.

Evaluation of nuclear β-catenin translocation

Immunofluorescence staining with a human vimentin antibody identified CCD18Co cell for determining nuclear β-catenin distribution. Therefore confocal images were opened in Photoshop CS6 and CCD18Co cells were identified as red-stained, hence vimentin positive cells. In the blue channel (DAPI) all nuclei of these vimentin positive cells were encircled and loaded as a selection. After switching to the green channel (β-catenin) this selection was inverted and filled with black, so that only the green staining of the nuclei remains. The channel was copied and saved as a new image. In the original image changes were undone until only nuclei were selected, which were thereafter filled with black, so that only cytoplasmic staining is left. The image was copied and saved as a new image. This procedure was repeated with all acquired images.

The nuclei-only and cytoplasm-only pictures where opened in ImageJ64. In the "set measurements" window ticks for Area, Integrated Density and Mean Grayvalue were set. First one nucleus and then a part near the nucleus of the corresponding cytoplasm was encircled and measured. This was repeated with all cells of one single image and measurements were exported to Microsoft Excel 2007. This procedure was done with all images.

In Microsoft Excel the intensity of green β-catenin staining was calculated using the following formula: Intensity of nucleus = Integrated Density of nucleus – (Area of nucleus x Mean Grayvalue of the corresponding cytoplasm) [481]

Table 3 List of antibodies and dyes for immunofluorescence stainings

Name	Fluorophor	Species	Conc.	Company	Cat. No.
vimentin	--	mouse	1:300	Invitrogen	18-0052
β-catenin	--	rabbit	1:100	Cell Signaling Technology	8480
goat-α-mouse Alexa Fluor 594	Alexa Fluor 594	goat	1:500	Invitrogen	A11003
goat-α-rabbit Alexa Fluor 488	Alexa Fluor 488	goat	1:500	Invitrogen	A11008
DAPI	--	--	1 µg/mL	Sigma-Aldrich	32670

Luciferase reporter assay

AP1 and TAGLN reporter plasmids

The AP1 plasmid was obtained from Addgene (ID 40342, 3xAP1pGL3). An insert containing 3 repeats of the AP1 canonical binding site (TGACTCA) in front of a minimal promoter containing a TATA box was introduced in a pGL3 basic backbone [482].
The TAGLN plasmid was prepared as described (refer to chapter: TAGLN reporter vector cloning).

Plasmid DNA transfection

For reporter gene assays CCD18Co were seeded in 6 cm tissue culture plates at 75 % confluency and cultivated in 3 mL of antibiotic-free growth medium for 16 hours at 37 °C in the incubator. Thereafter OptiMEM I was warmed to room temperature. A bulk solution of OptiMEM I and Lipofectamine was prepared for all transfections. Therefore for each 6 cm plate 219.4 µl of OptiMEM I and 5.6 µl of Lipofectamine 2000 was pipetted in one microcentrifuge tube that was then inverted three times, spinned shortly and incubated for 5 min. at room temperature. During this incubation step one separate microcentrifuge tube was prepared for every single transfection. The needed volume for 1 µg of plasmid DNA was pipetted in each tube and filled with OptiMEM I to a total volume of 225 µl. Tubes were inverted twice and spinned shortly. After incubation of the OptiMEM-Lipofectamine solution 225 µl was pipetted to every plasmid DNA containing microcentrifuge tube, inverted twice, spinned shortly and incubated for 20 min. at room temperature. Then 550 µl of the plasmid DNA-Lipofectamine solution was added to the tissue culture plates and were resuspended carefully. Cells were incubated at 37 °C in the incubator.

Measurement of luciferase activity

24 hours following transfection cells were trypsinized and equal amounts of cell suspension were seeded in 4 wells of a 24-well plate in complete growth medium. After an additional incubation period of 24 hours at 37 °C cells were washed twice with PBS and starved in 500 µl of growth medium containing 0.1 % FBS over night. To determine the effect of Wnt2 on AP1 dependent transcription and activation of TAGLN mRNA transcription cells transfected with the reporter vectors were incubated either with L929 or L Wnt2 cells or either with NCF3 or CAF3 in simple coculture. Therefore 8,000 cells of Wnt2 producer or control fibroblasts were resuspended in 500 µl of DMEM

supplemented with 10 % FBS and seeded on top of the starved CCD18Co for a co-culture period of 48 hours. For positive controls cells transfected with TAGLN reporter plasmid were incubated with 10 ng/mL of TGF-β for 16 hours, cells transfected with AP1 reporter plasmid were incubated with 10 ng/mL of PDGF-ββ. For determining luciferase activity the Dual-Luciferase® Reporter Assay System was used. Just before harvesting the reporter cells the needed amount of passive lysis buffer (PLB) was prepared by diluting the 5x concentrate to 1x in Aqua dest. For each well of a 24-well plate 100 µl of 1x PLB was required. Medium was removed from the cells, wells were washed with 1x PBS and 100 µl of 1x PLB was added to each well. Plates were put on a rocking platform and were incubated for 15 min. at room temperature. Cell lysates were then transferred to microcentrifuge tubes. Before measurement pre-dissolved Luciferase Assay Reagent II (LARII) in Luciferase Assay Buffer II was warmed to room temperature. Luciferase activity was measured using a luminometer. In a white 96-well plate 30 µl of cell lysate was preplated, 30 µl of LARII was added, mixed and firefly luminescence was read for 8 seconds. Measurements were carried out in duplicates. Relative luminescence units were exported to Microsoft Excel 2007.

Apoptosis assay

Apoptosis was determined by measuring caspase-3/7 activity using the Apo-ONE® Homogeneous Caspase-3/7 Assay. This assay uses the profluorescent consensus substrate rhodamine 110 bis-(N-CBZ-L-apartyl-L-glutamyl-L-valyl-aspartic acid amide) (Z-DEVD-R110), which can be cleaved by caspase-3/7. Active caspase-3 and/or -7 cleave the Z-DEVD-R110 peptide on its C-terminal side (aspartate residue) and rhodamine 110 becomes fluorescent when excited at a wavelength of 498 nm. Caspase-3 and -7 are expressed as procaspases; in this state they have no activity. Upon an apoptotic signaling event procaspase-3 and -7 are cleaved by caspase-8 [483] or by an apoptosome composed of cytochrome c, Apaf-1 and the initiator caspase-9 [484, 485]. Active caspases-3 and -7 then cleave the majority of cellular substrates in apoptotic cells [484] that harbor the DEVD amino acid sequence (Asp-Glu-Val-Asp) [486].

Therefore 5,000 cells of BJ1 GFP, BJ1 Wnt2, CCD18Co after 72 hours of co-culture with either L cells or L Wnt2 cells using co-culture inserts and CAF3 after siRNA mediated Wnt2 KD, respectively were seeded in duplicates in flat bottom 96-well plates in 100 µl of complete growth medium. For positive controls one further duplicate of each cell line was seeded and BJ1 were treated with 1µM of staurosporine for 3 hours for BJ1, CCD18Co with 0.5 µM for 2.5 hours and CAF3 with 0.5 µM for 3 hours. For medium-only controls 3 wells were filled with 100 µl of medium. After 16 hours of incubation the 100x Caspase Substrate Z-DEVD-R110 was diluted to 1x in Apo-One® Homogeneous Caspase-3/7 Buffer. Then 75 µl of medium was removed from each well and 25 µl of the freshly made reagent was added to each well. The plate was then incubated on a plate shaker at 350 rpm at room temperature for 1 hour in the dark. Fluorescence was then measured using a fluorescent plate reader at an excitation wavelength of 499 nm and an emission wavelength of 521 nm. Cleaved caspase-3/7 activity was calculated by subtracting the medium-only values from the values of the different conditions.

Proliferation assay

Buffers and Solutions

Washing solution:

- *1 % BSA*
- *1x PBS*

Reaction cocktail (for one sample):

- *109.5 µl of PBS*
- *2.5 µl of 2 mM $CuSO_4$*
- *0.625 µl of 1 mM of fluorescent dye azide Alexa Fluor 647*
- *2.5 µl of 1x Reaction Buffer Additive*
- *Aqua dest. to a total of 125 µl*

PI solution:

- *1.176 mg/ml of trisodiumcitrat*
- *0.25 mg/ml of RNAse A*
- *0.05 mg/ml of propidium iodide*
- *0.1 % Triton X-100*
- *Aqua dest.*

EdU incorporation and staining

For determination of proliferation the Click-iT® EdU Flow Cytometry Assay Kit was used. This assay is similar to the traditional bromodeoxyuridine (BrdU) incorporation, albeit the nucleoside analog has been changed to 5-ethynyl-2'deoxyuridine (EdU). This thymidine analog carries an alkyne that enables it to react with an azide that is coupled to a fluorophore in a copper mediated click-reaction. This type of reaction has the advantage that harsh DNA danaturation steps as required for BrdU detection are not necessary, since the reaction components are very small and therefore have easier access to incorporated nucleotides in non-denaturized DNA. This maintains the helical structure for cell cycle staining and antibody epitopes for labeling of other markers [487].

BJ1 GFP, BJ1 Wnt2 and CAF3 after Wnt2 KD were seeded in 6 cm tissue culture plates at a density of 100,000 cells per plate and were incubated for 48 hours at 37°C in the incubator. EdU was then added to the culture medium at a final concentration of 10 µM and incubated for 1 hour. Subsequently cells were harvested using TE and collected in microcentrifuge tubes. The Click reaction was carried out according to protocol with minor modifications. In short, cell pellets were fixed with 500 µl of pre-chilled (-20 °C) 100 % methanol and incubated for 10 min. at -20 °C. Thereafter cells were pelleted, methanol was discarded and cells were resuspended using 500 µl of washing solution. The reaction cocktail was prepared in a microcentrifuge tube. Thereafter 125 µl of the

reaction cocktail were added to each sample, cells were resuspended and incubated for 30 min. at room temperature in the dark. Cells were pelleted and resuspended with 500 µl of washing solution. Thereafter cells were pelleted and resuspended in 250 µl of PI solution for DNA staining. After 30 min. of incubation in the dark tubes were centrifuged, staining solution was discarded and cells were resuspended in 1x PBS and transferred to FACS tubes. Cells were analyzed using a BD FACSCalibur with Cell Quest Pro software.

In simple co-culture assays 150,000 CCD18Co and 150,000 L cells and L Wnt2 cells, respectively, were seeded in a 10 cm tissue culture dish. After 48 hours of incubation at 37 °C EdU was added to a final concentration of 10 µM and incubated for an additional hour at 37 °C. Cells were harvested, fixed and stained as described before. After incubation cells were pelleted and resuspended in 500 µl of washing solution. Cells were centrifuged, supernatants were discarded and each sample was resuspended in 100 µl of wash solution containing α-human vimentin antibody (1:300). Tubes were kept in the dark for one hour. Thereafter cells were washed once and were incubated in 100 µl of wash solution supplemented with goat-α-mouse Alexa Fluor 488 (1:500) for one hour in the dark. DNA was then stained using 250 µl of PI solution for 30 min. in the dark. Cells were then pelleted, resuspended in 1x PBS and transferred to FACS tubes. Cells were analyzed using a BD FACSCalibur with Cell Quest Pro software.

Evaluation of flow cytometric data

FACS data was analyzed in FlowJo. Raw data was opened in FlowJo and a FSC-SSC dot plot was opened. Live cells cluster as a compact sphere in the middle of the plot and were gated (**Figure 14A**). Single cells were discriminated from cell aggregates in a FL2-H-FL2-A dot plot. Cell aggregates display a shift towards FL2-A, single cells align in a straight line closest to FL2-H at an intensity of 200 to 400 at FL2-A. In a next step DNA amount was visualized in x-axis (FL2-A) and incorporated EdU was shown in y-axis (FL4-H). Cells in G1 and G2/M phase had not incorporated EdU and the two clusters at an intensity of 10^1 displayed auto-fluorescence. Cells in S-phase incorporated EdU and displayed higher intensities in FL4-H, which appeared as an arch. A gate was set around the EdU positive cells and numbers were exported to GraphPad Prism 5. In simple co-culture experiments human CCD18Co and mouse fibroblasts were cultivated in the same culture vessel. To evaluate S-phase only within the human cells a human vimentin specific antibody was used. After gating the live cells, the vimentin staining was visualized in a FL1-H histogram (**Figure 14B**). Two peaks could be observed; the left peak resembled the auto-fluorescent L cells and the right peak the human vimentin

positive CCD18Co, which were gated and further processed as described before. In GraphPad Prism 5 bar charts were generated out of three independent experiments and an unpaired t-test was carried out.

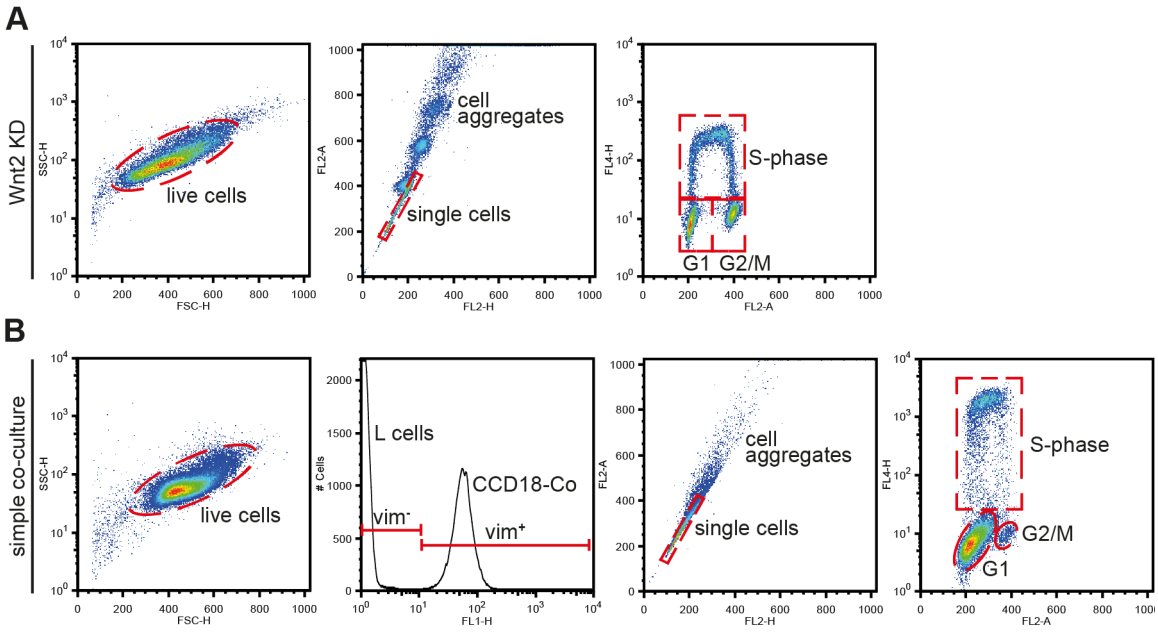

Figure 14 EdU FACS evaluation

A For evaluating BJ1 GFP, BJ1 Wnt2 and CAF3 after siRNA mediated Wnt2 KD live cells and single cells were gated before EdU incorporation was visualized in a FL2-A-FL4-H dot plot. Cells, which were in S-phase at the time of EdU incorporation, displayed a shift toward higher FL4-H intensities. **B** In simple co-culture experiments human CCD18Co were discriminated from mouse L cells with a human vimentin specific antibody. After gating of live cells CCD18Co were isolated in FL1-H, since they displayed higher fluorescence compared to L cells. Single cells were gated and cells being in S-phase were evaluated.

Migration assay

Buffers and Solutions

4 % Paraformaldehyde (PFA) pH 7.4:

- *4 % (w/v) PFA*
- *1 % 1M NaOH*
- *10 % 10x PBS*
- *Aqua dest.*

Crystal Violet:

- *0.03 % (w/v) Crystal Violet*
- *Aqua dest.*

Transwell Assay

A transwell assay was used to determine the migratory potential of CCD18Co upon co-cultivation with Wnt2 expressing fibroblasts, BJ1 GFP and BJ1 Wnt2 and of CAF3 after siRNA mediated Wnt2 KD, respectively. Transwell inserts harbor a porous membrane with a pore size of 8 µm. They were incubated with serum and growth factor free medium for one hour prior cell seeding at 37 °C. Thereafter medium was removed and 25,000 cells were added to the upper chamber in 100 µl of serum and growth factor free medium. The lower chamber was filled with 600 µl of complete growth medium. After 22 hours of incubation remaining cells were removed from the upper chamber using cotton swabs and migrated cells were fixed using 4 % PFA for 10 min. at room temperature. Transwell migration assays were carried out in duplicates.

Evaluation of migration assays

Transwell inserts were stained by adding 500 µl of 0.03 % (w/v) Crystal Violet solution in the culture well and 200 µl of the solution in the insert. After 30 min. membranes were washed once in tap water and were air-dried. 5 pictures of every membrane were taken in a cross-shaped manor and opened in Photoshop. Picture mode was set to CMYK-color. The magenta channel was selected and saved as a new grayscale picture. In ImageJ64 all pictures of one experiment were opened; in the first picture threshold window was opened (Image -> Adjust -> Treshold) and threshold levels were set as indicated by ImageJ. These values were used for all pictures of the same experiment. Next a binary was made (Process -> Binary -> Make Binary), picture was inverted and integrated density (IntDen) was measured. This was repeated with all images and with pictures of a membrane without cells for background measurements. To get values for membrane coverage images bearing the same pixel size as the experimental pictures were generated that were completely black or white. These pictures were

evaluated as described before. All values were exported to Microsoft Excel. With the black/white pictures percentages of membrane coverage was calculated (white – 100 % coverage; black – 0 % coverage). IntDen of the cell-free membrane was subtracted from every membrane measurement. Coverage was calculated with this formula: 100/(IntDen of 100 % coverage)*(IntDen of membrane picture). Values were exported to GraphPad Prism5 and Tukey Boxplots were generated.

Invasion assay

Buffers and Solutions

Methylcellulose (MC):	Collagen gel:
- 1.5 % (w/v) Methylcellulose	*- 40 % (v/v) MC*
- 2 mM l-glutamine	*- 2 mg/mL Collagen I*
- DMEM	*- 10 % (v/v) 10x PBS*
	- 1 % (v/v) 1M NaOH

Spheroid aggregation and harvesting

For determining invasiveness of CAF3 after siRNA mediated Wnt2 KD a spheroid-invasion assay was used. Spheroid formation was accomplished using u-shaped 96-well plates (**Figure 15A**). In every well 1,500 cells were seeded in 100 µl of complete growth medium supplemented with 20 % (v/v) MC. Therefore a bulk mixture for every plate was prepared that was filled in v-shaped reservoirs and 100 µl were transferred with a multichannel pipette in every well. Plates were centrifuged at 1,000 rpm for 5 min. and were incubated at 37 °C in the incubator for 6 hours. For each collagen gel one 96-well plate with spheroids was prepared.

After 6 hours of incubation the complete content of the 96-well plate was pipetted to v-shaped reservoirs and was then transferred to 10 mL centrifuge tubes. Tubes were centrifuged at 1,000 rpm for 5 min, 90 % of growth medium was aspirated by pipetting; spheroids were carefully resuspended in remaining growth medium and were transferred to 1.5 mL microcentrifuge tubes. Spheroids were pelleted again, supernatant was discarded and tubes were put on ice afterwards.

Collagen gel preparation

Collagen gels were produced as described in [488]. In brief, all ingredients were cooled on ice, except of 10x PBS that was kept at room temperature. For each gel 300 µl of gel was necessary and a bulk mixture for all gels was prepared. Two FACS were prepared, one for the gel and one for measuring the methylcellulose, since it has high viscosity and can therefore not be accurately be measured. This one was filled with as much water as methylcellulose would be needed. Then methylcellulose was transferred to the other FACS tube until both had the same fluid level. Next collagen I and 10x PBS were added to the tube. Silicone forms with a diameter of 1.5 cm and a height of 2 mm were put in tissue culture plates and ring-shaped PET meshes with 120 µm mesh size were ready at

hand. The last component of the gel was added when everything was prepared, since addition of NaOH induces polymerization of the gel. 1M NaoH was added, FACS was shaken well and centrifuged in a precooled centrifuge for 15 sec. at 1,000 rpm at 4 °C. Afterwards tubes were put on ice, air bubbles were removed with a pipette-tip and tube was put on ice again. Then 300 µl of collagen gel was transferred to the spheroids in the microcentrifuge tube. Spheroids were carefully resuspended in order not to introduce air-bubbles and the gel was then transferred into the silicone form, where it was evenly distributed with the pipette-tip. Then one mesh was added so that the fibroblasts could not contract the collagen gel. Since spheroids would sink to the bottom of the gel during polymerization resulting in tissue plate-like cell behavior the gels were incubated upside down for 3 min. then turned around on the right side. Gels were incubated until they were completely polymerized.

Afterwards 500 µl of growth medium was added on top of the gels and silicone forms were carefully removed. The gels were then transferred with a forceps into 24-well plates with 500 µl of complete growth medium and were incubated at 37 °C in the incubator where the fibroblasts start to invade the surrounding ECM (**Figure 15A**).

Evaluation of invasiveness

Images of spheroids were opened in ImageJ64. In the "Set scale" window the word "pixel" was added in the field "Unit of length". The ROI manager was opened, a tick was set for "Show all" and the "point" cursor was selected. The first point was set in the middle of the spheroid and was added to the ROI manager (**Figure 15B**). Then the tip of an invasive structure was selected and added to the manager; this was repeated for all structures of a spheroid. After the last added point "Measure" was clicked and the X and Y values were exported to Microsoft Excel 2007. This procedure was repeated for all spheroids. A straight line was drawn over the whole length of a scale bar that was then measured and the pixel length was exported for conversion from pixel to µm later on. In Excel the X and Y values of the spheroid center were subtracted from all X and Y values of invasive structures from the same spheroid resulting in *dX* and *dY* values. The distance (*D*) from the spheroid center to the tip of an invasive structure was calculated using this formula (**Figure 15B**):

$$D = \sqrt{(dX^2 + dY^2)}$$

The resulting length in pixel was now converted to µm using the before measured pixel length of the scale bar.

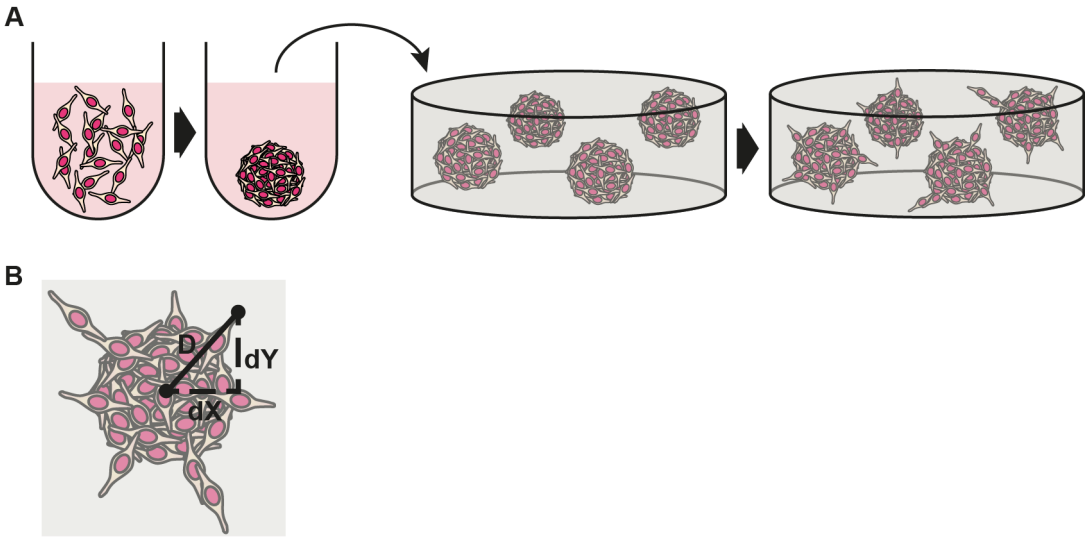

Figure 15 Invasion Assay

A Fibroblasts were seeded in u-shaped 96-well plates, where they aggregate to spheroids after 6 hours; they were harvested and embedded in collagen gel so that they could invade the surrounding ECM in an astral outgrowth. **B** Length of invasive structures were calculated by measuring the coordinates of the spheroid center and the tip of the invasive structure; subtraction of the coordinates resulted in *dX* and *dY* values that could be used to calculate the distance *D* between center and tip using the Pythagorean equation.

Organotypic coculture Assay

Buffers and Solutions

Collagen gel:	4 % Paraformaldehyde (PFA) pH 7.4:
- 2 mg/mL Collagen I	*- 4 % (w/v) PFA*
- 10 % (v/v) 10x PBS	*- 1 % 1M NaOH*
- 1 % (v/v) 1M NaOH	*- 10 % 10x PBS*
- in complete growth medium	*- Aqua dest.*

Production of collagen gels for organotypic assays

For organotypic assays BJ1 GFP or BJ1 Wnt2 cells and CAF3 Wnt2 KD or CAF3 NTC were used. Every type of fibroblast was embedded in three collagen gels. Since one silicone form was filled with 300 µl of gel a total of 1 mL collagen gel for every fibroblast type was needed. Therefore 2 mg of Collagen I were transferred to FACS tubes and chilled on ice. 10 % (v/v) of 10x PBS was added and 60,000 fibroblasts were transferred to the tubes. Tubes were filled with complete growth medium to 1 mL, 1 % (v/v) of 1 M NaOH was added and gel was mixed carefully by pipetting. Care was taken not to introduce air bubbles in the gel. Then 300 µl of collagen gel were transferred to each silicon form. Tissue plates with silicone forms were incubated at 37 °C for 30 min. Thereafter, when gels were completely polymerized, silicone forms were removed and gels were incubated in 6 cm tissue culture plates with 6 mL of complete growth medium at 37 °C in the incubator (**Figure 16A**). Three days later, when fibroblasts contracted and remodeled collagen gels, gels were transferred to 24-well plates with 250 µl of medium and 1,000,000 DLD1 tumor cells in 250 µl of growth medium were slowly added to each well drop by drop. Plates were incubated for 10 min. at room temperature and then carefully transferred in the incubator, where they were incubated for 2 days. After proper cell attachment collagen gels were transferred to a metal grid in 6 cm tissue culture dishes. Enough medium was added to establish an air-liquid interphase between the gels and the tumor cells. Medium was controlled every other day and if necessary a partial medium exchange was conducted. During incubation tumor cells could invade the ECM with different fibroblasts embedded within (**Figure 16B**). After 2 weeks of cultivation gels were fixed with 4 % PFA 10 min. at room temperature and were then transferred to 4 °C for over night fixation. For better sectioning gels were submerged in 1 % agarose, fixed with 4 % PFA and dehydrated in 70 % of EtOH. Agarose pads were then embedded in paraffin.

Collagen gel sectioning and Hematoxylin & Eosin (H&E) staining

In paraffin embedded gels were cut with a microtome in 5 µm thick sections and transferred to poly-l-lysine coated glass slides. Every 5th section and a total of 25 µm were H&E stained. Staining dishes were filled completely with the various solutions and slides were assembled in staining racks. After slides were baked at 60 °C sections were deparaffinized with 2 changes of xylene for 10 min. each. Sections were rehydrated for 2 min. in 96 % EtOH, 2 min. in 70 % EtOH, 2 min. in 50 % EtOH and were washed briefly in Aqua dest. Slides were stained in Mayer's hematoxylin solution for 2 min. and washed in 2 changes of tap water for 5 min. each. Slides were then dehydrated in 50 % EtOH for 2 min. and in 70 % EtOH for 2 min. Sections were then counterstained with eosin solution for 5 min. Slides were further dehydrated in 70 % EtOH for 30 sec., 96 % EtOH for additional 30 sec. and in isopropyl alcohol for 5 min. Thereafter sections were incubated for 5 min. each in two changes of xylene, slides were then mounted with Eukit and dried over night.

Evaluation of organotypic assays

Enough pictures to cover the complete collagen gel were taken from every stained section using a microscope with a color camera. In Adobe Photoshop CS6 pictures were merged to one image. Invasive structures were then counted using ImageJ64 cell counter tool. Care was taken to omit the outer most 500 µm of collagen gel since tumor cells also invade the gel from the sides and would lead to distortion of the evaluation. Counts and invasive area of invasive structures were plotted in GraphPad Prism 5 as Tukey box plots. Repetition of the evaluation by another colleague led to same numbers (data not shown).

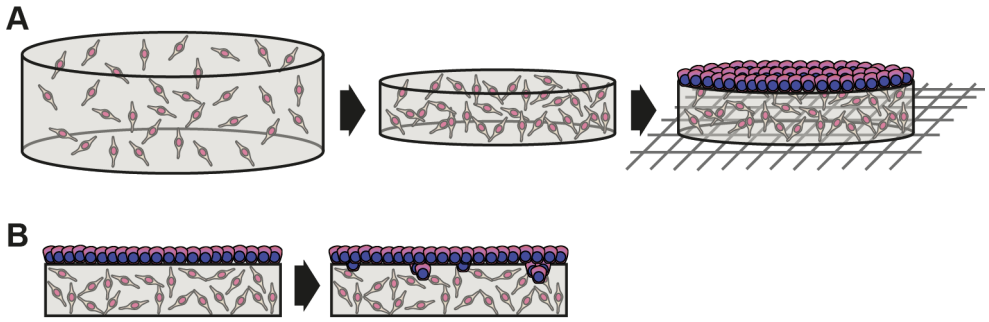

Figure 16 Organotypic co-culture assay
A Fibroblasts were embedded in collagen gel and after polymerization gels were incubated for 3 days at 37 °C in the incubator. During this time fibroblasts remodeled and contracted the gel. Then tumor cells were seeded on top of the gel, before they were transferred to metal grids. **B** Collagen gels were incubated for 2 weeks on metal grids with an air-liquid interphase in order to stimulate tumor cell invasion into the gel.

TAGLN reporter vector cloning

Buffers and Solutions

LB medium pH 7.0

- *0.01 % (w/v) tryptone*
- *0.005 % (w/v) yeast extract*
- *0.01 % NaCl*
- *Aqua dest*

LB-amp plates

- *0.01 % (w/v) tryptone*
- *0.005 % (w/v) yeast extract*
- *0.01 % (w/v) NaCl*
- *0.015 % (w/v) agarose*
- *100 µg/mL ampicillin*

TAGLN promoter PCR-amplification

A TAGLN promoter construct was molecular cloned as described in [489]. Therefore DNA was isolated with DNeasy Blood & Tissue Kit of 500,000 CCD18Co. DNA isolation was carried out according to protocol; in brief harvested cells were centrifuged at 300 g for 5 min at room temperature. Supernatant was discarded and pelleted cells were resuspended in 200 µl of 1x PBS. Then 20 µl of proteinase K and 4 µl of RNase A were added, vortexed and incubated for 2 min. at room temperature. Thereafter 200 µl of Buffer AL (without added ethanol) was added and mixed thoroughly by vortexing. Microcentrifuge tube was incubated at 56 °C for 10 min. Next 200 µl of ethanol was added and sample was mixed thoroughly by vortexing. The mixture was transferred to a DNeasy Mini spin column, which was placed in a 2 mL collection tube. Column was then centrifuged 6,000 g for 1 min., flow-through was discarded and collection tube was replaced by a fresh one. Then 500 µl of Buffer AW2 was added to column, which was thereafter centrifuged for 3 min. at 20,000 g to dry the membrane. The spin column was placed in a fresh 1.5 mL microcentrifuge tube, 100 µl of Buffer AE was pipetted directly on the membrane that was then incubated for 1 min. at room temperature, followed by 1 min. of centrifugation at 6,000 g. Eluted DNA was measured using Nanodrop and stored at -20 °C.

The TAGLN promoter was PCR-amplified from -1032 to +108 relative to the TAGLN transcriptional start site introducing a *MluI* site and a *XhoI* site at the 5' and 3' ends (Table 4) generating a PCR product of 1,142 bp. For PCR amplification Phusion HF DNA polymerase with proof reading ability was used. The PCR reaction was composed of 10 µl of 5x Phusion HF, 1 µl of 10 mM dNTP mix, 2.5 µl of 10 µM forward primer, 2.5 µl of 10 µM reverse primer, 0.5 µl of Phusion DNA polymerase, 27.5 µl of nuclease-

free water and 3 µl of template DNA (120 ng DNA). PCR-amplification was carried out in a Peqlab Primus 25 advanced themocycler (for detailed PCR program see Table 5). The PCR product was then stored at -20 °C until further processing.

Next step was to clean up the PCR product. Therefore 1 % agarose gel in 0.5x TBE supplemented with 4 µl of Midori Green to visualize DNA was loaded with 25 µl of PCR product mixed with 5 µl of loading dye and 5 µl of DNA ladder, respectively. Gel was run at 100 V for 30 min. The product was checked for its size, excised and transferred to a pre-weight microcentrifuge tube. The PCR product was cleaned up using the QIAquick Gel Extraction Kit. In brief, PCR product was weight and 3 volumes of Buffer QG was added to 1 volume of PCR sample (100 mg ≈ 100 µl). Microcentrifuge tubes were incubated at 50 °C until the gel slice has completely dissolved. Every 2 minutes tubes were mixed by vortexing. After gel has dissolved completely 1 gel volume of isopropanol was added and mixed. A QIAquick spin column was placed into a 2 mL collection tube and the sample was applied to the column. After a centrifugation step at 20,000 g for 1 min. at room temperature the flow-through was discarded and column was washed with 500 µl of Buffer QG. Centrifugation was repeated, the buffer was discarded and 750 µl of Buffer PE was added to the column. Before centrifugation tubes were incubated for 5 min. at room temperature, flow-through was discarded afterwards and columns were centrifuged for an additional minute to dry the membrane. Thereafter the column was placed in a clean 1.5 mL microcentrifuge tube, 30 µl of nuclease-free water was pipetted directly to the membrane. Tube was then centrifuged for 1 min. at 20,000 g, the column was discarded and PCR product was measured using the Nanodrop.

Blunt-end ligation

The cleaned up TAGLN promoter sequence was ligated into pJET 1.2/blunt Cloning Vector using CloneJET PCR Cloning Kit. Therefore 10 µl of 2x reaction buffer, 0.15 pmol of purified PCR product (113.85 ng of PCR product), 1 µl of pJET 1.2/blunt Cloning Vector, 1.6 µl of nuclease-free water and 1 µl of T4 DNA ligase was added in a microcentrifuge tube, mixed carefully and spinned. Tube was incubated at 22 °C for 5 minutes.

The pJET vector was introduced in the E. coli strain DH5α to amplify the plasmid. Therefore 1 mL of LB-medium was pre-warmed to 42°C. An aliquot of 100 µl of competent DH5α were thawed on ice. β-Mercaptoethanol was diluted 1:10 and 1.7 µl were then added to the aliquot and mixed carefully. Bacteria were incubated for 10 min.

on ice and mixed every 2 min. by snapping. Then 5 µl of the ligation reaction were added to E. coli and incubated for 30 min. on ice. Tube was placed in a themoblock equilibrated at 42 °C for 45 seconds, immediately chilled on ice for 2 min before 900 µl of pre-heated (42 °C) LB-medium was added. E. coli were then incubated for 1 hour at 37°C while shaking at 240 rpm. Microcentrifuge tube was centrifuged at 150 g for 2 min., 800 µl of the supernatant was discarded and E. coli were resuspended in the remaining LB-medium. On a pre-warmed LB-ampicillin plate (37 °C) 200 µl of transformation mix was plated and incubated over night. Next day 7 15 mL centrifuge tubes were each filled with 4 mL of LB-medium supplemented with 100 µg/mL of ampicillin. In every tube one colony of the over night culture was transferred using a yellow tip under a flame. Furthermore one additional centrifuge tube was inoculated with bacteria of a pGL3 basic bacterial stock. All tubes were incubated for 14 hours at 37 °C while shaking at 250 rpm.

Isolation of plasmids was accomplished using the GenElute Plasmid Miniprep Kit. Therefore 1.5 mL of the over night culture was transferred to microcentrifuge tubes and centrifuged at 12,000 g for 1 min. Bacteria were then resuspended with 200 µl of Resuspension Solution and mixed thoroughly by vortexing. Then 200 µl of Lysis Solution was added, tubes were inverted 6 times and incubated for 5 min. at room temperature. Lysis reaction was stopped by adding 350 µl of Neutralization/Binding Solution. Tubes were inverted 4 times and cell debris was pelleted by centrifugation at 12,000 g for 10 min. Meanwhile, GenElute Miniprep Binding Columns were filled with 500 µl of Column Preparation Solution and centrifuged at 12,000 g for 1 min. The flow-through was discarded. The cleared lysates were transferred to the columns, centrifuged at 12,000 g for 1 min. and flow-through was discarded. Then 500 µl of Optional Wash Solution were added to the columns, centrifuged at 12,000 g for 1 min. and flow-through was discarded. Thereafter 750 µl of Wash Solution were applied to the columns, which were then centrifuged at 12,000 g for 1 min. Liquid was removed and columns were centrifuged again at max. speed for 2 min. to remove residual ethanol. Columns were placed in fresh microcentrifuge tubes and 50 µl of nuclease-free water was added directly on the membrane. After the last centrifugation step a 12,000 g for 1 min. columns were discarded and amount of plasmid DNA was determined using Nanodrop. Plasmid DNA was then stored at -20 °C.

Restriction digest and ligation of TAGLN promoter and pGL3 basic

pGL3 basic vector and pJET vector clones were digested with the restriction enzymes *XhoI* and *MluI*. Therefore a bulk mixture for all clones and vectors was prepared by adding 2 µl of NEB buffer 3, 0.25 µl of each enzyme and 0.2 µl of BSA per reaction in a microcentrifuge tube. For each reaction a fresh microcentrifuge tube was prepared and 17.55 µl of plasmid DNA was added. Then 2.45 µl of the reaction mixture was transferred to each tube, mixed gently by snapping and incubated at 37°C for 2 hour.

Thereafter digested vectors mixed with 5 µl of loading dye were loaded on a fresh 1 % agarose gel supplemented with 4 µl of Midori Green and run at 100 V for 30 min. TAGLN promoter bands and pGL3 basic vector band were cut out and transferred to microcentrifuge tubes. Samples were cleaned up and DNA amount was determined as described before.

For the final ligation a vector-insert ratio of 5:1 was used. Therefore 2 µl of ligase buffer, 1 µl of T4 ligase, 0.0053 pmol of vector DNA (10 µl) and 0.0265 pmol of insert DNA (7 µl) were mixed in a microcentrifuge tube, incubated for 2 hours at 22 °C and stored afterwards at -20 °C

The final plasmid was introduced in One Shot TOP10 Chemically Competent E. coli. Bacteria were thawed on ice, 5 µl of the ligation mix was added and cells were incubated for 30 min. on ice. Microcentrifuge tubes were placed on a heat block equilibrated at 42 °C for 30 seconds and put back on ice for 2 min. Then 250 µl of S.O.C. Medium (room temperature) was added and microcentrifuge tubes were incubated for 1 hour at 37 °C while mixing at 300 rpm. A LB-amp plate was pre-warmed to 37 °C, 200 µl of the E. coli mixture were evenly dispensed and plate was incubated at 37 °C for 10 hours. In 8 15 mL centrifuge tubes 3 mL of LB-medium supplemented with 100 µg/mL ampicillin were transferred and each tube was inoculated with one colony using a yellow tip. Centrifuge tubes were incubated at 37 °C and shaken at 300 rpm for 16 hours. TAGLN-luciferase reporter clones were isolated using the GenElute Plasmid Miniprep Kit as described before. The remaining bacterial over night culture was kept on 4 °C.

Control restriction digest and midiprep

All plasmid clones were checked for TAGLN promoter insertion with restriction digest. Therefore plasmids were digested with *KpnI* and *HindIII*, which cut out a 1,170 bp fragment including the TAGLN promoter sequence. A bulk mixture for all reactions was prepared by mixing 3.4 µl of Aqua dest., 1 µl of NEB buffer 2, 0.5 µl of each enzyme and

0.1 µl of BSA in a microcentrifuge tube. In fresh tubes 5 µl of plasmid DNA were preplated and 5 µl of the bulk mixture were added, mixed by gentle snapping, spinned down and incubated at 37 °C for 2 hours. Digested plasmid DNA was then analyzed on a 1 % agarose gel supplemented with 4 µl of Midori Green as described before. Gel was examined for clones with bands at the appropriate height. The over night cultures of positive clones were used to prepare bacterial stocks in glycerol by mixing 700 µl of over night culture with 300 µl of 80 % (v/v) glycerol for long-term storage at -80 °C. One clone was used to inoculate a midiprep as described before. Isolated plasmid DNA was quantified using NanoDrop and was stored at -20 °C.

Table 4 Primer for promoter PCR-amplification

Gene	Sense	Sequence 5' to 3'	Tm
TAGLN promoter	fw	A<u>ACGCGT</u>[a] CCAGGGATCCCACTGTTAG	75.5 °C
	rev	A<u>CTCGAG</u>[b] GCTTCCTCAGGGCTCGCA	78.7 °C

[a]*MluI* site [b]*XhoI* site

Table 5 Temperatures for promoter PCR-amplification

Temp.	Time	Cycles	Comments
98 °C	30 sec.		
98 °C	10 sec.		
65 °C	30 sec.	1x	Tm of primer without *MluI* and *XhoI* sites
72 °C	40 sec.		
98 °C	10 sec.		
72 °C	30 sec	34x	Tm of whole primer
72 °C	40 sec.		
72 °C	10 min.		
4 °C	∞		

Senescence associated β-galactosidase assay (SA-β-gal)

Buffers and Solutions

Fixing solution:

- 2 % (v/v) formaldehyde

- 0.2 % (v/v) glutaraldehyde

- 1x PBS

Citric acid/sodium phosphate solution:

- 37 % (v/v) of 0.1 M citric acid

- 63 % (v/v) 0.2 M di-sodium hydrogen phosphate

- pH adjusted to 6.0 with 0.1 M citric acid

Staining solution:

- 50 µg/mL of Xgal

- 20 % (v/v) citric acid/sodium phosphate solution

- 5 mM potassium hexacyanoferrate (II)

- 5 mM potassium hexacyanoferrate (III)

- 150 mM NaCl

- 2 mM $MgCl_2$

- in Aqua dest.

SA-β-gal assay

SA-β-gal was determined in BJ1 GFP, BJ1 Wnt2 and CCD18Co after 72 hours of co-culture with L cells and L Wnt2 cells, respectively, using cell culture inserts. Furthermore SA-β-gal was tested in CAF3 72 hours after siRNA mediated Wnt2 KD. The experiment was carried out as described in Current Protocols in Cell Biology 2005 [490]. Therefore cells were harvested and 5,000 cells were seeded on 4-well chamber slides in complete growth medium. After 16 hours of incubation at 37 °C slides were washed three times with 1x PBS at room temperature on an orbital shaker for two min. each. After the last washing step cells were fixed with 500 µl of fixing solution for 5 min. on an orbital shaker at room temperature. Thereafter fixing solution was discarded and cells were washed with 1 ml of 1x PBS. Then 500 µl of staining solution was added to each well, chamber slides were put in a humidified chamber that was subsequently incubated at 37 °C in an incubator without CO_2 supply for 16 hours. Cells were washed with 1 mL of 1x PBS for 5 min. at room temperature, chambers were removed and slides were mounted with Vectashield mounting medium. Pictures were taken using an inverted light microscope with a color camera from Olympus. Cells were counted using ImageJ64s Cell Counter Tool, values were exported to Microsoft Excel and Tukey box plots were created using GraphPad Prism5.

Western blot analysis

Buffers and solutions

RIPA lysis buffer:

- *50 mM Tris pH 7.6*
- *150 mM NaCL*
- *1 % Triton X-100*
- *0.1 % SDS*
- *0.5 % Sodium deoxycholate*
- *Aqua dest.*

PIM:

- *2 µg/ml Leupeptin*
- *2 µg/ml Aprotinin*
- *0,3 µg/ml Benzamidine chloride*
- *10µg/ml Trypsin inhibitor*
- *Aqua dest.*

PMSF:

- *100 mM Phenylmethanesulfonyl fluoride*
- *Isopropyl alcohol*

Bradford solution:

- *20 % (v/v) Bradford*
- *Aqua dest.*

4x protein sample buffer:

- *200 mM Tris pH 6.8*
- *400 mM DTT*
- *8 % (w/v) SDS*
- *0.4 % (w/v) Bromphenol blue*
- *40 % Glycerol*
- *Aqua dest.*

Buffer B pH 8.8:

- *1.5 M Tris pH 8.8*
- *0.4 % (w/v) SDS*
- *Aqua dest.*

Buffer C pH 6.8:

- *0.5 M Tris pH 6.8*
- *0.4 % (v/v) SDS*
- *Aqua dest.*

APS:

- *10 % (w/v) APS*
- *Aqua dest.*

10x electrophoresis buffer:

- *250 mM Tris*
- *1.94 M glycine*
- *1 % (w/v) SDS*
- *Aqua dest.*

Harlow buffer:

- *48 mM Tris*
- *386 mM glycine*
- *0,1 % (w/v) SDS*
- *20 % (v/v) methanol*
- *Aqua dest.*

10x Ponceau S:

- *2 % (w/v) Ponceau S*
- *30 % (w/v) trichlor acetic acid*
- *30 % (w/v) sulfosalicylic acid*
- *Aqua dest.*

10x TBS:

- *1.5 M NaCL*
- *0.5 M Tris pH 7.4*
- *Aqua dest.*

1x TBS-T:

- *10 % (v/v) 10x TBS*
- *0.1 % (v/v) Triton X-100*
- *Aqua dest.*

5% blocking solution:

- *5 % (w/v) milk powder*
- *1x TBS-T*

TBS-T, 5% BSA:

- *5 % (w/v) BSA*
- *1x TBS-T*

Protein extraction

HCT116 and HT29 Wnt2 and GFP expressing cells were seeded in 6 cm tissue culture plates and incubated at 37 °C in the incubator. After 48 hours medium was removed, cells were washed twice with cold 1x PBS, that was then completely discarded. Afterwards 50 µl of RIPA lysis buffer supplemented with 2 % (v/v) PIM and 1 % (v/v) PMSF was added to each plate and cells were scrapped off using a rubber policeman. The cell suspension was then transferred to microcentrifuge tubes, vortexed vigorously and incubated for 5 min. on ice. Thereafter tubes were centrifuged at 20,000 g for 20 min. at 4 °C. The cleared supernatants were transferred to fresh microcentrifuge tubes and stored at -80 °C until further processing.

Protein preparation

The protein amount in cell lysates was determined with Bradford solution. Therefore 1 mL Bradford solution was pipetted in a cuvette and 1 µl of protein samples or RIPA lysis buffer as a reference probe was added, mixed by pipetting and incubated for 5 min. at room temperature. Protein amount was measured using a BioPhotometer. The amounts of protein lysate for 15 µg per sample were calculated and pipetted to fresh microcentrifuge tubes. Afterwards 4x protein sample buffer was diluted in the protein lysates to obtain 1x protein sample buffer, tubes were vortexed, spinned and boiled at 95 °C for 5 min. in a thermomixer. Samples were then cooled to room temperature.

SDS-PAGE

Before starting 1x electrophoresis buffer was prepared by diluting the 10x stock to 1x in Aqua dest. and buffer was then cooled to 4 °C. The Mini-PROTEAN Tetra Electrophoresis System from BioRad with a 15-slots comb was used. In a casting frame the 0.75 mm spacer plate and a short plate were combined and were then fastened in a casting stand. Thereafter separating gel was prepared by adding acrylamide, Buffer B, Aqua dest., APS and TEMED according to Table 6. After addition of TEMED tube was mixed thoroughly by vortexing and was then filled between spacer and short plate. In order to get a smooth edge 1 mL of isopropyl alcohol was added on top of the separating gel. After polymerization isopropyl alcohol was poured off and separating gel was washed three times with Aqua dest. To removed residual isopropyl alcohol. After drying with filter paper stacking gel was prepared (Table 6), mixed thoroughly and was then applied on top of the separating gel. A 15-slot comb was added.

After complete polmyerization the electrophoresis system was built with a buffer dam. The chamber was filled with the pre-chilled 1x electrophoresis buffer. The comb was removed and electrophoresis buffer was pipetted in every slot to remove residual acrylamide gel. First slot was loaded with 2.5 µl of PageRuler Prestained Protein Ladder, following slots were filled with the prepared samples. The equipment was run at 70 V until the samples formed a straight line. The voltage was then raised to 110 V.

Table 6 Recipe for 10 % separating gel and stacking gel

Component	10 % separating gel	stacking gel
acrylamide	4.2 mL	0.5 mL
Buffer B	3 mL	---
Buffer C	---	0.75 mL
Aqua dest.	4.8 mL	1.75 mL
APS	60 µl	30 µl
TEMED	5 µl	2.5 µl

Transfer

Before electrophoresis was finished a 8.5 x 6 cm piece of nitrocellulose membrane was cut and equilibrated in Harlow buffer to ensure proper protein transfer. Before the loading dye front reached the bottom of the glass plates the equipment was turned off. A Mini Trans-Blot Module was prepared. Therefore the buffer tank was filled with Harlow buffer and a cooling unit. One insert, one gel holder cassette, 2 foam pads, 4 pieces of 8 x 10 cm

sized 3MM Chr sheets were ready at hand. The foam pads and the 3MM Chr sheets were soaked in Harlow buffer. Then the sandwich for the western blot was assembled as follows: on top of the black side of the gel holder cassette a foam pad was placed, one Chr sheet was put on top of it. The SDS-PAGE equipment was removed, the spacer plate was lift off so that the gel stayed on the short plate. The stacking gel was removed and one Chr sheet was laid on the gel, which was then transferred on the filter paper. This sheet was then laid on the previous Chr sheet on the insert. The nitrocellulose membrane was added, covered with 2 Chr sheets and a foam pad. The gel holder cassette was closed and put in the chamber. Harlow buffer was filled to the top of the chamber, which was then closed with the lid and run for 1 hour at 350 mA. When transfer was finished the chamber was removed and the membrane was washed in a box with Aqua dest. on an orbital shaker for 5 min. Afterwards the membrane was stained in 10 mL of 1x Ponceau S for 15 min. on a rocking platform. The completely red membrane was destained in Aqua dest. until all lanes were visible as red bands on white background. The blot was scanned, saved and entirely destained in 1x TBS-T. Thereafter it was blocked for 1 hour at room temperature in a box filled with 10 mL of 5 % blocking solution. It was then washed 3 times for 10 min. in 1x TBS-T on an orbital shaker.

Protein detection

Primary antibodies were diluted in 5 mL of TBS-T, 5 % BSA (for dilution factors see Table 7) in 50 mL centrifuge tubes. Blots were placed inside the tubes and were incubated over night at 4 °C on a rocking mixer. Next day blots were washed 3 times for 10 min. with 1x TBS-T and were incubated in 10 mL of 5 % blocking solution supplemented with secondary antibodies (for dilution factors see Table 7) for 1 hour at room temperature. After that blots were washed three times with 1x TBS-T for 10 min. each. Signals were detected using enhanced chemiluminescence (ECL) that was prepared by mixing 1 mL of detection reagent 1 and 2. Blots were incubated with ECL for 1 min., drained on paper towels and wrapped in cling film. Blots were then tapped into cassettes and incubated with light-sensitive Amersham Hyperfilms and CL-XPosure films, which were thereafter fixed and developed using a Kodak Medical X-ray Processor MXP 2000.

Table 7 List of antibodies for Western blot detection

Name	Species	MW	Dilution	Company	Cat. No.
Wnt2	goat	34 kDa	1 μg/mL	R&D Systems	AF3464
GAPDH	rabbit	38 kDa	1:50,000	Trevigen	2275-PC-100
donkey-α-goat HRP IgG h+l	donkey	--	1:10,000	Bethyl Laboratories, Inc.	A90-116P
goat-α-rabbit HRP IgG h+l	goat	--	1:10,000	Bethyl Laboratories, Inc.	A120-101P

Xenograft tumor model

Handling, subcutaneous injection, tumor size measurement and sacrifice of the mice were conducted by skilled colleagues in the lab of our collaborator Prof. DI Dr. Richard Moriggl at the Ludwig Boltzmann Institute for Cancer Research (Vienna, Austria).

Assessment of Wnt2s impact on tumor progression was evaluated with a xenograft tumor model. Therefore 100,000 cells of HCT116 or HT29 either ectopically expressing Wnt2 or GFP, as control were subcutaneously injected in the groins of SCID mice. Tumor size was measured every week. After sacrifice tumors were explanted, tumor weight was assessed and pictures were taken.

Growth curves and box plots to illustrate tumor weight were created in GraphPad Prism5. Spheres and boxes represent mean values and whiskers indicate standard error of mean.

Statistical analyses

For statistical analysis Microsoft Excel 2007 and GraphPad Prism5 were used. Raw data was imported to Microsoft Excel 2007. Control conditions were set to 1 by dividing every single value with the mean of the control condition. Ratios of the other conditions to the aforementioned mean were calculated. This was repeated with every experiment and all ratios were exported to GraphPad Prism 5. Bar charts were generated, where bars show means and ticks standard deviation. In Tukey box plots the centerline represents the median, The difference between the 25^{th} and 75^{th} percentile is the interquartile range (IQR) that is presented as the box. The 75^{th} percentile is extended by 1.5 fold IQR and the largest value of the dataset that is smaller than this sum is indicated by a whisker. Outliers are shown with dots. The lower whisker is the 25^{th} percentile minus 1.5 fold IQR. A whisker indicates the smallest value within this range and outliers are represented with dots. P-values were calculated using GraphPad Prism5 (unpaired, two-tailed, 95 % confidence interval) and specified in the corresponding figures.

Results

WNT2 expression e*x vivo* and *in vitro*

In a previous experiment preceding this study patient-derived frozen tissue sections of colon cancer and normal tissue samples were laser capture microdissected in order to separate tumor stroma from tumor epithelium and normal stroma from normal epithelium, respectively. In brief, activated tumor stromal fibroblasts were identified using immunohistochemical staining of fibroblast activation protein α (FAP), an extensively studied marker for activated fibroblasts [491, 492], followed by immediate laser capture microdissection and RNA isolation. Gene expression profiling of these samples was conducted to identify molecular differences. Bioinformatic evaluation uncovered 1,299 genes that were differentially expressed between normal stroma and tumor stroma. More precisely, 672 genes were significantly down-regulated and 627 genes were up-regulated in the tumor stroma compared to normal stroma (false discovery rate $p<0.01$). Based on this screening a research article about one of the most significantly up-regulated genes in tumor stroma, namely IGFBP7, was recently published [480]. Another significantly up-regulated gene in tumor stroma was WNT2 (**Figure 17A**). Wnt2 was not or only expressed at very low levels in the other compartments. An *in silico* expression analysis of an independent large dataset derived from the BioExpress gene expression database (Gene Logic) confirmed that WNT2 mRNA expression was significantly elevated in 95 non-dissected colon cancer samples compared to normal colon mucosa (215 samples) (**Figure 17B**).

One of the major components of the tumor stroma are the cancer-associated fibroblasts (CAFs). Two CAF cultures (CAF1, CAF2) were established from native patient tumor material and were propagated as primary cultures. They were analyzed for WNT2 mRNA expression levels and compared with normal colon myofibroblasts (CCD18Co) and skin fibroblasts (BJ1) using full genome Affymetrix GeneChip arrays. Bioinformatic analysis revealed that high WNT2 mRNA expression is found in CAF1 and CAF2, leading to the assumption that major source of WNT2 in the tumor stroma are the CAFs (**Figure 17C**). The normal colon fibroblasts CCD18Co express lower levels of WNT2, whereas the skin fibroblasts do not endogenously express WNT2.

After completion of the gene expression profiling another CAF culture (CAF3) and its normal counterpart (normal colon fibroblasts 3, NCF3) derived from the same patient could be established successfully.

A first aim of this thesis was to analyze the expression pattern of WNT2 in NCF3 and CAF3 and to compare it with CCD18Co and BJ1. Therefore mRNA was isolated, cDNA was reverse transcribed and qPCR analysis was carried out in duplicates. Data were normalized to GAPDH expression and WNT2 qPCR analysis revealed CAF3 expressed significant amounts of Wnt2. NCF3, like BJ1, did not express endogenous WNT2 mRNA whereas CCD18Co did (**Figure 17D**). Again, as for CAF1 and CAF2 WNT2 mRNA was substantially higher in CAF3 as compared to CCD18Co.

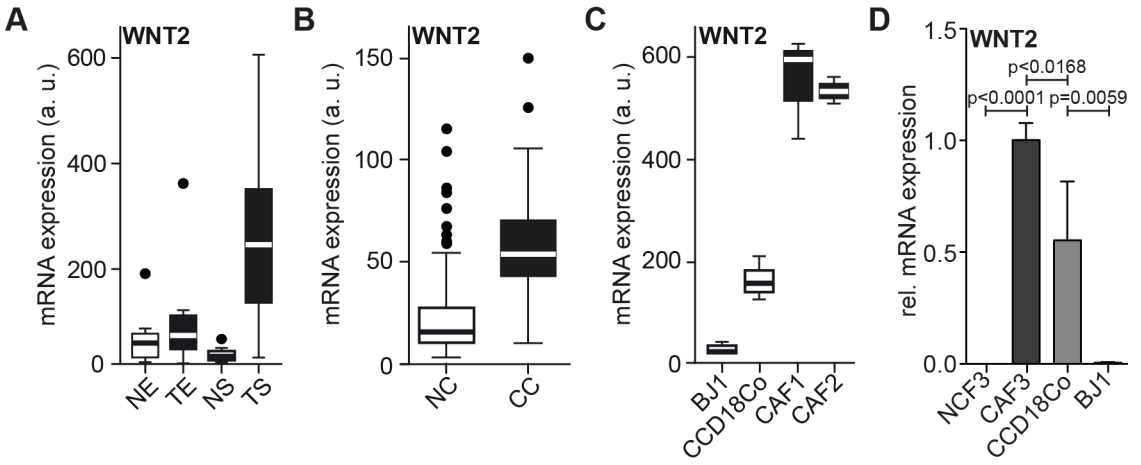

Figure 17 WNT2 expression *ex vivo* and *in vitro*
A Native patient samples were laser capture microdissected in normal epithelium (NE, n=6), normal stroma (NS, n=6), tumor epithelium (TE, n=26) and tumor stroma (TS, n=26) and mRNA was analyzed using full genome Affymetrix GeneChip arrays (false discovery rate p<0.01). **B** *In silico* expression analysis of non-dissected colon cancer (n=95) and normal colon mucosa (n=215) datasets derived from the BioExpress gene expression database (Gene Logic). **C** WNT2 mRNA expression was analyzed via full genome Affymetrix GeneChip arrays of BJ1, CCD18Co and the two patient derived fibroblast cultures CAF1 and CAF2 (n=6) (false discovery rate p<0.01). **D** WNT2 mRNA expression was analyzed in NCF3, CAF3, CCD18Co and BJ-1; mRNA was isolated, cDNA was reverse transcribed and qPCR analysis was carried out in duplicates of cells from two different passages (n=4); Data were normalized to GAPDH expression; Expression of WNT2 in CAF3 was set to 1 and corresponding values were calculated; Bars represent mean values and whiskers indicate standard deviation. Box plots represent median (bold center line), IQR (box), 1.5 fold extension of the IQR (whiskers) and outliers (dots).

Taken together we could demonstrate that WNT2 was expressed exclusively in tumor stroma, that the source of Wnt2 was dominantly CAFs which reside in the tumor stroma and that they kept their high expression of Wnt2 *in vitro*.

Modulating expression of Wnt2 in fibroblasts of different origins

Next, our goal was to examine the effects of Wnt2 on fibroblasts and tumor cells. Therefore BJ1 cells were used for over-expression experiments, since they do not express any endogenous WNT2 mRNA (**Figure 17C**, **D**). Hence, cells were stably transfected with Wnt2 and GFP as control, respectively. Stable WNT2 expression was achieved by puromycin (1 µg/mL) selection. High ectopic WNT2 expression was verified with qPCR (**Figure 18A**).

In order to test canonical Wnt signaling L cells expressing Wnt3a and Wnt5a are commonly used [15, 288] is used. Therefore the control L 929 cells (L par) were stably transfected with the same expression vector as previously used for BJ1 cells. qPCR analysis revealed high expression of Wnt2 (**Figure 18B**).

Since CAF3 express high amounts of Wnt2 we were interested in the effects of siRNA mediated Wnt2 knock-down (KD). As control CAF3 were transfected with non-targeting control (NTC) siRNA. After 72 hours mRNA was isolated, cDNA was reverse transcribed and qPCR analysis was carried out. We found that Wnt2 levels were reduced by 92.55 % on average in three independent experiments (**Figure 18C**).

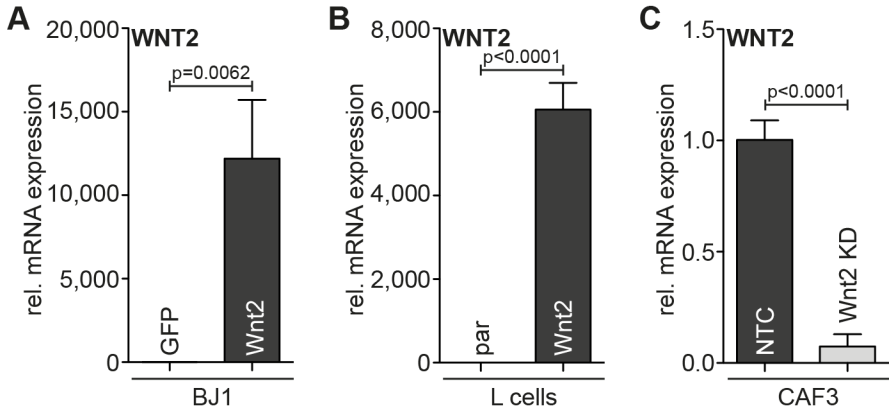

Figure 18 Modulating Wnt2 expression in fibroblasts
A BJ1 were stably transfected with Wnt2 and GFP as control, respectively and Wnt2 expression was measured (n=4). **B** For co-culture assays L par cells were stably transfected with Wnt2; mRNA expression was tested (n=4). **C** CAF3 were used for siRNA mediated Wnt2 KD experiments; NTC served as negative control; KD efficiency was analyzed (n=8). mRNA was isolated, cDNA was reverse transcribed and qPCR analyses were carried out in duplicates of two different passages (**A**, **B**) or of four independent experiments (**C**); Data was normalized to GAPDH expression; control conditions were set to one; since BJ-1 and L cells do not express endogenous Wnt2 cycle 40 was set as Cq value; bars represent means and whiskers illustrate standard deviation.

In summary, we demonstrated that we could exogenously express Wnt2 in BJ1 for over-expression experiments, generate Wnt2 expressing L cells for conditioned medium and co-culture experiments and that we were able to conduct highly efficient Wnt2 KD in CAF3. Therefore the tools to further study the influence of Wnt2 on colon cancer were established and validated.

Paracrine effects of Wnt2 on canonical Wnt signaling activation of tumor cells

First we wanted to test whether Wnt2 has the ability like Wnt3a [76] to activate canonical Wnt signaling. Therefore we used a 7TGP reporter vector, which exhibits 7 repeats of the TCF responsive element and GFP as a reporter gene and is commonly used to quantify canonical Wnt/β-catenin signaling [76] (for a map of 7TGP please refer to Material and Methods sections). When a Wnt ligand binds to the LRP/frizzled co-receptor complex the destruction complex disintegrates, β-catenin stabilizes and translocates to the nucleus. There it binds to members of the TCF family mediating target gene transcription. In case of the reporter vector β-catenin interacts with TCF and binds to TCF responsive elements of the vector, thereby inducing the transcription of GFP. The amount of fluorescence can then be measured using flow cytometric analysis. The tumor cell lines DLD1, HCT116, HT29 and LS174T were stably transfected with the 7TGP reporter vector and were incubated with conditioned medium from mouse L cells expressing different Wnt ligands (L Wnt5a, L Wnt3a, L Wnt2) or from control L cells (L par), respectively. L par and L Wnt5a CM, which do not activate canonical Wnt signaling, served as negative control [16], whereas L Wnt3a CM, a known activator of canonical Wnt signaling, was used as positive control. After 72 hours cells were harvested by trypsinization and fluorescence was measured via flow cytometric analysis. As expected, the reporter cells alone displayed high GFP fluorescence (**Figure 19A** and **B**). This activation results from different mutations in the canonical Wnt signaling pathway that were accumulated by epithelial cells during the process of adenoma formation [493]. Incubation with any Wnt conditioned medium did not show reporter activation, indicating that fibroblast derived paracrine Wnt signals did not lead to hyperactivation of the Wnt/β-catenin signaling pathway (**Figure 19A** and **B**).

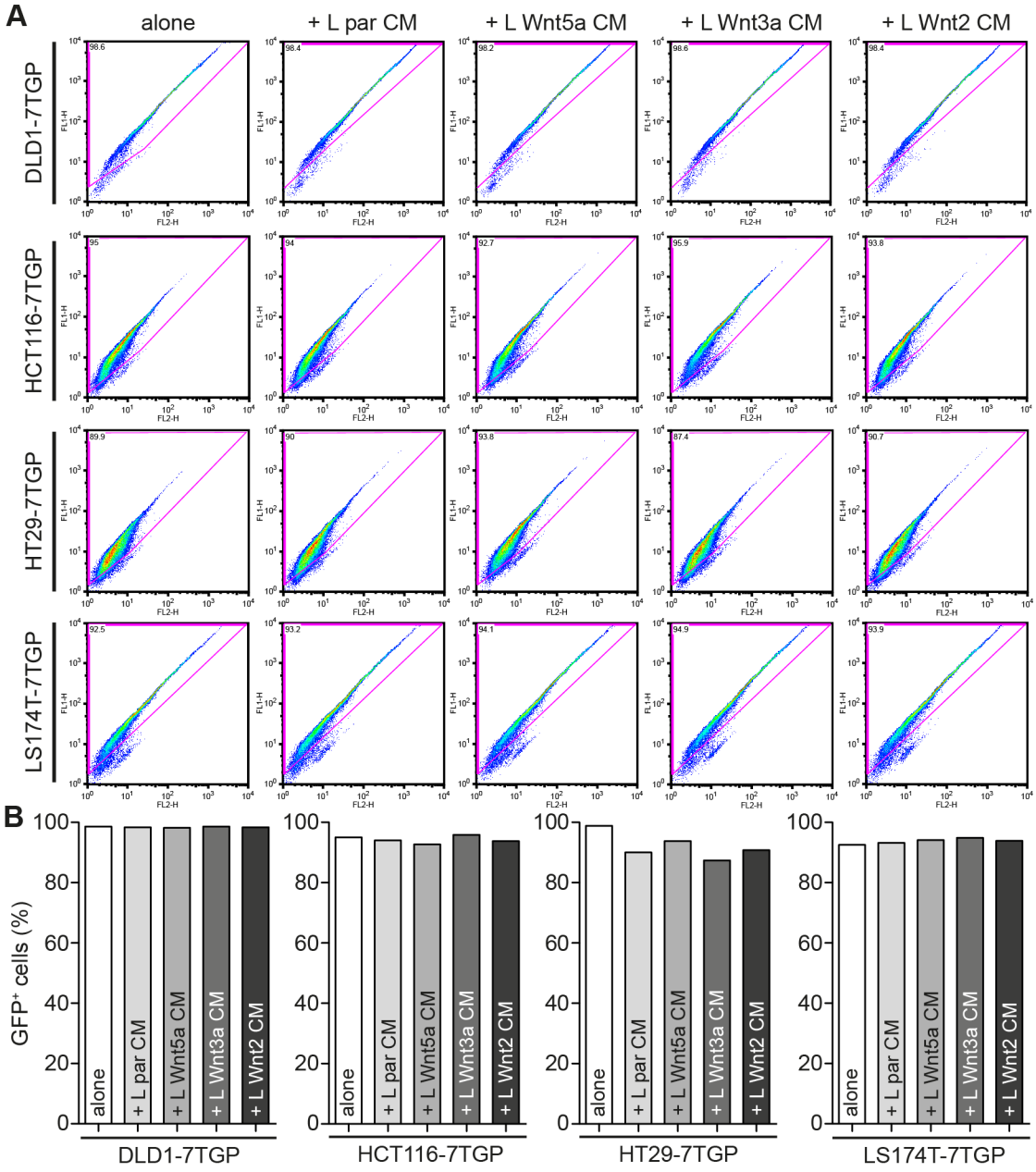

Figure 19 Incubation of 7TGP reporter tumor cells with conditioned medium
A Dot plots in the leftmost column show endogenous reporter activation; further columns indicate reporter activation upon treatment with conditioned media from L cells expressing different Wnt ligands. **B** Bar charts of reporter gene activation; bars indicate means and whiskers indicate standard deviation (n=1).

In a next step we evaluated whether direct cell-cell contact between the tumor cells and the Wnt producing fibroblasts had an effect on further pathway activation. Therefore 7TGP transfected DLD1, HCT116, HT29 and LS174T cells were "simple co-cultivated" with L par and Wnt ligand-expressing L cells, respectively. Flow cytometric analysis of 7TGP reporter activation showed no significant activation upon treatment with either Wnt2 containing CM or Wnt3a CM (**Figure 20A** and **B**).

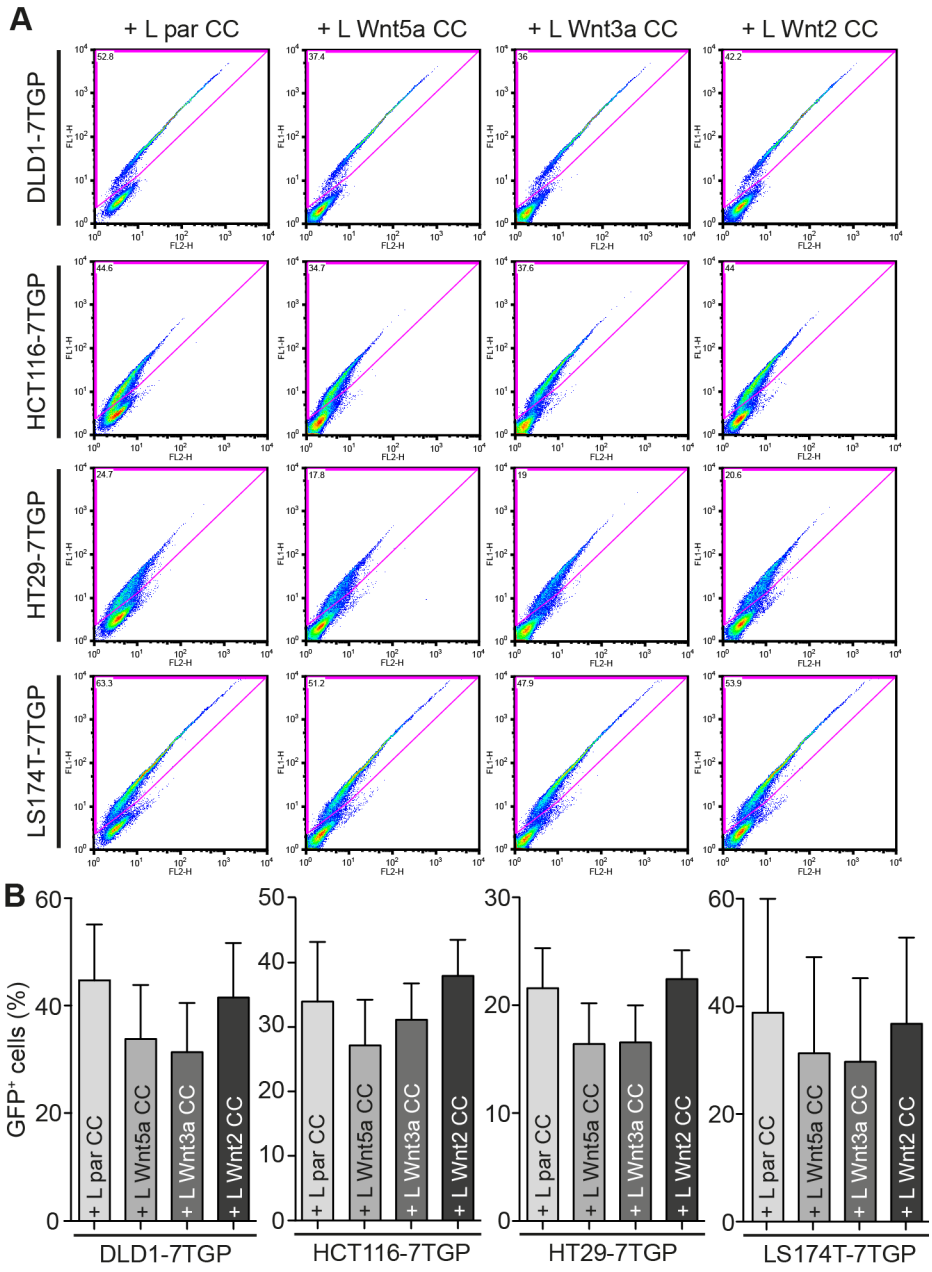

Figure 20 Co-cultures of 7TGP reporter cells with L cells

A Dot plots illustrate co-cultivation of different 7TGP reporter tumor cells with different Wnt ligand expressing L cells. **B** Bar charts of the FACS data; bars represent mean values and whiskers indicate standard deviation (n=3).

Autocrine effects of Wnt2 on fibroblasts

Our next goal was to determine the autocrine effects of Wnt2 on fibroblasts. Therefore canonical and non-canonical Wnt pathway activation and phenotypical parameters, like apoptosis, proliferation, migration and invasion were assessed in the presence or absence of Wnt2. Furthermore we were interested if autocrine Wnt2 alters the differentiation status of fibroblasts.

Wnt2 and canonical Wnt signaling activation

First we tested whether Wnt2 activates canonical Wnt signaling in fibroblasts. Therefore we used the same 7TGP reporter construct as described above. Immortalized human foreskin fibroblasts BJ1 and CCD18-Co colon myofibroblasts were transfected with the 7TGP reporter vector, selected with puromycin for 2 days. The reporter cells (designated BJ1-7TGP, CCD18Co-7TGP) were incubated with conditioned medium from mouse L cells expressing different Wnt ligands (L Wnt5a, L Wnt3a, L Wnt2) and parental L cells (L par) as control. After 72 hours cells were harvested by trypsinization and fluorescence was measured via flow cytometric analysis. Experiments were carried out in three independent experiments. One representative experiment is depicted in **Figure 21A**. All mean values of the three measurements are shown (**Figure 21B**). BJ1-7TGP cells alone display no endogenous activation of canonical Wnt signaling (**Figure 21A** and **B**). As expected, conditioned medium of the control L par cells and L Wnt5a could not activate the reporter gene. While 88.6 % of the reporter cells induced GFP expression upon Wnt3a conditioned medium ($p<0.0001$), Wnt2 conditioned medium had no effect on GFP expression in BJ1-7TGP.

In contrast to BJ1 10.4 % of the colon fibroblasts CCD18Co displayed active endogenous Wnt signaling without the addition of any conditioned medium (**Figure 21A** and **B**). However, treatment with Wnt2 resulted in slightly lower percentages (3.3 %) of pathway activation as compared to L par control (4.1 %, **Figure 21A** and **B**). Reduced activation upon L par CM compared to CCD18Co-7TGP cells alone was most likely due to the uptake of nutrients and release of metabolic byproducts of the L cells during conditioning of the medium. Wnt5a was able to reduce the number of GFP positive cells to 1.21 % by inhibiting canonical Wnt signaling as described in the literature [16]. In contrast Wnt3a conditioned medium significantly induced reporter activation in 99,36 % of CCD18-Co cells ($p=0.0005$).

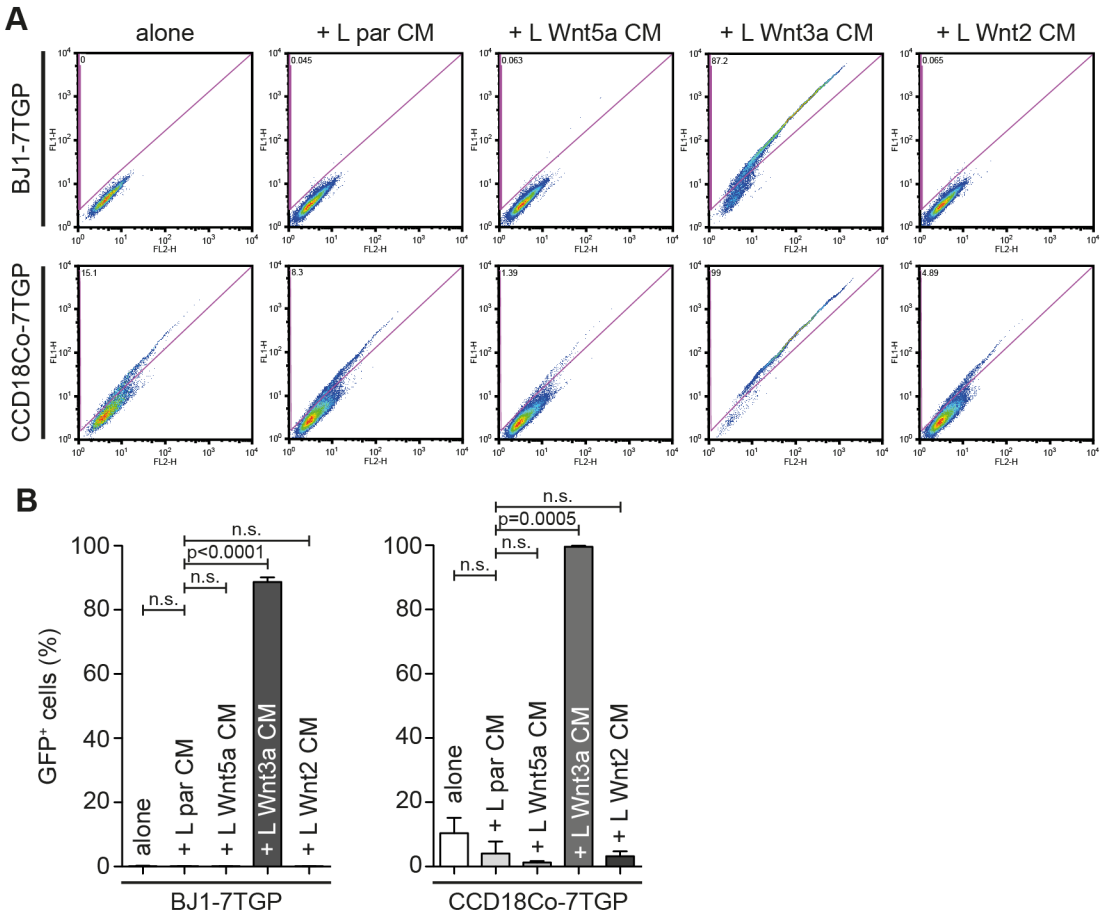

Figure 21 Treatment of 7TGP reporter cells with conditioned medium
A FACS results of BJ-1 7TGP cells (upper panel) and CCD18Co 7TGP cells (lower panel) incubated with conditioned medium of different Wnt ligand expressing mouse fibroblasts and control fibroblasts. Dot plots illustrate one representative experiment. **B** Graphs present percentages of reporter gene activation (n=3). Error bars indicate standard deviation

In a next experiment we were interested if direct cell-cell contact is necessary for Wnt2 to activate the canonical Wnt signaling pathway. Therefore BJ1-7TGP and CCD18Co-7TGP reporter cells were co-cultivated with L cells expressing different Wnt ligands or parental L cells as control. Cells were cultivated in the same culture vessels for 72 hours, then all cells were harvested by trypsinization and pathway activation was measured using flow cytometric analysis. In this setting the two cell types were analyzed together, precluding a quantitative readout and therefore percentage of reporter activation were lower compared to conditioned medium experiments. Results of BJ1 in co-culture were in concordance with previously collected data (**Figure 21**): L par, L Wnt5a and L Wnt2 cells did not activate canonical Wnt signaling in the BJ1 cells (**Figure 22A** and **B**). Whereas a mixture of both, BJ1 and L Wnt3a cells, resulted in the appearance of GFP positive BJ1 cells (p=0.0013).

Co-cultivation of CCD18Co-7TGP reporter cells with L par cells resulted in 3.3 % of GFP positive cells (**Figure 22A** and **B**). L Wnt5a cells mixed with CCD18Co-7TGP cells resulted in reduced pathway activation (1.1 %) as compared to control L par cells. As anticipated Wnt3a expressing fibroblasts activated 7TGP reporter cells in co-culture (24.4 %, p=0.0014). Most interestingly the co-culture setting with L Wnt2 cells led to canonical Wnt pathway activation in CCD18Co cells (13.3 % GFP^+, p=0.0015). These data suggest that direct cell-cell contact is needed for Wnt2 mediated activation of canonical Wnt signaling and that it is only activated in colon fibroblasts but not in skin fibroblasts.

Since this experiment could not reveal how many cells responded to Wnt2 and to rule out that the results were influenced by different proliferation of the different L cells the experiment was repeated using cell culture inserts. Therefore the L cells (L par, L Wnt5a, L Wnt3a and L Wnt2) were seeded on the bottom of a porous membrane of a cell culture inserts and CCD18Co reporter cells were cultivated for 72 hours on top of the inserts. The pore size (0.45 µm) of the permeable membrane was selected in a way, which hindered cell migration across the pores, but allowed direct cell-cell contact between the reporter and the producer cells. After the 72 hours of co-incubation the CCD18Co reporter cells residing in the upper part of the inserts were selectively typsinized and evaluated via flow cytometry analysis (**Figure 22C**). In this experiment 4.8 % of CCD18Co-7TGP cells express GFP upon endogenous activation of canonical Wnt signaling. Selective trypsinization revealed that with L par cells 5.6 % of the CCD18Co reporter cells were activated. With L Wnt5a cells the number of GFP positive cells was reduced to 4.3 %, whereas co-culture with Wnt3a led to 94.2 % of cells with activated signaling. Co-cultivation of L Wnt2 cells with CCD18Co-7TGP cells induced pathway activation in 51.4 % of the cell (**Figure 22D**).

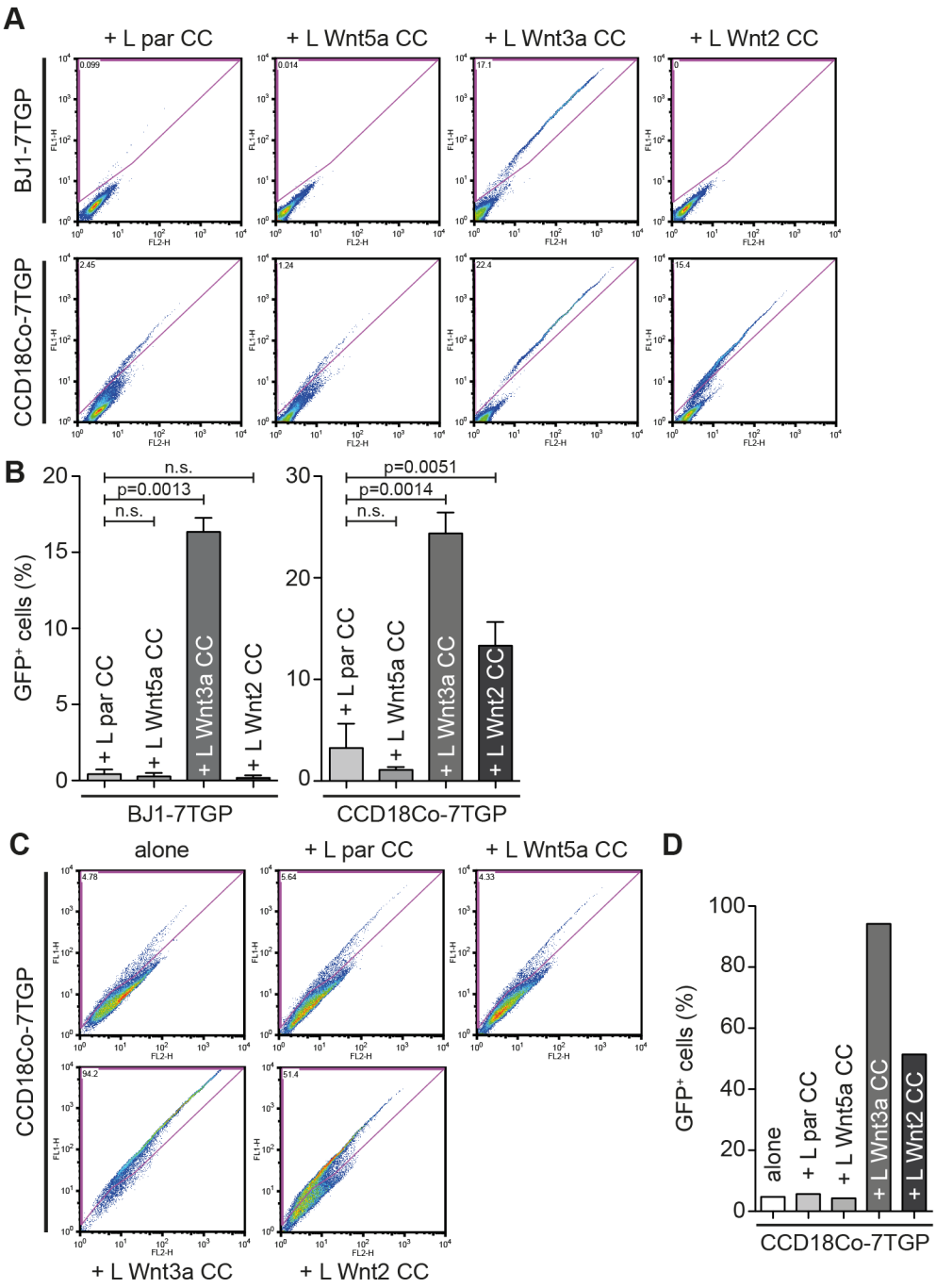

Figure 22 Co-cultures of 7TGP reporter cells with Wnt expressing L cells
A Dot plots in the upper panel illustrate GFP expression (y-axis) versus autofluorescence (x-axis) of BJ1-7TGP cells and CCD18Co-7TGP cells in co-culture with L cells. **B** Bar graphs indicate percentages of GFP means (n=3). Error bars indicate standard deviations. **C** CCD18Co 7TGP cells were co-cultivated with different L cells using cell culture inserts; CCD18Co were selectively harvested and analyzed. **D** Percentages of reporter cell activation after co-culture using co-culture inserts are shown (n=1)

To verify the results of the reporter gene assay we aimed to visualize the translocation of β-catenin to the nucleus upon activation of canonical Wnt signaling via immunofluorescence staining. Therefore CCD18-Co and different L cells (par, Wnt5a,

Wnt3a, Wnt2) were co-cultured in chamber slides. Cells were fixed after 72 hours cells and the human colonic fibroblasts CCD18Co were stained with a vimentin antibody (**Figure 23A**, red) that specifically recognizes human vimentin to distinguish the human from the mouse fibroblasts. Furthermore cells were stained with a β-catenin antibody (**Figure 23A**, green) and DNA was counterstained with DAPI (**Figure 23A**, blue). Pictures were acquired using a confocal microscope using the same optical section thickness, gain and exposure time. The intensity of β-catenin staining within the nucleus and the cytoplasm was quantified. Grey values of the cytoplasm were defined as basal levels and therefore subtracted from grey values of the nucleus in order to visualize the increase of β-catenin in the nucleus compared to the cytoplasm. Data of the immunofluorescence staining confined the results of the reporter gene assay (**Figure 22C** and **D**). CCD18Co cells alone displayed endogenous canonical Wnt signaling (**Figure 23A** and **B**) and nuclear β-catenin fluorescence was set to 1 arbitrary units (a.u.); ratios of the other conditions were plotted. Co-culture of L par cells with CCD18Co resulted in almost the same nuclear β-catenin intensity (1.2 a.u.). With L Wnt5a the amount of nuclear β-catenin was reduced to 0.5 a.u., whereas co-cultivation with Wnt3a resulted in almost 10-fold higher nuclear β-catenin levels compared to results of co-culture with L par cells, which is in good accordance to the reporter assay data. Wnt2 expressing cells induced nuclear β-catenin levels 3.3 fold in the CCD18Co cells. Differences of L Wnt5a, L Wnt3a and L Wnt2 co-cultures were highly significant ($p<0.0001$) compared to co-cultures with L par cells.

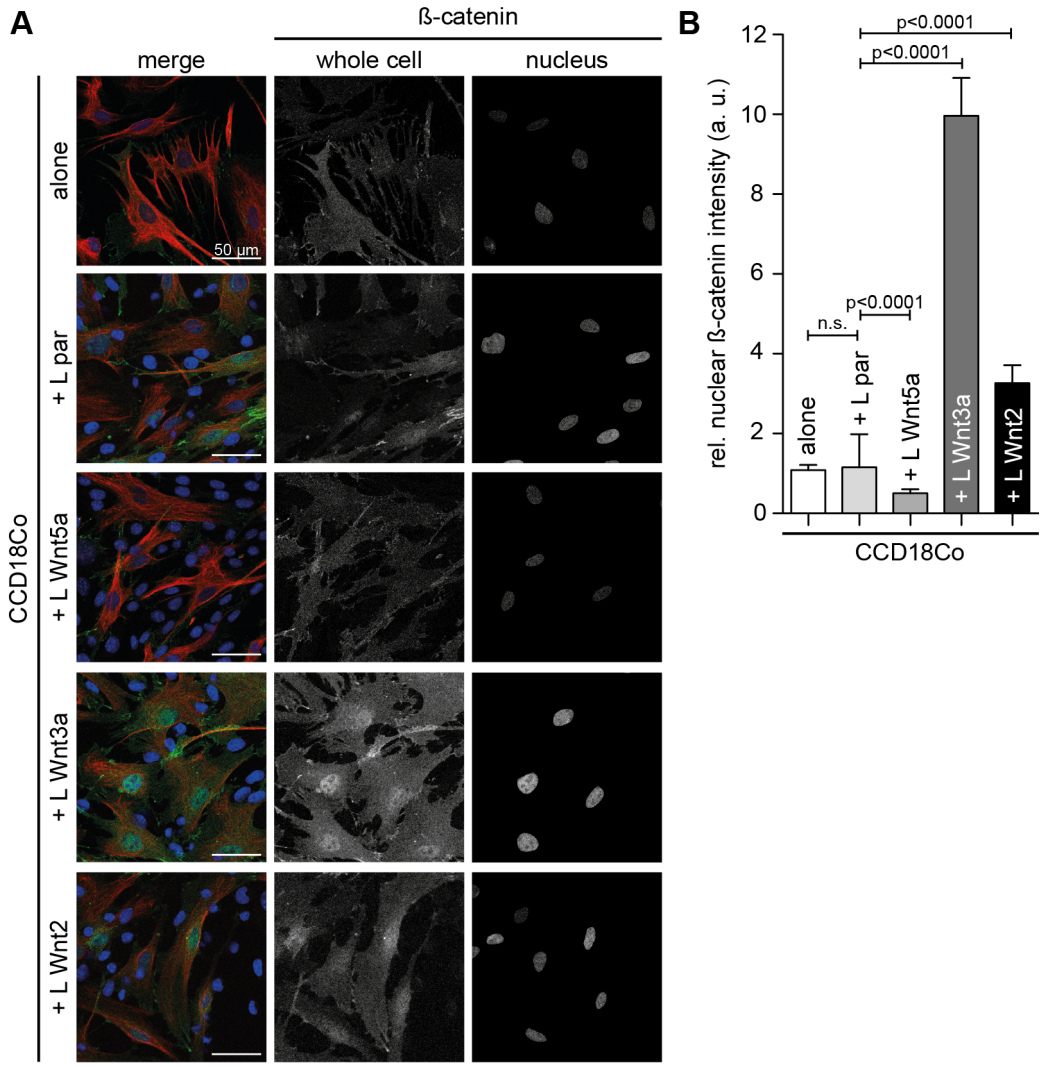

Figure 23 β-catenin nuclear translocation in CCD18Co upon co-culture with L cells expressing different Wnt ligands.
A CCD18Co were co-cultivated with different Wnt ligand expressing mouse L cells (L Wnt5a, L Wnt3a, L Wnt2) and control L cells (L par). Cells were fixed and stained with an α-β-catenin antibody (green) and an α-human vimentin antibody (red), nuclei were counterstained with DAPI (blue). β-catenin expression within the nuclei was visualized in new pictures; scale bars represent 50 µm. **B** β-catenin intensity in the nucleus was subtracted from the intensity in the cytoplasm. The condition without L cells was set to 1 and ratios for the other conditions were calculated. Bars indicate mean nuclear β-catenin intensity in arbitrary units (a.u.); error bars indicate standard deviation (alone n=54 cells; + L par n=69 cells; + L Wnt5a n=56 cells; + L Wnt3a n=59 cells; + L Wnt2 n=70 cells). **C** Whole cell lysates of CCD18Co either co-cultivated with L par or L Wnt2 cells using co-culture inserts; cell lysates of CAF3 after siRNA mediated Wnt2 KD.

So far, all previous experiments were carried out using Wnt2 over-expressing mouse fibroblasts as Wnt2-producer cells therefore we were interested whether endogenous Wnt2 of CAF3 are sufficient to induce canonical Wnt signaling in the colonic fibroblasts as compared to the corresponding NCF3, which did not express WNT2 mRNA. For this CCD18Co-7TGP reporter cells were co-cultivated with the same number of NCF3 and CAF3 and reporter gene activation was measured via flow cytometric analysis (**Figure**

24A and **B**). In line with our previous findings the mixture of NCF3 and CCD18Co-7TGP contained 4.3 % of GFP positive cells. In contrast, co-culture of CCD18Co-7TGP with CAF3 yielded 15.3 % of positive cells. This result demonstrated that the endogenous Wnt2 expression in the CAF3 is sufficient to drive canonical Wnt signaling activation.

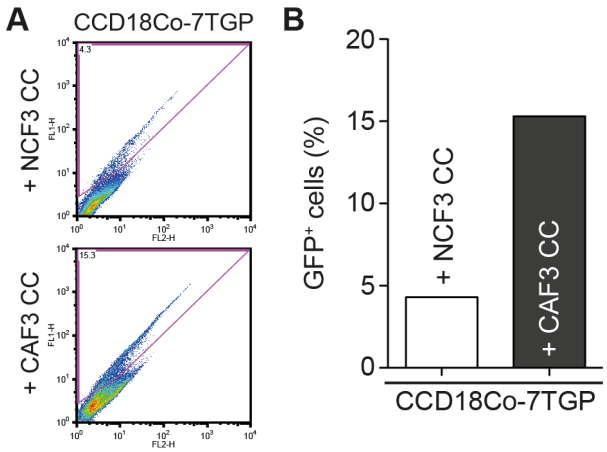

Figure 24 CAF3 as a source for Wnt2 signaling
A Dot plots show reporter gene activation of CCD18Co 7TGP cells upon co-cultivation with NCF3 and CAF3, respectively. **B** Amounts of GFP positive cells are presented as bar chart (n=1).

Taken together, we could demonstrate that Wnt2 activated canonical Wnt signaling solely in colonic fibroblasts and only upon direct cell-cell contact. The expression of Wnt2 in CAF3 was sufficient to activate canonical signaling in reporter fibroblasts, indicating that autocrine Wnt2 activates canonical Wnt signaling in cancer-associated fibroblasts.

Wnt2 and non-canonical Wnt pathway activation

The non-canonical Wnt pathway is comprised of the planar cell polarity pathway (PCP pathway) and the Wnt/calcium pathway. Both pathways function through β-catenin independent mechanisms and are activated by non-canonical Wnt ligands [494]. In order to assess the ability of Wnt2 to activate the non-canonical Wnt/PCP signaling pathway a luciferase reporter vector was used. This reporter contains three AP1 canonical binding sites (TGACTCA) upstream of a minimal promoter fragment comprising a TATA box. The vector was previously described [482, 495]. First, proper reporter activation upon stimulation of AP1 dependent target gene transcription was verified. Therefore CCD18Co cells were transfected with the AP1 reporter plasmid (CCD18Co-AP1). After starvation for 12 hours cells were treated for 6 hours with 20 ng/mL PDGF-BB a potent activator of AP1 dependent transcription [496]. Cells were then lysed and luciferase activity was measured. CCD18Co-AP1 reporter cells showed 1.75 fold induced AP1 activity upon PDGF-BB treatment (**Figure 25A**). Next CCD18Co-AP1 reporter cells were co-cultivated with either L par or L Wnt2 cells for 48 hours and 56 hours to assess if Wnt2 mediated signaling enhances AP1 dependent target gene transcription. Reporter cells and L cells were simple co-cultivated, since the mouse fibroblasts do not express any luciferase. After 48 hours of co-culture with Wnt2 expressing L cells increased reporter activity was detected, though this result was not significant (**Figure 25B**). However, 56 hours of co-culture revealed a 8-fold induction of AP1 dependent target gene transcription compared to L par co-cultures (**Figure 25C**). This induction seems to be a secondary effect of Wnt2, since the luciferase expression appeared relatively late. Co-culture experiments with NCF3 and CAF3, in order to test endogenous Wnt2 potency to activate AP1 dependent target gene transcription, resulted in twofold increased luciferase expression upon co-culture with CAF3 compared to NCF3 controls (**Figure 25D**).

In summary we could show that Wnt2 activates AP1 dependent target gene transcription after long-term co-culture using Wnt2 over-expressing cells and cells with endogenous Wnt2. This activation of AP1 dependent transcription is likely due to a secondary effect of Wnt2 inducing non-canonical Wnt signaling.

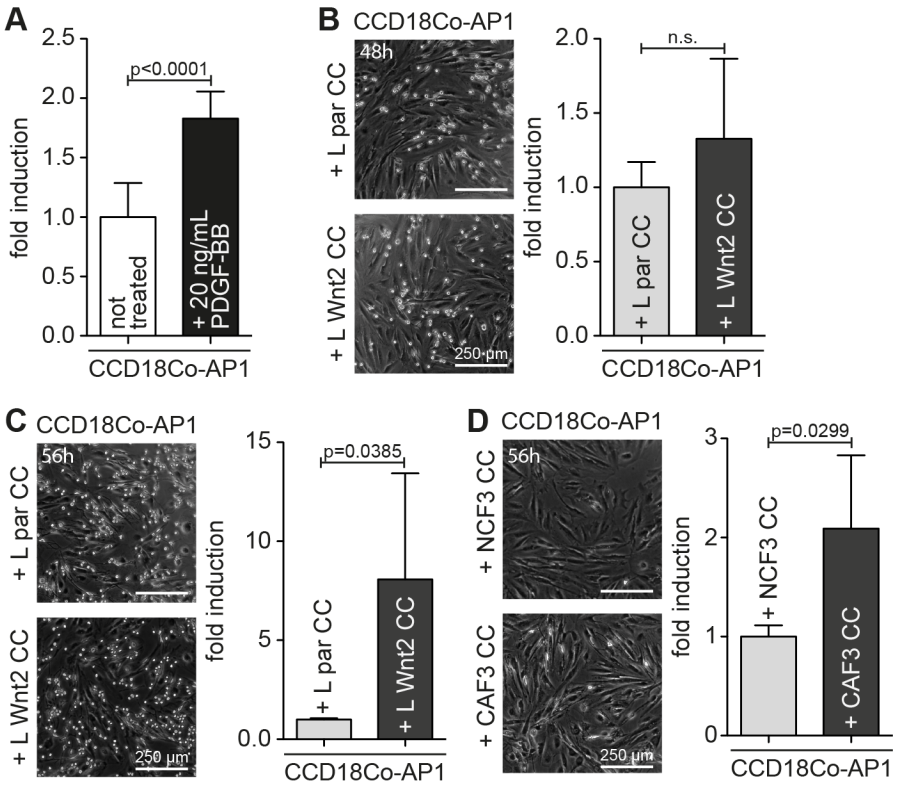

Figure 25 Wnt2 activates AP1 dependent transcription after long-term co-culture
CCD18-Co were bulk-transfected with AP1 reporter plasmid, seeded, starved over night and were either treated with 20 ng/mL PDGF-BB or co-cultured with L par, L Wnt2, NCF3 or CAF3, respectively; Cell lysates were harvested and luciferase activity was measured; Untreated conditions were set to one and fold induction was calculated; Data was collected from independent transfections, measured in duplicates. **A** AP1 reporter plasmid was checked for functionality; CCD18Co-AP1 were incubated with 20 ng/mL of PDGF-BB for 6 hours (n=6). **B, C** CCD18Co-AP1 were either co-cultivated with L par or L Wnt2 cells and were incubated for 48 hours (**B**, n=6) or for 56 hours (**C**, n=4). **D** CCD18Co-AP1 cells were seeded with NCF3 or CAF3, respectively and were analyzed after 56 hours (n=4). Images show one representative experiment (scale bar illustrate 250 µm). Data are presented as bar charts; whiskers indicate standard deviation.

The effect of Wnt2 on the phenotype of fibroblasts

Next we wanted to assess if treatment with Wnt2 or the KD of Wnt2 has any effect on phenotypical parameters of stromal fibroblasts. Therefore we analyzed caspase-3/7 activity as a read-out for apoptosis, EdU incorporation to determine proliferation effects, the migratory and invasive potential of fibroblasts either over-expressing Wnt2, co-cultivated with Wnt2 expressing cells or after siRNA mediated Wnt2 KD.

Apoptosis

In order to evaluate the effect of Wnt2 on apoptosis, we used the Apo-ONE® Homogeneous Caspase-3/7 Assay from Promega. This assay measures active caspase-3 and caspase-7 using a profluorescent consensus substrate rhodamine 110 bis-(N-CBZ-L-apartyl-L-glutamyl-L-valyl-aspartic acid amide) (Z-DEVD-R110), which can be cleaved by caspase-3/7.

To assess caspase-3/7 activity BJ1-GFP and BJ1-Wnt2 cells were seeded in 96-well plates and analyzed after 16 hours. BJ1 Wnt2 displayed no change of apoptosis compared to GFP controls (**Figure 26A**). As positive controls BJ1 were treated with 1 µM of the apoptosis inducer staurosporine for 3 hours. CCD18Co were co-cultivated with either L par or L Wnt2 cells for 72 hours using cell-culture inserts. The measured fluorescence of CCD18Co either co-cultivated with L par or L Wnt2 cells showed no differences (**Figure 26B**). In CAF3 Wnt2 was KD by siRNA and after 72 hours Wnt2 KD and NTC cells were seeded in 96-well plate for ApoOne measurement. As positive controls CCD18Co and CAF3 were treated with 0.5 µM of staurosporine for 2.5 hours and 3 hours, respectively to induce apoptosis [497]. Similarly, the KD of Wnt2 in CAF3 had no effect on apoptosis compared to NTC transfected CAFs (**Figure 26C**). Staurosporine treated controls showed high caspase-3/7 activities.

These results indicate that Wnt2 does not change apoptosis in fibroblasts.

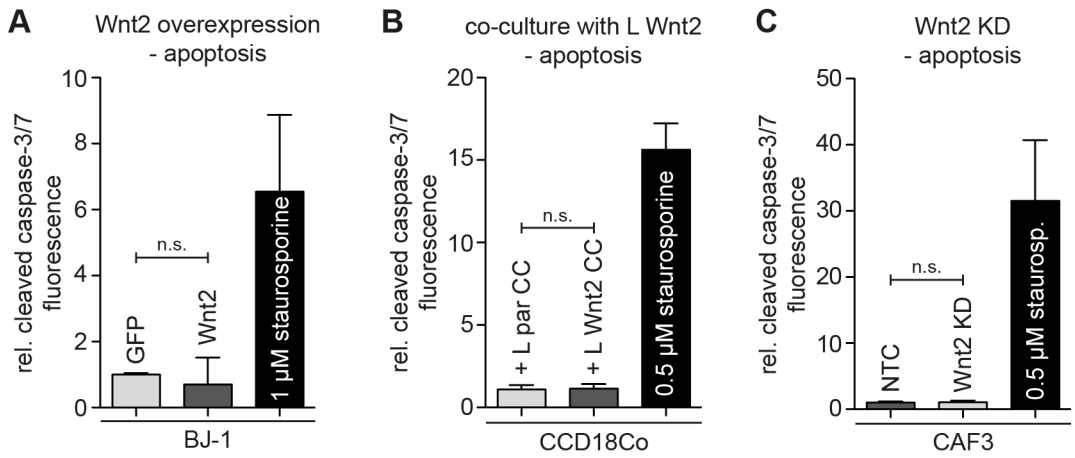

Figure 26 Assessment of apoptosis by measurement of caspase-3/7 activity

A BJ-1 GFP and BJ-1 Wnt2 cells were analyzed for caspase-3/7 activity 16 hours after seeding; as a positive control BJ-1 cells were incubated with 1 µM of staurosporine for 3 hours. **B** CCD18-Co were co-cultivated with L par and L Wnt2 cells, respectively using co-culture inserts; after 72 hours CCD18-Co were seeded and after additional 16 hours of incubation cleaved caspase-3/7 activity was measured; for positive controls CCD18-Co were incubated with 0.5 µM of staurosporine for 2.5 hours. **C** 72 hours after siRNA mediated Wnt2 KD in CAF3 cells were seeded and activity of cleaved caspase-3/7 was measured 16 hours later; CAF3 were treated with 0.5 µM of staurosporine as positive control for 3 hours. Data were derived from three biological replicates, measurements were done in duplicates (n=6); bars indicate mean values and error bars illustrate standard deviations.

Proliferation

Cell cycle distribution was measured using the Click-iT® EdU Alexa Fluor® 647 Flow Cytometry Assay Kit from Invitrogen. To measure EdU incorporation BJ1-GFP and BJ1-Wnt2 cells were seeded in tissue culture plates and were incubated for 72 hours 37 °C. At this point cells had not reached confluency as demonstrated by light microscopy (see images of **Figure 27A**). CCD18Co were co-cultivated with L par or L Wnt2 cells for 72 hours. CAF3 NTC and Wnt2 KD cells were reseeded 72 hours after conducting KD in new culture vessels and further incubated for additional 72 hours. After EdU incorporation (10 μM final concentration) for one hour cells were processed for flow cytometric analysis. To distinguish CCD18Co cells from the mouse L cells the colon fibroblasts were stained with a human specific vimentin antibody and positive cells were gated before assessment of EdU incorporation. Cells being in G1, S and G2/M-phase were quantified using flow cytometric analysis. Cells were counterstained with propidium iodide for DNA content analysis. In BJ1-Wnt2 G1-phase percentage was decreased, whereas S- and G2/M-phase fractions were elevated. However, these results were not significant. (**Figure 27A**). CCD18Co upon co-cultivation with Wnt2 producing cells showed no changes in G1, S and G2/M-phase compared to co-culture with L par cells (**Figure 27B**). Also Wnt2 KD in CAF3 had no influence on cell cycle distribution (**Figure 27C**).

These data clearly demonstrate that expression of Wnt2 does not affect cell cycle distribution and hence proliferation in fibroblasts.

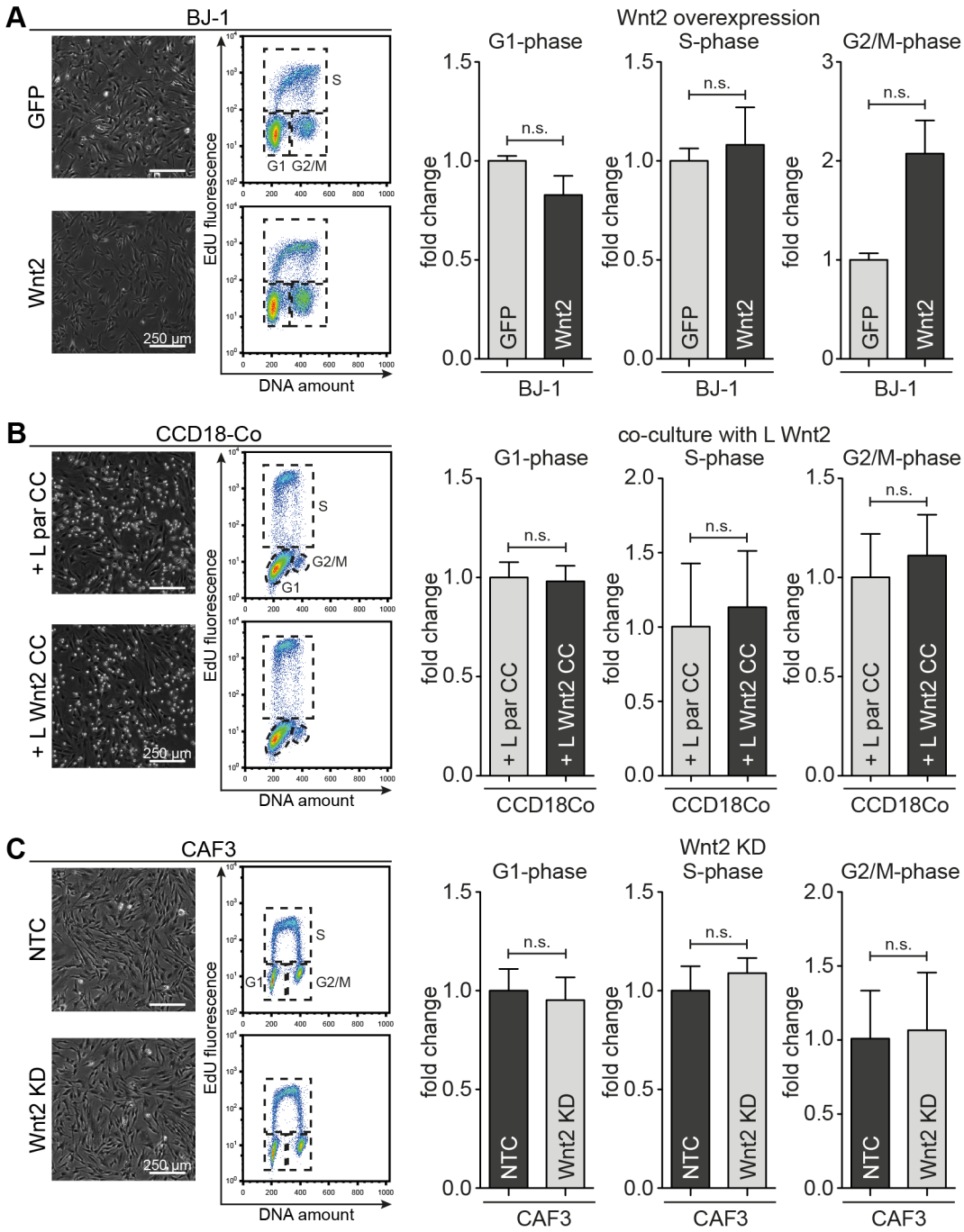

Figure 27 Wnt2 has no effect on cell cycle progression in fibroblasts
Cells were incubated with 10 µM EdU for one hour, fixed and incorporated EdU was labeled with a fluorescent dye azide that was measured via FACS analysis; in co-culture conditions CCD18-Co were stained with an α-vimentin antibody prior to the click-it reaction. **A** Cell Cycle analysis of BJ-1 GFP and BJ-1 Wnt2 cells. **B** Co-culture of CCD18-Co with L Wnt2 cells for 48 hours. **C** Comparison of CAF3 NTC and CAF3 Wnt2 KD 48 hours after reseed. Brightfield images and FACS dot plots show one representative experiment, scale bars illustrate 250 µm; bars indicate mean values of three biological replicates and error bars represent standard deviation.

Migration

Next we determined the migratory potential of fibroblasts in different culture conditions in transwell migration assays. Cells were seeded on the porous membrane of the upper chamber in serum- and growth factor-free medium. The lower chamber contained complete growth medium [498]. The growth factor gradient acted as a stimulus to trigger cell migration toward the serum-rich compartment. Our intent was to measure if the expression, co-cultivation or the KD of Wnt2 influences the migratory capacity of the fibroblasts toward the growth factors. Therefore BJ1-GFP and BJ1-Wnt2 were seeded on top of the membrane and were incubated for 22 hours. CCD18Co were co-cultivated with L par and L Wnt2 cells using co-culture inserts for 72 hours, thereafter CCD18Co were harvested and seeded in the top chambers, where they were incubated for 22 hours at 37 °C. CAF3 were used for siRNA mediated Wnt2 KD, NTC siRNA served as control. 72 hours post-transfection cells were seeded in the chamber and incubated for 22 hours in the incubator at 37 °C. After incubation non-migrated cells in the upper compartment of the transwell insert were removed, membranes were fixed and migrated cells were stained with crystal violet. Membrane coverage was measured and plotted. BJ1-GFP and BJ1-Wnt2 displayed no difference (**Figure 28A**). CCD18Co upon co-cultivation with Wnt2 expressing fibroblasts showed a tendency of higher migratory potential compared to co-culture with control fibroblasts, although this results was not significant (**Figure 28B**). This could possibly be explained by the fact that CCD18Co already express low levels of endogenous Wnt2 that was already sufficient to induce a migratory phenotype and that exogenous Wnt2 could not enhance its pro-migratory effect. However, more importantly in CAF3 we found that a Wnt2 KD led to significantly ($p>0.0001$) decreased migration compared to NTC transfected cells (**Figure 28C**).

Taken together, these data clearly indicate that Wnt2 has a pro-migratory effect on cancer-associated fibroblasts.

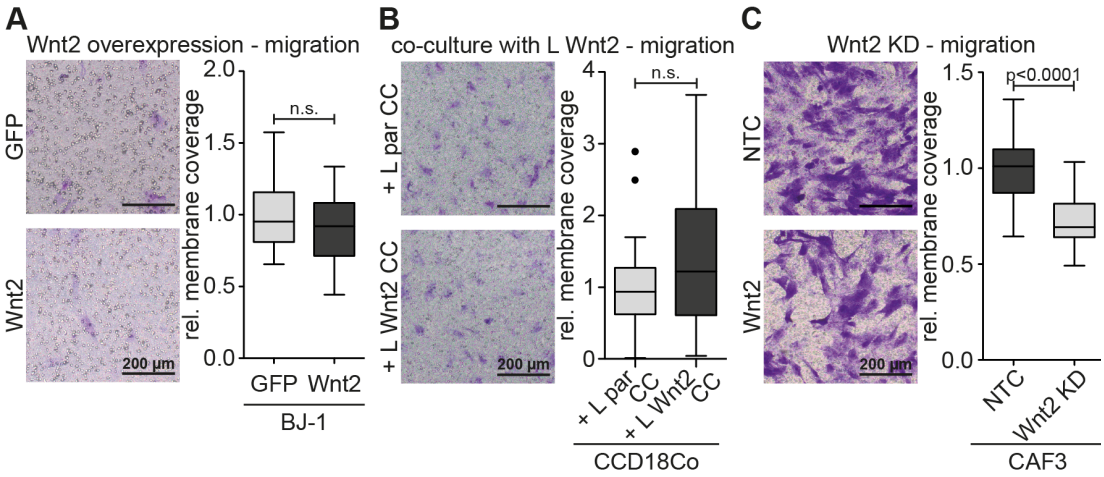

Figure 28 Effects of Wnt2 on fibroblast migration

Cells were seeded at a density of 25,000 cells per transwell chamber in serum- and supplement-free medium; lower chambers contained complete growth medium; 22 hours after seeding non-migrated cells on the upper surface of the porous membrane were removed, cells were fixed and stained with crystal violet. **A** Comparison of BJ-1 GFP and BJ-1 Wnt2 cells. **B** CCD18-Co and either L par or L Wnt2 cells were co-cultivated using co-culture inserts for 72 hours; CCD18-Co were seeded in transwell chambers afterwards. **C** CAF3 NTC and CAF Wnt2 KD cells were compared. Data were collected from three independent experiments that were carried out in duplicates (n=6); membrane coverage was calculated by measuring crystal violet positive area with ImageJ; scale bars represent 200 µm; data is presented in Tukey box plots, center line indicate the median, the box represents the IQR and whiskers present the 1.5 fold extension of the IQR, dots present outliers.

Invasion

Invasion assays were performed with CAF3 after siRNA mediated Wnt2 KD, since there was no effect on migration in BJ1 Wnt2 compared to GFP controls and the effect of co-culture of CCD18Co with L Wnt2 cells was not enough to clearly see a pro-migratory phenotype. A spheroid invasion assay was used to assess invasive potential of CAF3 72 hours after conducting Wnt2 KD. Therefore cells were aggregated to spheroids within 6 hours of incubation using v-shaped 96-well plates. Then spheroids were harvested and embedded into a collagen I matrix. Images were taken after polymerization of the collagen gel and after 16 hours of incubation. Within this time the fibroblasts invaded the surrounding ECM and displayed astral outgrowth. The number and invasion deepness of invasive structures were measured using ImageJ. CAF3-Wnt2 KD cells displayed a higher variety in the number of structures per spheroid than compared to NTC spheroids (**Figure 29A**), however the mean number of structures were comparable. Assessment of outgrowth length per spheroid revealed that upon Wnt2 KD complete outgrowth length was significantly reduced (p=0.0001) compared to NTC spheroids.

These results clearly demonstrate that Wnt2 induces the invasive capacity of colonic CAFs.

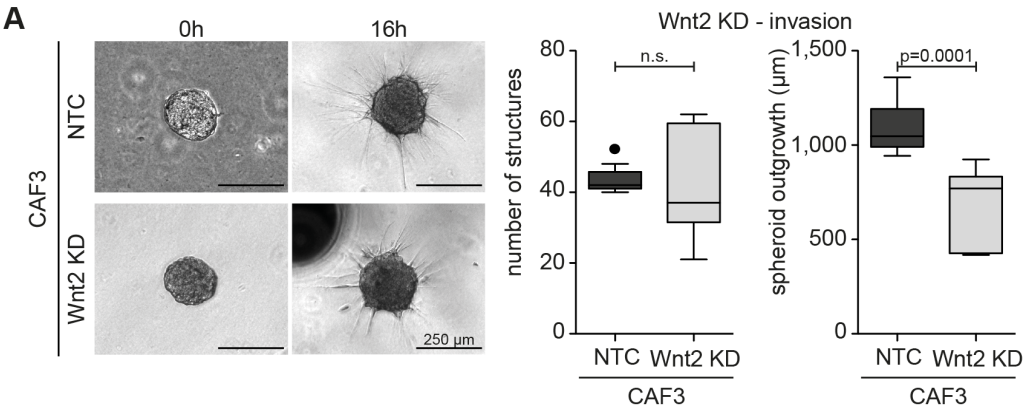

Figure 29 Effects of Wnt2 on CAF invasion
Spheroid aggregation was conducted by seeding either 1,500 CAF3-Wnt2 KD cells or 1,500 CAF3-NTC cells in v-shaped 96-well plates; cells were incubated for 6 hours at 37 °C; spheroids were harvested and embedded in collagen gels; pictures were taken directly after embedding and after 16 hours; invasive structures were evaluated using ImageJ (NTC n=10, Wnt2 KD n=7). Images of representative spheroids are shown, scale bars indicate 250 µm; Data is presented in Tukey box plots, center line indicate the median, the box represents the IQR and whiskers present the 1.5 fold extension of the IQR, dots present outliers.

Effect of Wnt2 on organotypic co-culture

We could show that Wnt2 KD alters the invasion capacity of CAF3, therefore we were interested if Wnt2 has also an impact in an organotypic co-culture model of fibroblasts and tumor cells, since Gaggioli et al demonstrated that fibroblasts have a leading role for squamous cell carcinoma collective invasion by generating tracks in the ECM [499]. Therefore BJ1 either Wnt2 or GFP over-expressing fibroblasts and CAF3 Wnt2 KD and NTC cells, respectively were embedded in collagen gels. When fibroblasts contracted and remodeled the collagen, DLD1 tumor cells were seeded on top of the gels. After proper cell attachment gels were transferred to metal grids to establish an air-liquid interface between the collagen gel and the tumor cells. Gels were incubated for three weeks in the incubator. They were then fixed in 4 % PFA and dehydrated in 70 % of ethanol. For better handling purpose gels were embedded in agarose gels, which were then embedded in paraffin. Collagen gels were cut in 5 µm sections using a microtome and every 5th section was H&E stained. Pictures of every section were acquired and number and area of invasive structures were evaluated. DLD1 tumor cells displayed only few invasive structures in the presence of BJ1 cells (**Figure 30A**). Expression of Wnt2 had no effect on tumor cell invasion compared to GFP expressing controls. Also the mean invasive area was not changed. However, the presence of colonic CAF3 fibroblasts led to increased invasion of tumor cells in contrast to co-cultures with the dermal fibroblasts BJ1 (**Figure 30B**). CAF3 after siRNA mediated Wnt2 KD displayed less invasive structures compared to CAF3 NTC transfected controls. Interestingly, mean invasive area was not altered, indicating that Wnt2 KD had only an effect on the number of invasive structures, not the size.

In summary, we could show that Wnt2 had an impact on tumor cell invasion, but only in the presence of colonic fibroblasts.

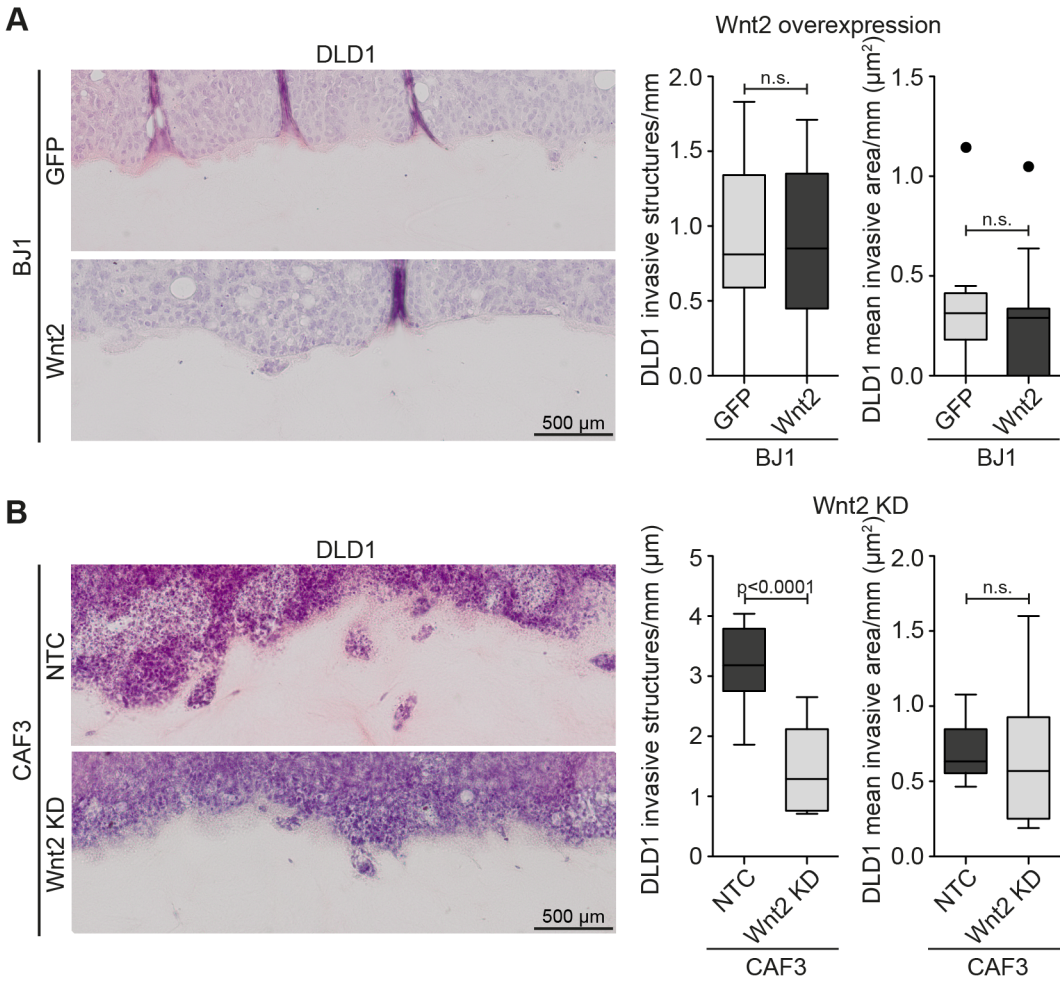

Figure 30 Decreased collective tumor cell invasion upon co-culture with CAFs harboring Wnt2 KD

BJ1 GFP and Wnt2 over-expressing fibroblasts (**A**) or CAF3 after siRNA mediated Wnt2 KD (**B**) were embedded in collagen gels; after contraction and remodeling of the ECM by the fibroblasts DLD1 tumor cells were seeded on top of the gels; they were transferred to a grid to establish an air-liquid interphase; gels were incubated for 14 days, fixed, sectioned and H&E stained; experiments were carried out in triplicates (BJ1) or in duplicates (CAF3); invasive structures of 5 sections per gel were counted and mean area was calculated; data was illustrated as Tukey box plots (BJ1 GFP and Wnt2 n=15, CAF NTC and Wnt2 KD n=10); scale bar indicate 500 µm.

Defining a Wnt2 fibroblast phenotype

So far we could provide evidence that Wnt2 has an impact on migration and invasion capacities of CAFs and that Wnt2 promotes cancer cell invasion in an organotypic assay. Furthermore it is well established that canonical Wnt signaling plays an important role in maintaining stemness in embryonic stem cells [500], neuronal stem cells [500], epithelial cells [356, 501] and in mesenchymal stem cells [502]. Therefore our next intent was to assess if Wnt2 alters the differentiation status of fibroblasts by testing a set of markers for mesenchymal stem cells (CD34 [503], THY1 [504], ENG [505]), activated fibroblasts (CD44 [505, 506], FAP [491, 492]) and smooth muscle cell-myofibroblast marker (PDGFRA [507], ACTA2 [508, 509], MKL2 [510, 511], TAGLN [512]). Furthermore we analyzed expression of FGF10, since Wnt2 was shown to regulate FGF10 in the developing mouse lung [307] and of PDGFRB, which is present in colorectal tumor stroma [513]. Expression of the above mentioned molecules was determined at the mRNA level. RT-qPCR was used to assess differences between CAFs and normal fibroblasts of the same patient (**Figure 31A**). Effects of Wnt2 were analyzed by co-cultivating CCD18Co with L par or L Wnt2 cells, respectively (**Figure 31B**) and by conducting Wnt2 KD in CAF3 (**Figure 31C**). The mesenchymal stem cell markers CD34 and THY1 were significantly increased in CAF3 compared to NCF3, however ENG was not regulated (**Figure 31A**). Co-cultivation of CCD18Co with Wnt2 did not significantly induce CD34 and THY1 transcription, although a tendency of increased mRNA level was visible. ENG was not induced (**Figure 31B**). Wnt2 KD in CAF3 resulted in slightly decreased mRNA levels of CD34 and THY1, compared to NTC siRNA. In contrast to co-culture with Wnt2, where ENG was not regulated, Wnt2 KD led to increased ENG expression (**Figure 31C**). These results allowed the assumption that Wnt2 has no significant impact on dedifferentiation of fibroblasts to mesenchymal stem cells.

CD44 and FAP, two markers for activated fibroblasts, were elevated in CAF3 compared to NCF3, however only changes of FAP mRNA were significantly altered (**Figure 31A**). Upon co-cultivation with Wnt2 both markers were increased significantly (**Figure 31B**) and after siRNA mediated Wnt2 KD mRNA levels of CD44 and FAP were significantly decreased (**Figure 31C**), indicating that expression of Wnt2 results in fibroblast activation.

The smooth muscle cell-myofibroblast markers PDGFRA and smooth muscle actin (SMA, ACTA2) were not significantly altered in CAF3 compared to NCF3 (**Figure 31A**).

Co-culture of CCD18Co with Wnt2 expressing fibroblasts resulted in a significant but small decrease of PDGFRA but not of ACTA2 compared to L par co-cultures (**Figure 31B**). However, after Wnt2 KD ACTA2 mRNA was significantly decreased and no changes in PDGFRA mRNA were detectable (**Figure 31C**). MKL2, a marker for smooth muscle cell differentiation, was only marginally increased in CAF3 compared to NCF3 (**Figure 31A**) and co-cultivation of CCD18Co with Wnt2 as well as Wnt2 KD in CAF3 had no effect on MKL2 levels (**Figure 31B** and **C**). However, transgelin (TAGLN) that is expressed from the beginning of smooth muscle cell differentiation, was 14-fold induced compared to NCF3, TAGLN expression almost doubled in CCD18Co upon Wnt2 co-culture and after siRNA mediated KD TAGLN transcription was decreased to nearly 50 % (**Figure 31A-C**). These data strongly suggested that expression of Wnt2 regulates TAGLN expression and drives fibroblasts in a smooth muscle cell-myofibroblast-like phenotype.

Wnt2 was shown to increase FGF10 expression during lung development; interestingly in colon derived CAF3 displayed very low FGF10 mRNA compared to NCF3 cells (**Figure 31A**). In Wnt2 treated CCD18Co FGF10 mRNA decreased to 73 % of the levels in co-culture with L par cells (**Figure 31B**) and intriguingly KD of Wnt2 in CAF3 could induce FGF10 levels to 1.5 fold compared to NTC siRNA transfected CAF3 (**Figure 31C**). These results demonstrated that Wnt2 had an impact on FGF10 mRNA expression.

PDGFRB mRNA expression was not altered in CAF3 compared to NCF3, after Wnt2 co-culture and upon Wnt2 KD (**Figure 31A-C**), indicating that Wnt2 does not alter PDGFRB mRNA levels in colonic fibroblasts.

In summary, these data suggest that Wnt2 had no impact on fibroblast dedifferentiation. Wnt2 induced markers for activated fibroblasts (CD44, FAP) and heavily induced TAGLN expression, indicating Wnt2 can direct fibroblasts in a more smooth muscle cell-like state.

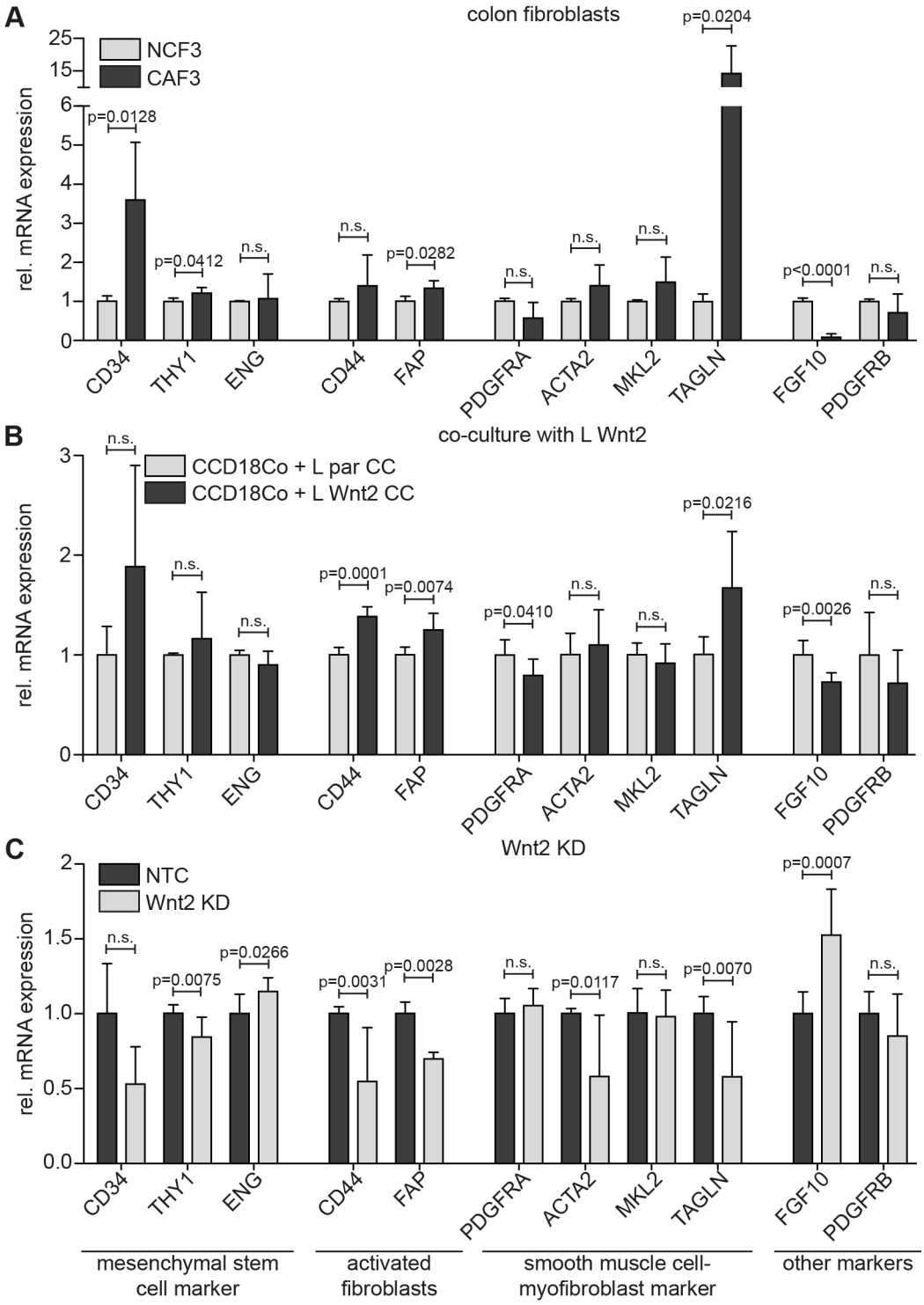

Figure 31 qPCR analysis of fibroblasts in different conditions

mRNA was isolated, reverse transcribed to cDNA and qPCR analysis was performed. **A** NCF3 and CAF3 were harvested 72 hours after splitting; qPCR was carried out from two passages and measured in duplicates (n=4). **B** CCD18Co were co-cultivated for 72 hours with L par or L Wnt2 cells on cell culture inserts and qPCR analysis of three biological experiments were performed in duplicates (n=6) **C** 72 hours after siRNA mediated Wnt2 KD CAF3 were harvested; NTC served as control; four independent KD were analyzed in duplicates (n=8). Data were normalized to GAPDH expression and control conditions were set to 1; bars represent mean values and error bars indicate standard deviation.

TAGLN expression is induced by Wnt2

In the previously described analysis Wnt2 induced mRNA expression of the early smooth muscle cell marker TAGLN (**Figure 31A-C**). In order to verify and further investigate this effect a TAGLN reporter vector was used, whether induction was due to direct transcriptional activation. A promoter fragment from −1031 to +108, relative to the transcriptional start site, was cloned upstream of the firefly luciferase gene to obtain a TAGLN reporter vector [489]. To verify the function of the reporter plasmid CCD18Co transfected with the TAGLN reporter plasmid (CCD18Co-TAGLN) were treated with TGFβ and induction of TAGLN was measured, since Yu et al could show that the TAGLN promoter is a target of TGFβ-/Smad3 dependent gene expression. ACTA2 served as control for proper TGFβ stimulation [514]. qPCR analysis revealed that treatment with 10 ng/mL of TGFβ for 24 hours induced ACTA2 mRNA 10-fold and TAGLN mRNA 12-fold in CCD18Co (**Figure 32A**). This indicated that CCD18Co cells responded properly to TGFβ treatment and induced both ACTA2 and TAGLN as reported in the literature [489]. Next, CCD18Co-TAGLN cells were treated with 10 ng/mL of TGFβ and firefly luciferase activity was measured. Luciferase activity in TGFβ treated CCD18Co-TAGLN reporter cells increased 20-fold to non-treated controls (**Figure 32B**), indicating that the reporter is functional. As a further proof of principle TAGLN reporter cells were incubated with Wnt3a expressing L cells, since it was shown, that Wnt3a induces TAGLN expression [515]. Reporter activation was enhanced twice upon co-cultivation of the CCD18Co-TAGLN reporter cells with LWnt3a cells compared to co-cultures with L par cells (**Figure 32B**). These data indicate that the reporter vector is functional and could be used for studying TAGLN promoter activation.

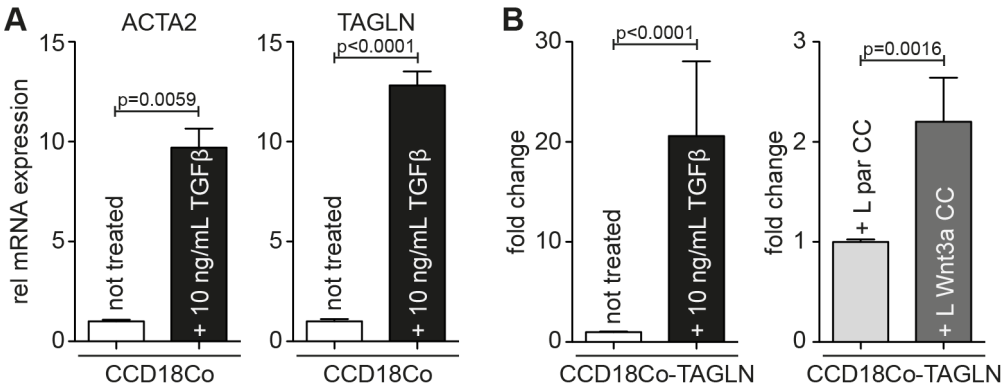

Figure 32 The TAGLN reporter plasmid is functional and displays response to TGFβ and Wnt3a

A CCD18Co were cultivated in the presence or absence of 10 ng/mL TGFβ for 24 hours; ACTA2 and TAGLN mRNA was measured in duplicates via RT-qPCR analysis; Cq values were normalized to GAPDH expression; controls were set to 1, corresponding values were calculated; data of three biological replicates were presented as bar charts (n=6), whiskers indicate standard deviation. **B** Cells were transfected with TAGLN plasmid (CCD18Co-TAGLN), after 24 hours of starvation cells were incubated with or without 10 ng/mL TGFβ or with L par and L Wnt3a cells, respectively for 24 hours; luciferase activity was measured; Control conditions were set to 1 a.u. and fold changes were calculated; three independent experiments were analyzed in duplicates (n=6), whiskers present standard deviation.

In a next step we assessed whether Wnt2 had an impact on the TAGLN reporter. Therefore CCD18Co-TAGLN cells were co-cultivated with either L par or L Wnt2 cells. After 48 hours cells were lysed and firefly luciferase activity was measured. Co-culture with Wnt2 expressing mouse fibroblasts resulted in two-fold induction of reporter activity compared to L par co-culture (**Figure 33A**). This finding verified the results from the qPCR analysis; TAGLN is a target of Wnt2 mediated signaling. Our next intent was to test if the endogenous Wnt2 expression of CAF3 is sufficient to activate TAGLN transcription. Hence, CCD18Co-TAGLN reporter cells were co-cultivated with NCF3 or CAF3. Promoter activity increased two-fold upon co-cultivation with CAF3 compared to NCF3 co-culture (**Figure 33B**), indicating that endogenous Wnt2 expressed in the CAFs could enhance TAGLN expression.

Schafer and Towler found that Wnt3a and TGFβ co-treatment enhanced TAGLN expression in mouse mesenchymal cells [515]. They further found that Wnt1, a known activator of canonical Wnt signaling [294] as Wnt3a, could not increase TAGLN expression in contrast to Wnt3a. Wnt2 had also the ability to enhance TAGLN promoter activity in combination with TGFβ treatment. CCD18Co-TAGLN cells were hence co-cultivated with L par and L Wnt2 cells, respectively either in the presence or absence of 10 ng/mL of TGFβ. Luciferase activity was measured and TGFβ treatment in

combination with L par cells resulted in a slightly but significant increase in TAGLN reporter activation (**Figure 33C**). In contrast combination of Wnt2 and TGFβ resulted in 10-fold increased reporter activation, compared to L par controls, whereas consistent to our previous findings. This dataset provide first evidence for a strong synergistic induction of TAGLN transcription by Wnt2/TGFβ in colon stromal fibroblasts. Wnt2 treatment alone increased luciferase activity by a factor of two.

Taken together, we found that Wnt2 mediates TAGLN expression in colonic fibroblasts, that endogenous Wnt2 in CAF3 is sufficient for TAGLN promoter activation and that Wnt2 signals in cooperation with TGFβ to enhance TAGLN expression.

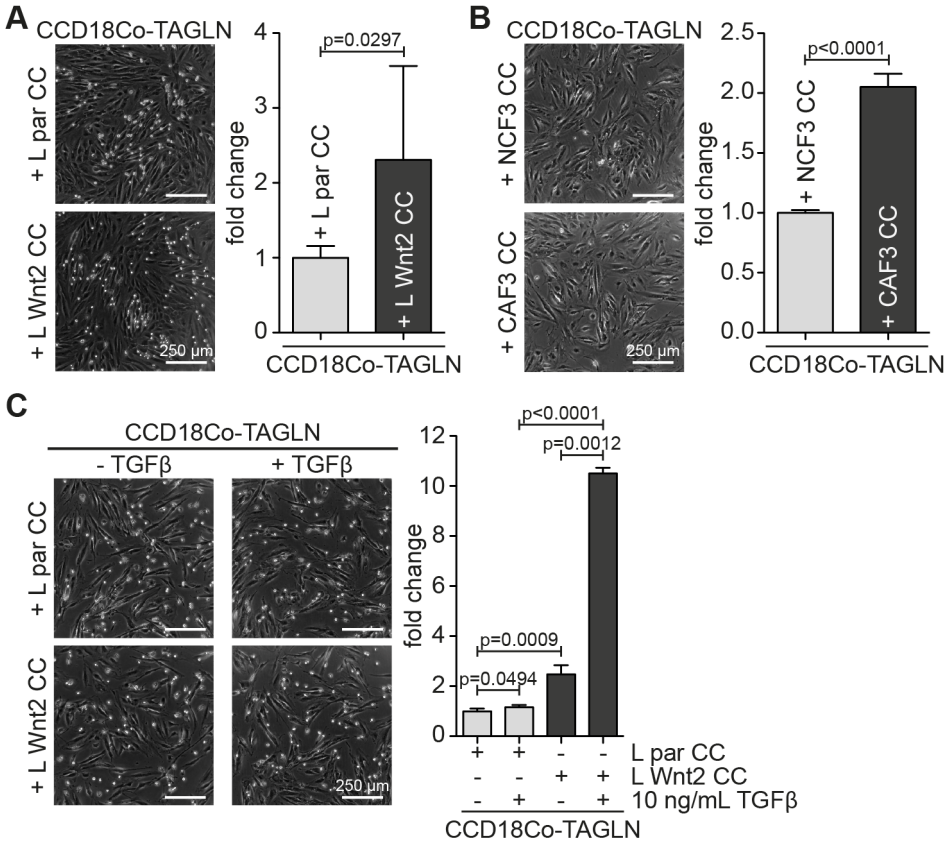

Figure 33 Wnt2 induces TAGLN expression that is potentiated by TGFβ
A CCD18Co-TAGLN cells were starved over night and incubated with either L par or L Wnt2 cells for 48 hours; luciferase activity was measured; Data of three independent experiments (n=6) were collected. **B** CCD18Co-TAGLN cells were starved and co-cultivated with NCF3 and CAF3, respectively for 48 hours; Cell lysates were collected and measured; Three independent experiments were measured in duplicates (n=6). **C** CCD18Co were transfected with TAGLN reporter plasmid and starved for 24 hours; cells were co-cultivated with L par or L Wnt2 cells, respectively either in the presence or absence of 10 ng/mL TGFβ for 16 hours; cells were then lysed and luciferase activity was measured in duplicates of two independent experiments (n=4). Images of representative experiments are shown; scale bars indicate 250 µm; data is presented as bar charts and whiskers indicate standard deviation.

Effect of Wnt2 on cellular senescence

TAGLN was first discovered as a smooth muscle protein that is over-expressed in senescent fibroblasts [516]. Therefore we wanted to test whether expression of Wnt2 has an effect on senescence of fibroblasts. In order to proof this hypothesis we used the senescence associated-β-galactosidase assay (SA-β-gal assay) [517]. The lysosomal hydrolase β-galactosidase cleaves galactose from glycoproteins in non-senescent cells at an optimum pH of 4.0 to 4.5. Its activity can be detected using cytochemical assays at pH 4.0, where X-gal is cleaved by β-galactosidase leading to the formation of blue precipitates [518]. It was found that lysosomal β-galactosidase levels and the overall size of lysosomes increase during senescence. This expansion of lysosomal content allows the detection of β-galactosidase activity even at a suboptimal pH of 6.0 [518] and therefore identifying senescent cells by adding X-gal at a pH of 6.0 [490]. We again made use of our triple fibroblast test system. The non-Wnt2 responsive BJ1 cells with (BJ1-Wnt2) and without (BJ1-GFP) Wnt2 were seeded on chamber slides and fixed after 16 hours. In parallel CCD18Co were co-cultivated with L par or L Wnt2 cells using cell-culture inserts for 72 hours. Thereafter CCD18Co were harvested and seeded on chamber slides, where they were fixed after 16 hours. siRNA mediated gene KD was conducted in CAF3 and 72 hours thereafter Wnt2 KD and NTC cells were harvested and seeded on chambers slides and were fixed as well after 16 hours. Chamber slides were incubated with X-gal staining solution over night, slides were then mounted and cover slips were added. Brightfield pictures of all cells and color images of the blue cells were taken. All cells per image and cells harboring blue precipitates were counted; relative numbers of SA-β-gal$^+$ were calculated and plotted. As expected from the previous results BJ1-GFP and BJ1-Wnt2 cells displayed no differences in senescence (**Figure 34A**). This result is in accordance with results of Dimri, et al They found that immortalized fibroblasts, like BJ1, do not show signs of senescence [517]. Co-cultivation of CCD18Co with Wnt2 expressing fibroblasts led to a significant increase ($p=0.0003$) in SA-β-gal$^+$ CCD18Co cells compared to cells co-cultivated with L par cells (**Figure 34B**). siRNA mediated Wnt2 KD significantly decreased ($p>0.0001$) the level of β-galactosidase activity in CAF3 compared to NTC transfected cells (**Figure 34C**).

This set of data strongly suggests that the expression of Wnt2 promotes cellular senescence in colonic fibroblasts via upregulation of TAGLN.

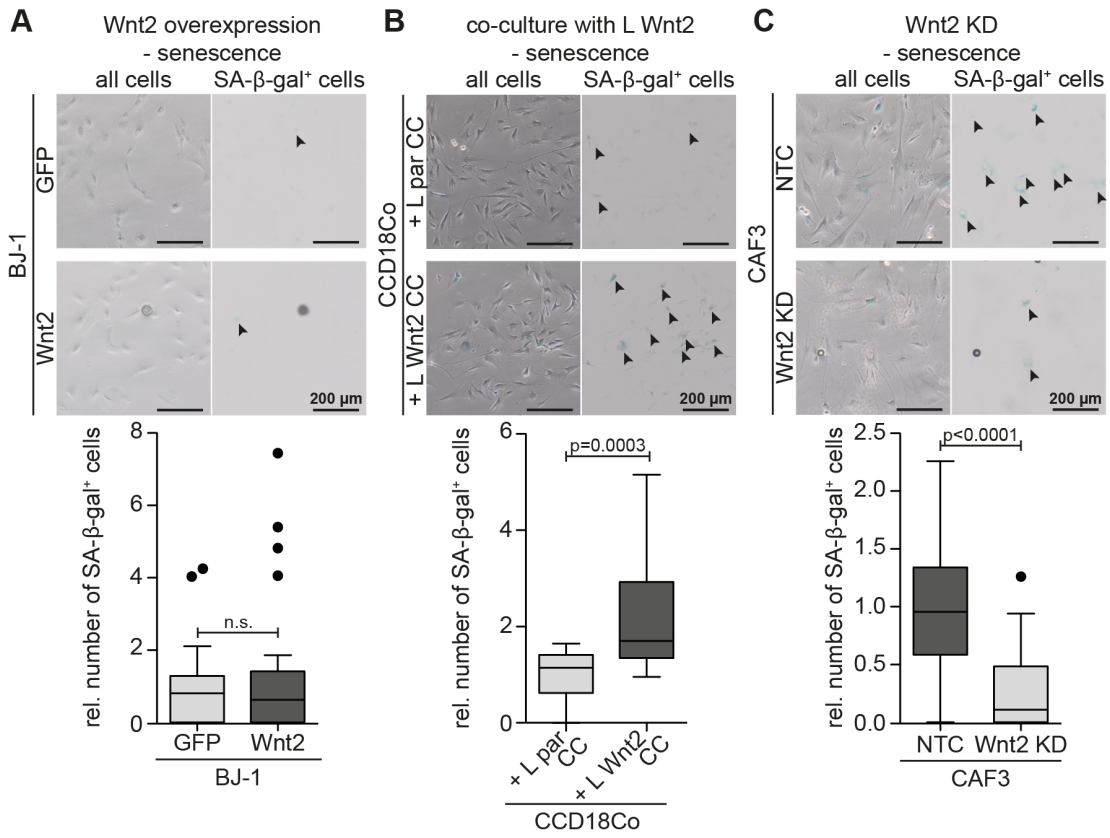

Figure 34 Wnt2 induces senescence in colonic fibroblasts
Cells were fixed 16 hours after seeding and incubated with X-gal staining solution for additional 16 hours. **A** BJ-1 GFP and BJ-1 Wnt2 cells were seeded after splitting. **B** CCD18-Co were co-cultivated with either L par or L Wnt2 cells using cell-culture inserts for 72 hours; cells were then seeded. **C** CAF3 NTC and CAF3 Wnt2 KD were seeded 72 hours after conducting WNT2 KD. Experiments were carried out in three biological replicates, 8 pictures were evaluated (n=24); one representative image pair (left panel - all cells; right panel - SA-β-gal positive cells) is shown; arrow heads indicate blue SA-β-gal positive cells; scale bars represent 200 µm; data is presented as Tukey box plots.

In vivo relevance

Previously we could demonstrate that Wnt2 is highly expressed in tumor stroma of colon cancer patients (**Figure 17A**). In order to test the effect of Wnt2 on tumor progression we used a xenograft tumor model that was conducted by our collaborator Univ. Prof. DI Dr. Richard Moriggl from the Ludwig Boltzmann Institute for Cancer Research.

Effect of Wnt2 on tumor cells in a xenograft tumor model

For xenograft tumor models mice with severe combined immunodeficiency (SCID) were used. These mice display impaired ability of T and B lineage-committed cells to develop to T or B lymphocytes [519] and therefore can not reject tumor cells [520]. For injection tumor cells (HCT116 and HT29) stably transfected with a Wnt2 expression vector or a GFP control vector were used. When tumor cells and fibroblasts are co-injected the fibroblasts would die and slowly be replaced by mouse fibroblasts (Dolznig, unpublished observations). We decided to keep Wnt2 expression high throughout the experiment and expressed Wnt2 ectopically in the tumor cells. Proper expression of Wnt2 was tested with Western blot analysis. Both HCT116 and HT29 showed high amounts of Wnt2 protein (**Figure 35A** and **C**). Blots were reprobed with GAPDH to test for equal loading. Injection of tumor cells and monitoring tumor growth was done in collaboration with Univ. Prof. DI Dr. Richard Moriggl. Mice were monitored daily and tumor measurements were taken every week. After two weeks first evidence for bigger Wnt2 expressing tumors were evident (**Figure 35B** and **D**). During the next weeks Wnt2 expressing tumors increased in size steadily. Before tumors reached a critical size mice were sacrificed and tumors were isolated and weighed. Both HCT116-Wnt2 and HT29-Wnt2 expressing tumors were twice as big as GFP controls, however it took longer until HT29 tumors reached the same volume compared to HCT116 tumors. Weight measurements after isolation of the tumors and images of the tumors showed that Wnt2 expressing tumors showed double the weight compared to GFP expressing controls (**Figure 35E** and **F**).

In summary ectopic expression of Wnt2 on tumor cells that were injected in SCID mice resulted in faster tumor growth and bigger tumor mass compared to GFP control transfected tumor cells. This data indicates that Wnt2 has an impact on tumor growth.

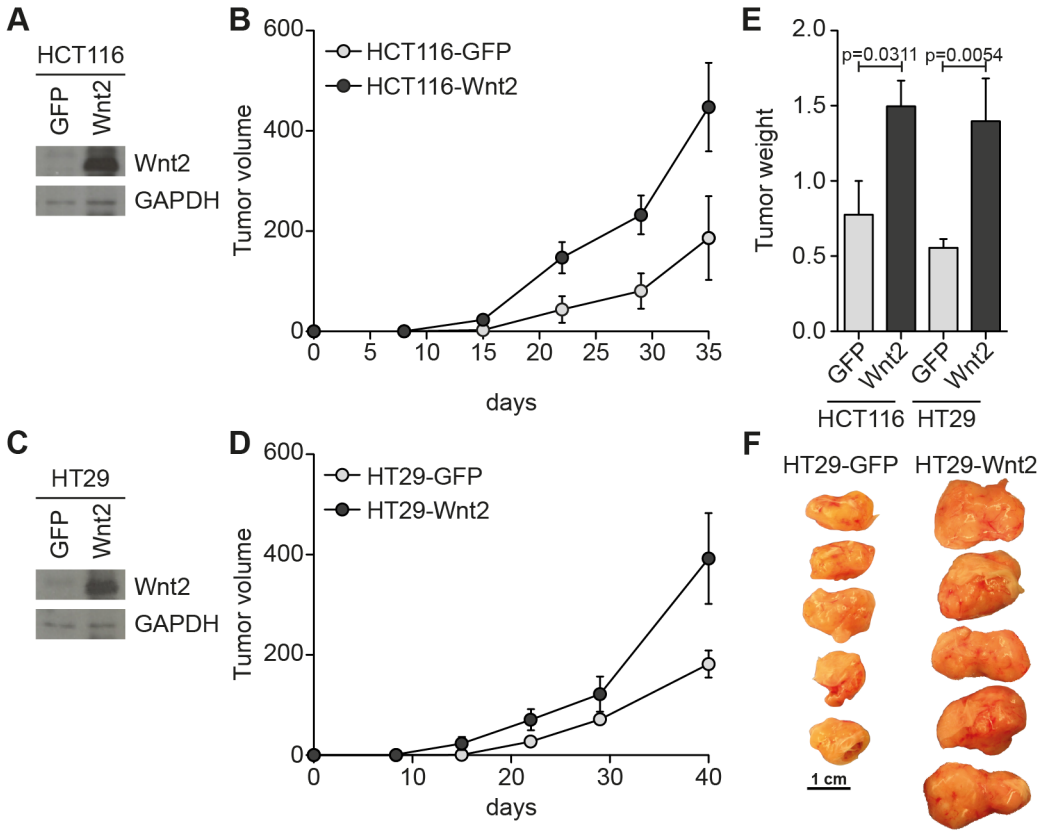

Figure 35 Wnt2 induces tumor growth in a xenograft mouse model
A and **C** The tumor cell line HCT116 and HT29 were stably transfected using a Wnt2 expression vector or a GFP control vector; Wnt2 expression was verified with Western blot analysis. **B** and **D** 100,000 cells were injected in SCID mice and tumor growth was assessed over time (n=5). **E** After sacrifice tumors were explanted and weight was measured. **F** Pictures of tumors were taken. Growth curves and bar charts display mean values; whiskers indicate standard error of mean; scale bar represents 1 cm.

Discussion

Tumor cells of solid cancers are interwoven by the tumor stroma, which has a major impact on tumor progression, metastasis and prognosis [438]. Although this influence is extensively studied many molecular mechanisms behind tumor cell to stroma cell communication remain widely elusive.

WNT2 expression in colon carcinomas

In order to gain more insights into tumor-stromal crosstalk, our goal was to evaluate differentially regulated genes in the tumor stroma of colon cancer compared to normal stroma of normal colonic mucosa and to identify its impact on tumor cells and on stromal cells themselves [479, 480]. One member of the Wnt signaling ligands, WNT2, was found to be one of the most significantly up-regulated genes in the tumor stroma compared to normal stroma (refer to **Figure 17A**). WNT2 was identified using a full-genome covering expression profiling screen of laser-assisted micro dissected colon cancer and normal colon samples, which were separated in tumor cells, tumor stroma, normal epithelium and normal stroma. Furthermore, we could show that CAFs (CAF1-3) isolated from primary colon cancers displayed high WNT2 mRNA expression in vitro. In an established primary culture of colon myofibroblasts (CCD18-Co, available from ATCC) WNT2 expression was less abundant. This was in contrast to skin fibroblasts (BJ1) or normal colon fibroblasts (NCF3) derived from the same patient as CAF3 that did not express Wnt2 (refer to **Figure 17D**). Our finding that colon cancers express high levels of WNT2 mRNA supports earlier findings that WNT2 was induced in intestinal cancers. Interestingly, it seems that WNT2 is selectively induced in malignant lesions of the digestive tract as high WNT2 levels were also reported in esophageal and gastric carcinomas [316, 323-327], whereas the normal epithelium of the digestive system did not show Wnt2 positivity [323]. This notion is underscored by our finding that other cancer types such as breast or cervix carcinoma were negative (Kramer et al, manuscript in preparation). In line with our observations, WNT2 was not found to be involved in the development of the lower digestive tract as demonstrated by mouse knockout models [306]. As Wnt2 is involved in lung development, normal lung displayed high expression, which was, however, decreased in lung cancers (Kramer et al, manuscript in preparation). In prostate cancer a similar expression pattern was found, indicating that Wnt2 induction and function might act in an organ specific way during tumor progression. To our knowledge we show for the first tie that Wnt2 is selectively expressed in stromal

fibroblast of colon cancers. These findings are indirectly corroborated by Katoh, who analyzed different gastric cancer cell lines and could not detect WNT2 mRNA in these cells. However, significantly induced WNT2 expression was found in primary gastric carcinomas leading to the prediction that WNT2 expression is up-regulated due to cancer-stromal interaction [316, 521]. Recently, WNT2 expression was found in CAFs isolated from esophageal carcinoma, further supporting our finding that CAFs of colorectal carcinomas express WNT2 mRNA [327]. Taken together, these data indicate that induction of WNT2 mRNA within the tumor stroma is a common feature in carcinomas of the digestive tract and that WNT2 is primarily expressed by CAFs. Why this WNT2 induction is taking place and what is its functional role during cancer progression in the digestive system was barely addressed so far.

Canonical Wnt signaling activation upon Wnt2 treatment

One major goal of this thesis was to elucidate if Wnt2 induced canonical Wnt signaling via paracrine crosstalk between Wnt2 expressing fibroblasts in the responding tumor cells or via autocrine signaling within the fibroblasts or both. Paracrine Wnt2 signaling could not hyper-activate a reporter construct for canonical Wnt signaling in colon cancer cell lines (refer to **Figure 19** and **Figure 20**). As expected, non-treated reporter tumor cell lines (DLD1-7TGP, HCT116-7TGP, HT29-7TGP and LS174T-7TGP) already displayed activated canonical signaling, since epithelial cells accumulate multiple genetic alterations during colon tumorigenesis thereby affecting the stability of β-catenin leading to constitutive pathway activation [493]. However, hyper-activation either upon co-cultivation or treatment with conditioned medium could not be induced by paracrine Wnt2 signaling. Nevertheless, some hyperactivation of the Wnt/beta catenin pathway has been reported in a study using myofibroblast-conditioned medium on primary colon cancer isolates in 3D culture [522]. So far we only can speculate that the tumor cells of these primary cultures were heterogeneous and a different reporter gene construct for canonical Wnt signaling was used (TOP/FOP Flash versus the 7TGP system used in our study). In esophageal squamous cell carcinoma (OSCC) Fu et al provided evidence that the epithelial cells responded to Wnt2 conditioned medium with accumulation of β-catenin within the nucleus as demonstrated by immunofluorescence analysis, thereby promoting tumor progression [327]. In this case, the accumulation of β-catenin is possibly enabled by the lack of mutations within the APC gene [523] or the CTNNB1 gene [524]

in the OSCC cells leading to normal induction of the canonical Wnt signaling by paracrine Wnt ligand. Paracrine Wnt2 had no effect on canonical Wnt signaling in well differentiated tumor cells (HCT116 - carcinoma Dukes' type A-stage, HT29 - adenocarcinoma Dukes' type B-stage, LS174T - adenocarcinoma Dukes' type B-stage, DLD-1 - adenocarcinoma Dukes' type C-stage) it could be well possible, that Wnt2 could have an impact on normal colon epithelial cells, thereby acting as a protumorigenic/mitogenic factor as reported for OSCC cells. However, so far effects of Wnt2 on colon cancer cells were subtle or not detectable at all and further research is needed to clarify the paracrine role of Wnt2 on primary colon epithelial cells or crypt organoid cultures.

A next step was to evaluate the autocrine effect of Wnt2 on canonical Wnt signaling activation. We found that exogenous Wnt2 did not activate canonical Wnt signaling in BJ1 skin fibroblasts upon treatment with Wnt2 conditioned medium or Wnt2 expressing cells. Interestingly, Wnt2 induced reporter gene activity of the normal colonic myofibroblasts CCD18Co reporter cells but only upon co-cultivation with Wnt2 producer cells, but not with Wnt2 conditioned medium, which will be discussed in detail below (refer to **Figure 21** and **Figure 22**). The fact that BJ1 skin fibroblasts, in contrast to CCD18Co, did not respond to exogenous Wnt2 with canonical Wnt signaling activation could possibly be explained by differential receptor expression. Expression profiling screens of BJ1 and CCD18Co revealed that Fzd4 and Fzd8 mRNAs were present in CCD18Co whereas BJ1 lacked expression (Kramer et al, manuscript in preparation). In the literature these receptors were reported to be associated with Wnt2 mediated signaling. Bravo and coworkers provided evidence that Wnt2 signals through Fzd8 in non-small cell lung cancer cells [321] and Wnt2 was shown to regulate the expression of Fzd4 [322]. We currently clarify, which receptor mediates Wnt2 signaling in BJ1-7TGP reporter cells by ectopic expression of Fzd4 and Fzd8 receptors and analysis of subsequent potential pathway activation upon Wnt2 treatment and/or knock-down of the respective receptors via siRNA mediated gene silencing in Wnt2 responding CCD18Co-7TGP reporter cells.

As mentioned above in contrast to the skin fibroblasts the colonic CCD18Co reporter cells displayed activation of canonical β–catenin signaling in co-culture experiments with Wnt2 producer cell lines. Expectedly, in non-treated controls a subset of cells showed activated canonical Wnt signaling. This is explained by the endogenous Wnt2 expression

in CCD18Co, which obviously stimulates pathway activation in an autocrine manner. However, a strong canonical Wnt signaling activation in these cells (50% positive cells) was achieved upon co-culture with Wnt2 over-expressing L cells and CAF3, which endogenously express high levels of Wnt2 (refer to **Figure 24**). In line with the activation of canonical signaling in our colon fibroblasts it was shown that Wnt2 activates canonical Wnt signaling in rat lung fibroblasts [525] and in NIH3T3 cells [526], however, this activation was very faint. We found that Wnt2 mediated induction of 7TGP reporter activation was strong but not as efficient as upon Wnt3a treatment. Co-culture using cell culture inserts demonstrated that 50 % of the reporter cells responded to Wnt2 producing L cells in contrast to co-culture with Wnt3a expressing L cells that resulted in pathway activation in 94 % of the reporter cells (refer to **Figure 22**). Interestingly, it seemed that the amplitude of beta-catenin response upon Wnt2 treatment was less pronounced than in cells treated with Wnt3a as judged by flow cytometric analysis. This observation was further substantiated by quantification of β-catenin levels localized in the nucleus in Wnt2 treated cells compared to Wnt3a controls (refer to **Figure 23**). This data indicates that Wnt2 drives canonical Wnt signaling activation only in a subset of stromal fibroblasts and to a lower extent as compared to Wnt3a, which could be important in order to drive an intermediate signaling response in stromal fibroblasts with potential different outcome as already supposed to be important in regulation of stem cell fate [527].

As described at the beginning of this section a Wnt2 response in the colonic fibroblasts was only seen in co-culture with Wnt2 producing cells and not with the conditioned medium alone. The lack of reporter activation using Wnt2 conditioned medium is not a surprising result, since Wnt ligands, as shown for Wnt1, were reported to be tightly bound to the cell surface, especially to heparan sulfate proteoglycans (HSPGs) [36, 37]. Blasband et al reported the same observation for Wnt2 [303]. However, Wnt2 conditioned medium was frequently used in many different studies [308, 312, 327, 528, 529]. In theses reports CHO, HEK293T or COS-7 cells were used to produce Wnt2 containing supernatants. A possible explanation could be that these cells do not or minor express Wnt-binding ECM components, like HSPGs, whereas our murine L cells used to produce the ligand might express more ECM components. Of note, L cells are fibroblast-derived cells and fibroblasts are well known to be the major contributors of ECM deposition *in vivo* [530]. Why Wnt3a acts in a paracrine manner whereas Wnt2 does not could not be solved in this study. However, it is known that Wnt3a expressed by L Wnt3a cells

associates with lipoprotein particles, thereby enabling paracrine signaling [531]. If Wnt2 has a similar binding ability was not analyzed so far.

Activation of non-canonical Wnt signaling pathways

A subset of Wnt ligands can also activate non-canonical Wnt signaling pathways, like the Wnt/Ca^{2+} or the Wnt/Rho pathway. In order to evaluate Wnt/Ca^{2+} pathway activation of a plasmid containing three NFAT binding sites upstream a luciferase reporter was used. However, CCD18Co cells transfected with this reporter were not able to induce reporter activity under positive control conditions like Wnt5a treatment or incubation with calcium ionophore A23187 but died after two days in culture. As Wnt2 was so far not reported to activate the Wnt/Ca2+ pathway we didn't invest excess time to assess the impact of Wnt2 on Wnt/Ca^{2+} pathway activation and focused instead on the Wnt/Rho pathway.

In order to evaluate the effect of Wnt2 on Wnt/Rho pathway AP1-dependent target gene transcription was assessed. We found that long-term co-culture of L Wnt2 cells and CCD18Co cells transfected with a reporter plasmid, which contains three AP1 binding sites upstream of a luciferase reporter, resulted in pathway activation compared to parental controls. This was also achieved upon co-cultivation of reporter cells with CAF3. Interestingly, shorter incubation times than 56 hours resulted in not significantly enhanced AP1 dependent target gene transcription at e.g. 48 hrs, compared to controls (refer to **Figure 25**). This indicates, that the effect of Wnt2 on AP1 reporter activation is more likely due to a secondary effect. However, in the literature Wnt2 was reported to activate AP1 dependent transcription in different cell types within 24 hours. Le Floch et al demonstrated that Wnt2 induced transcription of MMP7 mRNA via AP1 in colonic epithelial cells [528] and Onizuka and co-workers showed that during cardiomyocyte differentiation of ES cells Wnt2 activates JNK/AP1 dependent transcription [308]. In summary, this data indicate that Wnt2 mediates AP1 target gene transcription in a cell-type specific and context-dependent manner and that in stromal fibroblasts long-term exposure with Wnt2 leads to AP1 dependent transcription. Here further experiments beyond the scope of this thesis are necessary to elucidate the different roles of canonical and Wnt/Rho pathway in tumor-stroma crosstalk in colon cancer.

Impact of Wnt2 on fibroblast proliferation, apoptosis, migration and invasion

A next goal of this study was to clarify the effect of Wnt2 on the phenotype of fibroblasts. As expected ectopic expression of Wnt2 in BJ1 did not affect apoptosis due to the non-response in respect to canonical signaling as discussed above. Moreover, we observed no differences upon treatment with Wnt2 or KD of Wnt2 in responding colonic fibroblasts (refer to **Figure 26**). This is in contrast to Wnt2 knockdown experiments in non-small cell lung cancer cells [319], malignant glioma cells [317, 320] and colorectal cancer cells [318], which induced apoptosis. However, as colon cancer cells are concerned, in four commonly used colon cancer cell lines we could not detect Wnt2 expression at all.

Incubation with Wnt2 conditioned medium was shown to induce proliferation of esophageal squamous cell carcinoma cells (OSCC cells) [327], whereas in endothelial cells Wnt2, had no effect on proliferation [532]. Assessment of proliferation in CCD18Co co-cultured with Wnt2 expressing cells and in CAF3 upon Wnt2 KD revealed that Wnt2 did not change cell cycle distribution in both cell types (refer to **Figure 27**). However, we could show that Wnt2 enhanced, although not significantly, migration of CCD18Co co-cultivated with L Wnt2 cells. A Wnt2 KD in CAF3 decreased the migratory potential compared to NTC transfected CAFs, indicating that Wnt2 has a pro-migratory effect on colonic fibroblasts (refer to **Figure 28**). Interestingly, no results on cell migration upon Wnt2 administration in any cell type were reported so far.

Furthermore, CAF3 Wnt2 KD resulted in reduced invasion compared to controls as demonstrated by spheroid invasion into collagen I matrices (refer to **Figure 29**). Reduction of invasive potential in CAF3 after Wnt2 KD might be explained by altered AP1 dependent target gene transcription as induction of canonical signaling was so far never reported to be functionally involved in invasive potential. Supporting this notion, Le Floch et al showed that Wnt2 induced invasion of colonic and kidney epithelial cells was mediated via induction of MMP-7, which was mediated by JNK/AP1 dependent transcription [528]. Since, we were able to show that long-term treatment with Wnt2 resulted in activation of AP1 dependent target gene transcription in CCD18Co, it could be plausible, that the effect on invasion could be mediated by reduced AP1 activity in the CAF3 Wnt2 KD cells. In order to verify this hypothesis, transcriptional activation and

activity of different MMPs, including MMP-7, could be evaluated. Furthermore, invasion capacity should be monitored upon treatment with a Rock specific inhibitor.

Interestingly, so far, many studies analyzed the effect of Wnt2 on apoptosis [317, 318, 320, 533], proliferation [327, 532, 533], migration [533] and invasion [327, 528] on cancer cells; however, Wnt2 mediated changes on phenotypic parameters in fibroblasts were not reported. In summary, we provide first evidence that Wnt2 has an impact on migration and invasion of stromal fibroblasts.

Effect of Wnt2 on organotypic co-cultures

For many years invasion of carcinoma cells was reported by pathologists and was frequently explained by epithelial-to-mesenchymal transition (EMT) [534]. However, some carcinomas were also reported to retain their epithelial markers, while being invasive, like SCCs [535]. Gaggioli and coworkers provided evidence that in organotypic co-cultures of tumor cells and fibroblasts invading tumor cells were always following leading fibroblasts, which provide tracks within the ECM [499]. They showed that these tracks are sufficient for collective invasion, so that tumor cells invaded the gels even when fibroblasts were depleted after ECM remodeling. These data for the first time demonstrated that the fibroblasts in the tumor stroma have a vital role in carcinoma cell invasion. As we demonstrated that autocrine Wnt2 expression influenced the invasive potential of stromal fibroblasts, we were interested if the observed phenotype has an impact on collective invasion of tumor cells. In an organotypic co-culture model similar to the SCC model of Gaggioli et al [499] we found that Wnt2 KD in CAF3 significantly reduced collective invasion of DLD1 cells into the collagen gel compared to NTC transfected CAFs. KD of Wnt2 in CAF3 reduced the number of invasive structures of DLD1 cells to one third of control conditions (refer to **Figure 30B**). Interestingly, area measurements of invasive structures revealed that in NTC as well as in Wnt2 KD co-cultures the mean invasive area was comparable. This data shows that Wnt2 had only an effect on the number, but not the area of invasive structures, indicating that in Wnt2 KD conditions fewer tracks were provided by fibroblasts for DLD1 collective invasion due to decreased motility of the fibroblasts. However, leading fibroblasts promote equally large invasive structures in both conditions, suggesting that Wnt2 has no paracrine effect on the tumor cells. Convincingly, Wnt2 expression in BJ1 had no effect on DLD1 tumor cell invasion as we have previously shown that these fibroblasts were non-responsive in

respect to canonical signaling (refer to **Figure 30A**). In general tumor cells in co-culture with BJ1 hardly showed signs of collective invasion. This could be explained by observations of Magalhaes and coworkers. They found that hTERT immortalized BJ1, like the ones used in this study, display significantly decreased expression of MMP7, MMP2, MMP14, MMP11, MMP15 and do not express MMP3 compared to normal BJ1 [536], which leads to reduced invasion capacity of these immortalized BJ1.

Gaggioli and coworkers reported that in fibroblasts Rho/Rock signaling is necessary to provide tracks in the collagen gel for tumor cell invasion, but has no effect on fibroblast invasion [499]. As previously discussed, Le Floch et al demonstrated that Wnt2 activates JNK/AP1 target gene transcription via the non-canonical Wnt/Rho pathway resulting in enhanced invasion of epithelial cells. Taken together, a possible mechanism could be that Wnt2 regulates AP1 activity in stromal fibroblasts (refer to **Figure 25**), thereby altering their track-generation ability, which in turn affects collective invasion of tumor cells in an organotypic co-culture model and this mechanism might act also *in vivo*. In order to verify this hypothesis further spheroid invasion experiments of fibroblasts and organotypic co-cultures will be performed using a selective Rock inhibitor. Furthermore, invading spheroids, sections of organoytpic co-cultures or cells on cover slips upon treatment with Wnt2 could be stained with an affinity probe that exhibits the Rho-binding domain of rhotekin, which is coupled to GFP, in order to highlight cells with activated Rho signaling under the different conditions.

The Wnt2 fibroblast phenotype

Our next aim was to assess if Wnt2 has an impact on the differentiation status of fibroblast, since it is well established that Wnt signaling plays an important role in maintaining stemness in embryonic, neuronal, epithelial and mesenchymal stem cells [356, 500-502] and we demonstrated that Wnt2 affects migration and invasion in fibroblasts. Therefore, a set of markers for mesenchymal stem cells, activated fibroblasts and smooth muscle cell-myofibroblast markers were determined by RT-qPCR (refer to **Figure 31**).

The mesenchymal stem cell markers CD34 and THY1 were significantly increased in CAF3 compared to NCF3, however, in CCD18Co co-cultured with Wnt2 only marginally induced CD34 and THY1 mRNA expression. Upon Wnt2 KD in CAF3 CD34 was not

significantly decreased, whereas THY1 expression dropped by about 20 %. Expression of another stemness marker, ENG, was altered in CAF3 compared to NCF or in CCD18Co upon treatment with Wnt2, however, a Wnt2 KD in CAF3 led to increased ENG expression. Taken together, these data indicate that Wnt2 has no clear impact on dedifferentiation of colonic fibroblasts

The markers for activated fibroblasts CD44 and FAP were upregulated in CAF3 compared to NCF3. In accordance, both markers showed enhanced expression upon co-cultivation with Wnt2 and reduced expression after Wnt2 KD in CAF3. Since CAF3 were derived from "activated" stroma [537], it is not surprising that they express more CD44 and FAP than their normal counterpart. Interestingly, Wnt2 could induce expression of these markers, indicating that Wnt2 expression has an impact on the activation state of the stroma.

Transgelin (TAGLN) mRNA was found to be the most significantly regulated mRNA in our setting. It is a marker for smooth muscle cell and myofibroblast differentiation [512]. Its expression was 15 times higher in CAF3 compared to NCF3 and Wnt2 treatment of CCD18Co resulted in a highly significant two-fold induction. Concurrently, Wnt2 KD in CAF3 halved its expression. Surprisingly, expression of ACTA2 mRNA encoding for another prominent myofibroblast marker was not significantly induced in CAF3 and upon co-culture with Wnt2 in CCD18Co, but a Wnt2 KD significantly decreased its expression in CAF3. In conclusion expression of Wnt2 could drive fibroblasts in a smooth-muscle cell/myofibroblast state, since TAGLN was increased during fibroblast-to-myofibroblast transdifferentiation [538]. Supporting our findings ACTA2 expression is a hallmark of CAFs [440] that is induced by TGFβ treatment [514], however, it was shown that TGFβ-induced fibroblast invasion was mediated via LIF/Rho signaling and was independent of α-SMA (ACTA2) expression, indicating that cell contractility, ECM remodeling and fibroblast invasion are regulated by two distinct mechanism either in an alpha-SMA or an Rho dependent manner [539]. Our findings support this evidence for fibroblast heterogeneity within the tumor stroma.

Interestingly, FGF10 mRNA expression was almost completely abolished in CAF3 compared to NCF3, and consistently treatment of CCD18Co with Wnt2 resulted in decreased FGF10 mRNA expression and a Wnt2 KD in CAF3 induced its mRNA expression to 150 %. FGF10 is a member of the fibroblast growth factor family and is also referred to as keratinocyte growth factor 2 (KGF2). FGF10 -/- mice displayed lack of

fore- and hind limb development, lung agenesis, which led to perinatal lethality [540] and furthermore, absence of FGF10 expression during development resulted in colonic [541], duodenal [542] and cecal atresia [543]. Interestingly, it was shown that in 5 of 10 colorectal cancer tissues FGF10 mRNA expression was found in fibroblasts adjacent to tumor cells [544], indicating that every second colorectal tumor harbors CAFs lacking FGF10 expression, like our CAF3. Contrasting our results, it was show that Wnt2 induces FGF10 expression in the primitive lung mesenchyme in order to differentiate immature smooth muscle cells to mature airway smooth muscle cells [307]. However, there were no reports linking Wnt2 and FGF10 expression with colorectal cancer.

In summary we provide ample evidence that Wnt2 does not induce a mesenchymal stem cell phenotype in fibroblasts, but rather enhances markers for activated and smooth-muscle cell-myofibroblasts.

Impact of Wnt2 on transgelin expression

We demonstrated that Wnt2 regulates the expression of TAGLN in CCD18Co and in CAF3. Transgelin, also called SM22α, is an actin-binding protein and member of the calponin family [545]. It is expressed in smooth muscle tissue, like uterus, bladder, stomach and prostate, but also in other tissues including spinal chord and the heart [545, 546]. Furthermore, TAGLN is thought to be an early marker for smooth-muscle cell differentiation [547] and senescence [548]. Several studies proposed that TAGLN acts as a tumor suppressor. It blocked androgen stimulated cell growth in prostate carcinoma cells [549], suppressed the expression of MMP-9 [550] and re-expression of TAGLN in PC3 prostate cancer cells reduced their invasive capacity [551]. TAGLN expression was shown to be decreased in colon carcinoma samples compared to normal colon [552]; loss of TAGLN was correlated with lymph node metastasis and its re-expression in colon cancer cells had a negative impact on tumorigenicity [553]. However, we found that TAGLN expression was significantly increased in the tumor stroma compared to normal stroma as revealed by our previously described gene expression-profiling screen of laser-capture microdissected colon cancer and normal colon samples (Kramer et al, manuscript in preparation). Furthermore, in contrast to its proposed tumor suppressive function, transgelin expression was suggested as a candidate biomarker for lymph node metastasis of colorectal carcinomas [554] and its expression was upregulated in the invasive front of colorectal tumors in the liver of nude mice [555]. This data indicate that TAGLN

expression and its impact on colorectal carcinomas is contradictory. We provide evidence that exogenous Wnt2 delivered by co-cultures with L Wnt2 cells or CAF3 activated a TAGLN reporter plasmid in CCD18Co (refer to **Figure 33**). Induction of TAGLN expression by recombinant Wnt2 in murine sarcoma-derived 10T1/2 fibroblasts and in murine lung bud extracts, supported this observation [307]. Interestingly, Shafer and Towler investigated the effect of different Wnt ligands on TAGLN expression and found that canonical Wnt3a and not Wnt1, which is the prototype for canonical Wnts, activated TAGLN expression in C3H10T1/2 fibroblasts [515]. The authors conclude that the function of different Wnt ligands is highly dependent on the available Fzd/LRP expression of the responder cells. These data imply that Wnt2 shares more similarities with Wnt3a than Wnt1 in respect to TAGLN induction. Shafer and Towler further observed that simultaneous treatment with Wnt3a and TGFβ resulted in augmented TAGLN expression via a CAGAG promoter element sharing features of the TCF (CAAAG) and the Smad binding motifs (CAGA) [515]. This elevating effect on transgelin expression was of specific interest, since high levels of TGFβ1 were found in serum of CRC patients, which was associated with poor clinical outcome [448]. Indeed we also found that concomitant treatment of CCD18Co-TAGLN reporter cells with Wnt2 and TGFβ enhanced luciferase expression more than 4-fold compared to Wnt2 only condition and 9-fold compared if TGFβ was administered in the presence of L par cells (refer to **Figure 33C**). In line with the current thinking, Calon and coworkers provide evidence that TGFβ expression in CRCs acts on tumor stromal cells, including CAFs, thereby inducing a pro-metastatic program [448]. Taking these findings into account, it could be hypothesized that CAF-derived Wnt2 and TGFβ cooperatively induce TAGLN expression in stromal fibroblasts, thereby possibly mediating a pro-metastatic effect, which was previously described for TGFβ [448] and TAGLN [554, 555].

Transgelin was previously also identified as a protein, which is over-expressed in fibroblasts that have undergone replicative senescence [516]. Therefore, we were interested if Wnt2 has an effect on senescence of fibroblasts. We showed that treatment with Wnt2 induced SA-β-gal staining in CCD18Co and a Wnt2 KD resulted in reduced senescence mediated β-gal activity in CAF3. As expected for an established cell line, BJ1 GFP and Wnt2 cells displayed no differences and only minor SA-β-gal staining (refer to **Figure 34**), as immortalized fibroblasts were shown to lack any signs of senescence [517]. Our findings are in contrast to the literature, where replicative senescence is

associated with reduced Wnt2 signaling in human fibroblasts (WI-38) and human epithelial cells (RPE) [556]. Furthermore, loss of Wnt2 via siRNA led to increased senescence markers, like senescence-associated heterochromatin foci [556, 557]. It may well be that the spatial origin (different organs) of distinct fibroblasts is responsible for a completely opposite behavior. In order to elucidate this discrepancy more senescence markers, like stabilization of p21, phosphorylation of histone H2A.X and reduction pRB, should be tested to confirm the SA-β-gal staining results.

Recently, Dvorakova and colleagues published a review about transgelin and its implications in cancer development. They state that transformation of premalignant cells can be promoted by senescent fibroblasts, since they over-produce cytokines, growth factors and ECM components thereby resembling a myofibroblast phenotype [558]. This notion is supported by Krtolica and coworkers, who demonstrated that senescent fibroblasts produce soluble and insoluble factors, which promote proliferation and tumor formation of premalignant and malignant cells [559]. To put it another way, myofibroblasts and senescent fibroblasts share a similar secretion pattern that differs from normal fibroblasts. This assumption is supported by Sobral et al They isolated SMA^- CAFs and SMA^+ CAFs from oral squamous cell carcinoma samples and found that a differentially expressed growth factor (activin A) of SMA^+ CAFs promoted proliferation of OSCC cells and enhanced tumor growth in a xenograft tumor model [560]. In another study with CAFs that exhibited features of myofibroblasts (SMA^+, enhanced collagen gel contraction) a pro-tumorigenic and pro-angiogenic phenotype of CAFs compared to NCFs was found [561]. These studies indicate that myofibroblasts have an impact on tumor progression, which is further substantiated by the fact that abundant presence of myofibroblasts associates with decreased patient survival and enhanced disease recurrence [562]. Considering these arguments, it could be possible that Wnt2 in concert with TGFβ enhance the expression of TAGLN, thereby leading to a smooth-muscle cell-myofibroblast phenotype with a consequently changed secretion pattern that could stimulate tumor progression and metastasis of colorectal carcinomas. In order to investigate this hypothesis the effect of cooperatively induced TAGLN expression in CAFs on the invasion and proliferation potential of tumor cells and endothelial cells should be addressed. Furthermore, we propose to perform *in vivo* experiments, where colorectal carcinomas are induced using AOM/DSS treatment [563, 564] in conditional

TAGLN and Wnt2 knock-out mice and to study effects of TAGLN$^{-/-}$ and Wnt2$^{-/-}$ on colon cancer initiation, progression and metastasis.

Effect of Wnt2 on tumor cells in a xenograft tumor model

Our next intent was to assess if Wnt2 has an effect on tumor progression *in vivo*. A xenograft tumor model revealed that HCT116 and HT29 stably expressing Wnt2 were growing faster and therefore display bigger tumor mass compared to GFP control conditions (refer to **Figure 35**). One drawback of this experiment is that we had to use tumor cells ectopically expressing Wnt2, in order to keep constant Wnt2 expression throughout the experiment, since co-injected fibroblasts would diminish and slowly be replaced by mouse fibroblasts (Dolznig, unpublished observations). At this point, the results are only descriptive. Further analysis of H&E and immunohistochemically stained sections for different proteins (KI67, cleaved caspase-7, CD31, FAP) is currently done to investigate histological differences and to elucidate, why Wnt2 expressing tumors had a growth advantage compared to GFP control tumors. However, our finding is supported by experiments showing that dominant negative Wnt2 in A549 cells, which express endogenous Wnt2, subcutaneously injected in Nu/Nu mice resulted in decreased tumor mass due to reduced c-Myc and cyclin D1 expression [321]. Furthermore subcutaneous U251 glioma xenograft model treated with Wnt2 or β-catenin siRNA every 4 days showed reduced growth rate via down-regulation of PI3K/AKT signaling [317]. Taken together, we found that Wnt2 has a pro-tumorigenic effect in a xenograft mouse model.

Conclusion

In this thesis I provide evidence that Wnt2, which is expressed by tumor stroma-residing CAFs, has a major impact on tumor progression. We could show for the first time that Wnt2 activates canonical Wnt signaling in colonic fibroblasts, that Wnt2 induces migration and invasion in CAFs thereby leading to enhanced collective tumor cell invasion. Furthermore, Wnt2 induces a smooth-muscle cell-myofibroblast phenotype via TAGLN expression, which could probably induce tumor progression and metastasis. Although some major hypotheses remain uncorroborated, this work gives first insights in the role of Wnt2 within the tumor stroma, thereby providing basic information for further research projects in order to elucidate possible mechanisms of colon tumor initiation, progression and metastasis.

Bibliography

1. Sharma, R.P., *Wingless - a new mutant in D. melanogaster.* Drosophila Information Service, 1973. **50**.
2. Sharma, R.P. and V.L. Chopra, *Effect of the Wingless (wg1) mutation on wing and haltere development in Drosophila melanogaster.* Dev Biol, 1976. **48**(2): p. 461-5.
3. Nusse, R. and H.E. Varmus, *Many tumors induced by the mouse mammary tumor virus contain a provirus integrated in the same region of the host genome.* Cell, 1982. **31**(1): p. 99-109.
4. Nusse, R., et al., *Mode of proviral activation of a putative mammary oncogene (int-1) on mouse chromosome 15.* Nature, 1984. **307**(5947): p. 131-6.
5. Rijsewijk, F., et al., *The Drosophila homolog of the mouse mammary oncogene int-1 is identical to the segment polarity gene wingless.* Cell, 1987. **50**(4): p. 649-57.
6. Christian, J.L., et al., *Isolation of cDNAs partially encoding four Xenopus Wnt-1/int-1-related proteins and characterization of their transient expression during embryonic development.* Dev Biol, 1991. **143**(2): p. 230-4.
7. Du, S.J., et al., *Identification of distinct classes and functional domains of Wnts through expression of wild-type and chimeric proteins in Xenopus embryos.* Mol Cell Biol, 1995. **15**(5): p. 2625-34.
8. Moon, R.T., *In pursuit of the functions of the Wnt family of developmental regulators: insights from Xenopus laevis.* Bioessays, 1993. **15**(2): p. 91-7.
9. Wodarz, A. and R. Nusse, *Mechanisms of Wnt signaling in development.* Annu Rev Cell Dev Biol, 1998. **14**: p. 59-88.
10. Kikuchi, A., H. Yamamoto, and S. Kishida, *Multiplicity of the interactions of Wnt proteins and their receptors.* Cell Signal, 2007. **19**(4): p. 659-71.
11. Miller, J.R., *The Wnts.* Genome Biol, 2002. **3**(1): p. REVIEWS3001.
12. Nusse, R., *An ancient cluster of Wnt paralogues.* Trends Genet, 2001. **17**(8): p. 443.
13. Logan, C.Y. and R. Nusse, *The Wnt signaling pathway in development and disease.* Annu Rev Cell Dev Biol, 2004. **20**: p. 781-810.
14. Kishida, S., H. Yamamoto, and A. Kikuchi, *Wnt-3a and Dvl induce neurite retraction by activating Rho-associated kinase.* Mol Cell Biol, 2004. **24**(10): p. 4487-501.
15. Willert, K., et al., *Wnt proteins are lipid-modified and can act as stem cell growth factors.* Nature, 2003. **423**(6938): p. 448-52.
16. Mikels, A.J. and R. Nusse, *Purified Wnt5a protein activates or inhibits beta-catenin-TCF signaling depending on receptor context.* PLoS Biol, 2006. **4**(4): p. e115.
17. Kurayoshi, M., et al., *Expression of Wnt-5a is correlated with aggressiveness of gastric cancer by stimulating cell migration and invasion.* Cancer Res, 2006. **66**(21): p. 10439-48.
18. Kurayoshi, M., et al., *Post-translational palmitoylation and glycosylation of Wnt-5a are necessary for its signalling.* Biochem J, 2007. **402**(3): p. 515-23.
19. Bradley, R.S. and A.M. Brown, *A soluble form of Wnt-1 protein with mitogenic activity on mammary epithelial cells.* Mol Cell Biol, 1995. **15**(8): p. 4616-22.

20. Nakagawa, S., et al., *Identification of the laminar-inducing factor: Wnt-signal from the anterior rim induces correct laminar formation of the neural retina in vitro.* Dev Biol, 2003. **260**(2): p. 414-25.
21. Hwang, S.G., et al., *Wnt-7a causes loss of differentiated phenotype and inhibits apoptosis of articular chondrocytes via different mechanisms.* J Biol Chem, 2004. **279**(25): p. 26597-604.
22. Hirabayashi, Y., et al., *The Wnt/beta-catenin pathway directs neuronal differentiation of cortical neural precursor cells.* Development, 2004. **131**(12): p. 2791-801.
23. Pandur, P., et al., *Wnt-11 activation of a non-canonical Wnt signalling pathway is required for cardiogenesis.* Nature, 2002. **418**(6898): p. 636-41.
24. Smolich, B.D., et al., *Wnt family proteins are secreted and associated with the cell surface.* Mol Biol Cell, 1993. **4**(12): p. 1267-75.
25. Hofmann, K., *A superfamily of membrane-bound O-acyltransferases with implications for wnt signaling.* Trends Biochem Sci, 2000. **25**(3): p. 111-2.
26. Zhai, L., D. Chaturvedi, and S. Cumberledge, *Drosophila wnt-1 undergoes a hydrophobic modification and is targeted to lipid rafts, a process that requires porcupine.* J Biol Chem, 2004. **279**(32): p. 33220-7.
27. Takada, R., et al., *Monounsaturated fatty acid modification of Wnt protein: its role in Wnt secretion.* Dev Cell, 2006. **11**(6): p. 791-801.
28. Komekado, H., et al., *Glycosylation and palmitoylation of Wnt-3a are coupled to produce an active form of Wnt-3a.* Genes Cells, 2007. **12**(4): p. 521-34.
29. Banziger, C., et al., *Wntless, a conserved membrane protein dedicated to the secretion of Wnt proteins from signaling cells.* Cell, 2006. **125**(3): p. 509-22.
30. Bartscherer, K., et al., *Secretion of Wnt ligands requires Evi, a conserved transmembrane protein.* Cell, 2006. **125**(3): p. 523-33.
31. Goodman, R.M., et al., *Sprinter: a novel transmembrane protein required for Wg secretion and signaling.* Development, 2006. **133**(24): p. 4901-11.
32. MacDonald, B.T., K. Tamai, and X. He, *Wnt/beta-catenin signaling: components, mechanisms, and diseases.* Dev Cell, 2009. **17**(1): p. 9-26.
33. Hausmann, G., C. Banziger, and K. Basler, *Helping Wingless take flight: how WNT proteins are secreted.* Nat Rev Mol Cell Biol, 2007. **8**(4): p. 331-6.
34. Belenkaya, T.Y., et al., *The retromer complex influences Wnt secretion by recycling wntless from endosomes to the trans-Golgi network.* Dev Cell, 2008. **14**(1): p. 120-31.
35. Franch-Marro, X., et al., *Wingless secretion requires endosome-to-Golgi retrieval of Wntless/Evi/Sprinter by the retromer complex.* Nat Cell Biol, 2008. **10**(2): p. 170-7.
36. Bradley, R.S. and A.M. Brown, *The proto-oncogene int-1 encodes a secreted protein associated with the extracellular matrix.* EMBO J, 1990. **9**(5): p. 1569-75.
37. Reichsman, F., L. Smith, and S. Cumberledge, *Glycosaminoglycans can modulate extracellular localization of the wingless protein and promote signal transduction.* J Cell Biol, 1996. **135**(3): p. 819-27.
38. Tsuda, M., et al., *The cell-surface proteoglycan Dally regulates Wingless signalling in Drosophila.* Nature, 1999. **400**(6741): p. 276-80.
39. Zecca, M., K. Basler, and G. Struhl, *Direct and long-range action of a wingless morphogen gradient.* Cell, 1996. **87**(5): p. 833-44.

40. Katanaev, V.L., et al., *Reggie-1/flotillin-2 promotes secretion of the long-range signalling forms of Wingless and Hedgehog in Drosophila.* EMBO J, 2008. **27**(3): p. 509-21.
41. Greco, V., M. Hannus, and S. Eaton, *Argosomes: a potential vehicle for the spread of morphogens through epithelia.* Cell, 2001. **106**(5): p. 633-45.
42. Panakova, D., et al., *Lipoprotein particles are required for Hedgehog and Wingless signalling.* Nature, 2005. **435**(7038): p. 58-65.
43. Clevers, H. and R. Nusse, *Wnt/beta-catenin signaling and disease.* Cell, 2012. **149**(6): p. 1192-205.
44. Bhanot, P., et al., *A new member of the frizzled family from Drosophila functions as a Wingless receptor.* Nature, 1996. **382**(6588): p. 225-30.
45. Wang, Y., et al., *A large family of putative transmembrane receptors homologous to the product of the Drosophila tissue polarity gene frizzled.* J Biol Chem, 1996. **271**(8): p. 4468-76.
46. Dann, C.E., et al., *Insights into Wnt binding and signalling from the structures of two Frizzled cysteine-rich domains.* Nature, 2001. **412**(6842): p. 86-90.
47. Hsieh, J.C., et al., *Biochemical characterization of Wnt-frizzled interactions using a soluble, biologically active vertebrate Wnt protein.* Proc Natl Acad Sci U S A, 1999. **96**(7): p. 3546-51.
48. Pinson, K.I., et al., *An LDL-receptor-related protein mediates Wnt signalling in mice.* Nature, 2000. **407**(6803): p. 535-8.
49. Tamai, K., et al., *LDL-receptor-related proteins in Wnt signal transduction.* Nature, 2000. **407**(6803): p. 530-5.
50. Nishita, M., et al., *Cell/tissue-tropic functions of Wnt5a signaling in normal and cancer cells.* Trends Cell Biol, 2010. **20**(6): p. 346-54.
51. Forrester, W.C., et al., *A C. elegans Ror receptor tyrosine kinase regulates cell motility and asymmetric cell division.* Nature, 1999. **400**(6747): p. 881-5.
52. Jones, S.E. and C. Jomary, *Secreted Frizzled-related proteins: searching for relationships and patterns.* Bioessays, 2002. **24**(9): p. 811-20.
53. Marsit, C.J., et al., *Epigenetic inactivation of SFRP genes and TP53 alteration act jointly as markers of invasive bladder cancer.* Cancer Res, 2005. **65**(16): p. 7081-5.
54. Suzuki, H., et al., *Epigenetic inactivation of SFRP genes allows constitutive WNT signaling in colorectal cancer.* Nat Genet, 2004. **36**(4): p. 417-22.
55. Leyns, L., et al., *Frzb-1 is a secreted antagonist of Wnt signaling expressed in the Spemann organizer.* Cell, 1997. **88**(6): p. 747-56.
56. Lin, K., et al., *The cysteine-rich frizzled domain of Frzb-1 is required and sufficient for modulation of Wnt signaling.* Proc Natl Acad Sci U S A, 1997. **94**(21): p. 11196-200.
57. Wang, S., et al., *Frzb, a secreted protein expressed in the Spemann organizer, binds and inhibits Wnt-8.* Cell, 1997. **88**(6): p. 757-66.
58. Lopez-Rios, J., et al., *The Netrin-related domain of Sfrp1 interacts with Wnt ligands and antagonizes their activity in the anterior neural plate.* Neural Dev, 2008. **3**: p. 19.
59. Bhat, R.A., et al., *Structure-function analysis of secreted frizzled-related protein-1 for its Wnt antagonist function.* J Cell Biochem, 2007. **102**(6): p. 1519-28.

60. Swain, R.K., et al., *Xenopus frizzled-4S, a splicing variant of Xfz4 is a context-dependent activator and inhibitor of Wnt/beta-catenin signaling.* Cell Commun Signal, 2005. **3**: p. 12.
61. Cruciat, C.M. and C. Niehrs, *Secreted and transmembrane wnt inhibitors and activators.* Cold Spring Harb Perspect Biol, 2013. **5**(3): p. a015081.
62. Wawrzak, D., et al., *Wnt3a binds to several sFRPs in the nanomolar range.* Biochem Biophys Res Commun, 2007. **357**(4): p. 1119-23.
63. Bafico, A., et al., *Interaction of frizzled related protein (FRP) with Wnt ligands and the frizzled receptor suggests alternative mechanisms for FRP inhibition of Wnt signaling.* J Biol Chem, 1999. **274**(23): p. 16180-7.
64. Rodriguez, J., et al., *SFRP1 regulates the growth of retinal ganglion cell axons through the Fz2 receptor.* Nat Neurosci, 2005. **8**(10): p. 1301-9.
65. Glinka, A., et al., *Dickkopf-1 is a member of a new family of secreted proteins and functions in head induction.* Nature, 1998. **391**(6665): p. 357-62.
66. Bafico, A., et al., *Novel mechanism of Wnt signalling inhibition mediated by Dickkopf-1 interaction with LRP6/Arrow.* Nat Cell Biol, 2001. **3**(7): p. 683-6.
67. Mao, B., et al., *LDL-receptor-related protein 6 is a receptor for Dickkopf proteins.* Nature, 2001. **411**(6835): p. 321-5.
68. Mao, B., et al., *Kremen proteins are Dickkopf receptors that regulate Wnt/beta-catenin signalling.* Nature, 2002. **417**(6889): p. 664-7.
69. Ahn, Y., et al., *Inhibition of Wnt signaling by Wise (Sostdc1) and negative feedback from Shh controls tooth number and patterning.* Development, 2010. **137**(19): p. 3221-31.
70. Yamamoto, H., et al., *Wnt3a and Dkk1 regulate distinct internalization pathways of LRP6 to tune the activation of beta-catenin signaling.* Dev Cell, 2008. **15**(1): p. 37-48.
71. Willnow, T.E., A. Christ, and A. Hammes, *Endocytic receptor-mediated control of morphogen signaling.* Development, 2012. **139**(23): p. 4311-9.
72. Hsieh, J.C., et al., *A new secreted protein that binds to Wnt proteins and inhibits their activities.* Nature, 1999. **398**(6726): p. 431-6.
73. Surmann-Schmitt, C., et al., *Wif-1 is expressed at cartilage-mesenchyme interfaces and impedes Wnt3a-mediated inhibition of chondrogenesis.* J Cell Sci, 2009. **122**(Pt 20): p. 3627-37.
74. Zhang, X., et al., *Tiki1 is required for head formation via Wnt cleavage-oxidation and inactivation.* Cell, 2012. **149**(7): p. 1565-77.
75. Dijksterhuis, J.P., J. Petersen, and G. Schulte, *WNT/Frizzled signalling: receptor-ligand selectivity with focus on FZD-G protein signalling and its physiological relevance: IUPHAR Review 3.* Br J Pharmacol, 2014. **171**(5): p. 1195-209.
76. Fuerer, C. and R. Nusse, *Lentiviral vectors to probe and manipulate the Wnt signaling pathway.* PLoS One, 2010. **5**(2): p. e9370.
77. Veeman, M.T., J.D. Axelrod, and R.T. Moon, *A second canon. Functions and mechanisms of beta-catenin-independent Wnt signaling.* Dev Cell, 2003. **5**(3): p. 367-77.
78. Lien, W.H. and E. Fuchs, *Wnt some lose some: transcriptional governance of stem cells by Wnt/beta-catenin signaling.* Genes Dev, 2014. **28**(14): p. 1517-1532.

79. Atlasi, Y., L. Looijenga, and R. Fodde, *Cancer stem cells, pluripotency, and cellular heterogeneity: a WNTer perspective.* Curr Top Dev Biol, 2014. **107**: p. 373-404.
80. Holland, J.D., et al., *Wnt signaling in stem and cancer stem cells.* Curr Opin Cell Biol, 2013. **25**(2): p. 254-64.
81. Kishida, M., et al., *Axin prevents Wnt-3a-induced accumulation of beta-catenin.* Oncogene, 1999. **18**(4): p. 979-85.
82. Price, M.A., *CKI, there's more than one: casein kinase I family members in Wnt and Hedgehog signaling.* Genes Dev, 2006. **20**(4): p. 399-410.
83. Ikeda, S., et al., *Axin, a negative regulator of the Wnt signaling pathway, forms a complex with GSK-3beta and beta-catenin and promotes GSK-3beta-dependent phosphorylation of beta-catenin.* EMBO J, 1998. **17**(5): p. 1371-84.
84. Hsu, W., L. Zeng, and F. Costantini, *Identification of a domain of Axin that binds to the serine/threonine protein phosphatase 2A and a self-binding domain.* J Biol Chem, 1999. **274**(6): p. 3439-45.
85. Seeling, J.M., et al., *Regulation of beta-catenin signaling by the B56 subunit of protein phosphatase 2A.* Science, 1999. **283**(5410): p. 2089-91.
86. Stamos, J.L. and W.I. Weis, *The beta-catenin destruction complex.* Cold Spring Harb Perspect Biol, 2013. **5**(1): p. a007898.
87. Amit, S., et al., *Axin-mediated CKI phosphorylation of beta-catenin at Ser 45: a molecular switch for the Wnt pathway.* Genes Dev, 2002. **16**(9): p. 1066-76.
88. Liu, C., et al., *Control of beta-catenin phosphorylation/degradation by a dual-kinase mechanism.* Cell, 2002. **108**(6): p. 837-47.
89. Yost, C., et al., *The axis-inducing activity, stability, and subcellular distribution of beta-catenin is regulated in Xenopus embryos by glycogen synthase kinase 3.* Genes Dev, 1996. **10**(12): p. 1443-54.
90. Hagen, T., et al., *Expression and characterization of GSK-3 mutants and their effect on beta-catenin phosphorylation in intact cells.* J Biol Chem, 2002. **277**(26): p. 23330-5.
91. Wu, G. and X. He, *Threonine 41 in beta-catenin serves as a key phosphorylation relay residue in beta-catenin degradation.* Biochemistry, 2006. **45**(16): p. 5319-23.
92. Orford, K., et al., *Serine phosphorylation-regulated ubiquitination and degradation of beta-catenin.* J Biol Chem, 1997. **272**(40): p. 24735-8.
93. Wu, G., et al., *Structure of a beta-TrCP1-Skp1-beta-catenin complex: destruction motif binding and lysine specificity of the SCF(beta-TrCP1) ubiquitin ligase.* Mol Cell, 2003. **11**(6): p. 1445-56.
94. Hart, M., et al., *The F-box protein beta-TrCP associates with phosphorylated beta-catenin and regulates its activity in the cell.* Curr Biol, 1999. **9**(4): p. 207-10.
95. Kitagawa, M., et al., *An F-box protein, FWD1, mediates ubiquitin-dependent proteolysis of beta-catenin.* EMBO J, 1999. **18**(9): p. 2401-10.
96. Latres, E., D.S. Chiaur, and M. Pagano, *The human F box protein beta-Trcp associates with the Cul1/Skp1 complex and regulates the stability of beta-catenin.* Oncogene, 1999. **18**(4): p. 849-54.
97. Liu, C., et al., *beta-Trcp couples beta-catenin phosphorylation-degradation and regulates Xenopus axis formation.* Proc Natl Acad Sci U S A, 1999. **96**(11): p. 6273-8.

98. Winston, J.T., et al., *The SCFbeta-TRCP-ubiquitin ligase complex associates specifically with phosphorylated destruction motifs in IkappaBalpha and beta-catenin and stimulates IkappaBalpha ubiquitination in vitro.* Genes Dev, 1999. **13**(3): p. 270-83.
99. Aberle, H., et al., *beta-catenin is a target for the ubiquitin-proteasome pathway.* EMBO J, 1997. **16**(13): p. 3797-804.
100. Gates, J. and M. Peifer, *Can 1000 reviews be wrong? Actin, alpha-Catenin, and adherens junctions.* Cell, 2005. **123**(5): p. 769-72.
101. Rubinfeld, B., et al., *Association of the APC gene product with beta-catenin.* Science, 1993. **262**(5140): p. 1731-4.
102. Rubinfeld, B., et al., *Loss of beta-catenin regulation by the APC tumor suppressor protein correlates with loss of structure due to common somatic mutations of the gene.* Cancer Res, 1997. **57**(20): p. 4624-30.
103. Behrens, J., et al., *Functional interaction of beta-catenin with the transcription factor LEF-1.* Nature, 1996. **382**(6592): p. 638-42.
104. Molenaar, M., et al., *XTcf-3 transcription factor mediates beta-catenin-induced axis formation in Xenopus embryos.* Cell, 1996. **86**(3): p. 391-9.
105. Huber, O., et al., *Nuclear localization of beta-catenin by interaction with transcription factor LEF-1.* Mech Dev, 1996. **59**(1): p. 3-10.
106. Ikeda, S., et al., *GSK-3beta-dependent phosphorylation of adenomatous polyposis coli gene product can be modulated by beta-catenin and protein phosphatase 2A complexed with Axin.* Oncogene, 2000. **19**(4): p. 537-45.
107. Yamamoto, H., et al., *Phosphorylation of axin, a Wnt signal negative regulator, by glycogen synthase kinase-3beta regulates its stability.* J Biol Chem, 1999. **274**(16): p. 10681-4.
108. Rubinfeld, B., D.A. Tice, and P. Polakis, *Axin-dependent phosphorylation of the adenomatous polyposis coli protein mediated by casein kinase 1epsilon.* J Biol Chem, 2001. **276**(42): p. 39037-45.
109. Yamamoto, H., et al., *Inhibition of the Wnt signaling pathway by the PR61 subunit of protein phosphatase 2A.* J Biol Chem, 2001. **276**(29): p. 26875-82.
110. Behrens, J., et al., *Functional interaction of an axin homolog, conductin, with beta-catenin, APC, and GSK3beta.* Science, 1998. **280**(5363): p. 596-9.
111. Kishida, S., et al., *Axin, a negative regulator of the wnt signaling pathway, directly interacts with adenomatous polyposis coli and regulates the stabilization of beta-catenin.* J Biol Chem, 1998. **273**(18): p. 10823-6.
112. Spink, K.E., P. Polakis, and W.I. Weis, *Structural basis of the Axin-adenomatous polyposis coli interaction.* EMBO J, 2000. **19**(10): p. 2270-9.
113. Dajani, R., et al., *Structural basis for recruitment of glycogen synthase kinase 3beta to the axin-APC scaffold complex.* EMBO J, 2003. **22**(3): p. 494-501.
114. Ha, N.C., et al., *Mechanism of phosphorylation-dependent binding of APC to beta-catenin and its role in beta-catenin degradation.* Mol Cell, 2004. **15**(4): p. 511-21.
115. Zeng, L., et al., *The mouse Fused locus encodes Axin, an inhibitor of the Wnt signaling pathway that regulates embryonic axis formation.* Cell, 1997. **90**(1): p. 181-92.
116. Yamamoto, H., et al., *Axil, a member of the Axin family, interacts with both glycogen synthase kinase 3beta and beta-catenin and inhibits axis formation of Xenopus embryos.* Mol Cell Biol, 1998. **18**(5): p. 2867-75.

117. Jho, E.H., et al., *Wnt/beta-catenin/Tcf signaling induces the transcription of Axin2, a negative regulator of the signaling pathway.* Mol Cell Biol, 2002. **22**(4): p. 1172-83.
118. Leung, J.Y., et al., *Activation of AXIN2 expression by beta-catenin-T cell factor. A feedback repressor pathway regulating Wnt signaling.* J Biol Chem, 2002. **277**(24): p. 21657-65.
119. Chia, I.V. and F. Costantini, *Mouse axin and axin2/conductin proteins are functionally equivalent in vivo.* Mol Cell Biol, 2005. **25**(11): p. 4371-6.
120. Munemitsu, S., et al., *Deletion of an amino-terminal sequence beta-catenin in vivo and promotes hyperphosporylation of the adenomatous polyposis coli tumor suppressor protein.* Mol Cell Biol, 1996. **16**(8): p. 4088-94.
121. Korinek, V., et al., *Constitutive transcriptional activation by a beta-catenin-Tcf complex in APC-/- colon carcinoma.* Science, 1997. **275**(5307): p. 1784-7.
122. Morin, P.J., et al., *Activation of beta-catenin-Tcf signaling in colon cancer by mutations in beta-catenin or APC.* Science, 1997. **275**(5307): p. 1787-90.
123. Clevers, H., *Wnt/beta-catenin signaling in development and disease.* Cell, 2006. **127**(3): p. 469-80.
124. Ahmed, Y., A. Nouri, and E. Wieschaus, *Drosophila Apc1 and Apc2 regulate Wingless transduction throughout development.* Development, 2002. **129**(7): p. 1751-62.
125. Day, C.L. and T. Alber, *Crystal structure of the amino-terminal coiled-coil domain of the APC tumor suppressor.* J Mol Biol, 2000. **301**(1): p. 147-56.
126. Hirschl, D., P. Bayer, and O. Muller, *Secondary structure of an armadillo single repeat from the APC protein.* FEBS Lett, 1996. **383**(1-2): p. 31-6.
127. Eklof Spink, K., S.G. Fridman, and W.I. Weis, *Molecular mechanisms of beta-catenin recognition by adenomatous polyposis coli revealed by the structure of an APC-beta-catenin complex.* EMBO J, 2001. **20**(22): p. 6203-12.
128. Su, Y., et al., *APC is essential for targeting phosphorylated beta-catenin to the SCFbeta-TrCP ubiquitin ligase.* Mol Cell, 2008. **32**(5): p. 652-61.
129. Valvezan, A.J., et al., *Adenomatous polyposis coli (APC) regulates multiple signaling pathways by enhancing glycogen synthase kinase-3 (GSK-3) activity.* J Biol Chem, 2012. **287**(6): p. 3823-32.
130. Rubinfeld, B., et al., *Binding of GSK3beta to the APC-beta-catenin complex and regulation of complex assembly.* Science, 1996. **272**(5264): p. 1023-6.
131. Liu, J., et al., *The third 20 amino acid repeat is the tightest binding site of APC for beta-catenin.* J Mol Biol, 2006. **360**(1): p. 133-44.
132. Xing, Y., et al., *Crystal structure of a beta-catenin/axin complex suggests a mechanism for the beta-catenin destruction complex.* Genes Dev, 2003. **17**(22): p. 2753-64.
133. Xing, Y., et al., *Crystal structure of a beta-catenin/APC complex reveals a critical role for APC phosphorylation in APC function.* Mol Cell, 2004. **15**(4): p. 523-33.
134. Major, M.B., et al., *Wilms tumor suppressor WTX negatively regulates WNT/beta-catenin signaling.* Science, 2007. **316**(5827): p. 1043-6.
135. Crosas, B., et al., *Ubiquitin chains are remodeled at the proteasome by opposing ubiquitin ligase and deubiquitinating activities.* Cell, 2006. **127**(7): p. 1401-13.
136. Lee, M.J., et al., *Trimming of ubiquitin chains by proteasome-associated deubiquitinating enzymes.* Mol Cell Proteomics, 2011. **10**(5): p. R110 003871.

137. Woodgett, J.R., *Molecular cloning and expression of glycogen synthase kinase-3/factor A.* EMBO J, 1990. **9**(8): p. 2431-8.
138. Doble, B.W., et al., *Functional redundancy of GSK-3alpha and GSK-3beta in Wnt/beta-catenin signaling shown by using an allelic series of embryonic stem cell lines.* Dev Cell, 2007. **12**(6): p. 957-71.
139. McManus, E.J., et al., *Role that phosphorylation of GSK3 plays in insulin and Wnt signalling defined by knockin analysis.* EMBO J, 2005. **24**(8): p. 1571-83.
140. Patel, S., et al., *Tissue-specific role of glycogen synthase kinase 3beta in glucose homeostasis and insulin action.* Mol Cell Biol, 2008. **28**(20): p. 6314-28.
141. Kaidanovich-Beilin, O., et al., *Abnormalities in brain structure and behavior in GSK-3alpha mutant mice.* Mol Brain, 2009. **2**: p. 35.
142. Davidson, G., et al., *Casein kinase 1 gamma couples Wnt receptor activation to cytoplasmic signal transduction.* Nature, 2005. **438**(7069): p. 867-72.
143. Wu, C.H. and R. Nusse, *Ligand receptor interactions in the Wnt signaling pathway in Drosophila.* J Biol Chem, 2002. **277**(44): p. 41762-9.
144. Umbhauer, M., et al., *The C-terminal cytoplasmic Lys-thr-X-X-X-Trp motif in frizzled receptors mediates Wnt/beta-catenin signalling.* EMBO J, 2000. **19**(18): p. 4944-54.
145. Yanagawa, S., et al., *The dishevelled protein is modified by wingless signaling in Drosophila.* Genes Dev, 1995. **9**(9): p. 1087-97.
146. Bilic, J., et al., *Wnt induces LRP6 signalosomes and promotes dishevelled-dependent LRP6 phosphorylation.* Science, 2007. **316**(5831): p. 1619-22.
147. Gao, C. and Y.G. Chen, *Dishevelled: The hub of Wnt signaling.* Cell Signal, 2010. **22**(5): p. 717-27.
148. Ahumada, A., et al., *Signaling of rat Frizzled-2 through phosphodiesterase and cyclic GMP.* Science, 2002. **298**(5600): p. 2006-10.
149. Katanaev, V.L., et al., *Trimeric G protein-dependent frizzled signaling in Drosophila.* Cell, 2005. **120**(1): p. 111-22.
150. Liu, X., J.S. Rubin, and A.R. Kimmel, *Rapid, Wnt-induced changes in GSK3beta associations that regulate beta-catenin stabilization are mediated by Galpha proteins.* Curr Biol, 2005. **15**(22): p. 1989-97.
151. Halleskog, C., et al., *Heterotrimeric G protein-dependent WNT-5A signaling to ERK1/2 mediates distinct aspects of microglia proinflammatory transformation.* J Neuroinflammation, 2012. **9**: p. 111.
152. Zeng, X., et al., *A dual-kinase mechanism for Wnt co-receptor phosphorylation and activation.* Nature, 2005. **438**(7069): p. 873-7.
153. Mao, J., et al., *Low-density lipoprotein receptor-related protein-5 binds to Axin and regulates the canonical Wnt signaling pathway.* Mol Cell, 2001. **7**(4): p. 801-9.
154. Tolwinski, N.S., et al., *Wg/Wnt signal can be transmitted through arrow/LRP5,6 and Axin independently of Zw3/Gsk3beta activity.* Dev Cell, 2003. **4**(3): p. 407-18.
155. Itoh, K., et al., *Interaction of dishevelled and Xenopus axin-related protein is required for wnt signal transduction.* Mol Cell Biol, 2000. **20**(6): p. 2228-38.
156. Cliffe, A., F. Hamada, and M. Bienz, *A role of Dishevelled in relocating Axin to the plasma membrane during wingless signaling.* Curr Biol, 2003. **13**(11): p. 960-6.
157. Tamai, K., et al., *A mechanism for Wnt coreceptor activation.* Mol Cell, 2004. **13**(1): p. 149-56.

158. Beagle, B., K. Mi, and G.V. Johnson, *Phosphorylation of PPP(S/T)P motif of the free LRP6 intracellular domain is not required to activate the Wnt/beta-catenin pathway and attenuate GSK3beta activity.* J Cell Biochem, 2009. **108**(4): p. 886-95.
159. Lee, E., et al., *The roles of APC and Axin derived from experimental and theoretical analysis of the Wnt pathway.* PLoS Biol, 2003. **1**(1): p. E10.
160. Cadigan, K.M., *Wnt signaling--20 years and counting.* Trends Genet, 2002. **18**(7): p. 340-2.
161. Bienz, M. and H. Clevers, *Armadillo/beta-catenin signals in the nucleus--proof beyond a reasonable doubt?* Nat Cell Biol, 2003. **5**(3): p. 179-82.
162. Yang, J., et al., *PP2A:B56epsilon is required for Wnt/beta-catenin signaling during embryonic development.* Development, 2003. **130**(23): p. 5569-78.
163. Tolwinski, N.S. and E. Wieschaus, *A nuclear function for armadillo/beta-catenin.* PLoS Biol, 2004. **2**(4): p. E95.
164. Miller, J.R. and R.T. Moon, *Analysis of the signaling activities of localization mutants of beta-catenin during axis specification in Xenopus.* J Cell Biol, 1997. **139**(1): p. 229-43.
165. Cox, R.T., et al., *Membrane-tethered Drosophila Armadillo cannot transduce Wingless signal on its own.* Development, 1999. **126**(6): p. 1327-35.
166. Fagotto, F., U. Gluck, and B.M. Gumbiner, *Nuclear localization signal-independent and importin/karyopherin-independent nuclear import of beta-catenin.* Curr Biol, 1998. **8**(4): p. 181-90.
167. Yokoya, F., et al., *beta-catenin can be transported into the nucleus in a Ran-unassisted manner.* Mol Biol Cell, 1999. **10**(4): p. 1119-31.
168. Eleftheriou, A., M. Yoshida, and B.R. Henderson, *Nuclear export of human beta-catenin can occur independent of CRM1 and the adenomatous polyposis coli tumor suppressor.* J Biol Chem, 2001. **276**(28): p. 25883-8.
169. Sharma, M., et al., *Specific armadillo repeat sequences facilitate beta-catenin nuclear transport in live cells via direct binding to nucleoporins Nup62, Nup153, and RanBP2/Nup358.* J Biol Chem, 2012. **287**(2): p. 819-31.
170. Zhang, N., et al., *FoxM1 promotes beta-catenin nuclear localization and controls Wnt target-gene expression and glioma tumorigenesis.* Cancer Cell, 2011. **20**(4): p. 427-42.
171. van de Wetering, M., et al., *Armadillo coactivates transcription driven by the product of the Drosophila segment polarity gene dTCF.* Cell, 1997. **88**(6): p. 789-99.
172. Brantjes, H., et al., *TCF: Lady Justice casting the final verdict on the outcome of Wnt signalling.* Biol Chem, 2002. **383**(2): p. 255-61.
173. Galceran, J., et al., *Wnt3a-/--like phenotype and limb deficiency in Lef1(-/-)Tcf1(-/-) mice.* Genes Dev, 1999. **13**(6): p. 709-17.
174. Merrill, B.J., et al., *Tcf3: a transcriptional regulator of axis induction in the early embryo.* Development, 2004. **131**(2): p. 263-74.
175. Yi, F., et al., *Opposing effects of Tcf3 and Tcf1 control Wnt stimulation of embryonic stem cell self-renewal.* Nat Cell Biol, 2011. **13**(7): p. 762-70.
176. Wu, C.I., et al., *Function of Wnt/beta-catenin in counteracting Tcf3 repression through the Tcf3-beta-catenin interaction.* Development, 2012. **139**(12): p. 2118-29.
177. Cavallo, R.A., et al., *Drosophila Tcf and Groucho interact to repress Wingless signalling activity.* Nature, 1998. **395**(6702): p. 604-8.

178. Roose, J., et al., *The Xenopus Wnt effector XTcf-3 interacts with Groucho-related transcriptional repressors.* Nature, 1998. **395**(6702): p. 608-12.
179. Chen, G., et al., *A functional interaction between the histone deacetylase Rpd3 and the corepressor groucho in Drosophila development.* Genes Dev, 1999. **13**(17): p. 2218-30.
180. Daniels, D.L. and W.I. Weis, *Beta-catenin directly displaces Groucho/TLE repressors from Tcf/Lef in Wnt-mediated transcription activation.* Nat Struct Mol Biol, 2005. **12**(4): p. 364-71.
181. Hecht, A., et al., *The p300/CBP acetyltransferases function as transcriptional coactivators of beta-catenin in vertebrates.* EMBO J, 2000. **19**(8): p. 1839-50.
182. Takemaru, K.I. and R.T. Moon, *The transcriptional coactivator CBP interacts with beta-catenin to activate gene expression.* J Cell Biol, 2000. **149**(2): p. 249-54.
183. Barker, N., et al., *The chromatin remodelling factor Brg-1 interacts with beta-catenin to promote target gene activation.* EMBO J, 2001. **20**(17): p. 4935-43.
184. Mosimann, C., G. Hausmann, and K. Basler, *Parafibromin/Hyrax activates Wnt/Wg target gene transcription by direct association with beta-catenin/Armadillo.* Cell, 2006. **125**(2): p. 327-41.
185. Kramps, T., et al., *Wnt/wingless signaling requires BCL9/legless-mediated recruitment of pygopus to the nuclear beta-catenin-TCF complex.* Cell, 2002. **109**(1): p. 47-60.
186. Parker, D.S., J. Jemison, and K.M. Cadigan, *Pygopus, a nuclear PHD-finger protein required for Wingless signaling in Drosophila.* Development, 2002. **129**(11): p. 2565-76.
187. Thompson, B., et al., *A new nuclear component of the Wnt signalling pathway.* Nat Cell Biol, 2002. **4**(5): p. 367-73.
188. Townsley, F.M., A. Cliffe, and M. Bienz, *Pygopus and Legless target Armadillo/beta-catenin to the nucleus to enable its transcriptional co-activator function.* Nat Cell Biol, 2004. **6**(7): p. 626-33.
189. Hoffmans, R., R. Stadeli, and K. Basler, *Pygopus and legless provide essential transcriptional coactivator functions to armadillo/beta-catenin.* Curr Biol, 2005. **15**(13): p. 1207-11.
190. He, T.C., et al., *Identification of c-MYC as a target of the APC pathway.* Science, 1998. **281**(5382): p. 1509-12.
191. Shtutman, M., et al., *The cyclin D1 gene is a target of the beta-catenin/LEF-1 pathway.* Proc Natl Acad Sci U S A, 1999. **96**(10): p. 5522-7.
192. Tetsu, O. and F. McCormick, *Beta-catenin regulates expression of cyclin D1 in colon carcinoma cells.* Nature, 1999. **398**(6726): p. 422-6.
193. Hoffmeyer, K., et al., *Wnt/beta-catenin signaling regulates telomerase in stem cells and cancer cells.* Science, 2012. **336**(6088): p. 1549-54.
194. Lustig, B., et al., *Negative feedback loop of Wnt signaling through upregulation of conductin/axin2 in colorectal and liver tumors.* Mol Cell Biol, 2002. **22**(4): p. 1184-93.
195. Cadigan, K.M., et al., *Wingless repression of Drosophila frizzled 2 expression shapes the Wingless morphogen gradient in the wing.* Cell, 1998. **93**(5): p. 767-77.
196. Muller, H.A., R. Samanta, and E. Wieschaus, *Wingless signaling in the Drosophila embryo: zygotic requirements and the role of the frizzled genes.* Development, 1999. **126**(3): p. 577-86.

197. Sato, A., et al., *Dfrizzled-3, a new Drosophila Wnt receptor, acting as an attenuator of Wingless signaling in wingless hypomorphic mutants.* Development, 1999. **126**(20): p. 4421-30.
198. Willert, J., et al., *A transcriptional response to Wnt protein in human embryonic carcinoma cells.* BMC Dev Biol, 2002. **2**: p. 8.
199. Wu, Z.Q., et al., *Canonical Wnt suppressor, Axin2, promotes colon carcinoma oncogenic activity.* Proc Natl Acad Sci U S A, 2012. **109**(28): p. 11312-7.
200. Hovanes, K., et al., *Beta-catenin-sensitive isoforms of lymphoid enhancer factor-1 are selectively expressed in colon cancer.* Nat Genet, 2001. **28**(1): p. 53-7.
201. Roose, J., et al., *Synergy between tumor suppressor APC and the beta-catenin-Tcf4 target Tcf1.* Science, 1999. **285**(5435): p. 1923-6.
202. Takemaru, K., et al., *Chibby, a nuclear beta-catenin-associated antagonist of the Wnt/Wingless pathway.* Nature, 2003. **422**(6934): p. 905-9.
203. Tago, K., et al., *Inhibition of Wnt signaling by ICAT, a novel beta-catenin-interacting protein.* Genes Dev, 2000. **14**(14): p. 1741-9.
204. Daniels, D.L. and W.I. Weis, *ICAT inhibits beta-catenin binding to Tcf/Lef-family transcription factors and the general coactivator p300 using independent structural modules.* Mol Cell, 2002. **10**(3): p. 573-84.
205. Graham, T.A., et al., *The crystal structure of the beta-catenin/ICAT complex reveals the inhibitory mechanism of ICAT.* Mol Cell, 2002. **10**(3): p. 563-71.
206. Ishitani, T., et al., *The TAK1-NLK-MAPK-related pathway antagonizes signalling between beta-catenin and transcription factor TCF.* Nature, 1999. **399**(6738): p. 798-802.
207. Ishitani, T., J. Ninomiya-Tsuji, and K. Matsumoto, *Regulation of lymphoid enhancer factor 1/T-cell factor by mitogen-activated protein kinase-related Nemo-like kinase-dependent phosphorylation in Wnt/beta-catenin signaling.* Mol Cell Biol, 2003. **23**(4): p. 1379-89.
208. Henderson, B.R., *Nuclear-cytoplasmic shuttling of APC regulates beta-catenin subcellular localization and turnover.* Nat Cell Biol, 2000. **2**(9): p. 653-60.
209. Cong, F. and H. Varmus, *Nuclear-cytoplasmic shuttling of Axin regulates subcellular localization of beta-catenin.* Proc Natl Acad Sci U S A, 2004. **101**(9): p. 2882-7.
210. Bienz, M., *The subcellular destinations of APC proteins.* Nat Rev Mol Cell Biol, 2002. **3**(5): p. 328-38.
211. Sierra, J., et al., *The APC tumor suppressor counteracts beta-catenin activation and H3K4 methylation at Wnt target genes.* Genes Dev, 2006. **20**(5): p. 586-600.
212. Perissi, V. and M.G. Rosenfeld, *Controlling nuclear receptors: the circular logic of cofactor cycles.* Nat Rev Mol Cell Biol, 2005. **6**(7): p. 542-54.
213. Willert, K. and K.A. Jones, *Wnt signaling: is the party in the nucleus?* Genes Dev, 2006. **20**(11): p. 1394-404.
214. Habas, R. and I.B. Dawid, *Dishevelled and Wnt signaling: is the nucleus the final frontier?* J Biol, 2005. **4**(1): p. 2.
215. Caspi, M., et al., *Nuclear GSK-3beta inhibits the canonical Wnt signalling pathway in a beta-catenin phosphorylation-independent manner.* Oncogene, 2008. **27**(25): p. 3546-55.
216. Doble, B.W. and J.R. Woodgett, *GSK-3: tricks of the trade for a multi-tasking kinase.* J Cell Sci, 2003. **116**(Pt 7): p. 1175-86.

217. Kirkham, M. and R.G. Parton, *Clathrin-independent endocytosis: new insights into caveolae and non-caveolar lipid raft carriers.* Biochim Biophys Acta, 2005. **1746**(3): p. 349-63.
218. Razani, B., S.E. Woodman, and M.P. Lisanti, *Caveolae: from cell biology to animal physiology.* Pharmacol Rev, 2002. **54**(3): p. 431-67.
219. Yamamoto, H., H. Komekado, and A. Kikuchi, *Caveolin is necessary for Wnt-3a-dependent internalization of LRP6 and accumulation of beta-catenin.* Dev Cell, 2006. **11**(2): p. 213-23.
220. Khan, Z., et al., *Analysis of endogenous LRP6 function reveals a novel feedback mechanism by which Wnt negatively regulates its receptor.* Mol Cell Biol, 2007. **27**(20): p. 7291-301.
221. Zerial, M. and H. McBride, *Rab proteins as membrane organizers.* Nat Rev Mol Cell Biol, 2001. **2**(2): p. 107-17.
222. Schafer, D.A., *Regulating actin dynamics at membranes: a focus on dynamin.* Traffic, 2004. **5**(7): p. 463-9.
223. Mi, K., P.J. Dolan, and G.V. Johnson, *The low density lipoprotein receptor-related protein 6 interacts with glycogen synthase kinase 3 and attenuates activity.* J Biol Chem, 2006. **281**(8): p. 4787-94.
224. Blitzer, J.T. and R. Nusse, *A critical role for endocytosis in Wnt signaling.* BMC Cell Biol, 2006. **7**: p. 28.
225. Chen, W., et al., *beta-Arrestin1 modulates lymphoid enhancer factor transcriptional activity through interaction with phosphorylated dishevelled proteins.* Proc Natl Acad Sci U S A, 2001. **98**(26): p. 14889-94.
226. Bryja, V., et al., *Beta-arrestin is a necessary component of Wnt/beta-catenin signaling in vitro and in vivo.* Proc Natl Acad Sci U S A, 2007. **104**(16): p. 6690-5.
227. Taelman, V.F., et al., *Wnt signaling requires sequestration of glycogen synthase kinase 3 inside multivesicular endosomes.* Cell, 2010. **143**(7): p. 1136-48.
228. Jin, T., I. George Fantus, and J. Sun, *Wnt and beyond Wnt: multiple mechanisms control the transcriptional property of beta-catenin.* Cell Signal, 2008. **20**(10): p. 1697-704.
229. Yang, L., C. Lin, and Z.R. Liu, *P68 RNA helicase mediates PDGF-induced epithelial mesenchymal transition by displacing Axin from beta-catenin.* Cell, 2006. **127**(1): p. 139-55.
230. Yang, L., et al., *Phosphorylation of p68 RNA helicase plays a role in platelet-derived growth factor-induced cell proliferation by up-regulating cyclin D1 and c-Myc expression.* J Biol Chem, 2007. **282**(23): p. 16811-9.
231. Inoki, K., et al., *TSC2 integrates Wnt and energy signals via a coordinated phosphorylation by AMPK and GSK3 to regulate cell growth.* Cell, 2006. **126**(5): p. 955-68.
232. Xu, Q., et al., *Vascular development in the retina and inner ear: control by Norrin and Frizzled-4, a high-affinity ligand-receptor pair.* Cell, 2004. **116**(6): p. 883-95.
233. Kazanskaya, O., et al., *R-Spondin2 is a secreted activator of Wnt/beta-catenin signaling and is required for Xenopus myogenesis.* Dev Cell, 2004. **7**(4): p. 525-34.
234. Kim, K.A., et al., *R-Spondin proteins: a novel link to beta-catenin activation.* Cell Cycle, 2006. **5**(1): p. 23-6.

235. Kim, K.A., et al., *R-Spondin family members regulate the Wnt pathway by a common mechanism.* Mol Biol Cell, 2008. **19**(6): p. 2588-96.
236. Nam, J.S., et al., *Mouse cristin/R-spondin family proteins are novel ligands for the Frizzled 8 and LRP6 receptors and activate beta-catenin-dependent gene expression.* J Biol Chem, 2006. **281**(19): p. 13247-57.
237. Binnerts, M.E., et al., *R-Spondin1 regulates Wnt signaling by inhibiting internalization of LRP6.* Proc Natl Acad Sci U S A, 2007. **104**(37): p. 14700-5.
238. Wei, Q., et al., *R-spondin1 is a high affinity ligand for LRP6 and induces LRP6 phosphorylation and beta-catenin signaling.* J Biol Chem, 2007. **282**(21): p. 15903-11.
239. de Lau, W., et al., *Lgr5 homologues associate with Wnt receptors and mediate R-spondin signalling.* Nature, 2011. **476**(7360): p. 293-7.
240. Peng, W.C., et al., *Structure of stem cell growth factor R-spondin 1 in complex with the ectodomain of its receptor LGR5.* Cell Rep, 2013. **3**(6): p. 1885-92.
241. Jaks, V., et al., *Lgr5 marks cycling, yet long-lived, hair follicle stem cells.* Nat Genet, 2008. **40**(11): p. 1291-9.
242. Sato, T., et al., *Single Lgr5 stem cells build crypt-villus structures in vitro without a mesenchymal niche.* Nature, 2009. **459**(7244): p. 262-5.
243. van der Flier, L.G. and H. Clevers, *Stem cells, self-renewal, and differentiation in the intestinal epithelium.* Annu Rev Physiol, 2009. **71**: p. 241-60.
244. Carmon, K.S., et al., *LGR5 interacts and cointernalizes with Wnt receptors to modulate Wnt/beta-catenin signaling.* Mol Cell Biol, 2012. **32**(11): p. 2054-64.
245. Sato, T., et al., *Paneth cells constitute the niche for Lgr5 stem cells in intestinal crypts.* Nature, 2011. **469**(7330): p. 415-8.
246. Semenov, M.V., et al., *SnapShot: Noncanonical Wnt Signaling Pathways.* Cell, 2007. **131**(7): p. 1378.
247. Keller, R., *Shaping the vertebrate body plan by polarized embryonic cell movements.* Science, 2002. **298**(5600): p. 1950-4.
248. Schlessinger, K., A. Hall, and N. Tolwinski, *Wnt signaling pathways meet Rho GTPases.* Genes Dev, 2009. **23**(3): p. 265-77.
249. Djiane, A., et al., *Role of frizzled 7 in the regulation of convergent extension movements during gastrulation in Xenopus laevis.* Development, 2000. **127**(14): p. 3091-100.
250. Sugimura, R. and L. Li, *Noncanonical Wnt signaling in vertebrate development, stem cells, and diseases.* Birth Defects Res C Embryo Today, 2010. **90**(4): p. 243-56.
251. Habas, R., Y. Kato, and X. He, *Wnt/Frizzled activation of Rho regulates vertebrate gastrulation and requires a novel Formin homology protein Daam1.* Cell, 2001. **107**(7): p. 843-54.
252. Jaffe, A.B. and A. Hall, *Rho GTPases: biochemistry and biology.* Annu Rev Cell Dev Biol, 2005. **21**: p. 247-69.
253. Tu, D., et al., *Crystal structure of a coiled-coil domain from human ROCK I.* PLoS One, 2011. **6**(3): p. e18080.
254. Winter, C.G., et al., *Drosophila Rho-associated kinase (Drok) links Frizzled-mediated planar cell polarity signaling to the actin cytoskeleton.* Cell, 2001. **105**(1): p. 81-91.
255. Sato, A., et al., *Profilin is an effector for Daam1 in non-canonical Wnt signaling and is required for vertebrate gastrulation.* Development, 2006. **133**(21): p. 4219-31.

256. Habas, R., I.B. Dawid, and X. He, *Coactivation of Rac and Rho by Wnt/Frizzled signaling is required for vertebrate gastrulation.* Genes Dev, 2003. **17**(2): p. 295-309.
257. Saadeddin, A., et al., *The links between transcription, beta-catenin/JNK signaling, and carcinogenesis.* Mol Cancer Res, 2009. **7**(8): p. 1189-96.
258. Weber, U., et al., *Combinatorial signaling by the Frizzled/PCP and Egfr pathways during planar cell polarity establishment in the Drosophila eye.* Dev Biol, 2008. **316**(1): p. 110-23.
259. Jochum, W., E. Passegue, and E.F. Wagner, *AP-1 in mouse development and tumorigenesis.* Oncogene, 2001. **20**(19): p. 2401-12.
260. Paricio, N., et al., *The Drosophila STE20-like kinase misshapen is required downstream of the Frizzled receptor in planar polarity signaling.* EMBO J, 1999. **18**(17): p. 4669-78.
261. Kim, G.H. and J.K. Han, *JNK and ROKalpha function in the noncanonical Wnt/RhoA signaling pathway to regulate Xenopus convergent extension movements.* Dev Dyn, 2005. **232**(4): p. 958-68.
262. Nomachi, A., et al., *Receptor tyrosine kinase Ror2 mediates Wnt5a-induced polarized cell migration by activating c-Jun N-terminal kinase via actin-binding protein filamin A.* J Biol Chem, 2008. **283**(41): p. 27973-81.
263. Nishita, M., et al., *Ror2/Frizzled complex mediates Wnt5a-induced AP-1 activation by regulating Dishevelled polymerization.* Mol Cell Biol, 2010. **30**(14): p. 3610-9.
264. Hakeda-Suzuki, S., et al., *Rac function and regulation during Drosophila development.* Nature, 2002. **416**(6879): p. 438-42.
265. Munoz-Descalzo, S., et al., *Analysis of the role of the Rac/Cdc42 GTPases during planar cell polarity generation in Drosophila.* Int J Dev Biol, 2007. **51**(5): p. 379-87.
266. Eaton, S., et al., *CDC42 and Rac1 control different actin-dependent processes in the Drosophila wing disc epithelium.* J Cell Biol, 1995. **131**(1): p. 151-64.
267. Slusarski, D.C., et al., *Modulation of embryonic intracellular Ca2+ signaling by Wnt-5A.* Dev Biol, 1997. **182**(1): p. 114-20.
268. Slusarski, D.C., V.G. Corces, and R.T. Moon, *Interaction of Wnt and a Frizzled homologue triggers G-protein-linked phosphatidylinositol signalling.* Nature, 1997. **390**(6658): p. 410-3.
269. Ma, L. and H.Y. Wang, *Suppression of cyclic GMP-dependent protein kinase is essential to the Wnt/cGMP/Ca2+ pathway.* J Biol Chem, 2006. **281**(41): p. 30990-1001.
270. De, A., *Wnt/Ca2+ signaling pathway: a brief overview.* Acta Biochim Biophys Sin (Shanghai), 2011. **43**(10): p. 745-56.
271. Kuhl, M., et al., *Ca(2+)/calmodulin-dependent protein kinase II is stimulated by Wnt and Frizzled homologs and promotes ventral cell fates in Xenopus.* J Biol Chem, 2000. **275**(17): p. 12701-11.
272. Sheldahl, L.C., et al., *Protein kinase C is differentially stimulated by Wnt and Frizzled homologs in a G-protein-dependent manner.* Curr Biol, 1999. **9**(13): p. 695-8.
273. Saneyoshi, T., et al., *The Wnt/calcium pathway activates NF-AT and promotes ventral cell fate in Xenopus embryos.* Nature, 2002. **417**(6886): p. 295-9.
274. Kohn, A.D. and R.T. Moon, *Wnt and calcium signaling: beta-catenin-independent pathways.* Cell Calcium, 2005. **38**(3-4): p. 439-46.

275. Hogan, P.G., et al., *Transcriptional regulation by calcium, calcineurin, and NFAT.* Genes Dev, 2003. **17**(18): p. 2205-32.
276. Feske, S., et al., *Ca2+/calcineurin signalling in cells of the immune system.* Biochem Biophys Res Commun, 2003. **311**(4): p. 1117-32.
277. Wang, H., Y. Lee, and C.C. Malbon, *PDE6 is an effector for the Wnt/Ca2+/cGMP-signalling pathway in development.* Biochem Soc Trans, 2004. **32**(Pt 5): p. 792-6.
278. Sheldahl, L.C., et al., *Dishevelled activates Ca2+ flux, PKC, and CamKII in vertebrate embryos.* J Cell Biol, 2003. **161**(4): p. 769-77.
279. Ma, L., et al., *Dishevelled-3 C-terminal His single amino acid repeats are obligate for Wnt5a activation of non-canonical signaling.* J Mol Signal, 2010. **5**: p. 19.
280. Kuhl, M., et al., *Antagonistic regulation of convergent extension movements in Xenopus by Wnt/beta-catenin and Wnt/Ca2+ signaling.* Mech Dev, 2001. **106**(1-2): p. 61-76.
281. Gonzalez-Sancho, J.M., et al., *Wnt proteins induce dishevelled phosphorylation via an LRP5/6- independent mechanism, irrespective of their ability to stabilize beta-catenin.* Mol Cell Biol, 2004. **24**(11): p. 4757-68.
282. Choi, S.C. and J.K. Han, *Xenopus Cdc42 regulates convergent extension movements during gastrulation through Wnt/Ca2+ signaling pathway.* Dev Biol, 2002. **244**(2): p. 342-57.
283. Dejmek, J., et al., *Wnt-5a/Ca2+-induced NFAT activity is counteracted by Wnt-5a/Yes-Cdc42-casein kinase 1alpha signaling in human mammary epithelial cells.* Mol Cell Biol, 2006. **26**(16): p. 6024-36.
284. Yang, G.Y., et al., *Calpain activation by Wingless-type murine mammary tumor virus integration site family, member 5A (Wnt5a) promotes axonal growth.* J Biol Chem, 2011. **286**(8): p. 6566-76.
285. Li, L., B.I. Hutchins, and K. Kalil, *Wnt5a induces simultaneous cortical axon outgrowth and repulsive axon guidance through distinct signaling mechanisms.* J Neurosci, 2009. **29**(18): p. 5873-83.
286. O'Connell, M.P., et al., *Wnt5A activates the calpain-mediated cleavage of filamin A.* J Invest Dermatol, 2009. **129**(7): p. 1782-9.
287. Nishita, M., et al., *Filopodia formation mediated by receptor tyrosine kinase Ror2 is required for Wnt5a-induced cell migration.* J Cell Biol, 2006. **175**(4): p. 555-62.
288. Chen, W., et al., *Dishevelled 2 recruits beta-arrestin 2 to mediate Wnt5A-stimulated endocytosis of Frizzled 4.* Science, 2003. **301**(5638): p. 1391-4.
289. Yu, A., et al., *Association of Dishevelled with the clathrin AP-2 adaptor is required for Frizzled endocytosis and planar cell polarity signaling.* Dev Cell, 2007. **12**(1): p. 129-41.
290. O'Connell, M.P., et al., *Heparan sulfate proteoglycan modulation of Wnt5A signal transduction in metastatic melanoma cells.* J Biol Chem, 2009. **284**(42): p. 28704-12.
291. Ohkawara, B., A. Glinka, and C. Niehrs, *Rspo3 binds syndecan 4 and induces Wnt/PCP signaling via clathrin-mediated endocytosis to promote morphogenesis.* Dev Cell, 2011. **20**(3): p. 303-14.
292. Wu, X., et al., *Rac1 activation controls nuclear localization of beta-catenin during canonical Wnt signaling.* Cell, 2008. **133**(2): p. 340-53.

293. Sen, M., *Wnt signalling in rheumatoid arthritis.* Rheumatology (Oxford), 2005. **44**(6): p. 708-13.
294. Grumolato, L., et al., *Canonical and noncanonical Wnts use a common mechanism to activate completely unrelated coreceptors.* Genes Dev, 2010. **24**(22): p. 2517-30.
295. Ziemer, L.T., D. Pennica, and A.J. Levine, *Identification of a mouse homolog of the human BTEB2 transcription factor as a beta-catenin-independent Wnt-1-responsive gene.* Mol Cell Biol, 2001. **21**(2): p. 562-74.
296. Lu, W., et al., *Mammalian Ryk is a Wnt coreceptor required for stimulation of neurite outgrowth.* Cell, 2004. **119**(1): p. 97-108.
297. He, X., et al., *A member of the Frizzled protein family mediating axis induction by Wnt-5A.* Science, 1997. **275**(5306): p. 1652-4.
298. Lin, X., *Functions of heparan sulfate proteoglycans in cell signaling during development.* Development, 2004. **131**(24): p. 6009-21.
299. Yamamoto, S., et al., *Cthrc1 selectively activates the planar cell polarity pathway of Wnt signaling by stabilizing the Wnt-receptor complex.* Dev Cell, 2008. **15**(1): p. 23-36.
300. Wainwright, B.J., et al., *Isolation of a human gene with protein sequence similarity to human and murine int-1 and the Drosophila segment polarity mutant wingless.* EMBO J, 1988. **7**(6): p. 1743-8.
301. Betsholtz, C., et al., *Efficient reversion of simian sarcoma virus-transformation and inhibition of growth factor-induced mitogenesis by suramin.* Proc Natl Acad Sci U S A, 1986. **83**(17): p. 6440-4.
302. Williams, L.T., et al., *Platelet-derived growth factor receptors form a high affinity state in membrane preparations. Kinetics and affinity cross-linking studies.* J Biol Chem, 1984. **259**(8): p. 5287-94.
303. Blasband, A., B. Schryver, and J. Papkoff, *The biochemical properties and transforming potential of human Wnt-2 are similar to Wnt-1.* Oncogene, 1992. **7**(1): p. 153-61.
304. Farrall, M., et al., *Recombinations between IRP and cystic fibrosis.* Am J Hum Genet, 1988. **43**(4): p. 471-5.
305. Levay-Young, B.K. and M. Navre, *Growth and developmental regulation of wnt-2 (irp) gene in mesenchymal cells of fetal lung.* Am J Physiol, 1992. **262**(6 Pt 1): p. L672-83.
306. Goss, A.M., et al., *Wnt2/2b and beta-catenin signaling are necessary and sufficient to specify lung progenitors in the foregut.* Dev Cell, 2009. **17**(2): p. 290-8.
307. Goss, A.M., et al., *Wnt2 signaling is necessary and sufficient to activate the airway smooth muscle program in the lung by regulating myocardin/Mrtf-B and Fgf10 expression.* Dev Biol, 2011. **356**(2): p. 541-52.
308. Onizuka, T., et al., *Wnt2 accelerates cardiac myocyte differentiation from ES-cell derived mesodermal cells via non-canonical pathway.* J Mol Cell Cardiol, 2012. **52**(3): p. 650-9.
309. Wayman, G.A., et al., *Activity-dependent dendritic arborization mediated by CaM-kinase I activation and enhanced CREB-dependent transcription of Wnt-2.* Neuron, 2006. **50**(6): p. 897-909.
310. Rawal, N., et al., *Dynamic temporal and cell type-specific expression of Wnt signaling components in the developing midbrain.* Exp Cell Res, 2006. **312**(9): p. 1626-36.

311. Sousa, K.M., et al., *Wnt2 regulates progenitor proliferation in the developing ventral midbrain.* J Biol Chem, 2010. **285**(10): p. 7246-53.
312. Klein, D., et al., *Wnt2 acts as a cell type-specific, autocrine growth factor in rat hepatic sinusoidal endothelial cells cross-stimulating the VEGF pathway.* Hepatology, 2008. **47**(3): p. 1018-31.
313. Ding, B.S., et al., *Inductive angiocrine signals from sinusoidal endothelium are required for liver regeneration.* Nature, 2010. **468**(7321): p. 310-5.
314. Klein, D., et al., *Wnt2 acts as an angiogenic growth factor for non-sinusoidal endothelial cells and inhibits expression of stanniocalcin-1.* Angiogenesis, 2009. **12**(3): p. 251-65.
315. Dale, T.C., et al., *Compartment switching of WNT-2 expression in human breast tumors.* Cancer Res, 1996. **56**(19): p. 4320-3.
316. Katoh, M., *WNT2 and human gastrointestinal cancer (review).* Int J Mol Med, 2003. **12**(5): p. 811-6.
317. Pu, P., et al., *Downregulation of Wnt2 and beta-catenin by siRNA suppresses malignant glioma cell growth.* Cancer Gene Ther, 2009. **16**(4): p. 351-61.
318. Shi, Y., et al., *Inhibition of Wnt-2 and galectin-3 synergistically destabilizes beta-catenin and induces apoptosis in human colorectal cancer cells.* Int J Cancer, 2007. **121**(6): p. 1175-81.
319. You, L., et al., *Inhibition of Wnt-2-mediated signaling induces programmed cell death in non-small-cell lung cancer cells.* Oncogene, 2004. **23**(36): p. 6170-4.
320. You, L., et al., *An anti-Wnt-2 monoclonal antibody induces apoptosis in malignant melanoma cells and inhibits tumor growth.* Cancer Res, 2004. **64**(15): p. 5385-9.
321. Bravo, D.T., et al., *Frizzled-8 receptor is activated by the Wnt-2 ligand in non-small cell lung cancer.* BMC Cancer, 2013. **13**: p. 316.
322. Planutis, K., et al., *Regulation of norrin receptor frizzled-4 by Wnt2 in colon-derived cells.* BMC Cell Biol, 2007. **8**: p. 12.
323. Vider, B.Z., et al., *Evidence for the involvement of the Wnt 2 gene in human colorectal cancer.* Oncogene, 1996. **12**(1): p. 153-8.
324. Holcombe, R.F., et al., *Expression of Wnt ligands and Frizzled receptors in colonic mucosa and in colon carcinoma.* Mol Pathol, 2002. **55**(4): p. 220-6.
325. Smith, K., et al., *Up-regulation of macrophage wnt gene expression in adenoma-carcinoma progression of human colorectal cancer.* Br J Cancer, 1999. **81**(3): p. 496-502.
326. Park, J.K., et al., *Overexpression of Wnt-2 in colorectal cancers.* Neoplasma, 2009. **56**(2): p. 119-23.
327. Fu, L., et al., *Wnt2 secreted by tumour fibroblasts promotes tumour progression in oesophageal cancer by activation of the Wnt/beta-catenin signalling pathway.* Gut, 2011. **60**(12): p. 1635-43.
328. Liu, X., et al., *Wnt2 inhibits enteric bacterial-induced inflammation in intestinal epithelial cells.* Inflamm Bowel Dis, 2012. **18**(3): p. 418-29.
329. Boyer, L.A., et al., *Core transcriptional regulatory circuitry in human embryonic stem cells.* Cell, 2005. **122**(6): p. 947-56.
330. Sato, N., et al., *Maintenance of pluripotency in human and mouse embryonic stem cells through activation of Wnt signaling by a pharmacological GSK-3-specific inhibitor.* Nat Med, 2004. **10**(1): p. 55-63.
331. ten Berge, D., et al., *Embryonic stem cells require Wnt proteins to prevent differentiation to epiblast stem cells.* Nat Cell Biol, 2011. **13**(9): p. 1070-5.

332. Lindsley, R.C., et al., *Canonical Wnt signaling is required for development of embryonic stem cell-derived mesoderm.* Development, 2006. **133**(19): p. 3787-96.
333. Bakre, M.M., et al., *Generation of multipotential mesendodermal progenitors from mouse embryonic stem cells via sustained Wnt pathway activation.* J Biol Chem, 2007. **282**(43): p. 31703-12.
334. Merrill, B.J., *Wnt pathway regulation of embryonic stem cell self-renewal.* Cold Spring Harb Perspect Biol, 2012. **4**(9): p. a007971.
335. Yi, F., L. Pereira, and B.J. Merrill, *Tcf3 functions as a steady-state limiter of transcriptional programs of mouse embryonic stem cell self-renewal.* Stem Cells, 2008. **26**(8): p. 1951-60.
336. Williams, R.L., et al., *Myeloid leukaemia inhibitory factor maintains the developmental potential of embryonic stem cells.* Nature, 1988. **336**(6200): p. 684-7.
337. Wray, J., et al., *Inhibition of glycogen synthase kinase-3 alleviates Tcf3 repression of the pluripotency network and increases embryonic stem cell resistance to differentiation.* Nat Cell Biol, 2011. **13**(7): p. 838-45.
338. Ying, Q.L., et al., *The ground state of embryonic stem cell self-renewal.* Nature, 2008. **453**(7194): p. 519-23.
339. Niwa, H., *Wnt: what's needed to maintain pluripotency?* Nat Cell Biol, 2011. **13**(9): p. 1024-6.
340. Lyashenko, N., et al., *Differential requirement for the dual functions of beta-catenin in embryonic stem cell self-renewal and germ layer formation.* Nat Cell Biol, 2011. **13**(7): p. 753-61.
341. Mendelson, A. and P.S. Frenette, *Hematopoietic stem cell niche maintenance during homeostasis and regeneration.* Nat Med, 2014. **20**(8): p. 833-46.
342. Kolf, C.M., E. Cho, and R.S. Tuan, *Mesenchymal stromal cells. Biology of adult mesenchymal stem cells: regulation of niche, self-renewal and differentiation.* Arthritis Res Ther, 2007. **9**(1): p. 204.
343. Ladran, I., et al., *Neural stem and progenitor cells in health and disease.* Wiley Interdiscip Rev Syst Biol Med, 2013. **5**(6): p. 701-15.
344. Fujii, M. and T. Sato, *Culturing intestinal stem cells: applications for colorectal cancer research.* Front Genet, 2014. **5**: p. 169.
345. Barker, N., *Adult intestinal stem cells: critical drivers of epithelial homeostasis and regeneration.* Nat Rev Mol Cell Biol, 2014. **15**(1): p. 19-33.
346. Cheng, H. and C.P. Leblond, *Origin, differentiation and renewal of the four main epithelial cell types in the mouse small intestine. V. Unitarian Theory of the origin of the four epithelial cell types.* Am J Anat, 1974. **141**(4): p. 537-61.
347. Potten, C.S., et al., *The segregation of DNA in epithelial stem cells.* Cell, 1978. **15**(3): p. 899-906.
348. Barker, N., et al., *Identification of stem cells in small intestine and colon by marker gene Lgr5.* Nature, 2007. **449**(7165): p. 1003-7.
349. Sangiorgi, E. and M.R. Capecchi, *Bmi1 is expressed in vivo in intestinal stem cells.* Nat Genet, 2008. **40**(7): p. 915-20.
350. Yan, K.S., et al., *The intestinal stem cell markers Bmi1 and Lgr5 identify two functionally distinct populations.* Proc Natl Acad Sci U S A, 2012. **109**(2): p. 466-71.
351. van Es, J.H., et al., *Dll1+ secretory progenitor cells revert to stem cells upon crypt damage.* Nat Cell Biol, 2012. **14**(10): p. 1099-104.

352. Carulli, A.J., L.C. Samuelson, and S. Schnell, *Unraveling intestinal stem cell behavior with models of crypt dynamics.* Integr Biol (Camb), 2014. **6**(3): p. 243-57.
353. Durand, A., et al., *Functional intestinal stem cells after Paneth cell ablation induced by the loss of transcription factor Math1 (Atoh1).* Proc Natl Acad Sci U S A, 2012. **109**(23): p. 8965-70.
354. Kim, T.H., S. Escudero, and R.A. Shivdasani, *Intact function of Lgr5 receptor-expressing intestinal stem cells in the absence of Paneth cells.* Proc Natl Acad Sci U S A, 2012. **109**(10): p. 3932-7.
355. Farin, H.F., J.H. Van Es, and H. Clevers, *Redundant sources of Wnt regulate intestinal stem cells and promote formation of Paneth cells.* Gastroenterology, 2012. **143**(6): p. 1518-1529 e7.
356. Korinek, V., et al., *Depletion of epithelial stem-cell compartments in the small intestine of mice lacking Tcf-4.* Nat Genet, 1998. **19**(4): p. 379-83.
357. Pinto, D., et al., *Canonical Wnt signals are essential for homeostasis of the intestinal epithelium.* Genes Dev, 2003. **17**(14): p. 1709-13.
358. Ireland, H., et al., *Inducible Cre-mediated control of gene expression in the murine gastrointestinal tract: effect of loss of beta-catenin.* Gastroenterology, 2004. **126**(5): p. 1236-46.
359. Greco, V., et al., *A two-step mechanism for stem cell activation during hair regeneration.* Cell Stem Cell, 2009. **4**(2): p. 155-69.
360. Tian, H., et al., *A reserve stem cell population in small intestine renders Lgr5-positive cells dispensable.* Nature, 2011. **478**(7368): p. 255-9.
361. Buczacki, S.J., et al., *Intestinal label-retaining cells are secretory precursors expressing Lgr5.* Nature, 2013. **495**(7439): p. 65-9.
362. Ritsma, L., et al., *Intestinal crypt homeostasis revealed at single-stem-cell level by in vivo live imaging.* Nature, 2014. **507**(7492): p. 362-5.
363. Barker, N., M. van de Wetering, and H. Clevers, *The intestinal stem cell.* Genes Dev, 2008. **22**(14): p. 1856-64.
364. Beausejour, M., et al., *Suppression of anoikis in human intestinal epithelial cells: differentiation state-selective roles of alpha2beta1, alpha3beta1, alpha5beta1, and alpha6beta4 integrins.* BMC Cell Biol, 2013. **14**: p. 53.
365. Bjerknes, M. and H. Cheng, *Gastrointestinal stem cells. II. Intestinal stem cells.* Am J Physiol Gastrointest Liver Physiol, 2005. **289**(3): p. G381-7.
366. Ireland, H., et al., *Cellular inheritance of a Cre-activated reporter gene to determine Paneth cell longevity in the murine small intestine.* Dev Dyn, 2005. **233**(4): p. 1332-6.
367. Munoz, J., et al., *The Lgr5 intestinal stem cell signature: robust expression of proposed quiescent '+4' cell markers.* EMBO J, 2012. **31**(14): p. 3079-91.
368. Ferlay, J., et al., *Estimates of worldwide burden of cancer in 2008: GLOBOCAN 2008.* Int J Cancer, 2010. **127**(12): p. 2893-917.
369. Haggar, F.A. and R.P. Boushey, *Colorectal cancer epidemiology: incidence, mortality, survival, and risk factors.* Clin Colon Rectal Surg, 2009. **22**(4): p. 191-7.
370. Willett, W.C., *Diet and cancer: an evolving picture.* JAMA, 2005. **293**(2): p. 233-4.
371. Boyle, P. and J. Ferlay, *Mortality and survival in breast and colorectal cancer.* Nat Clin Pract Oncol, 2005. **2**(9): p. 424-5.

372. Janout, V. and H. Kollarova, *Epidemiology of colorectal cancer.* Biomed Pap Med Fac Univ Palacky Olomouc Czech Repub, 2001. **145**(1): p. 5-10.
373. Larsson, S.C. and A. Wolk, *Meat consumption and risk of colorectal cancer: a meta-analysis of prospective studies.* Int J Cancer, 2006. **119**(11): p. 2657-64.
374. Santarelli, R.L., F. Pierre, and D.E. Corpet, *Processed meat and colorectal cancer: a review of epidemiologic and experimental evidence.* Nutr Cancer, 2008. **60**(2): p. 131-44.
375. Kabat, G.C., et al., *A cohort study of dietary iron and heme iron intake and risk of colorectal cancer in women.* Br J Cancer, 2007. **97**(1): p. 118-22.
376. Sinha, R., *An epidemiologic approach to studying heterocyclic amines.* Mutat Res, 2002. **506-507**: p. 197-204.
377. Irabor, D.O., *Colorectal carcinoma: why is there a lower incidence in Nigerians when compared to Caucasians?* J Cancer Epidemiol, 2011. **2011**: p. 675154.
378. Janakiram, N.B. and C.V. Rao, *The role of inflammation in colon cancer.* Adv Exp Med Biol, 2014. **816**: p. 25-52.
379. Huttenhower, C., A.D. Kostic, and R.J. Xavier, *Inflammatory bowel disease as a model for translating the microbiome.* Immunity, 2014. **40**(6): p. 843-54.
380. Lakatos, P.L. and L. Lakatos, *Risk for colorectal cancer in ulcerative colitis: changes, causes and management strategies.* World J Gastroenterol, 2008. **14**(25): p. 3937-47.
381. Askling, J., et al., *Family history as a risk factor for colorectal cancer in inflammatory bowel disease.* Gastroenterology, 2001. **120**(6): p. 1356-62.
382. Thun, M.J., M.M. Namboodiri, and C.W. Heath, Jr., *Aspirin use and reduced risk of fatal colon cancer.* N Engl J Med, 1991. **325**(23): p. 1593-6.
383. Smalley, W.E. and R.N. DuBois, *Colorectal cancer and nonsteroidal anti-inflammatory drugs.* Adv Pharmacol, 1997. **39**: p. 1-20.
384. Hawk, E.T. and B. Levin, *Colorectal cancer prevention.* J Clin Oncol, 2005. **23**(2): p. 378-91.
385. Brenner, H., M. Kloor, and C.P. Pox, *Colorectal cancer.* Lancet, 2014. **383**(9927): p. 1490-502.
386. Ferretti, S., et al., *[TNM classification of malignant tumours, VII edition 2009. Changes and practical effects on cancer epidemiology].* Epidemiol Prev, 2010. **34**(3): p. 125-8.
387. Sheth, K.R. and B.M. Clary, *Management of hepatic metastases from colorectal cancer.* Clin Colon Rectal Surg, 2005. **18**(3): p. 215-23.
388. Mitry, E., et al., *Epidemiology, management and prognosis of colorectal cancer with lung metastases: a 30-year population-based study.* Gut, 2010. **59**(10): p. 1383-8.
389. Nozue, M., et al., *Treatment and prognosis in colorectal cancer patients with bone metastasis.* Oncol Rep, 2002. **9**(1): p. 109-12.
390. Mongan, J.P., et al., *Brain metastases from colorectal cancer: risk factors, incidence, and the possible role of chemokines.* Clin Colorectal Cancer, 2009. **8**(2): p. 100-5.
391. Tanaka, T., *Colorectal carcinogenesis: Review of human and experimental animal studies.* J Carcinog, 2009. **8**: p. 5.
392. Giles, R.H., J.H. van Es, and H. Clevers, *Caught up in a Wnt storm: Wnt signaling in cancer.* Biochim Biophys Acta, 2003. **1653**(1): p. 1-24.
393. Fearon, E.R., *Molecular genetics of colorectal cancer.* Annu Rev Pathol, 2011. **6**: p. 479-507.

394. Segditsas, S. and I. Tomlinson, *Colorectal cancer and genetic alterations in the Wnt pathway.* Oncogene, 2006. **25**(57): p. 7531-7.
395. Laurent-Puig, P., C. Beroud, and T. Soussi, *APC gene: database of germline and somatic mutations in human tumors and cell lines.* Nucleic Acids Res, 1998. **26**(1): p. 269-70.
396. Fearnhead, N.S., M.P. Britton, and W.F. Bodmer, *The ABC of APC.* Hum Mol Genet, 2001. **10**(7): p. 721-33.
397. Smits, R., et al., *Somatic Apc mutations are selected upon their capacity to inactivate the beta-catenin downregulating activity.* Genes Chromosomes Cancer, 2000. **29**(3): p. 229-39.
398. Mahmoud, N.N., et al., *Genotype-phenotype correlation in murine Apc mutation: differences in enterocyte migration and response to sulindac.* Cancer Res, 1999. **59**(2): p. 353-9.
399. Dihlmann, S., et al., *Dominant negative effect of the APC1309 mutation: a possible explanation for genotype-phenotype correlations in familial adenomatous polyposis.* Cancer Res, 1999. **59**(8): p. 1857-60.
400. Samowitz, W.S., et al., *Beta-catenin mutations are more frequent in small colorectal adenomas than in larger adenomas and invasive carcinomas.* Cancer Res, 1999. **59**(7): p. 1442-4.
401. Polakis, P., *The oncogenic activation of beta-catenin.* Curr Opin Genet Dev, 1999. **9**(1): p. 15-21.
402. Webster, M.T., et al., *Sequence variants of the axin gene in breast, colon, and other cancers: an analysis of mutations that interfere with GSK3 binding.* Genes Chromosomes Cancer, 2000. **28**(4): p. 443-53.
403. Lengauer, C., K.W. Kinzler, and B. Vogelstein, *Genetic instability in colorectal cancers.* Nature, 1997. **386**(6625): p. 623-7.
404. Armaghany, T., et al., *Genetic alterations in colorectal cancer.* Gastrointest Cancer Res, 2012. **5**(1): p. 19-27.
405. Miyaki, M., et al., *Higher frequency of Smad4 gene mutation in human colorectal cancer with distant metastasis.* Oncogene, 1999. **18**(20): p. 3098-103.
406. Shi, Y., et al., *A structural basis for mutational inactivation of the tumour suppressor Smad4.* Nature, 1997. **388**(6637): p. 87-93.
407. Woodford-Richens, K.L., et al., *SMAD4 mutations in colorectal cancer probably occur before chromosomal instability, but after divergence of the microsatellite instability pathway.* Proc Natl Acad Sci U S A, 2001. **98**(17): p. 9719-23.
408. Levine, A.J., *p53, the cellular gatekeeper for growth and division.* Cell, 1997. **88**(3): p. 323-31.
409. Fearon, E.R. and B. Vogelstein, *A genetic model for colorectal tumorigenesis.* Cell, 1990. **61**(5): p. 759-67.
410. Greenblatt, M.S., et al., *Mutations in the p53 tumor suppressor gene: clues to cancer etiology and molecular pathogenesis.* Cancer Res, 1994. **54**(18): p. 4855-78.
411. Bettington, M., et al., *The serrated pathway to colorectal carcinoma: current concepts and challenges.* Histopathology, 2013. **62**(3): p. 367-86.
412. Frank, S.A., in *Dynamics of Cancer: Incidence, Inheritance, and Evolution*2007: Princeton (NJ).
413. Shih, I.M., et al., *Top-down morphogenesis of colorectal tumors.* Proc Natl Acad Sci U S A, 2001. **98**(5): p. 2640-5.

414. Preston, S.L., et al., *Bottom-up histogenesis of colorectal adenomas: origin in the monocryptal adenoma and initial expansion by crypt fission.* Cancer Res, 2003. **63**(13): p. 3819-25.
415. Barker, N., et al., *Crypt stem cells as the cells-of-origin of intestinal cancer.* Nature, 2009. **457**(7229): p. 608-11.
416. Schwitalla, S., et al., *Intestinal tumorigenesis initiated by dedifferentiation and acquisition of stem-cell-like properties.* Cell, 2013. **152**(1-2): p. 25-38.
417. Roy, H.K. and H.T. Lynch, *Diagnosing Lynch syndrome: is the answer in the mouth?* Gut, 2003. **52**(12): p. 1665-7.
418. Sloane, J., et al., *Familial adenomatous polyposis: not all masses are desmoids.* Fam Cancer, 2013. **12**(3): p. 525-8.
419. Matsumoto, T., et al., *Serrated adenoma in familial adenomatous polyposis: relation to germline APC gene mutation.* Gut, 2002. **50**(3): p. 402-4.
420. Boland, C.R. and H.T. Lynch, *The history of Lynch syndrome.* Fam Cancer, 2013. **12**(2): p. 145-57.
421. Warthin, A.S., *The further study of a cancer family.* J Cancer Research, 1925. **9**: p. 279-286.
422. Lynch, H.T. and A.J. Krush, *Cancer family "G" revisited: 1895-1970.* Cancer, 1971. **27**(6): p. 1505-11.
423. Lynch, H.T., et al., *Hereditary nonpolyposis colorectal cancer (Lynch syndromes I and II). I. Clinical description of resource.* Cancer, 1985. **56**(4): p. 934-8.
424. Lynch, H.T., et al., *Hereditary nonpolyposis colorectal cancer (Lynch syndromes I and II). II. Biomarker studies.* Cancer, 1985. **56**(4): p. 939-51.
425. Douglas, J.A., et al., *History and molecular genetics of Lynch syndrome in family G: a century later.* JAMA, 2005. **294**(17): p. 2195-202.
426. Bronner, C.E., et al., *Mutation in the DNA mismatch repair gene homologue hMLH1 is associated with hereditary non-polyposis colon cancer.* Nature, 1994. **368**(6468): p. 258-61.
427. Peltomaki, P., *Epigenetic mechanisms in the pathogenesis of Lynch syndrome.* Clin Genet, 2014. **85**(5): p. 403-12.
428. Lynch, H.T., T. Smyrk, and J. Lynch, *An update of HNPCC (Lynch syndrome).* Cancer Genet Cytogenet, 1997. **93**(1): p. 84-99.
429. Vasen, H.F., et al., *The International Collaborative Group on Hereditary Non-Polyposis Colorectal Cancer (ICG-HNPCC).* Dis Colon Rectum, 1991. **34**(5): p. 424-5.
430. Vasen, H.F., et al., *New clinical criteria for hereditary nonpolyposis colorectal cancer (HNPCC, Lynch syndrome) proposed by the International Collaborative group on HNPCC.* Gastroenterology, 1999. **116**(6): p. 1453-6.
431. Boland, C.R., et al., *A National Cancer Institute Workshop on Microsatellite Instability for cancer detection and familial predisposition: development of international criteria for the determination of microsatellite instability in colorectal cancer.* Cancer Res, 1998. **58**(22): p. 5248-57.
432. Lindor, N.M., et al., *Lower cancer incidence in Amsterdam-I criteria families without mismatch repair deficiency: familial colorectal cancer type X.* JAMA, 2005. **293**(16): p. 1979-85.
433. Boland, C.R. and M. Shike, *Report from the Jerusalem workshop on Lynch syndrome-hereditary nonpolyposis colorectal cancer.* Gastroenterology, 2010. **138**(7): p. 2197 e1-7.

434. de Vos tot Nederveen Cappel, W.H., et al., *Colorectal surveillance in Lynch syndrome families.* Fam Cancer, 2013. **12**(2): p. 261-5.
435. Augsten, M., *Cancer-associated fibroblasts as another polarized cell type of the tumor microenvironment.* Front Oncol, 2014. **4**: p. 62.
436. Dvorak, H.F., *Tumors: wounds that do not heal. Similarities between tumor stroma generation and wound healing.* N Engl J Med, 1986. **315**(26): p. 1650-9.
437. Bissell, M.J., et al., *Tissue structure, nuclear organization, and gene expression in normal and malignant breast.* Cancer Res, 1999. **59**(7 Suppl): p. 1757-1763s; discussion 1763s-1764s.
438. Goubran, H.A., et al., *Regulation of tumor growth and metastasis: the role of tumor microenvironment.* Cancer Growth Metastasis, 2014. **7**: p. 9-18.
439. Cirri, P. and P. Chiarugi, *Cancer associated fibroblasts: the dark side of the coin.* Am J Cancer Res, 2011. **1**(4): p. 482-97.
440. Kalluri, R. and M. Zeisberg, *Fibroblasts in cancer.* Nat Rev Cancer, 2006. **6**(5): p. 392-401.
441. Vaheri, A., et al., *Nemosis, a novel way of fibroblast activation, in inflammation and cancer.* Exp Cell Res, 2009. **315**(10): p. 1633-8.
442. Elkabets, M., et al., *Human tumors instigate granulin-expressing hematopoietic cells that promote malignancy by activating stromal fibroblasts in mice.* J Clin Invest, 2011. **121**(2): p. 784-99.
443. Radisky, D.C., P.A. Kenny, and M.J. Bissell, *Fibrosis and cancer: do myofibroblasts come also from epithelial cells via EMT?* J Cell Biochem, 2007. **101**(4): p. 830-9.
444. Zeisberg, E.M., et al., *Endothelial-to-mesenchymal transition contributes to cardiac fibrosis.* Nat Med, 2007. **13**(8): p. 952-61.
445. Gabbiani, G., G.B. Ryan, and G. Majne, *Presence of modified fibroblasts in granulation tissue and their possible role in wound contraction.* Experientia, 1971. **27**(5): p. 549-50.
446. Ina, K., et al., *Significance of alpha-SMA in myofibroblasts emerging in renal tubulointerstitial fibrosis.* Histol Histopathol, 2011. **26**(7): p. 855-66.
447. Trimboli, A.J., et al., *Pten in stromal fibroblasts suppresses mammary epithelial tumours.* Nature, 2009. **461**(7267): p. 1084-91.
448. Calon, A., et al., *Dependency of colorectal cancer on a TGF-beta-driven program in stromal cells for metastasis initiation.* Cancer Cell, 2012. **22**(5): p. 571-84.
449. Jia, C.C., et al., *Cancer-associated fibroblasts from hepatocellular carcinoma promote malignant cell proliferation by HGF secretion.* PLoS One, 2013. **8**(5): p. e63243.
450. Owens, P., et al., *Bone Morphogenetic Proteins stimulate mammary fibroblasts to promote mammary carcinoma cell invasion.* PLoS One, 2013. **8**(6): p. e67533.
451. Comito, G., et al., *Cancer-associated fibroblasts and M2-polarized macrophages synergize during prostate carcinoma progression.* Oncogene, 2014. **33**(19): p. 2423-31.
452. Watnick, R.S., *The role of the tumor microenvironment in regulating angiogenesis.* Cold Spring Harb Perspect Med, 2012. **2**(12): p. a006676.
453. Scott, R.W., et al., *LIM kinases are required for invasive path generation by tumor and tumor-associated stromal cells.* J Cell Biol, 2010. **191**(1): p. 169-85.

454. Tomasek, J.J., et al., *Myofibroblasts and mechano-regulation of connective tissue remodelling.* Nat Rev Mol Cell Biol, 2002. **3**(5): p. 349-63.
455. Simian, M., et al., *The interplay of matrix metalloproteinases, morphogens and growth factors is necessary for branching of mammary epithelial cells.* Development, 2001. **128**(16): p. 3117-31.
456. Levental, K.R., et al., *Matrix crosslinking forces tumor progression by enhancing integrin signaling.* Cell, 2009. **139**(5): p. 891-906.
457. Lyu, Y.Y., et al., *Substituent effect on the luminescent properties of a series of deep blue emitting mixed ligand Ir(III) complexes.* J Phys Chem B, 2006. **110**(21): p. 10303-14.
458. Vered, M., et al., *Cancer-associated fibroblasts and epithelial-mesenchymal transition in metastatic oral tongue squamous cell carcinoma.* Int J Cancer, 2010. **127**(6): p. 1356-62.
459. Giannoni, E., et al., *Reciprocal activation of prostate cancer cells and cancer-associated fibroblasts stimulates epithelial-mesenchymal transition and cancer stemness.* Cancer Res, 2010. **70**(17): p. 6945-56.
460. Qian, B.Z. and J.W. Pollard, *Macrophage diversity enhances tumor progression and metastasis.* Cell, 2010. **141**(1): p. 39-51.
461. Sica, A., et al., *Macrophage polarization in tumour progression.* Semin Cancer Biol, 2008. **18**(5): p. 349-55.
462. Bunt, S.K., et al., *Reduced inflammation in the tumor microenvironment delays the accumulation of myeloid-derived suppressor cells and limits tumor progression.* Cancer Res, 2007. **67**(20): p. 10019-26.
463. Lewis, C. and C. Murdoch, *Macrophage responses to hypoxia: implications for tumor progression and anti-cancer therapies.* Am J Pathol, 2005. **167**(3): p. 627-35.
464. Weber, C.E. and P.C. Kuo, *The tumor microenvironment.* Surg Oncol, 2012. **21**(3): p. 172-7.
465. Van Linthout, S., K. Miteva, and C. Tschope, *Crosstalk between fibroblasts and inflammatory cells.* Cardiovasc Res, 2014. **102**(2): p. 258-69.
466. Murray, P.J. and T.A. Wynn, *Protective and pathogenic functions of macrophage subsets.* Nat Rev Immunol, 2011. **11**(11): p. 723-37.
467. Solinas, G., et al., *Tumor-associated macrophages (TAM) as major players of the cancer-related inflammation.* J Leukoc Biol, 2009. **86**(5): p. 1065-73.
468. Zhang, W., et al., *Expression of tumor-associated macrophages and vascular endothelial growth factor correlates with poor prognosis of peripheral T-cell lymphoma, not otherwise specified.* Leuk Lymphoma, 2011. **52**(1): p. 46-52.
469. Baglole, C.J., et al., *More than structural cells, fibroblasts create and orchestrate the tumor microenvironment.* Immunol Invest, 2006. **35**(3-4): p. 297-325.
470. Egeblad, M., E.S. Nakasone, and Z. Werb, *Tumors as organs: complex tissues that interface with the entire organism.* Dev Cell, 2010. **18**(6): p. 884-901.
471. Nagy, J.A., et al., *Vascular permeability, vascular hyperpermeability and angiogenesis.* Angiogenesis, 2008. **11**(2): p. 109-19.
472. Vaupel, P., F. Kallinowski, and P. Okunieff, *Blood flow, oxygen and nutrient supply, and metabolic microenvironment of human tumors: a review.* Cancer Res, 1989. **49**(23): p. 6449-65.
473. Bensaad, K., et al., *TIGAR, a p53-inducible regulator of glycolysis and apoptosis.* Cell, 2006. **126**(1): p. 107-20.

474. Pouyssegur, J., F. Dayan, and N.M. Mazure, *Hypoxia signalling in cancer and approaches to enforce tumour regression.* Nature, 2006. **441**(7092): p. 437-43.
475. Chiche, J., M.C. Brahimi-Horn, and J. Pouyssegur, *Tumour hypoxia induces a metabolic shift causing acidosis: a common feature in cancer.* J Cell Mol Med, 2010. **14**(4): p. 771-94.
476. Martinez-Zaguilan, R., et al., *Acidic pH enhances the invasive behavior of human melanoma cells.* Clin Exp Metastasis, 1996. **14**(2): p. 176-86.
477. Lardner, A., *The effects of extracellular pH on immune function.* J Leukoc Biol, 2001. **69**(4): p. 522-30.
478. Colegio, O.R., et al., *Functional polarization of tumour-associated macrophages by tumour-derived lactic acid.* Nature, 2014. **513**(7519): p. 559-63.
479. Rupp, C., et al., *Laser capture microdissection of epithelial cancers guided by antibodies against fibroblast activation protein and endosialin.* Diagn Mol Pathol, 2006. **15**(1): p. 35-42.
480. Rupp, C., et al., *IGFBP7, a novel tumor stroma marker, with growth-promoting effects in colon cancer through a paracrine tumor-stroma interaction.* Oncogene, 2014. **0**.
481. Burgess, A., et al., *Loss of human Greatwall results in G2 arrest and multiple mitotic defects due to deregulation of the cyclin B-Cdc2/PP2A balance.* Proc Natl Acad Sci U S A, 2010. **107**(28): p. 12564-9.
482. Vasanwala, F.H., et al., *Repression of AP-1 function: a mechanism for the regulation of Blimp-1 expression and B lymphocyte differentiation by the B cell lymphoma-6 protooncogene.* J Immunol, 2002. **169**(4): p. 1922-9.
483. Stennicke, H.R., et al., *Pro-caspase-3 is a major physiologic target of caspase-8.* J Biol Chem, 1998. **273**(42): p. 27084-90.
484. Kumar, S., *Caspase function in programmed cell death.* Cell Death Differ, 2007. **14**(1): p. 32-43.
485. Logue, S.E. and S.J. Martin, *Caspase activation cascades in apoptosis.* Biochem Soc Trans, 2008. **36**(Pt 1): p. 1-9.
486. Lazebnik, Y.A., et al., *Cleavage of poly(ADP-ribose) polymerase by a proteinase with properties like ICE.* Nature, 1994. **371**(6495): p. 346-7.
487. Buck, S.B., et al., *Detection of S-phase cell cycle progression using 5-ethynyl-2'-deoxyuridine incorporation with click chemistry, an alternative to using 5-bromo-2'-deoxyuridine antibodies.* Biotechniques, 2008. **44**(7): p. 927-9.
488. Dolznig, H., et al., *Modeling colon adenocarcinomas in vitro a 3D co-culture system induces cancer-relevant pathways upon tumor cell and stromal fibroblast interaction.* Am J Pathol, 2011. **179**(1): p. 487-501.
489. Yu, H., et al., *Transgelin is a direct target of TGF-beta/Smad3-dependent epithelial cell migration in lung fibrosis.* FASEB J, 2008. **22**(6): p. 1778-89.
490. Bandyopadhyay, D., et al., *Analysis of cellular senescence in culture in vivo: the senescence-associated beta-galactosidase assay.* Curr Protoc Cell Biol, 2005. **Chapter 18**: p. Unit 18 9.
491. Niedermeyer, J., et al., *Targeted disruption of mouse fibroblast activation protein.* Mol Cell Biol, 2000. **20**(3): p. 1089-94.
492. Garin-Chesa, P., L.J. Old, and W.J. Rettig, *Cell surface glycoprotein of reactive stromal fibroblasts as a potential antibody target in human epithelial cancers.* Proc Natl Acad Sci U S A, 1990. **87**(18): p. 7235-9.
493. Polakis, P., *Wnt signaling and cancer.* Genes Dev, 2000. **14**(15): p. 1837-51.

494. Rao, T.P. and M. Kuhl, *An updated overview on Wnt signaling pathways: a prelude for more.* Circ Res, 2010. **106**(12): p. 1798-806.
495. Patel, P., et al., *The expression of HIV-1 Vpu in monocytes causes increased secretion of TGF-beta that activates profibrogenic genes in hepatic stellate cells.* PLoS One, 2014. **9**(2): p. e88934.
496. Monje, P., M.J. Marinissen, and J.S. Gutkind, *Phosphorylation of the carboxyl-terminal transactivation domain of c-Fos by extracellular signal-regulated kinase mediates the transcriptional activation of AP-1 and cellular transformation induced by platelet-derived growth factor.* Mol Cell Biol, 2003. **23**(19): p. 7030-43.
497. Thuret, G., et al., *Mechanisms of staurosporine induced apoptosis in a human corneal endothelial cell line.* Br J Ophthalmol, 2003. **87**(3): p. 346-52.
498. Kramer, N., et al., *In vitro cell migration and invasion assays.* Mutat Res, 2012.
499. Gaggioli, C., et al., *Fibroblast-led collective invasion of carcinoma cells with differing roles for RhoGTPases in leading and following cells.* Nat Cell Biol, 2007. **9**(12): p. 1392-400.
500. Nusse, R., *Wnt signaling and stem cell control.* Cell Res, 2008. **18**(5): p. 523-7.
501. Zeng, Y.A. and R. Nusse, *Wnt proteins are self-renewal factors for mammary stem cells and promote their long-term expansion in culture.* Cell Stem Cell, 2010. **6**(6): p. 568-77.
502. Ling, L., V. Nurcombe, and S.M. Cool, *Wnt signaling controls the fate of mesenchymal stem cells.* Gene, 2009. **433**(1-2): p. 1-7.
503. Diaz-Flores, L., et al., *CD34+ stromal cells/fibroblasts/fibrocytes/telocytes as a tissue reserve and a principal source of mesenchymal cells. Location, morphology, function and role in pathology.* Histol Histopathol, 2014. **29**(7): p. 831-870.
504. Wiesmann, A., et al., *Decreased CD90 expression in human mesenchymal stem cells by applying mechanical stimulation.* Head Face Med, 2006. **2**: p. 8.
505. Tsai, M.S., et al., *Isolation of human multipotent mesenchymal stem cells from second-trimester amniotic fluid using a novel two-stage culture protocol.* Hum Reprod, 2004. **19**(6): p. 1450-6.
506. Spaeth, E.L., et al., *Mesenchymal CD44 expression contributes to the acquisition of an activated fibroblast phenotype via TWIST activation in the tumor microenvironment.* Cancer Res, 2013. **73**(17): p. 5347-59.
507. Lin, C., et al., *Differential regulation of Gli proteins by Sufu in the lung affects PDGF signaling and myofibroblast development.* Dev Biol, 2014.
508. Hinz, B., et al., *The myofibroblast: one function, multiple origins.* Am J Pathol, 2007. **170**(6): p. 1807-16.
509. Gan, Q., et al., *Smooth muscle cells and myofibroblasts use distinct transcriptional mechanisms for smooth muscle alpha-actin expression.* Circ Res, 2007. **101**(9): p. 883-92.
510. Xie, W.B., et al., *Smad2 and myocardin-related transcription factor B cooperatively regulate vascular smooth muscle differentiation from neural crest cells.* Circ Res, 2013. **113**(8): p. e76-86.
511. Li, J., et al., *Myocardin-like protein 2 regulates TGFbeta signaling in embryonic stem cells and the developing vasculature.* Development, 2012. **139**(19): p. 3531-42.
512. Solway, J., et al., *Structure and expression of a smooth muscle cell-specific gene, SM22 alpha.* J Biol Chem, 1995. **270**(22): p. 13460-9.

513. Steller, E.J., et al., *PDGFRB promotes liver metastasis formation of mesenchymal-like colorectal tumor cells.* Neoplasia, 2013. **15**(2): p. 204-17.
514. Desmouliere, A., et al., *Transforming growth factor-beta 1 induces alpha-smooth muscle actin expression in granulation tissue myofibroblasts and in quiescent and growing cultured fibroblasts.* J Cell Biol, 1993. **122**(1): p. 103-11.
515. Shafer, S.L. and D.A. Towler, *Transcriptional regulation of SM22alpha by Wnt3a: convergence with TGFbeta(1)/Smad signaling at a novel regulatory element.* J Mol Cell Cardiol, 2009. **46**(5): p. 621-35.
516. Thweatt, R., C.K. Lumpkin, Jr., and S. Goldstein, *A novel gene encoding a smooth muscle protein is overexpressed in senescent human fibroblasts.* Biochem Biophys Res Commun, 1992. **187**(1): p. 1-7.
517. Dimri, G.P., et al., *A biomarker that identifies senescent human cells in culture and in aging skin in vivo.* Proc Natl Acad Sci U S A, 1995. **92**(20): p. 9363-7.
518. Kurz, D.J., et al., *Senescence-associated (beta)-galactosidase reflects an increase in lysosomal mass during replicative ageing of human endothelial cells.* J Cell Sci, 2000. **113 (Pt 20)**: p. 3613-22.
519. Bosma, M.J. and A.M. Carroll, *The SCID mouse mutant: definition, characterization, and potential uses.* Annu Rev Immunol, 1991. **9**: p. 323-50.
520. Richmond, A. and Y. Su, *Mouse xenograft models vs GEM models for human cancer therapeutics.* Dis Model Mech, 2008. **1**(2-3): p. 78-82.
521. Katoh, M., *Frequent up-regulation of WNT2 in primary gastric cancer and colorectal cancer.* Int J Oncol, 2001. **19**(5): p. 1003-7.
522. Vermeulen, L., et al., *Wnt activity defines colon cancer stem cells and is regulated by the microenvironment.* Nat Cell Biol, 2010. **12**(5): p. 468-76.
523. Ogasawara, S., et al., *Lack of mutations of the adenomatous polyposis coli gene in oesophageal and gastric carcinomas.* Virchows Arch, 1994. **424**(6): p. 607-11.
524. de Castro, J., et al., *beta-catenin expression pattern in primary oesophageal squamous cell carcinoma. Relationship with clinicopathologic features and clinical outcome.* Virchows Arch, 2000. **437**(6): p. 599-604.
525. Miller, M.F., et al., *Wnt ligands signal in a cooperative manner to promote foregut organogenesis.* Proc Natl Acad Sci U S A, 2012. **109**(38): p. 15348-53.
526. Najdi, R., et al., *A uniform human Wnt expression library reveals a shared secretory pathway and unique signaling activities.* Differentiation, 2012. **84**(2): p. 203-13.
527. Hoppler, S.P. and R.T. Moon, *Wnt Signaling in Development and Disease: Molecular Mechanisms and Biological Functions.*2014, Hoboken, NJ, USA: John Wiley & Sons.
528. Le Floch, N., et al., *The proinvasive activity of Wnt-2 is mediated through a noncanonical Wnt pathway coupled to GSK-3beta and c-Jun/AP-1 signaling.* FASEB J, 2005. **19**(1): p. 144-6.
529. Wang, Y., et al., *Endocardial to myocardial notch-wnt-bmp axis regulates early heart valve development.* PLoS One, 2013. **8**(4): p. e60244.
530. Frantz, C., K.M. Stewart, and V.M. Weaver, *The extracellular matrix at a glance.* J Cell Sci, 2010. **123**(Pt 24): p. 4195-200.
531. Neumann, S., et al., *Mammalian Wnt3a is released on lipoprotein particles.* Traffic, 2009. **10**(3): p. 334-43.

532. Goodwin, A.M., J. Kitajewski, and P.A. D'Amore, *Wnt1 and Wnt5a affect endothelial proliferation and capillary length; Wnt2 does not.* Growth Factors, 2007. **25**(1): p. 25-32.
533. Bilir, B., O. Kucuk, and C.S. Moreno, *Wnt signaling blockage inhibits cell proliferation and migration, and induces apoptosis in triple-negative breast cancer cells.* J Transl Med, 2013. **11**: p. 280.
534. Thiery, J.P., *Epithelial-mesenchymal transitions in tumour progression.* Nat Rev Cancer, 2002. **2**(6): p. 442-54.
535. Macpherson, I.R., et al., *p120-catenin is required for the collective invasion of squamous cell carcinoma cells via a phosphorylation-independent mechanism.* Oncogene, 2007. **26**(36): p. 5214-28.
536. de Magalhaes, J.P., et al., *Gene expression and regulation in H2O2-induced premature senescence of human foreskin fibroblasts expressing or not telomerase.* Exp Gerontol, 2004. **39**(9): p. 1379-89.
537. Mueller, M.M. and N.E. Fusenig, *Friends or foes - bipolar effects of the tumour stroma in cancer.* Nat Rev Cancer, 2004. **4**(11): p. 839-49.
538. Untergasser, G., et al., *Profiling molecular targets of TGF-beta1 in prostate fibroblast-to-myofibroblast transdifferentiation.* Mech Ageing Dev, 2005. **126**(1): p. 59-69.
539. Albrengues, J., et al., *LIF mediates proinvasive activation of stromal fibroblasts in cancer.* Cell Rep, 2014. **7**(5): p. 1664-78.
540. Min, H., et al., *Fgf-10 is required for both limb and lung development and exhibits striking functional similarity to Drosophila branchless.* Genes Dev, 1998. **12**(20): p. 3156-61.
541. Fairbanks, T.J., et al., *Colonic atresia without mesenteric vascular occlusion. The role of the fibroblast growth factor 10 signaling pathway.* J Pediatr Surg, 2005. **40**(2): p. 390-6.
542. Kanard, R.C., et al., *Fibroblast growth factor-10 serves a regulatory role in duodenal development.* J Pediatr Surg, 2005. **40**(2): p. 313-6.
543. Fairbanks, T.J., et al., *A genetic mechanism for cecal atresia: the role of the Fgf10 signaling pathway.* J Surg Res, 2004. **120**(2): p. 201-9.
544. Matsuike, A., et al., *Expression of fibroblast growth factor (FGF)-10 in human colorectal adenocarcinoma cells.* J Nippon Med Sch, 2001. **68**(5): p. 397-404.
545. Lawson, D., M. Harrison, and C. Shapland, *Fibroblast transgelin and smooth muscle SM22alpha are the same protein, the expression of which is down-regulated in many cell lines.* Cell Motil Cytoskeleton, 1997. **38**(3): p. 250-7.
546. Camoretti-Mercado, B., et al., *Expression and cytogenetic localization of the human SM22 gene (TAGLN).* Genomics, 1998. **49**(3): p. 452-7.
547. Assinder, S.J., J.A. Stanton, and P.D. Prasad, *Transgelin: an actin-binding protein and tumour suppressor.* Int J Biochem Cell Biol, 2009. **41**(3): p. 482-6.
548. Murano, S., et al., *Diverse gene sequences are overexpressed in werner syndrome fibroblasts undergoing premature replicative senescence.* Mol Cell Biol, 1991. **11**(8): p. 3905-14.
549. Yang, Z., et al., *Transgelin functions as a suppressor via inhibition of ARA54-enhanced androgen receptor transactivation and prostate cancer cell growth.* Mol Endocrinol, 2007. **21**(2): p. 343-58.
550. Nair, R.R., J. Solway, and D.D. Boyd, *Expression cloning identifies transgelin (SM22) as a novel repressor of 92-kDa type IV collagenase (MMP-9) expression.* J Biol Chem, 2006. **281**(36): p. 26424-36.

551. Thompson, O., et al., *Depletion of the actin bundling protein SM22/transgelin increases actin dynamics and enhances the tumourigenic phenotypes of cells.* BMC Cell Biol, 2012. **13**: p. 1.
552. Shields, J.M., K. Rogers-Graham, and C.J. Der, *Loss of transgelin in breast and colon tumors and in RIE-1 cells by Ras deregulation of gene expression through Raf-independent pathways.* J Biol Chem, 2002. **277**(12): p. 9790-9.
553. Yeo, M., et al., *Loss of SM22 is a characteristic signature of colon carcinogenesis and its restoration suppresses colon tumorigenicity in vivo and in vitro.* Cancer, 2010. **116**(11): p. 2581-9.
554. Lin, Y., et al., *Association of the actin-binding protein transgelin with lymph node metastasis in human colorectal cancer.* Neoplasia, 2009. **11**(9): p. 864-73.
555. Bandapalli, O.R., et al., *Global analysis of host tissue gene expression in the invasive front of colorectal liver metastases.* Int J Cancer, 2006. **118**(1): p. 74-89.
556. Kuilman, T. and D.S. Peeper, *Senescence-messaging secretome: SMS-ing cellular stress.* Nat Rev Cancer, 2009. **9**(2): p. 81-94.
557. Ye, X., et al., *Downregulation of Wnt signaling is a trigger for formation of facultative heterochromatin and onset of cell senescence in primary human cells.* Mol Cell, 2007. **27**(2): p. 183-96.
558. Dvorakova, M., R. Nenutil, and P. Bouchal, *Transgelins, cytoskeletal proteins implicated in different aspects of cancer development.* Expert Rev Proteomics, 2014. **11**(2): p. 149-65.
559. Krtolica, A., et al., *Senescent fibroblasts promote epithelial cell growth and tumorigenesis: a link between cancer and aging.* Proc Natl Acad Sci U S A, 2001. **98**(21): p. 12072-7.
560. Sobral, L.M., et al., *Myofibroblasts in the stroma of oral cancer promote tumorigenesis via secretion of activin A.* Oral Oncol, 2011. **47**(9): p. 840-6.
561. Orimo, A., et al., *Stromal fibroblasts present in invasive human breast carcinomas promote tumor growth and angiogenesis through elevated SDF-1/CXCL12 secretion.* Cell, 2005. **121**(3): p. 335-48.
562. Lucio, P.S., et al., *Myofibroblasts and their relationship with oral squamous cell carcinoma.* Braz J Otorhinolaryngol, 2013. **79**(1): p. 112-8.
563. Neufert, C., C. Becker, and M.F. Neurath, *An inducible mouse model of colon carcinogenesis for the analysis of sporadic and inflammation-driven tumor progression.* Nat Protoc, 2007. **2**(8): p. 1998-2004.
564. De Robertis, M., et al., *The AOM/DSS murine model for the study of colon carcinogenesis: From pathways to diagnosis and therapy studies.* J Carcinog, 2011. **10**: p. 9.

Curriculum Vitae

NAME Mag.[a] Nina Kramer (geb. Slabina)

AUSBILDUNG

seit 2011	PhD Studium **Biologie** Universität Wien Thema der Dissertation: The role of Wnt2 in human colon carcinoma development
21. Jänner 2011	**Magistra rer. nat.**
2005 – 2011	Diplomstudium **Biologie,** Stzw. **Anthropologie,** Schwerpunkt **Humangenetik** Universität Wien Thema der Diplomarbeit: mTOR signalling in primary human lung fibroblasts in 3D cultures
2004 – 2005	Diplomstudium **Veterinärmedizin** Veterinärmedizinische Universität Wien
15. Juni 2004	**Matura** ORG Anton Kriegergasse, Wien

BERUFSERFAHRUNG

2014 – laufend	**Projektmitarbeiterin** Institut für Medizinische Genetik, Medizinische Universität Wien, Währingerstrasse 10, 1090 Wien
2011 – 2014	**Projektmitarbeiterin im Rahmen der Dissertation** Donau Universität Krems (in Kooperation mit dem Institut für Medizinische Genetik, Medizinische Universität Wien), Dr. Karl Dorrek-Strasse 30, 3500 Krems
2009 – 2011	**Diplomarbeit** Institut für Medizinische Genetik, Medizinische Universität Wien, Währingerstrasse 10, 1090 Wien

KONFERENZTEILNAHMEN UND TAGUNGEN

Beatson International Cancer Conference – Targeting the Tumour Stroma
7. Juli 2013 – 10. Juli 2013, Glasgow, Schottland

6. ÖGMBT Jahrestagung
15. September 2014 – 18. September 2014, Wien, Österreich

POSTER PRÄSENTATIONEN

1. *Stromal fibroblast Wnt2 expression in colon cancer*
   Nina Kramer, Harini Nivarthi, Richard Moriggl, Markus Hengstschläger, Wolfgang Sommergruber, Dagmar Schwanzer-Pfeiffer, Helmut Dolznig
   2013, Beatson International Cancer Conference, Glasgow, Schottland

2. *Stromal fibroblast Wnt2 expression in colon cancer*
   Nina Kramer, Harini Nivarthi, Richard Moriggl, Markus Hengstschläger, Wolfgang Sommergruber, Dagmar Schwanzer-Pfeiffer, Helmut Dolznig
   2014, 6. ÖGMBT Jahrestagung, Wien, Österreich

3. *Stromal-derived IGF2 in colon cancer development and progression*
   Christine Unger, **Nina Kramer**, Angelika Walzl, Markus Hengstschläger, Helmut Dolznig
   2014, 6. ÖGMBT Jahrestagung, Wien, Österreich

PUBLIKATIONSLISTE

1. *Modeling human carcinomas: Physiological relevant 3D models to improve anticancer drug development*. C. Unger, **N. Kramer**, A. Walzl, M. Scherzer, M. Hengstschläger and H. Dolznig. *Advanced Drug Delivery Reviews*, 2014, in press.
2. *Lobatin B inhibits NPM/ALK and NK-κB attenuating anaplastic-large-cell-lymphomagenesis and lymphendothelial tumour intravasation.* I. Kiss, C. Unger, H. Nguyen, A. Atanasov, **N. Kramer**, W. Chatuphonprasert, S. Brenner, R. McKinnon, A. Peschel, A. Vasas, I. Lajter, R. Kain, P. Saiko, T. Szekeres, L. Kenner Lukas, M. Hassler, R. Diaz, R. Frisch, V. Dirsch, W. Jäger, R. de Martin, V. Bochkov, C. Passreiter, B. Peter-Vörösmarty, R. Mader, M. Grusch, H. Dolznig, B. Kopp, I. Zupko, J. Hohmann and G. Krupitza. *Cancer Letters*, 2014, in press.
3. *The Resazurin Reduction Assay Can Distinguish Cytotoxic from Cytostatic Compounds in Spheroid Screening Assays.* A. Walzl, C. Unger, **N. Kramer**, D. Unterleuthner, M. Scherzer, M. Hengstschläger, D. Schwanzer-Pfeiffer and H. Dolznig. *J Biomol Screen*. 2014 Apr 23.
4. *In vitro cell migration and invasion assays.* **N. Kramer**, A. Walzl, C. Unger, M. Rosner, G. Krupitza, M. Hengstschläger and H. Dolznig. *Mutat Res*. 2012 Jan-Mar;752(1):10-24.

5. *Simple and Cost Efficient Method to Avoid Unequal Evaporation in Cellular Screening Assays, Which Restores Cellular Metabolic Activity*. A. Walzl, **N. Kramer**, G. Mazza, M. Rosner, D. Falkenhagen, M. Hengstschläger, D. Schwanzer-Pfeiffer and H. Dolznig. *Int J App Sciences and Technology*. 2012; 2(6):17-25.
6. *Tuberin and PRAS40 are anti-apoptotic gatekeepers during early human amniotic fluid stem cell differentiation*. C. Fuchs, M. Rosner, H. Dolznig, M. Mikula, **N. Kramer** and M. Hengstschläger. *Hum Mol Genet*. 2011 Mar 1;21(5):1049-61.
7. *Organotypic spheroid cultures to study tumor–stroma interaction during cancer development.* H. Dolznig, A. Walzl, **N. Kramer**, M. Rosner, P. Garin-Chesa and M. Hengstschläger. *Drug Discov Today Dis Models*. 2011 Sep;8(2-3):113-119.
8. *Contribution of human amniotic fluid stem cells to renal tissue formation depends on mTOR*. N. Siegel, M. Rosner, M. Unbekandt, C. Fuchs, **N. Slabina (Kramer)**, H. Dolznig, J. A. Davies, G. Lubec and M. Hengstschläger. *Hum Mol Genet*. 2010 Sep 1;19(17):3320-31.
9. *Efficient siRNA-mediated prolonged gene silencing in human amniotic fluid stem cells.* M. Rosner, N. Siegel, C. Fuchs, **N. Slabina (Kramer)**, H. Dolznig and M. Hengstschläger. *Nat Protoc*. 2010 Jun;5(6):1081-95.

MANUSKRIPTE IN BEARBEITUNG

1. *The ratio of STAT1 to STAT3 expression influences colorectal cancer growth.* H. Nivarthi, C. Gordziel, **N. Kramer**, M. Themanns, M. Eberl, B. Rabe, M. Schlederer, S. Rose-John, T. Knösel, L. Kenner, F. Aberger, H. Dolznig, K. Friedrich and R. Moriggl. *Submitted to Clinical Cancer Research, under revision*
2. *The germacranolide sesquiterpene lactone Neurolenin B of the healing plant Neurolaena lobata inhibits NPM/ALK-driven cell expansion and NF-kB-driven tumour intravasation.* C. Unger, I. Kiss, **N. Kramer**, A. Atanasov, N. H. Chi, W. Chatuphonprasert, S. Brenner, R. McKinnon-Popescu, A. Peschel, R. Kain, P. Saiko, L. Kenner, M. Hassler, R. Diaz, R. Frisch, V. Dirsch, W. Jäger, R. de Martin, V. Bochkov, C. Passreiter, R. Mader, M. Grusch, H. Dolznig, B. Kopp, I. Zupko, J. Hohmann and G. Krupitza. *Submitted to Britisch Journal of Cancer*
3. *WNT2 - a novel colon tumor stroma marker - induces migration and invasion by activation of canonical β-catenin signaling in colonic fibroblasts.* **N. Kramer**, D. Unterleuthner, J. Schmöllerl, H. Nivarthi, A. Rudisch, A. Walzl, C. Unger, M. Scherzer, M. Artaker, M. Schlederer, M. Hengstschläger, R. Moriggl, W. Sommergruber and H. Dolznig. *In preparation for submisison to Oncogene*
4. *The role of REG1A in colon cancer development.* C. Unger, A. Rudisch, H. Nivarthi, **N. Kramer**, A. Walzl, M. Scherzer, M. Hengstschläger, D. Pfeiffer and H. Dolznig. *In prepartion for submission to Cancer Research*

Appendix

Chemicals, reagents and equipment used in this study

Table 8 Chemicals and reagents

Product name	Company	Article no.
10x PBS, pH 7.4	Life Technologies, Carlsbad, California, USA	70011-044
2-Mercaptoethanol, min. 98 %	Merck, Darmstadt, Germany	8.05740.0250
30 % Acrylamide/ bis-Acrylamide Solution	Sigma-Aldrich, St. Louis, MO, USA	A3699
3xAP1pGL3	Addgene, Cambridge, MA, USA	40342
4',6-Diamidino-2-phenylindole dihydrochloride (DAPI)	Sigma-Aldrich, St. Louis, MO, USA	32670
5-Bromo-4-chloro-3-indolyl β-D-galactopyranoside (X-gal)	Sigma-Aldrich, St. Louis, MO, USA	B4252
5-Bromo-4-chloro-3-indolyl β-D-galactopyranoside (X-gal)	Sigma-Aldrich, St. Louis, MO, USA	B4252
5-Sulfosalicylic acid dihydrate	Sigma-Aldrich, St. Louis, MO, USA	S2130
5x siRNA buffer	Dharmacon, Lafayette, CO, USA	B-002000-UB-015
7-Aminoactinomycin D (7-AAD)	Sigma-Aldrich, St. Louis, MO, USA	A9400
Agarose Electrophoresis Grade	Invitrogen, Carlsbad, CA, USA	15510-027
Alexa Fluor® 488 Goat Anti-Mouse IgG (H+L) Antibody	Invitrogen, Carlsbad, CA, USA	A-11001
Alexa Fluor® 488 Goat Anti-Rabbit IgG (H+L) Antibody	Invitrogen, Carlsbad, CA, USA	A 11034
Alexa Fluor® 546 Phalloidin	Invitrogen, Carlsbad, CA, USA	A 22283
Alexa Fluor® 594 Goat Anti-Mouse IgG (H+L) Antibody	Invitrogen, Carlsbad, CA, USA	A 11032
Ammonium persulfate (APS)	BioRad, Hercules, CA, USA	1610700
Ampicillin sodium salt	Sigma-Aldrich, St. Louis, MO, USA	A0166
Apo-ONE® Homogeneous Caspase-3/7 Assay	Promega, Madison, WI, USA	G7790
Aprotinin from bovine lung	Sigma-Aldrich, St. Louis, MO, USA	A1153
Benzamidine chloride Hydrochlorid: Hydrate	Sigma-Aldrich, St. Louis, MO, USA	B6506

Product name	Company	Article no.
BioRad - Protein Assay Dye reagent Concentrate	BioRad, Hercules, CA, USA	500-0006
Bovine Serum Albumin (BSA) Fraction V	GE Healthcare, Little Chalfont, United Kingdom	K41-001
Bromophenol blue	Merck, Darmstadt, Germany	L961422
Calcium chloride dihydrate ($CaCl_2$)	Merck, Darmstadt, Germany	2382
Citric acid	Sigma-Aldrich, St. Louis, MO, USA	C2404
Click-iT® EdU Flow Cytometry Assay Kit	Life Technologies, Carlsbad, California, USA	C10425
CloneJET PCR Cloning Kit	Thermo Scientific, Waltham, MA, USA	K1231
Collagen I, Rat Tail	Corning, Bedford, MA, USA	354236
Crystal Violet	Sigma-Aldrich, St. Louis, MO, USA	C3886
DEPC treated water	Invitrogen, Carlsbad, CA, USA	10813-012
di-Sodium hydrogen phosphate dihydrate	Merck, Darmstadt, Germany	1.06580
Dimethyl sulfoxide (DMSO)	Sigma-Aldrich, St. Louis, MO, USA	D5879
Dithiothreitol (DTT)	Sigma-Aldrich, St. Louis, MO, USA	646563
DMEM 1x (4.5 g/l D-Glucose, 0.11 g/l Sodium Pyruvate)	Life Technologies, Carlsbad, California, USA	21969-035
DNeasy Blood & Tissue Kit	Qiagen, Valencia, CA, USA	69504
DPBS 1x	Lonza, Verviers, Belgium	17-512F
Dual-Luciferase® Reporter Assay System	Promega, Madison, WI, USA	E1910
EGM-2 MV BulletKit	Lonza, Verviers, Belgium	LONCC-3202 (CC-3156+CC-4147)
Ethanol absolute for analysis	VWR, West Chester, PA, USA	20821.310
Ethylenediaminetetraacetic acid (EDTA)	Sigma-Aldrich, St. Louis, MO, USA	E5134
FGM Fibroblast BulletKit	Lonza, Verviers, Belgium	LONCC-3130 (CC-3131+CC-4134)
Fixmilch Instant	Maresi, Vienna, Austria	

Product name	Company	Article no.
GenElute Plasmid Miniprep Kit	Sigma-Aldrich, St. Louis, MO, USA	PLN70
Glutaraldehyde solution	Sigma-Aldrich, St. Louis, MO, USA	G5882
Glutaraldehyde solution, 25 % in H2O	Sigma-Aldrich, St. Louis, MO, USA	G6257
Glycerol	Merck, Darmstadt, Germany	1.04093
Glycine for electrophoresis	Sigma-Aldrich, St. Louis, MO, USA	G8898
GoScript™ Reverse Transcription System	Promega, Madison, WI	A5001
GoTaq™ qPCR Master Mix	Promega, Madison, WI, USA	A6002
Heat Inactivated Fetal bovine serum (FBS)	Life Technologies, Carlsbad, California, USA	10500-064
HindIII	New England Biolabs, Ipswich, MA, USA	R0104
KpnI	New England Biolabs, Ipswich, MA, USA	R0142
L-glutamine	Lonza, Verviers, Belgium	BE17-605E
Leupeptin	Sigma-Aldrich, St. Louis, MO, USA	L2023
Lipofectamine 2000	Invitrogen, Carlsbad, CA, USA	11668-027
Lipofectamine RNAiMAX	Invitrogen, Carlsbad, CA, USA	13778-075
Magnesium chloride hexahydrate ($MgCl_2$)	Merck, Darmstadt, Germany	5833
Methanol	Sigma-Aldrich, St. Louis, MO, USA	179957
Methylcellulose (4,000 centipoises)	Sigma-Aldrich, St. Louis, MO, USA	M0512
Midori Green Advanced	Nippon Genetics Europe, Düren, Germany	MG04
MluI	New England Biolabs, Ipswich, MA, USA	R0198
Mouse IgG-heavy and light chain Antibody	Bethyl Laboratories Inc., Montgomery, TX, USA	A90-116P
ON-TARGETplus Non-targeting Control Pool	GE Dharmacon, Lafayette, CO, USA	D-001810-10-05
ON-TARGETplus SMARTpool siRNA Wnt2 siRNA	GE Dharmacon, Lafayette, CO, USA	L-003938-00-0005

Product name	Company	Article no.
One Shot TOP10 Chemically Competent E. coli	Life Technologies, Carlsbad, California, USA	C4040
OptiMEM I	Life Technologies, Carlsbad, California, USA	31985
PageRuler Prestained Protein Ladder	Fermentas, Thermo Fisher Scrientific, Waltham, MA, USA	SM0671
Paraformaldehyde	Sigma-Aldrich, St. Louis, MO, USA	P6148
Penicillin	Sigma-Aldrich, St. Louis, MO, USA	P3032
pGL3 basic	Promega, Madison, WI, USA	E1751
Phenyl-methyl-sulfonyl-fluorid (PMSF)	Sigma-Aldrich, St. Louis, MO, USA	P7626
Phusion HF	New England Biolabs, Ipswich, MA, USA	M0530
Ponceau S	Sigma-Aldrich, St. Louis, MO, USA	P3504
Potassium chloride (KCl)	Merck, Darmstadt, Germany	1.04936
Potassium hexacyanoferrate (II) trihydrate	Sigma-Aldrich, St. Louis, MO	31254
Potassium hexacyanoferrate (III)	Sigma-Aldrich, St. Louis, MO	31253
Propidium iodide	Sigma-Aldrich, St. Louis, MO, USA	P4170
Puromycin dihydrochloride	Sigma-Aldrich, St. Louis, MO, USA	P7255
QIAquick Gel Extraction Kit	Qiagen, Valencia, CA, USA	28704
Rabbit IgG-heavy and light chain Antibody	Bethyl Laboratories Inc., Montgomery, TX, USA	A120-101P
ReliaPrep™ RNA Cell Miniprep System	Promega, Madison, WI	Z6011
RNAse A	Sigma-Aldrich, St. Louis, MO, USA	R5125
Select Yeast extract	Sigma-Aldrich, St. Louis, MO, USA	Y0500
Sodium chloride (NaCl)	Sigma-Aldrich, St. Louis, MO, USA	S9625
Sodium citrate tribasic dihydrate	Sigma-Aldrich, St. Louis, MO, USA	C7254

Product name	Company	Article no.
Sodium deoxycholate	Sigma-Aldrich, St. Louis, MO, USA	30970
Sodium dodecyl sulfate (SDS)	Sigma-Aldrich, St. Louis, MO, USA	L4390
Sodium hydroxide (NaOH) pellets	Merck, Darmstadt, Germany	1.06498
Staurosporine	Sigma-Aldrich, St. Louis, MO, USA	S4400
Streptomycin sulfate	Sigma-Aldrich, St. Louis, MO, USA	S6501
Tetramethylethylenediamine (TEMED)	Sigma-Aldrich, St. Louis, MO, USA	T9281
Trichlor acetic adid	Merck, Darmstadt, Germany	807
Trisma Base	Sigma-Aldrich, St. Louis, MO, USA	T1503
Triton X-100	Sigma-Aldrich, St. Louis, MO, USA	T8787
Trypsin	Serwa, Heidelberg, Germany	37290
Trypsin inhibitor	Sigma-Aldrich, St. Louis, MO, USA	T9003
Tryptone	Sigma-Aldrich, St. Louis, MO, USA	T9410
Tween 20	BioRad, Hercules, CA, USA	170-6531
Vectashield Mounting Medium for Fluorescence	Vector Laboratories Inc., Burlingame, CA, USA	H-1000
Vimentin V9 antibody	Life Technologies, Carlsbad, California, USA	18-0052
XhoI	New England Biolabs, Ipswich, MA, USA	R0146
β-catenin antibody	Cell Signaling Technologies, Danvers, MA, USA	8480

Tabelle 9 Equipment used in this study

Product name	Company	Article no.
1.5 ml microcentrifuge tubes	VWR, West Chester, PA, USA	211-0015 (Europe)
100 x 20 mm Tissue Culture Dish	CytoOne STARLAB International, Hamburg, Germany	CC7682-3394
15 ml centrifuge tubes	Sarstedt, Nümbrecht, Germany	62.554.502
15-slots comb	BioRad, Hercules, CA, USA	165-3355
24-well plate with lid	CytoOne STARLAB International, Hamburg, Germany	CC7682-7524
3MM Chr sheets	Whatman, Dassel, Germany	3030 917
4-well chamber slide	Lab-Tek®, Nalge Nunc International, Naperville, IL, USA	177437
500 µl microcentrifuge tubes	Eppendorf, Hamburg, Germany	0030 121.023
6-well plate with lid	CytoOne STARLAB International, Hamburg, Germany	CC7682-7506
60 x 15 mm Tissue Culture Dish	CytoOne STARLAB International, Hamburg, Germany	CC7682-3359
96-well plate flat bottom	CytoOne STARLAB International, Hamburg, Germany	CC7682-7596
96-well plates V-shaped	Sterillin, Aberbargoed, Caerphilly, UK	microtiter plate 612V96 lid 642000
BioPhotometer	Eppendorf, Hamburg, Germany	
Bright-Line hemacytometer	Hausser Scientific, Horsham, PA, USA	3120
Cellquest Version 6.0	BD Immunocytometry Systems	
CL-XPosure films	Thermo Scientific, Waltham, MA, USA	34089
Corning® Transwell® polycarbonate membrane cell culture inserts	Sigma-Aldrich, St. Louis, MO, USA	CLS3422-48EA

Product name	Company	Article no.
cover slide	Thermo Scientific, Waltham, MA, USA	DXD-10143263 24x60 mm #1
CryoTubes™	Nalge Nunc International, Naperville, IL, USA	343958
cuvette	Sarstedt, Nümbrecht, Germany	67.746
Eppendorf Centrifuge 5417R	Eppendorf, Hamburg, Germany	
FACS-tube	BD Falcon™, BD Biosciences, Erembodegem, Belgium	352054
FACSCalibur	Beckton Dickinson, Franklin Lakes, NJ, USA	
FlowJo Version 7.5.5	Tree Star Inc., Ashland, OR, USA	
glass slide	Thermo Scientific, Waltham, MA, USA	DXD-10143560
GraphPad Prism 4	GraphPad Software Inc., La Jolla, CA, USA	
Heraeus BBD 6220 incubators	Thermo Scientific, Waltham, MA, USA	
Kodak Medical X-ray Processor 2000	Kodak, Stuttgart, Germany	
light-sensitive Amersham Hyperfilms	GE Healthcare, Buckinghamshire, UK	28906837
Low Multiplate 96 Natl 25/BX	BioRad, Hercules, CA, USA	MLL9601
Microseal B Adhesive Seals	BioRad, Hercules, CA, USA	MSB1001
Microsoft Excel 2008	Microsoft Corporation, Redmond WA, USA	
Millicell Cell Culture Insert	Merck Millipore Ltd, Darmstadt, Germany	PICM0RG50
Mini-PROTEAN Tetra Electrophoresis System	Hercules, CA, USA	165-8002
Mini-Trans-Blot Module	BioRad, Hercules, CA, USA	170-3935
Nanodrop 2000	Thermo Scientific, Waltham, MA, USA	
nitrocellulose membrane	Watman, Dassel, Germany	10401396
Nunc-Immuno MicroWell 96 well polystyrene plates	Sigma-Aldrich, St. Louis, MO, USA	P8616-50EA

Product name	Company	Article no.
orbital shaker	Rocky® 3D	
Parafilm “M”®	VWR, West Chester, Pa, USA	291-1213
PCR tubes 0.2 mL flat cap	Peqlab, Erlangen, Germany	82-0620-A
PET mesh with 120 µm mesh size	Bückmann, Mönchengladbach, Germany	PET-100/77-32
pipette-tips	Starlab, Ahrensburg, Germany	0,1-10 µl S1111-3000 1-200 µl S1111-1006 101-1000 µl S1111-2021
rocking platform	VWR, West Chester, Pa, USA	40000300
single-use syringe	B Braun, Bethlehem, PA, USA	460 6051 V
Synergy HT	Biotek, Winooski, VT, USA	
syringe filter with 0,2 µm pore size	Whatman, Dassel, Germany	6809-2122
Thermocycler Primus25 advanced	Peqlab, Erlangen, Germany	
thermomixer comfort	Eppendorf, Hamburg, Germany	
v-shaped reservoir	Eppendorf, Hamburg, Deutschland	D5063-85
watherbath shaker Julabo W22	JULABO Labortechnik GmbH, Seelbach, Germany	